**Lara Mills**

# Modeling the impact of sea level rise in the Guadiana Estuary

**UNIVERSIDADE DO ALGARVE**
FACULDADE DE CIÊNCIAS E TECNOLOGIA
2019

**Lara Mills**

# Modeling the impact of sea level rise in the Guadiana Estuary

**Master in Marine and Coastal Sciences**
Work performed under the supervision of:
Flávio Martins, Prof. Coordinator, University of Algarve
João Janeiro, Researcher, CIMA

**UNIVERSIDADE DO ALGARVE**
FACULDADE DE CIÊNCIAS E TECNOLOGIA
2019

Modeling the impact of sea level rise in the Guadiana Estuary

Declaração de autoria de trabalho

Declaro ser o(a) autor(a) deste trabalho, que é original e inédito. Autores e trabalhos consultados estão devidamente citados no texto e constam da listagem de referências incluída.

---

Declaration of authorship of work

I declare to be the author of this work, which is original and unpublished. Authors and works consulted are duly cited in the text and are included in the list of references.

---

Copyright © 2019 Lara Mills

A Universidade do Algarve reserva para si o direito, em conformidade com o disposto no Código do Direito de Autor e dos Direitos Conexos, de arquivar, reproduzir e publicar a obra, independentemente do meio utilizado, bem como de a divulgar através de repositórios científicos e de admitir a sua cópia e distribuição para fins meramente educacionais ou de investigação e não comerciais, conquanto seja dado o devido crédito ao autor e editor respetivos.

The University of Algarve reserves the right, in accordance with the provisions of the Code of the Copyright Law and related rights, to file, reproduce and publish the work, regardless of the used mean, as well as to disseminate it through scientific repositories and to allow its copy and distribution for purely educational or research purposes and non-commercial purposes, although be given due credit to the respective author and publisher.

**Acknowledgements**

First, I would like to thank my supervisors Flávio Martins and João Janeiro for being the best supervisors ever and for sharing their extensive knowledge of the MOHID modeling system with me. Their encouragement and guidance throughout this past year is greatly appreciated and I am truly grateful for all the opportunities they have let me be part of in relation to this work. I would also like to thank them for providing me with such a wonderful working space in the Hidrotec lab and for making me feel part of the team. I would further like to thank everyone in Hidrotec for providing a calm, fun and warm environment to complete this project.

I would also like to thank the IT department at the University of Algarve for giving me access to a virtual machine as well as a VPN, allowing me to run my model simulations from anywhere in the world.

I would like to thank Bentley Systems, namely the general director, Frank Braunschwieg for the use of MOHID studio. This project would not have been possible without the development of this software.

Next, I would like to thank all my professors in the Marine and Coastal Systems master for sharing their deep knowledge in marine and coastal systems. I would also like to thank my classmates for their support and friendship over these last two years and for making this master program a happy and positive experience. I would like to give a special thank you to the one and only Dream Team for being the best late-night study buddies.

**Abstract**

Sea level rise is a global concern as a large percentage of the population live on the coast. The focus of this study is the impact of sea level rise on the Guadiana Estuary, an estuary in the Iberian Peninsula formed at the interface of the Guadiana River and the Gulf of Cadiz. Estuaries will be largely affected by sea level rise as these transitional environments host highly diverse and complex marine ecosystems. Model-based projections of sea level rise demonstrate that global mean sea level rise is accelerating. Major consequences of sea level rise are the intrusion of salt from the sea into fresh water as well as an increase in flooding area. Not yet fully explored in the literature are the effects of sea level rise on salinity concentrations in estuarine environments. As the physical, chemical and biological components of estuaries are sensitive to changes in salinity, the purpose of this study is to further evaluate salt intrusion and flooding in the Guadiana Estuary caused by sea level rise and the socioeconomic effects of areas surrounding the estuary.

Hydrodynamics of the Guadiana Estuary were simulated in a two-dimensional numerical model with the MOHID water modeling system. A previously developed hydrodynamic model was used to further examine evolution of salinity transport in the estuary as well as flooding areas in response to sea level rise. Varying tidal amplitudes, freshwater discharge from the Guadiana River and bathymetries of the estuary were incorporated in the model to fully evaluate the impacts of sea level rise on salinity transport and flooding areas of the estuary. Results show an overall increase in salinity and land inundation in the estuary in response to sea level rise. The salinity extends westward and eastward to the saltmarshes of the estuary when there is a high freshwater discharge from the Guadiana River. Salinity extends further up the main channel when the freshwater discharge is low.

**Keywords:** Guadiana Estuary; numerical model; MOHID; sea level rise; salinity intrusion

**Abstrato**

A elevação do nível do mar é uma preocupação global, pois uma grande percentagem da população mundial vive na costa. O foco deste estudo é o impacto do aumento do nível do mar no estuário do Guadiana, um estuário da Península Ibérica formado na interface do rio Guadiana e do Golfo de Cádiz. Os estuários serão amplamente afetados pela elevação do nível do mar, pois esses ambientes de transição hospedam ecossistemas marinhos altamente diversificados e complexos. Projeções baseadas em modelos de aumento do nível do mar demonstram que o aumento médio global do nível do mar está a acelerar. As principais consequências do aumento do nível do mar são a intrusão de sal do mar em água doce, bem como o aumento da área de inundação. Ainda não são totalmente explorados na literatura os efeitos do aumento do nível do mar nas concentrações de salinidade em ambientes estuarinos. Como os componentes físicos, químicos e biológicos dos estuários são sensíveis a mudanças na salinidade, o objetivo deste estudo é avaliar ainda mais a intrusão e inundação de sal no estuário do Guadiana causada pelo aumento do nível do mar e os efeitos socioeconômicos das áreas ao redor do estuário.

A hidrodinâmica do estuário do Guadiana foi simulada em um modelo numérico bidimensional com o sistema de modelagem de água MOHID. Um modelo hidrodinâmico da área em estudo, desenvolvido anteriormente, foi usado para examinar melhor a evolução do transporte de salinidade no estuário, bem como nas áreas de inundação em resposta à elevação do nível do mar. Diferentes amplitudes de maré, caudais de água doce do rio Guadiana e batimetrias do estuário foram incorporadas no modelo para avaliar os impactos do aumento do nível do mar no transporte de salinidade e nas áreas de inundação do estuário. Os resultados mostram um aumento geral na salinidade e inundação de terras no estuário em resposta ao aumento do nível do mar. A salinidade estende-se para oeste e leste até os sapais salgados do estuário, quando há uma alta descarga de água doce do Guadiana. A salinidade estende-se ainda mais pelo canal principal quando a descarga de água doce é baixa.

**Palavras-chave**: Estuário do Guadiana; modelo numérico; MOHID; aumento do nível do mar; intrusão salina

**Resumo**

A subida do nível médio global do mar ocorre atualmente a uma taxa de aproximadamente 3,2 milímetros por ano. O último relatório do Painel Intergovernamental de Mudanças Climáticas (IPCC) concluiu que a taxa de aumento médio do nível do mar está a acelerar bem como o número de pessoas que ocupam as áreas costeiras. A elevação do nível do mar impactará amplamente a sociedade, pois os seus efeitos negativos incluem aumento das áreas de inundação, aumento da salinidade e mudanças nos ecossistemas. A elevação do nível do mar terá um grande impacto nos estuários, pois os estuários servem como interface entre a água doce da terra e a água salgada do mar. Esses ambientes sensíveis hospedam ecossistemas altamente diversos e complexos e serão impactados pelas mudanças climáticas.

O principal objetivo deste trabalho é analisar mudanças na salinidade e áreas de inundação em resposta ao aumento do nível do mar num grande estuário da Península Ibérica, o estuário do Guadiana. O estuário de Guadiana fica entre o rio Guadiana e o Golfo de Cádiz. A foz do estuário fica entre duas regiões altamente povoadas: Vila de Real de Santo António, no lado português, e Ayamonte, no lado espanhol. O estuário de Guadiana possui um regime mesotidal semidiurno com influência da maré 50 quilómetros a montante de onde encontra o Golfo de Cádiz. O estuário do Guadiana é bem misturado e estratificado apenas sob condições extremas.

O estudo baseia-se nas metodologias e nos resultados de um modelo hidrodinâmico e de transporte já desenvolvido e validado, baseado no sistema de modelação MOHID (Mills et al., 2019) para fornecer uma análise mais quantitativa de como o Estuário do Guadiana evoluirá ao longo do século atual. Como o estuário é bem misturado e as propriedades da água não mudam ao longo da coluna de água, foi decidido modelar a hidrodinâmica do estuário em 2D.

O modelo implementa cenários de elevação do nível do mar projetados pelo IPCC até ao ano 2100, variando o caudal de água doce do rio Guadiana e diferentes batimetrias baseadas em um litoral estático ou em mudança. O fluxo de água doce no estuário do Guadiana foi fortemente regulado devido à recente construção de barragens. Dois cenários de caudal de água doce foram implementados no modelo: (1) elevada descarga de água doce de 100 m3 / s, representando o fluxo do rio no inverno e (2) baixa descarga de água doce de 10 m3 / s, representando o fluxo do rio no verão. O sistema de modelação MOHID foi usado para analisar como os cenários mencionados anteriormente afetarão as propriedades hidrodinâmicas e hídricas do estuário do Guadiana. O MOHID simula processos físicos, biogeoquímicos e sedimentos na coluna de água usando uma abordagem de programação orientada a objetos. É

composto por modelos de hidrodinâmica, transporte euleriano, transporte lagrangiano, qualidade da água e sedimentos.

Todas as simulações foram executadas em uma malha cartesiana de 1400 x 350 células computacionais com um passo espacial de 30 metros, que foi escolhido por fornecer a resolução espacial mais apropriada sem incorrer em tempo de cálculo excessivo. O estuário do Guadiana tem um tempo de residência alto, especialmente quando o fluxo do rio é baixo. Por exemplo, são necessários dois meses para estabilizar o campo de salinidade para uma descarga do rio de 10 m3 / s, o que se traduz em mais de duas semanas no tempo de simulação. Os locais das séries temporais também foram escolhidos ao longo do canal principal e nos sapais a oeste do estuário de Guadiana, no lado português. Os resultados das séries temporais permitiram uma avaliação da velocidade e salinidade por um período de dois ciclos de maré ou 24 horas.

Os resultados do modelo mostraram que a dinâmica do estuário do Guadiana é bastante complexa. As mudanças na salinidade são muito mais variáveis em relação à batimetria atual em resposta ao aumento do nível do mar em comparação com as mudanças na salinidade de uma batimetria que permite inundações. A batimetria que permite inundações resulta na extensão da salinidade para oeste e leste no estuário inferior, em direção aos pântanos de Espanha e Portugal. Para altos fluxos de água doce, a salinidade estende-se horizontalmente e para baixos fluxos de água doce, a salinidade estende-se ainda mais no canal principal. No geral, a salinidade aumenta em resposta ao aumento médio do nível do mar. A distribuição horizontal da salinidade varia de acordo com o fluxo de água doce e batimetria. Os valores de salinidade são muito mais altos na maré alta em comparação com os valores de salinidade obtidos na maré baixa, o que demonstra a forte influência da maré na dinâmica do estuário.

A quantidade de terra submersa durante um ciclo de maré também foi calculada. Os resultados mostram um aumento consistente da área inundada em resposta ao aumento do nível do mar. As classes de inundação também foram calculadas com base na quantidade de tempo que a terra fica submersa durante um ciclo de maré. Classes de inundação mais altas estão associadas a um tempo de inundação mais longo e classes de inundação mais baixas estão associadas a um tempo de inundação mais curto. Os resultados do modelo demonstraram uma quantidade maior de área em classes de inundação mais altas em resposta à elevação do nível do mar.

No geral, os resultados mostram um aumento da salinidade e inundação da terra em resposta à elevação do nível do mar. Os resultados obtidos neste trabalho podem ser úteis no processo de tomada de decisão por forma a manter e preservar as áreas estuarinas e costeiras à medida que o nível do mar aumenta.

# Table of Contents

1 Introduction ..... 1
1.1 Motivation ..... 1
1.2 Objectives ..... 3
1.3 Dissertation Structure ..... 3
2 Literature Review & State of the Art ..... 4
2.1 What Is Sea Level Change? ..... 4
2.1.1 Definition of Sea Level ..... 4
2.1.2 Global Sea Level Change ..... 4
2.1.3 Regional Sea Level Change ..... 5
2.1.4 The Impact of Sea Level Rise on Estuaries ..... 6
2.2 The Guadiana Estuary ..... 7
2.2.1 Physical Characteristics ..... 7
2.2.2 Hydrodynamic Characterization ..... 9
2.2.3 Guadiana River Outflow ..... 10
2.2.4 Socioeconomic Characterization of the Guadiana Estuary ..... 11
2.2.5 Managing the Guadiana Estuary: the SPICOSA Project ..... 11
2.3 Salinity Intrusion ..... 12
2.4 Modeling the Impacts of Sea Level Change ..... 12
2.4.1 Definition of Numerical Model ..... 12
2.4.2 Previous Models of the Guadiana Estuary ..... 13
3 Methods ..... 14
3.1 MOHID ..... 14
3.2 Model Simulations ..... 15
3.2.1 Model Setup ..... 15
3.2.2 Model Bathymetries ..... 16
3.2.3 Sea Level Rise Scenarios ..... 17

3.2.4 Freshwater Flow Scenarios ..... 18
3.2.5 Tidal Scenarios ..... 19
3.2.6 Model Runs ..... 20
3.2.7 Areas of Inundation ..... 21
4 Results ..... 22
4.1 Time Series Locations ..... 22
4.2 Temporal Evolution of Velocity ..... 23
4.2.1 Velocity Time Series at Neap Tide for a High Freshwater Flow ..... 23
4.2.2 Velocity Time Series at Neap Tide for a Low Freshwater Flow ..... 27
4.2.3 Velocity Time Series at Spring Tide for a High Freshwater flow ..... 31
4.2.4 Velocity Time Series at Spring Tide for a Low Freshwater Discharge ..... 35
4.3 Evolution of Water Elevation ..... 39
4.4 Temporal Evolution of Salinity ..... 43
4.4.1 Salinity Time Series at Neap Tide with a High Freshwater Discharge ..... 43
4.4.2 Salinity Time Series at Neap Tide with a Low Freshwater Discharge ..... 46
4.4.3 Salinity Time Series at Spring Tide with a High Freshwater Discharge ..... 50
4.4.4 Salinity Time Series at Spring Tide with a Low Freshwater Discharge ..... 54
4.5 Horizontal Distribution Maps of Salinity ..... 57
4.5.1 Salinity Distribution Maps at Neap Tide with a High Freshwater Flow ..... 58
4.5.2 Salinity Distribution Maps at Neap Tide with a Low Freshwater Flow ..... 60
4.5.3 Salinity Distribution Maps at Spring Tide with a High Freshwater Flow ..... 63
4.5.4 Salinity Distribution Maps at Spring Tide with a Low Freshwater Flow ..... 65
4.5.5 Areas of Inundation: Flooding Classes ..... 67
4.5.6 Areas of Inundation: Flood Distribution Maps ..... 72
5 Discussion ..... 77
5.1 Hydrodynamic and Salinity Results ..... 77
5.1.1 Evolution of Salinity for a High Freshwater Discharge at Neap Tide ..... 77

5.1.2 Evolution of Salinity for a Low Freshwater Discharge at Neap Tide.....81
5.1.3 Evolution of Salinity for a High Freshwater Discharge at Spring Tide.....84
5.1.4 Temporal Evolution of Salinity for a Low Freshwater Discharge at Spring Tide 87
5.1.5 Overall Impact of Salinity Change on the Guadiana Estuary.....91
5.1.6 Impact of Land Inundation.....92
6 Conclusion.....93
References.....95
Appendix A Time Series Results of Water Elevation.....100
Appendix B Time Series Results of Velocity.....113
Appendix C Salinity Time Series.....117
Appendix D ICCS Conference Paper – "The Impact of Sea Level Rise in the Guadiana Estuary" 122

## List of Figures

Figure 1.1 Paleo sea level data, tide gauge data and future predictions for very high greenhouse gas emissions (red) and very low greenhouse gas emissions (blue) obtained from the IPCC AR5 (Church et al., 2013).....2
Figure 2.1 Location and geomorphology of the Guadiana Estuary (Garel, 2017).....9
Figure 3.1 Computational bathymetry of the Guadiana Estuary if the coastline is maintained on a mesh of 1400 x 350 cells with a space step of 30 m (Mills et al., 2019).....16
Figure 3.2 Computational bathymetry of the Guadiana Estuary, allowing flooding (1400 x 350 cells with a space step of 30 m). The grey area represents land. (Sampath et al., 2011).....17
Figure 3.3 Model setup for one simulation.....21
Figure 4.1 Location and nomenclature for points used in the time series along the main channel (left) and saltmarshes (right).....23
Figure 4.2 Velocity time series over two tidal cycles for a river discharge of 100 $m^3/s$ at neap tide in the upper estuary for the present bathymetry (left) and bathymetry that allows flooding (right).....24

Figure 4.3 Velocity time series over two tidal cycles for a river discharge of 100 $m^3/s$ at neap tide in the middle estuary for the present bathymetry (left) and bathymetry that allows flooding (right). ....24
Figure 4.4 Velocity time series over two tidal cycles for a river discharge of 100 $m^3/s$ at neap tide at the inlet into the marshes for the present bathymetry (left) and bathymetry that allows flooding (right). ....24
Figure 4.5 Velocity time series over two tidal cycles for a river discharge of 100 $m^3/s$ at neap tide in the westernmost region of Castro Marim for the present bathymetry (left) and bathymetry that allows flooding (right). ....25
Figure 4.6 Velocity time series over two tidal cycles for a river discharge of 100 $m^3/s$ at neap tide at the easternmost region of Castro Marim for the present bathymetry (left) and bathymetry that allows flooding (right). ....25
Figure 4.7 Velocity time series over two tidal cycles for a river discharge of 100 $m^3/s$ at neap tide downstream Esteiro da Carrasqueira for the present bathymetry (left) and bathymetry that allows flooding (right). ....25
Figure 4.8 Velocity time series over two tidal cycles for a river discharge of 100 $m^3/s$ at neap tide in the lower estuary for the present bathymetry (left) and bathymetry that allows flooding (right). ....26
Figure 4.9 Velocity time series over two tidal cycles for a river discharge of 10 $m^3/s$ at neap tide in the upper estuary for the present bathymetry (left) and bathymetry that allows flooding (right). ....28
Figure 4.10 Velocity time series over two tidal cycles for a river discharge of 10 $m^3/s$ at neap tide in the middle estuary for the present bathymetry (left) and bathymetry that allows flooding (right). ....28
Figure 4.11 Velocity time series over two tidal cycles for a river discharge of 10 $m^3/s$ at neap tide at the inlet into the marshes for the present bathymetry (left) and bathymetry that allows flooding (right). ....28
Figure 4.12 Velocity time series over two tidal cycles for a river discharge of 10 $m^3/s$ at neap tide in the westernmost region of Castro Marim for the present bathymetry (left) and bathymetry that allows flooding (right). ....29
Figure 4.13 Velocity time series over two tidal cycles for a river discharge of 10 $m^3/s$ at neap tide in the marsh area for the present bathymetry (left) and bathymetry that allows flooding (right). ....29

Figure 4.14 Velocity time series over two tidal cycles for a river discharge of 10 $m^3/s$ at neap tide downstream Esteiro da Carrasqueira for the present bathymetry (left) and bathymetry that allows flooding (right). .....29
Figure 4.15 Velocity time series over two tidal cycles for a river discharge of 10 $m^3/s$ at neap tide in the lower estuary for the present bathymetry (left) and bathymetry that allows flooding (right). .....30
Figure 4.16 Velocity time series over two tidal cycles for a river discharge of 100 $m^3/s$ at spring tide in the upper estuary for the present bathymetry (left) and bathymetry that allows flooding (right). .....31
Figure 4.17 Velocity time series over two tidal cycles for a river discharge of 100 $m^3/s$ at spring tide in the middle estuary for the present bathymetry (left) and bathymetry that allows flooding (right). .....32
Figure 4.18 Velocity time series over two tidal cycles for a river discharge of 100 $m^3/s$ at spring tide at the inlet into the marshes for the present bathymetry (left) and bathymetry that allows flooding (right).....32
Figure 4.19 Velocity time series over two tidal cycles for a river discharge of 100 $m^3/s$ at neap tide in the marsh area at the westernmost region of Castro Marim for the present bathymetry (left) and bathymetry that allows flooding (right). .....32
Figure 4.20 Velocity time series over two tidal cycles for a river discharge of 100 $m^3/s$ at spring tide in the easternmost area of Castro Marim for the present bathymetry (left) and bathymetry that allows flooding (right). .....33
Figure 4.21 Velocity time series over two tidal cycles for a river discharge of 100 $m^3/s$ at spring tide downstream Esteiro da Carrasqueira for the present bathymetry (left) and bathymetry that allows flooding (right). .....33
Figure 4.22 Velocity time series over two tidal cycles for a river discharge of 100 $m^3/s$ at spring tide in the lower estuary for the present bathymetry (left) and bathymetry that allows flooding (right). .....33
Figure 4.23 Velocity time series over two tidal cycles for a river discharge of 10 $m^3/s$ at spring tide in the upper estuary for the present bathymetry (left) and bathymetry allowing flooding (right). .....35
Figure 4.24 Velocity time series over two tidal cycles for a river discharge of 10 $m^3/s$ at spring tide in the middle estuary for the present bathymetry (left) and bathymetry allowing flooding (right). .....36

Figure 4.25 Velocity time series over two tidal cycles for a river discharge of 10 $m^3/s$ at spring tide in the inlet into the marshes for the present bathymetry (left) and bathymetry allowing flooding (right).....36
Figure 4.26 Velocity time series over two tidal cycles for a river discharge of 10 $m^3/s$ at spring tide in the westernmost region of Castro Marim for the present bathymetry (left) and bathymetry allowing flooding (right).....36
Figure 4.27 Velocity time series over two tidal cycles for a river discharge of 10 $m^3/s$ at spring tide in the marsh area for the present bathymetry (left) and bathymetry allowing flooding (right). .....37
Figure 4.28 Velocity time series over two tidal cycles for a river discharge of 10 $m^3/s$ at spring tide downstream Esteiro da Carrasqueira for the present bathymetry (left) and bathymetry that allows flooding (right). .....37
Figure 4.29 Velocity time series over two tidal cycles for a river discharge of 10 $m^3/s$ at spring tide in the lower estuary for the present bathymetry (left) and bathymetry allowing flooding (right). .....37
Figure 4.30 Salinity time series over two tidal cycles for a river discharge of 100 $m^3/s$ at neap tide in the upper estuary for the present bathymetry (left) and bathymetry allowing flooding (right). .....43
Figure 4.31 Salinity time series over two tidal cycles for a river discharge of 100 $m^3/s$ at neap tide in the middle estuary for the present bathymetry (left) and bathymetry allowing flooding (right). .....43
Figure 4.32 Salinity time series over two tidal cycles for a river discharge of 100 $m^3/s$ at neap tide at the inlet into the marshes for the present bathymetry (left) and bathymetry allowing flooding (right).....44
Figure 4.33 Salinity time series over two tidal cycles for a river discharge of 100 $m^3/s$ at neap tide at the westernmost region of Castro Marim for the present bathymetry (left) and bathymetry allowing flooding (right).....44
Figure 4.34 Salinity time series over two tidal cycles for a river discharge of 100 $m^3/s$ at neap tide in the easternmost region of Castro Marim for the present bathymetry (left) and bathymetry allowing flooding (right).....44
Figure 4.35 Salinity time series over two tidal cycles for a river discharge of 100 $m^3/s$ at neap tide downstream Esteiro da Carrasqueira for the present bathymetry (left) and bathymetry that allows flooding (right). .....44

Figure 4.36 Salinity time series over two tidal cycles for a river discharge of 100 $m^3/s$ at neap tide in the lower estuary for the present bathymetry (left) and bathymetry allowing flooding (right). .....45
Figure 4.37 Salinity time series over two tidal cycles for a river discharge of 10 $m^3/s$ at neap tide in the upper estuary for the present bathymetry (left) and bathymetry allowing flooding (right). .....47
Figure 4.38 Salinity time series over two tidal cycles for a river discharge of 10 $m^3/s$ at neap tide in the middle estuary for the present bathymetry (left) and bathymetry allowing flooding (right). .....47
Figure 4.39 Salinity time series over two tidal cycles for a river discharge of 10 $m^3/s$ at neap tide at the inlet into the marshes for the present bathymetry (left) and bathymetry allowing flooding (right).....47
Figure 4.40 Salinity time series over two tidal cycles for a river discharge of 10 $m^3/s$ at neap tide at the westernmost region of Castro Marim for the present bathymetry (left) and bathymetry allowing flooding (right).....48
Figure 4.41 Salinity time series over two tidal cycles for a river discharge of 10 $m^3/s$ at neap tide in the easternmost region of Castro Marim for the present bathymetry (left) and bathymetry allowing flooding (right).....48
Figure 4.42 Salinity time series over two tidal cycles for a river discharge of 10 $m^3/s$ at neap tide downstream Esteiro da Carrasqueira for the present bathymetry (left) and bathymetry that allows flooding (right). .....48
Figure 4.43 Salinity time series over two tidal cycles for a river discharge of 10 $m^3/s$ at neap tide in the lower estuary for the present bathymetry (left) and bathymetry allowing flooding (right). .....49
Figure 4.44 Salinity time series over two tidal cycles for a river discharge of 100 $m^3/s$ at spring tide in the upper estuary for the present bathymetry (left) and bathymetry allowing flooding (right). .....50
Figure 4.45 Salinity time series over two tidal cycles for a river discharge of 100 $m^3/s$ at spring tide in the middle estuary for the present bathymetry (left) and bathymetry allowing flooding (right). .....51
Figure 4.46 Salinity time series over two tidal cycles for a river discharge of 100 $m^3/s$ at spring tide at the inlet into the marshes for the present bathymetry (left) and bathymetry allowing flooding (right).....51

Figure 4.47 Salinity time series over two tidal cycles for a river discharge of 100 $m^3/s$ at spring tide at the westernmost region of Castro Marim for the present bathymetry (left) and bathymetry allowing flooding (right).....51
Figure 4.48 Salinity time series over two tidal cycles for a river discharge of 100 $m^3/s$ at spring tide in the marsh area for the present bathymetry (left) and bathymetry allowing flooding (right). .....51
Figure 4.49 Salinity time series over two tidal cycles for a river discharge of 100 $m^3/s$ at spring tide downstream Esteiro da Carrasqueira for the present bathymetry (left) and bathymetry that allows flooding (right). .....52
Figure 4.50 Salinity time series over two tidal cycles for a river discharge of 100 $m^3/s$ at spring tide in the lower estuary for the present bathymetry (left) and bathymetry allowing flooding (right). .....52
Figure 4.51 Salinity time series over two tidal cycles for a river discharge of 10 $m^3/s$ at spring tide in the upper estuary for the present bathymetry (left) and bathymetry allowing flooding (right). .....54
Figure 4.52 Salinity time series over two tidal cycles for a river discharge of 10 $m^3/s$ at spring tide in the middle estuary for the present bathymetry (left) and bathymetry allowing flooding (right). .....54
Figure 4.53 Salinity time series over two tidal cycles for a river discharge of 10 $m^3/s$ at spring tide at the inlet into the marshes for the present bathymetry (left) and bathymetry allowing flooding (right).....54
Figure 4.54 Salinity time series over two tidal cycles for a river discharge of 10 $m^3/s$ at spring tide at the westernmost region of Castro Marim for the present bathymetry (left) and bathymetry allowing flooding (right).....55
Figure 4.55 Salinity time series over two tidal cycles for a river discharge of 10 $m^3/s$ at spring tide in the marsh area for the present bathymetry (left) and bathymetry allowing flooding (right). .....55
Figure 4.56 Salinity time series over two tidal cycles for a river discharge of 10 $m^3/s$ at spring tide downstream Esteiro da Carrasqueira for the present bathymetry (left) and bathymetry that allows flooding (right). .....55
Figure 4.57 Salinity time series over two tidal cycles for a river discharge of 10 $m^3/s$ at spring tide in the lower estuary for the present bathymetry (left) and bathymetry allowing flooding (right). .....56

Figure 4.58 Salinity distribution maps in high water conditions for a river discharge of 100 $m^3/s$ for the present year, 2040, 2070 and 2100 at neap tide over the present bathymetry. ....58
Figure 4.59 Salinity distribution maps in low water conditions for a river discharge of 100 $m^3/s$ for the present year, 2040, 2070 and 2100 at neap tide over the present bathymetry.....59
Figure 4.60 Salinity distribution maps in high water conditions for a river discharge of 100 $m^3/s$ for the present year, 2040, 2070 and 2100 at neap tide over the bathymetry allowing flooding. .....59
Figure 4.61 Salinity distribution maps in low water conditions for a river discharge of 100 $m^3/s$ for the present year, 2040, 2070 and 2100 at neap tide over the bathymetry allowing flooding. .....60
Figure 4.62 Salinity distribution maps in high water conditions for a river discharge of 10 $m^3/s$ for the present year, 2040, 2070 and 2100 at neap tide over the present bathymetry.....61
Figure 4.63 Salinity distribution maps in low water conditions for a river discharge of 10 $m^3/s$ for the present year, 2040, 2070 and 2100 at neap tide over the present bathymetry.....61
Figure 4.64 Salinity distribution maps in high water conditions for a river discharge of 10 $m^3/s$ for the present year, 2040, 2070 and 2100 at neap tide over the bathymetry allowing flooding. .....62
Figure 4.65 Salinity distribution maps in low water conditions for a river discharge of 10 $m^3/s$ for the present year, 2040, 2070 and 2100 at neap tide over the bathymetry allowing flooding. .....62
Figure 4.66 Salinity distribution maps in high water conditions for a river discharge of 100 $m^3/s$ for the present year, 2040, 2070 and 2100 at spring tide over the present bathymetry. ..63
Figure 4.67 Salinity distribution maps in low water conditions for a river discharge of 100 $m^3/s$ for the present year, 2040, 2070 and 2100 at spring tide over the present bathymetry. .....63
Figure 4.68 Salinity distribution maps in high water conditions for a river discharge of 100 $m^3/s$ for the present year, 2040, 2070 and 2100 at spring tide over the bathymetry allowing flooding. .....64
Figure 4.69 Salinity distribution maps in low water conditions for a river discharge of 100 $m^3/s$ for the present year, 2040, 2070 and 2100 at spring tide over the bathymetry allowing flooding. .....64
Figure 4.70 Salinity distribution maps in high water conditions for a river discharge of 10 $m^3/s$ for the present year, 2040, 2070 and 2100 at spring tide over the present bathymetry. .....65
Figure 4.71 Salinity distribution maps in low water conditions for a river discharge of 10 $m^3/s$ for the present year, 2040, 2070 and 2100 at spring tide over the present bathymetry. .....65

Figure 4.72 Salinity distribution maps in high water conditions for a river discharge of 10 $m^3/s$ for the present year, 2040, 2070 and 2100 at spring tide over the bathymetry allowing flooding. .....66
Figure 4.73 Salinity distribution maps in low water conditions for a river discharge of 10 $m^3/s$ for the present year, 2040, 2070 and 2100 at spring tide over the bathymetry allowing flooding. .....66
Figure 4.74 Histogram showing classes of flooding as a function of submersion time for one tidal cycle for the various scenarios of sea level rise at neap tide with a high freshwater flow. .....68
Figure 4.75 Histogram showing classes of flooding as a function of submersion time for one tidal cycle for the various scenarios of sea level rise at neap tide with a low freshwater flow. .....69
Figure 4.76 Histogram showing classes of flooding as a function of submersion time for one tidal cycle for the various scenarios of sea level rise at spring tide with a high freshwater flow. .....70
Figure 4.77 Histogram showing classes of flooding as a function of submersion time for one tidal cycle for the various scenarios of sea level rise at spring tide with a low freshwater flow. .....71
Figure 4.78 Flood distribution maps for a high freshwater discharge during neap tide for the various scenarios of sea level rise. .....73
Figure 4.79 Flood distribution maps for a low freshwater discharge during neap tide for the various scenarios of sea level rise. .....74
Figure 4.80 Flood distribution maps for a high freshwater discharge during spring tide for the various scenarios of sea level rise. .....75
Figure 4.81 Flood distribution maps for a low freshwater discharge during spring tide for the various scenarios of sea level rise. .....76
Figure 5.1 Velocity direction and salinity distribution near the inlet into the marshes for a high freshwater flow at neap tide over the present bathymetry for the various scenarios of sea level rise at a time instant of one hour before high tide. .....78
Figure 5.2 Velocity direction and salinity distribution near the inlet into the marshes for a high freshwater flow at neap tide over the bathymetry allowing flooding for the various scenarios of sea level rise at a time instant of one hour before high tide. .....80

Figure 5.3 Velocity direction and salinity distribution for a low freshwater flow at neap tide over the present bathymetry for the various scenarios of sea level rise at a time instant of one hour before high tide. ..... 82
Figure 5.4 Velocity direction and salinity distribution at all areas affected by the salinity front for a low freshwater flow at neap tide over the bathymetry allowing flooding one hour before high tide. ..... 83
Figure 5.5 Velocity direction and salinity distribution at all areas affected by the salinity front for a high freshwater flow at spring tide over the present bathymetry one hour before high tide. ..... 85
Figure 5.6 Velocity direction and salinity distribution at all areas affected by the salinity front for a high freshwater flow at spring tide over the bathymetry allowing flooding. ..... 86
Figure 5.7 Velocity direction and salinity distribution at all areas affected by the salinity front for a high freshwater flow at spring tide over the bathymetry allowing flooding. ..... 88
Figure 5.8 Velocity direction and salinity distribution at all areas affected by the salinity front for a high freshwater flow at spring tide over the bathymetry allowing flooding. ..... 90
Figure 5.9 Area of inundation in 2100 near the Esuri housing development at spring tide for a high freshwater flow. ..... 92
Figure 5.10 Land submerged at Castro Marim during one tidal cycle at neap tide (left) and spring tide (right) in the year 2100. ..... 93
Figure A.1 Time series of water elevation over two tidal cycles for a river discharge of 100 $m^3/s$ at neap tide in the upper estuary for the present bathymetry (left) and bathymetry that allows flooding (right). ..... 100
Figure A.2 Time series of water elevation over two tidal cycles for a river discharge of 100 $m^3/s$ at neap tide in the upper estuary for the present bathymetry (left) and bathymetry that allows flooding (right). ..... 100
Figure A.3 Time series of water elevation over two tidal cycles for a river discharge of 100 $m^3/s$ at neap tide in the middle estuary for the present bathymetry (left) and bathymetry that allows flooding (right). ..... 100
Figure A.4 Time series of water elevation over two tidal cycles for a river discharge of 100 $m^3/s$ at neap tide in the middle estuary for the present bathymetry (left) and bathymetry that allows flooding (right). ..... 101
Figure A.5 Time series of water elevation over two tidal cycles for a river discharge of 100 $m^3/s$ at neap tide in the northernmost region of Castro Marim for the present bathymetry (left) and bathymetry that allows flooding (right). ..... 101

Figure A.6 Time series of water elevation over two tidal cycles for a river discharge of 100 $m^3/s$ at neap tide in the westernmost region of Esteiro da Leziria for the present bathymetry (left) and bathymetry that allows flooding (right). .....101
Figure A.7 Time series of water elevation over two tidal cycles for a river discharge of 100 $m^3/s$ at neap tide in the easternmost region of Castro Marim for the present bathymetry (left) and bathymetry that allows flooding (right). .....102
Figure A.8 Time series of water elevation over two tidal cycles for a river discharge of 100 $m^3/s$ at neap tide in the inlet into Castro Marim for the present bathymetry (left) and bathymetry that allows flooding (right). .....102
Figure A.9 Time series of water elevation over two tidal cycles for a river discharge of 100 $m^3/s$ at neap tide downstream Esteiro da Carrasqueira for the present bathymetry (left) and bathymetry that allows flooding (right). .....102
Figure A.10 Time series of water elevation over two tidal cycles for a river discharge of 100 $m^3/s$ at neap tide in the lower estuary for the present bathymetry (left) and bathymetry that allows flooding (right). .....103
Figure A.11 Time series of water elevation over two tidal cycles for a river discharge of 100 $m^3/s$ at neap tide in the westernmost region of Esteiro da Carrasqueira for the present bathymetry (left) and bathymetry that allows flooding (right). .....103
Figure A.12 Time series of water elevation over two tidal cycles for a river discharge of 10 $m^3/s$ at neap tide in the upper estuary for the present bathymetry (left) and bathymetry that allows flooding (right). .....103
Figure A.13 Time series of water elevation over two tidal cycles for a river discharge of 10 $m^3/s$ at neap tide in the upper estuary for the present bathymetry (left) and bathymetry that allows flooding (right). .....104
Figure A.14 Time series of water elevation over two tidal cycles for a river discharge of 10 $m^3/s$ at neap tide in the middle estuary for the present bathymetry (left) and bathymetry that allows flooding (right). .....104
Figure A.15 Time series of water elevation over two tidal cycles for a river discharge of 10 $m^3/s$ at neap tide in the middle estuary for the present bathymetry (left) and bathymetry that allows flooding (right). .....104
Figure A.16 Time series of water elevation over two tidal cycles for a river discharge of 10 $m^3/s$ at neap tide in the northernmost region of Castro Marim for the present bathymetry (left) and bathymetry that allows flooding (right). .....105

Figure A.17 Time series of water elevation over two tidal cycles for a river discharge of 10 $m^3/s$ at neap tide in the westernmost region of Esteiro da Leziria for the present bathymetry (left) and bathymetry that allows flooding (right). .....105
Figure A.18 Time series of water elevation over two tidal cycles for a river discharge of 10 $m^3/s$ at neap tide in the easternmost region of Castro Marim for the present bathymetry (left) and bathymetry that allows flooding (right). .....105
Figure A.19 Time series of water elevation over two tidal cycles for a river discharge of 10 $m^3/s$ at neap tide in the inlet into Castro Marim for the present bathymetry (left) and bathymetry that allows flooding (right). .....106
Figure A.20 Time series of water elevation over two tidal cycles for a river discharge of 10 $m^3/s$ at neap tide downstream Esteiro da Carrasqueira for the present bathymetry (left) and bathymetry that allows flooding (right). .....106
Figure A.21 Time series of water elevation over two tidal cycles for a river discharge of 10 $m^3/s$ at neap tide in the lower estuary for the present bathymetry (left) and bathymetry that allows flooding (right). .....106
Figure A.22 Time series of water elevation over two tidal cycles for a river discharge of 10 $m^3/s$ at neap tide in the westernmost region of Esteiro da Carrasqueira for the present bathymetry (left) and bathymetry that allows flooding (right). .....106
Figure A.23 Time series of water elevation over two tidal cycles for a river discharge of 100 $m^3/s$ at spring tide in the upper estuary for the present bathymetry (left) and bathymetry that allows flooding (right). .....107
Figure A.24 Time series of water elevation over two tidal cycles for a river discharge of 100 $m^3/s$ at spring tide in the upper estuary for the present bathymetry (left) and bathymetry that allows flooding (right). .....107
Figure A.25 Time series of water elevation over two tidal cycles for a river discharge of 100 $m^3/s$ at spring tide in the middle estuary for the present bathymetry (left) and bathymetry that allows flooding (right). .....107
Figure A.26 Time series of water elevation over two tidal cycles for a river discharge of 100 $m^3/s$ at spring tide in the middle estuary for the present bathymetry (left) and bathymetry that allows flooding (right). .....108
Figure A.27 Time series of water elevation over two tidal cycles for a river discharge of 100 $m^3/s$ at spring tide in the northernmost region of Castro Marim for the present bathymetry (left) and bathymetry that allows flooding (right). .....108

Figure A.28 Time series of water elevation over two tidal cycles for a river discharge of 100 $m^3/s$ at spring tide in the westernmost region of Esteiro da Leziria for the present bathymetry (left) and bathymetry that allows flooding (right). .....108
Figure A.29 Time series of water elevation over two tidal cycles for a river discharge of 100 $m^3/s$ at spring tide in the easternmost region of Castro Marim for the present bathymetry (left) and bathymetry that allows flooding (right). .....108
Figure A.30 Time series of water elevation over two tidal cycles for a river discharge of 100 $m^3/s$ at spring tide at the inlet into Castro Marim for the present bathymetry (left) and bathymetry that allows flooding (right). .....109
Figure A.31 Time series of water elevation over two tidal cycles for a river discharge of 100 $m^3/s$ at spring tide downstream Esteiro da Carrasqueira for the present bathymetry (left) and bathymetry that allows flooding (right). .....109
Figure A.32 Time series of water elevation over two tidal cycles for a river discharge of 100 $m^3/s$ at spring tide in the lower estuary for the present bathymetry (left) and bathymetry that allows flooding (right). .....109
Figure A.33 Time series of water elevation over two tidal cycles for a river discharge of 100 $m^3/s$ at spring tide in the westernmost region of Esteiro da Carresqueira for the present bathymetry (left) and bathymetry that allows flooding (right). .....109
Figure A.34 Time series of water elevation over two tidal cycles for a river discharge of 10 $m^3/s$ at spring tide in the upper estuary for the present bathymetry (left) and bathymetry that allows flooding (right). .....110
Figure A.35 Time series of water elevation over two tidal cycles for a river discharge of 10 $m^3/s$ at spring tide in the upper estuary for the present bathymetry (left) and bathymetry that allows flooding (right). .....110
Figure A.36 Time series of water elevation over two tidal cycles for a river discharge of 10 $m^3/s$ at spring tide in the middle estuary for the present bathymetry (left) and bathymetry that allows flooding (right). .....110
Figure A.37 Time series of water elevation over two tidal cycles for a river discharge of 10 $m^3/s$ at spring tide in the middle estuary for the present bathymetry (left) and bathymetry that allows flooding (right). .....110
Figure A.38 Time series of water elevation over two tidal cycles for a river discharge of 10 $m^3/s$ at spring tide in the northernmost region of Castro Marim for the present bathymetry (left) and bathymetry that allows flooding (right). .....111

Figure A.39 Time series of water elevation over two tidal cycles for a river discharge of 10 $m^3/s$ at spring tide in the westernmost region of Esteiro da Leziria for the present bathymetry (left) and bathymetry that allows flooding (right). .....111
Figure A.40 Time series of water elevation over two tidal cycles for a river discharge of 10 $m^3/s$ at spring tide in the easternmost region of Castro Marim for the present bathymetry (left) and bathymetry that allows flooding (right). .....111
Figure A.41 Time series of water elevation over two tidal cycles for a river discharge of 10 $m^3/s$ at spring tide at the inlet into Castro Marim for the present bathymetry (left) and bathymetry that allows flooding (right). .....111
Figure A.42 Time series of water elevation over two tidal cycles for a river discharge of 10 $m^3/s$ at spring tide downstream Esteiro da Carrasqueira for the present bathymetry (left) and bathymetry that allows flooding (right). .....112
Figure A.43 Time series of water elevation over two tidal cycles for a river discharge of 10 $m^3/s$ at spring tide in the lower estuary for the present bathymetry (left) and bathymetry that allows flooding (right). .....112
Figure A.44 Time series of water elevation over two tidal cycles for a river discharge of 10 $m^3/s$ at spring tide in the westernmost region of Esteiro da Carrasqueira the present bathymetry (left) and bathymetry that allows flooding (right). .....112
Figure B.1 Velocity time series over two tidal cycles for a river discharge of 100 $m^3/s$ at neap tide in the upper estuary for the present bathymetry (left) and bathymetry that allows flooding (right). .....113
Figure B.2 Velocity time series over two tidal cycles for a river discharge of 100 $m^3/s$ at neap tide in the middle estuary for the present bathymetry (left) and bathymetry that allows flooding (right). .....113
Figure B.3 Velocity time series over two tidal cycles for a river discharge of 100 $m^3/s$ at neap tide in the northernmost region of Castro Marim for the present bathymetry (left) and bathymetry that allows flooding (right). .....113
Figure B.4 Velocity time series over two tidal cycles for a river discharge of 100 $m^3/s$ at neap tide in the westernmost region of Esteiro da Carrasqueira for the present bathymetry (left) and bathymetry that allows flooding (right). .....114
Figure B.5 Velocity time series over two tidal cycles for a river discharge of 10 $m^3/s$ at neap tide in the upper estuary for the present bathymetry (left) and bathymetry that allows flooding (right). .....114

Figure B.6 Velocity time series over two tidal cycles for a river discharge of 10 $m^3/s$ at neap tide in the middle estuary for the present bathymetry (left) and bathymetry that allows flooding (right). .....114
Figure B.7 Velocity time series over two tidal cycles for a river discharge of 10 $m^3/s$ at neap tide in the northernmost region of Castro Marim for the present bathymetry (left) and bathymetry that allows flooding (right). .....114
Figure B.8 Velocity time series over two tidal cycles for a river discharge of 10 $m^3/s$ at neap tide in the westernmost region of Esteiro da Carrasqueira for the present bathymetry (left) and bathymetry that allows flooding (right). .....115
Figure B.9 Velocity time series over two tidal cycles for a river discharge of 100 $m^3/s$ at spring tide in the upper estuary for the present bathymetry (left) and bathymetry that allows flooding (right). .....115
Figure B.10 Velocity time series over two tidal cycles for a river discharge of 100 $m^3/s$ at spring tide in the middle estuary for the present bathymetry (left) and bathymetry that allows flooding (right). .....115
Figure B.11 Velocity time series over two tidal cycles for a river discharge of 100 $m^3/s$ at spring tide in the northernmost region of Castro Marim for the present bathymetry (left) and bathymetry that allows flooding (right). .....115
Figure B.12 Velocity time series over two tidal cycles for a river discharge of 100 $m^3/s$ at spring tide in the westernmost region of Esteiro da Carrasqueira for the present bathymetry (left) and bathymetry that allows flooding (right). .....116
Figure B.13 Velocity time series over two tidal cycles for a river discharge of 10 $m^3/s$ at spring tide in the upper estuary for the present bathymetry (left) and bathymetry that allows flooding (right). .....116
Figure B.14 Velocity time series over two tidal cycles for a river discharge of 10 $m^3/s$ at spring tide in the middle estuary for the present bathymetry (left) and bathymetry that allows flooding (right). .....116
Figure B.15 Velocity time series over two tidal cycles for a river discharge of 10 $m^3/s$ at spring tide in the northernmost region of Castro Marim for the present bathymetry (left) and bathymetry that allows flooding (right). .....116
Figure B.16 Velocity time series over two tidal cycles for a river discharge of 10 $m^3/s$ at spring tide in the westernmost region of Esteiro da Carrasqueira for the present bathymetry (left) and bathymetry that allows flooding (right). .....117

Figure C.1 Salinity time series over two tidal cycles for a river discharge of 100 $m^3/s$ at neap tide in the upper estuary for the present bathymetry (left) and bathymetry that allows flooding (right). ..... 117
Figure C.2 Salinity time series over two tidal cycles for a river discharge of 100 $m^3/s$ at neap tide in the middle estuary for the present bathymetry (left) and bathymetry that allows flooding (right). ..... 117
Figure C.3 Salinity time series over two tidal cycles for a river discharge of 100 $m^3/s$ at neap tide in the northernmost region of Castro Marim for the present bathymetry (left) and bathymetry that allows flooding (right). ..... 118
Figure C.4 Salinity time series over two tidal cycles for a river discharge of 100 $m^3/s$ at neap tide in the westernmost region of Esteiro da Carrasqueira for the present bathymetry (left) and bathymetry that allows flooding (right). ..... 118
Figure C.5 Salinity time series over two tidal cycles for a river discharge of 10 $m^3/s$ at neap tide in the upper estuary for the present bathymetry (left) and bathymetry that allows flooding (right). ..... 118
Figure C.6 Salinity time series over two tidal cycles for a river discharge of 10 $m^3/s$ at neap tide in the middle estuary for the present bathymetry (left) and bathymetry that allows flooding (right). ..... 118
Figure C.7 Velocity time series over two tidal cycles for a river discharge of 10 $m^3/s$ at neap tide in the northernmost region of Castro Marim for the present bathymetry (left) and bathymetry that allows flooding (right). ..... 119
Figure C.8 Salinity time series over two tidal cycles for a river discharge of 10 $m^3/s$ at neap tide in the westernmost region of Esteiro da Carrasqueira for the present bathymetry (left) and bathymetry that allows flooding (right). ..... 119
Figure C.9 Salinity time series over two tidal cycles for a river discharge of 100 $m^3/s$ at spring tide in the upper estuary for the present bathymetry (left) and bathymetry that allows flooding (right). ..... 119
Figure C.10 Salinity time series over two tidal cycles for a river discharge of 100 $m^3/s$ at spring tide in the middle estuary for the present bathymetry (left) and bathymetry that allows flooding (right). ..... 119
Figure C.11 Salinity time series over two tidal cycles for a river discharge of 100 $m^3/s$ at spring tide in the northernmost region of Castro Marim for the present bathymetry (left) and bathymetry that allows flooding (right). ..... 120

Figure C.12 Salinity time series over two tidal cycles for a river discharge of 100 $m^3/s$ at spring tide in the westernmost region of Esteiro da Carrasqueira for the present bathymetry (left) and bathymetry that allows flooding (right). ..... 120
Figure C.13 Salinity time series over two tidal cycles for a river discharge of 10 $m^3/s$ at spring tide in the upper estuary for the present bathymetry (left) and bathymetry that allows flooding (right). ..... 120
Figure C.14 Salinity time series over two tidal cycles for a river discharge of 100 $m^3/s$ at spring tide in the middle estuary for the present bathymetry (left) and bathymetry that allows flooding (right). ..... 120
Figure C.15 Salinity time series over two tidal cycles for a river discharge of 10 $m^3/s$ at spring tide in the northernmost region of Castro Marim for the present bathymetry (left) and bathymetry that allows flooding (right). ..... 121
Figure C.16 Salinity time series over two tidal cycles for a river discharge of 10 $m^3/s$ at spring tide in the westernmost region of Esteiro da Carrasqueira for the present bathymetry (left) and bathymetry that allows flooding (right). ..... 121

## List of Tables

Table 3.1 Predictions for the rise in global mean sea level in meter based on sea level rise from the years 1986-2005 for RCP 4.5 and RCP 8.5 (Adapted from the 5th IPCC Report, Church et al. (2013) along with scenarios used by Mills et al. (2019) ..... 18
Table 3.2 Bathymetry Scenarios ..... 19
Table 3.3 Sea Level Rise Scenarios ..... 20
Table 3.4 Freshwater Flow Scenarios ..... 20
Table 3.5 Tidal Scenarios ..... 20
Table 3.6 Histogram chart computed in Python to calculate land inundation for each class of flooding. ..... 22
Table 4.1 Changes in velocity modulus for a discharge of 100 $m^3/s$ at neap tide over the present bathymetry. ..... 26
Table 4.2 Changes in velocity modulus for a discharge of 100 $m^3/s$ at neap tide over the bathymetry allowing flooding. ..... 27
Table 4.3 Changes in velocity modulus for a discharge of 10 $m^3/s$ at neap tide over the present bathymetry. ..... 30

Table 4.4 Changes in velocity modulus for a discharge of 10 $m^3/s$ at neap tide over the bathymetry allowing flooding. ..... 31
Table 4.5 Changes in velocity modulus for a discharge of 100 $m^3/s$ at spring tide over the present bathymetry. ..... 34
Table 4.6 Changes in velocity modulus for a discharge of 100 $m^3/s$ at spring tide over the bathymetry allowing flooding. ..... 35
Table 4.7 Changes in velocity modulus for a discharge of 10 $m^3/s$ at spring tide over the present bathymetry. ..... 38
Table 4.8 Changes in velocity modulus for a discharge of 10 $m^3/s$ at spring tide over the bathymetry allowing flooding. ..... 38
Table 4.9 Change in water elevation for a freshwater discharge of 100 $m^3/s$ at neap tide over the present bathymetry. ..... 39
Table 4.10 Change in water elevation for a freshwater discharge of 100 $m^3/s$ at neap tide over the bathymetry allowing flooding. ..... 40
Table 4.11 Change in water elevation for a freshwater discharge of 10 $m^3/s$ at neap tide over the present bathymetry. ..... 40
Table 4.12 Change in water elevation for a freshwater discharge of 10 $m^3/s$ at neap tide over the bathymetry allowing flooding. ..... 40
Table 4.13 Change in water elevation for a freshwater discharge of 100 $m^3/s$ at spring tide over the present bathymetry. ..... 41
Table 4.14 Change in water elevation for a freshwater discharge of 100 $m^3/s$ at spring tide over the bathymetry allowing flooding. ..... 41
Table 4.15 Change in water elevation for a freshwater discharge of 10 $m^3/s$ at spring tide over the present bathymetry. ..... 42
Table 4.16 Change in water elevation for a freshwater discharge of 10 $m^3/s$ at spring tide over the bathymetry allowing flooding. ..... 42
Table 4.17 Change in salinity for a discharge of 100 $m^3/s$ at neap tide over the present bathymetry. ..... 45
Table 4.18 Changes in salinity for a discharge of 100 $m^3/s$ at neap tide over bathymetry allowing flooding. ..... 46
Table 4.19 Changes in salinity for a discharge of 10 $m^3/s$ at neap tide over the present bathymetry ..... 49
Table 4.20 Changes in salinity for a discharge of 10 $m^3/s$ at neap tide over the bathymetry allowing flooding. ..... 50

Table 4.21 Changes in salinity for a discharge of 100 $m^3$/s at spring tide over the present bathymetry. ..... 53
Table 4.22 Changes in salinity for a discharge of 100 $m^3$/s at spring tide over the bathymetry allowing flooding. ..... 53
Table 4.23 Changes in salinity for a discharge of 10 $m^3$/s at spring tide over the present bathymetry. ..... 56
Table 4.24 Changes in salinity for a discharge of 10 m3/s at spring tide over the bathymetry allowing flooding. ..... 57
Table 4.25 Areas of inundation over one tidal cycle at neap tide with a high freshwater flow. ..... 68
Table 4.26 Areas of inundation over one tidal cycle at neap tide with a low freshwater flow. ..... 69
Table 4.27 Areas of inundation over one tidal cycle at spring tide with a high freshwater flow. ..... 70
Table 4.28 Areas of inundation over one tidal cycle at spring tide with a low freshwater flow. ..... 71

# 1 Introduction

## 1.1 Motivation

Global mean sea level is currently rising at a rate of roughly 3.2 millimeters per year (Church et al., 2013). The most recent report from the Intergovernmental Panel on Climate Change (IPCC) has concluded that the rate of global mean sea level rise has been increasing over the last two centuries and continues to accelerate. With over 10% of the world's population living within 10 meters elevation of the present sea level (Carrasco et al., 2016), this should be a large concern. Even more concerning is the fact that as the rate of sea level rise is accelerating, the human population is expanding more rapidly than global trends (Nicholls et al., 2011). As the number of people inhabiting coastal areas increases, there will be detrimental effects on both society and the economy. More specifically, sea level rise will result in land submergence, an increase in flooding area, an increase in erosion, an increase in salinity and changes in ecosystems (Nicholls et al., 2011).

The IPCC has released several reports assessing the impacts of climate change and future projections of climate change. Models of sea level rise projected by the IPCC are typically only based on thermal expansion (Nicholls et al., 2011). The 4$^{th}$ assessment report (AR4) showed a rate of sea level rise of 1 mm/year since 1980 based on tide gauge data from Church and White (2011). A study based on satellite data by Rahmstorf et al. (2012) found the AR4 to be biased low as it underestimated sea level projections by about 60%. The AR4 did not account for components of sea level rise not related to climate change such as water storage in artificial reservoirs on land and extraction of fossil groundwater for irrigation purposes (Rahmstorf et al., 2012). Furthermore, projections made by the IPCC in the AR4 assumed that Antarctica would gain enough mass in the future to compensate for the mass lost in Greenland, when in fact the ice sheets in both Greenland and Antarctica are increasingly losing mass (Rahmstorf et al., 2012). Spring and summer sea-ice extent has decreased by approximately 10 – 15% since the 1950s based on observations in the northern hemisphere (McLean et al., 2001). Furthermore, sea ice in the arctic has thinned out significantly, which underestimates the decline in ice volume (McLean et al., 2001). Information from the IPCC reports are used by policymakers all around the world when it comes to making decisions about adaptation strategies for changes in sea level. It is therefore crucial to validate models before relying on them as accurate measures of future sea level rise projections.

The latest IPCC 5th assessment report (AR5) published in 2014 has not received much criticism compared to the AR4 and has predicted a global sea level rise of 52 to 98 centimeters by the end of this century based on a model scenario of very high greenhouse gas emissions (Church et al., 2013). A compilation of paleo sea level data, tide gauge data for the present sea level and likely sea level projections of global mean sea level rise as assessed by the IPCC AR5 can be seen in Figure 1.1. Other studies predict that the rise in sea level will be close to 1 meter by 2100 (Rahmstorf et al., 2012). While studies and reports in the literature may not agree with the precise projected rate of sea level rise, they are all in agreement that the global mean sea level is rising and will rise close to 1 meter by the end of 2100. It is virtually certain that sea level rise will continue beyond the year 2500 unless global temperature declines (Wong et al., 2014). As a rising sea level is to be expected, the impacts and consequences should be assessed.

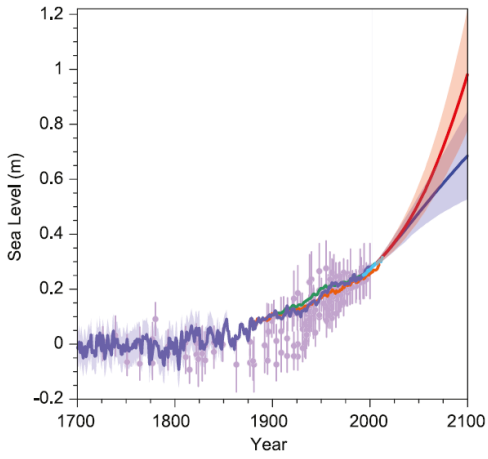


*Figure 1.1* Paleo sea level data, tide gauge data and future predictions for very high greenhouse gas emissions (red) and very low greenhouse gas emissions (blue) obtained from the IPCC AR5 (Church et al., 2013).

Of relevance to the present study is the impact of sea level rise on estuaries, where rivers meet sea and freshwater mixes with saltwater. It is crucial to understand the impacts of climate change on these transitional environments and the underlying processes that will occur as a result of climate change. An increase in sea temperature and rise in sea level will impact hydrological cycles and change the freshwater flow into estuaries (Chua & Xu, 2014). The amount of seawater in an estuary will increase, which will further increase the salinity. A long-term increase in salinity will cause irreversible damage to estuarine ecosystems (Hilton et al., 2008). The projected sea level rise will potentially negatively impact marine organisms over the next few decades (McLean et al., 2001). A negative impact on marine life will further impact the economic activities that rely on the abundance and quality of marine organisms. Many studies have evaluated the biological and physical impacts of sea level rise on estuaries. Not yet fully explored in the literature is a quantifiable relationship between sea level rise and salinity. It is therefore the aim of this work to evaluate how sea level rise will directly impact

the hydrodynamics and water properties, namely salinity in the Guadiana Estuary, an estuary in the Iberian Peninsula between Portugal and Spain.

## 1.2 Objectives

The objective of this dissertation is to analyze the effects of sea level rise and variations in freshwater discharge in the Guadiana Estuary due to climate change. The study builds upon the methodologies and results of an already developed and validated hydrodynamic and transport model, based on the MOHID modeling system (Mills et al., 2019) to provide a more quantitative analysis of how the Guadiana Estuary will evolve throughout the present century. The model simulates various scenarios of sea level rise and freshwater discharge along different bathymetries at both spring and neap tide to evaluate (1) changes in salinity in the estuary and (2) areas of inundation. Impacts on habitat and traditional socioeconomic activities in the region will also be considered. The results will provide vulnerability indices for coastal managers to examine the extent of the impacts of sea level rise in the Guadiana Estuary.

## 1.3 Dissertation Structure

This dissertation is structured as follows: the next chapter: Literature Review & State of the Art begins with a review of previous works published on the hydrodynamics of the Guadiana Estuary as well as how estuarine dynamics change due to climate change. The third chapter includes the methods used to set up and run the simulations for the model. The fourth chapter contains the results of the model as well as a summary of each major result. The fifth chapter discusses the major findings and compares them with previous published work. The final chapter concludes all the major findings of this work. Appendix A includes time series results of water elevation. Appendix B contains the remaining time series results of velocity that are not included in the main text. Appendix C contains the remaining time series results of salinity that are not included in the main text. Appendix D consists of the peer-reviewed paper by Mills et al. (2019) that was published for the International Conference on Computational Science (ICCS) in June 2019 after the start of this dissertation.

# 2 Literature Review & State of the Art

## 2.1 What Is Sea Level Change?

### 2.1.1 Definition of Sea Level

Sea level can be defined as the height of the ocean surface at any location on Earth (Church et al., 2013). Sea level measured with respect to the surface of the solid Earth is known as relative sea level (RSL), whereas sea level measured with respect to an ellipsoid is known as geocentric sea level. RSL is measured with tide gauges and has been estimated for longer time spans from geological records, whereas geocentric sea level is measured from satellite altimetry (Church et al., 2013). The focus of this study will be RSL, as it is more relevant in terms of coastal impacts on sea level change. The change in ocean water volume is calculated by integrating RSL change over the ocean area (Church et al., 2013). This change in volume currently has a positive linear trend with temperature (Church et al., 2013). However, projections of sea level rise and temperature on a century time scale are likely to be non-linear due to the climate system responding at different times to surface temperatures and the input of heat to the deep ocean and ice-sheet adjustment (Nicholls et al., 2011).

### 2.1.2 Global Sea Level Change

Sea level rise does not occur uniformly throughout the globe, so it is important to distinguish between global sea level change and regional sea level change. A change in global mean sea level is referred to as a eustatic change and is linked to the volume of the Earth ocean. On the other hand, a change in regional sea level is referred to as an isostatic change and is caused by local factors such as tectonic uplift moving coastal areas upwards (Rovere et al., 2016). The main components of Eustatic sea level rise are: (1) the amount of ice transferred between the continents and oceans during glacial cycles (Fleming et al., 1998); (2) thermal expansion due to warming temperatures of the oceans; (3) melting of continental ice (Brown et al., 2018). There is also a strong contribution of sea level rise form natural and human-induced land storage (Church et al., 2013). The largest increase in the storage of heat in the climate systems is in the ocean (Church et al., 2013). This poses a serious threat to sea level rise as sea level rise is a direct consequence of temperature increase. It takes time for the sea level to respond to changes in temperature, but when mass is added to the ocean all regions experience a sea level change within days (Church et al., 2013).

Spatial variability in the rates of sea level rise are to be expected based on tide gauge and satellite data (Chua & Xu, 2014). Furthermore, prior to the development of high-quality

satellite altimeters in 1992 to measure global mean sea level, estimates of sea level were obtained from sparsely networked coastal and island tide-gauge measurements (Church & White, 2011). There are several gaps in the tide gauge data, which can cause uncertainty for future sea level predictions (Church & White, 2011). It is therefore crucial to improve estimates for global mean sea level rise as many studies of climate change use individual sea level records that have been correct for vertical land motion to determine the rate of regional sea level rise (Church & White, 2011).

### 2.1.3 Regional Sea Level Change

Sea level is a dynamic quantity and does not rise at the same rate around the globe, which is why it is important to distinguish regional sea level change from global sea level change (Church & White, 2011). As sea level varies over time, the solid Earth responds with a glacial isostatic adjustment also known as a postglacial rebound (Sella et al., 2007). An isostatic change in sea level is not a change in water volume, but rather a change in sea level with respect to a land-based reference (Rovere et al., 2016). This isostatic adjustment is not only caused by sea level rise but is also due to the redistribution of ice as ice freezes on land in the form of glaciers during glacial periods and then melts during interglacial periods. When ice accumulates on land, Earth's lithosphere responds by sinking into the mantle. This further causes material from the mantle to uplift from the glacial areas and a relative sea level fall is observed. The opposite effect takes place during interglacial periods when ice melts, resulting in a sea level rise (Rovere et al., 2016).

Of relevance to the present study is the assessment of regional sea level rise as the study evaluates the impacts of sea level rise on a specific coastal area in the Iberian Peninsula, the Guadiana Estuary. Regional sea level rise is a consequence of not only thermal expansion and melting ice, but also local and regional meteorological effects such as storm surges, modes of climate variability and the impact of anthropogenic climate change (Church & White, 2011). Other major factors of regional sea level rise include changes in salinity and changes in atmospheric pressure anomalies from atmospheric loading (Church et al., 2013). Patterns in regional sea level change are a reflection of the redistribution of heat, salt and water mass due to changes in ocean circulation (Cazenave & Cozannet, 2013). Regional sea level varies much more over a short period of time compared to global mean sea level because the ocean volume is nearly constant, but the distribution of volume has high variability over time due to local and regional meteorological effects and climate variability (Church & White, 2011). Predictions

made by the IPCC AR5 have found that beyond the end of the 21st century both regional and local areas will experience significant deviations from the global mean sea level (Church et al., 2013).

Direct impacts of regional sea level rise on coastal areas include a decrease in biodiversity and an increase in the magnitude and spatial extent of a hazard for storm surge floods (Carrasco et al., 2016). A study by Bilskie et al. (2014) concluded that sea level rise will impact how storm surges behave along the coastline and impact coastal communities throughout the world. The magnitude and frequency of floods around the world will increase due to sea level rise, which is consistent with previous studies on the effects of coastal flooding induced by sea level rise (Bilskie et al., 2014).

### 2.1.4 The Impact of Sea Level Rise on Estuaries

An estuary is defined as the interface between fresh water from land and saltwater from the sea, extending to the river as far as the upper limit of the tide. The interaction between land and sea in this semi-enclosed body of water connects both terrestrial and marine environments and includes sub-tidal, intertidal and surrounding terrestrial habitat. Coastal plain estuaries formed along drowned fluvial valleys as a result of the eustatic sea level rise over the last 15,000 years. Estuaries have an adaptive capacity to sea level rise in which an increase in sea level deepens the channel and increases the accommodation space of sediments, further enhancing ebb and flood asymmetry (Sampath et al., 2015). Estuaries are areas of transition where less dense freshwater from rivers meets more dense saltwater from the sea. A water column is stratified when less dense water lies over more dense water, hence the stratification of an estuary is dependent on the amount of saltwater in the estuary, the flow rate of freshwater and the turbulence of the system.

Estuaries display strong chemical gradients and dynamic mixing of continental and marine waters (Delgado et al., 2012). As a large component of estuaries consists of freshwater from land, contaminated elements from anthropogenic activities can easily be accumulated in the catchment and along the entire estuary (Delgado et al., 2012). Estuaries are sensitive to natural forcing such as sea level rise and direct human activities (Sampath et al., 2015). The development of harbors, shipping channels and recreational facilities change the hydrodynamics as well as the physical, chemical and biological processes of estuaries. A major consequence of sea level rise in estuaries is the intrusion of salt (McLean et al., 2001) as an increase in sea level allows more salt water to enter the estuary (Ross et al., 2015).

Several factors control the circulation in estuaries such as density difference, mixing of saltwater and freshwater, freshwater flow and the tides (Garel et al., 2009). A study by Chua and Xu (2014) found that sea level rise results in a stronger longitudinal salinity gradient in estuaries, which in turn drives a stronger gravitational circulation. Natural and anthropogenic factors shape the physical, chemical and biological processes of estuaries. This can have a profound effect on ecosystem services and marine habitat since estuaries hold highly diverse and complex ecosystems (Sampath et al., 2015). Estuarine ecosystems along with saltmarshes host distinctive biodiversity and ecosystem services (Sampath & Boski, 2016). Recreational and commercial fishing, aquaculture, ecotourism and port facilities will all be affected by changes in estuaries. These industries further contribute to both regional and national economies, culture and society. The worst outcome of sea level rise would be a forced migration of a large proportion of the population that live on the coast (Nicholls et al., 2011). As sea level rise is inevitable, it is crucial to develop protection plans and invest money into coastal defenses and other forms of adaptation (Nicholls et al., 2011).

## 2.2 The Guadiana Estuary

### 2.2.1 Physical Characteristics

The Guadiana Estuary was formed after the last glacial low stand. It had previously been a subaerial valley where sediments bypassed the valley towards the present-day middle and outer shelf (Lobo et al., 2003). The morphological characteristics of the Guadiana during this period did not allow for significant accumulation of fluvial deposits. It was not until the end of the postglacial transgression period when this subaerial valley transformed into an estuary and sediments began accumulating in structural depressions (Lobo et al., 2003). The transition from fluvial to estuarine sedimentation took place 13,300 years ago but stopped during the Younger Dryas when the climate briefly returned to glacial conditions (Delgado et al., 2012). During the Holocene, the lower portion of the estuary was excavated and filled with sediments (Garel et al., 2009). This resulted in extensive salt marshes on both sides of the inlet, but active sedimentation during the Holocene as well as anthropogenic pressures has greatly reduced the magnitude of the area (Garel et al., 2009).

The Guadiana Estuary lies between the Guadiana River and the Gulf of Cadiz in a semi-arid environment. The head of the Guadiana River begins in Spain and extends 810 kilometers south toward the Gulf of Cadiz (Delgado et al., 2012). The Guadiana River is the fourth longest river in the Iberian peninsula and holds a catchment area of 66,960 $km^2$ (Quesada et al., 2019).

From its mouth in front of Vila Real de Santo António, the Guadiana Estuary extends north to its tidal limit near Mértola, Portugal. The estuary is most narrow at the head near Mértola with a width of 70 meters. The estuary is widest with a width of 800 meters at its mouth in between Vila Real de Santo António on the Portuguese side and Ayamonte on the Spanish side (Fortunato et al., 2002).

The Guadiana Estuary can be described as a rock-bound estuary due to its narrow and moderate depth where the volume of water entering the estuary during the flood tide is larger than the freshwater discharge from the Guadiana River (Garel, 2017). Because of its narrow width, the entire length of the estuary will be affected by moderate to high river inflows (Quesada et al., 2019). There is wave influence from the Atlantic Ocean only in the lower portion of the estuary (Lobo et al., 2003). The wave energy is moderate and is most significant at the submerged delta, the furthest extension of the lower portion of the estuary (Garel et al., 2009). At the submerged delta, fluvial sediment mixes with marine material from longitudinal transport along the coast (Gonzalez et al., 2004). Tidal and riverine processes are the dominant forces in the estuary, thus the action of the waves is considered negligible (Garel et al., 2009).

The Guadiana Estuary can be characterized by two physiographic domains: (1) an estuarine valley with complex interactions between fluvial and marine processes and (2) a progradation of a complex formed by sand areas and marshes in the fluvial plain (Lobo et al., 2003). The western margin of the estuary is characterized by a salt marsh sheltered by a littoral sand spit that drains into the estuarine channel (Garel et al., 2009). The eastern margin is composed of barrier islands and sand spits separated by wide salt marshes that drain to the Gulf of Cadiz through a tidal inlet (Garel et al., 2009). The maximum turbidity occurs in the lower portion of the estuary where the sea intrudes the estuary with salinity (Garel et al., 2009). A map showing the location and geomorphological features of the study area is shown in Figure 2.1.

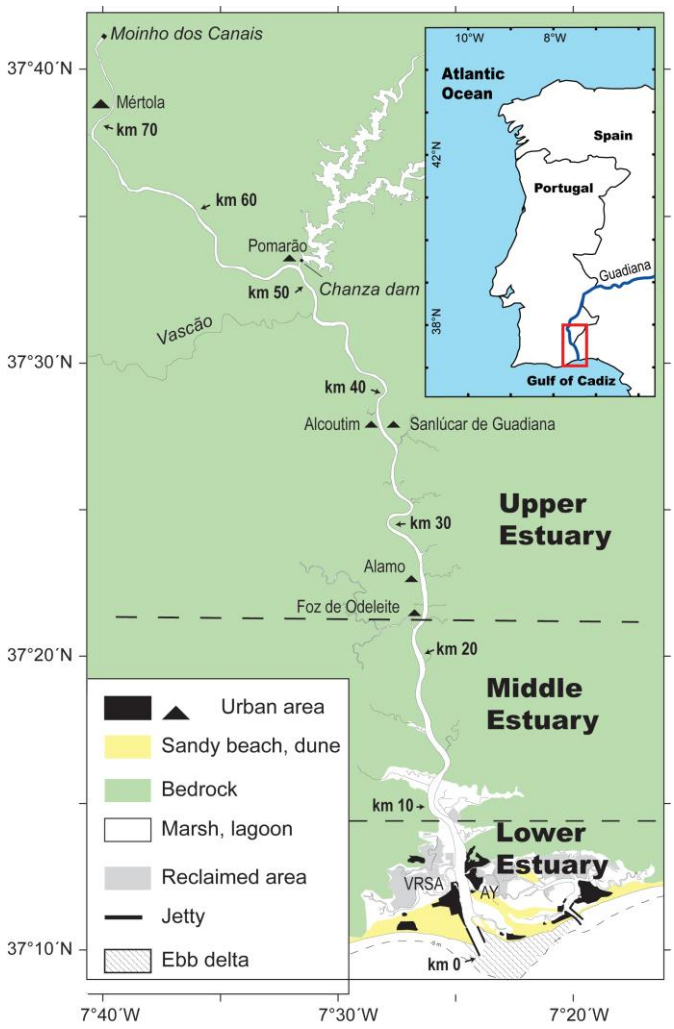


*Figure 2.1* Location and geomorphology of the Guadiana Estuary (Garel, 2017)

### 2.2.2 Hydrodynamic Characterization

The Guadiana Estuary is characterized by a semidiurnal mesotidal regime with tidal influence 50 kilometers upstream from where it meets the Gulf of Cadiz (Delgado et al., 2012). The average neap tidal range is 1.28 meters and the average spring tidal range is 2.56 meters with a maximum spring tidal range up to 3.44 meters based on long-term tide gauge data taken in front of Vila Real de Santo António (Garel et al., 2009). Tidal forcing has a large influence on spring-neap variability when there is low river inflow (Quesada et al., 2019). A non-linear relationship between velocity and friction also plays a role in spring-neap variability (Garel, 2017). There is less bed friction at neap tide due to the smaller magnitude of velocity, which results in the tide being slightly amplified at the mouth and lower estuary (Garel, 2017). On the other hand, the tidal wave is damped at spring tide due to stronger bed friction from larger velocity magnitudes (Garel, 2017). The upper portion of the estuary exhibits reflection and enhanced morphological convergence, resulting in enhanced tidal amplitudes upstream (Garel & Cai, 2018).

The stratification of the Guadiana Estuary ranges from very well mixed to very well stratified as both the tides and freshwater inputs control the vertical mixing and stratification (Garel et al., 2009). The mixing of the water column varies by season, with a well-mixed water column when there is low discharge from the Guadiana River in the summer and a partially stratified water column in the winter when the river delivers nutrients towards the continental shelf. At spring tide and when the river discharge is low, tidal processes control the water circulation of the estuary and the estuary becomes well-mixed (Garel & D'Alimonte, 2017). The estuary is weakly stratified when it is neap tide and the river discharge is low (Garel & D'Alimonte, 2017). In the latter case, density-driven processes control the mixing of the estuary. The water column is stratified only under extreme conditions (Basos, 2013). The formation of a salt wedge was observed during a very high discharge (2000 $m^3/s$) during the flood tide, while the estuary was filled with freshwater at the ebb-tide (Garel & D'Alimonte, 2017). Garel et al. (2009) found that in general, ebb currents are faster than flood currents even when the flow from the Guadiana River is low. The ebb-dominance is strongest near the mouth of the estuary and is most likely due to the large hydraulic depth of the estuarine channel and is enhanced when the river discharge increases (Garel et al., 2009). Furthermore, the ebb-dominance is more pronounced in high freshwater discharge cases, which results in horizontal advection in the main channel. The horizontal advection enhances the tidal asymmetry (Garel et al., 2009). Velocities are generally higher at the mouth of the estuary and decrease upstream (Garel et al., 2009). At spring tide, there is a longer ebb phase and at neap tide there is a long flood phase (Garel, 2017). Observations taken from the deeper main channel have found the ebb tide to be longer and faster during spring tides, whereas the flood is longer and faster during neap tides (Garel, 2017).

### 2.2.3 Guadiana River Outflow

The river inputs from the Guadiana River into the estuary vary by season. Both severe droughts and episodic floods are known to occur in the river basin (Garel et al., 2009). The flow rate from the Guadiana river varies widely from less than 10 $m^3/s$ to 4660 $m^3/s$. One major factor contributing to the freshwater flow rate is the construction of dams. Since the 1950s, over 100 large dams were constructed in the Guadiana River basin for water storage and irrigation (Garel et al., 2009). 70% of the drainage basin was controlled by dams by the end of 2000 (Garel et al., 2009). Of relevance is the Alqueva Dam, located 60 kilometers upstream the head of the estuary (Garel & D'Alimonte, 2017). The Alqueva Dam is the largest reservoir

in southern and western Europe storing 4150 $hm^3$ of water (Garel et al., 2009). The dam's closure in 2002 has significantly reduced the freshwater discharge into the estuary from a yearly average of 143 $m^3/s$ to 16 $m^3/s$ (Garel et al., 2009). Downstream the dam, the river has ephemeral flows and is dry for 40% of the year (Fortunato et al., 2002). The scarce rainfall and storage of freshwater has reduced the current flow into the estuary. The reduction in flowrate also has an impact on residence time, the time it takes a particle to exit the system (Oliveira et al., 2006). The residence time of salinity for a discharge of 50 $m^3/s$ is roughly 5 days, whereas for a discharge of 2 $m^3/s$ the residence time ranges between 14 and 37 days, based on the results of a 1-dimensional ecohydrology model of the estuary (Wolanski et al., 2006). Thus, the discharge of the Guadiana River, has a large effect on the horizontal distribution of salinity in the estuary.

### 2.2.4 Socioeconomic Characterization of the Guadiana Estuary

According to Guimarães et al. (2012), 50,000 people reside near the Guadiana Estuary, 45% of which live on the Portuguese side. Most of these people have jobs in tourisms and in the service industry. The population increases significantly in the high season by up to 300,000 people on the Spanish side and up to 212,000 people on the Portuguese side as a result of tourism. The population is concentrated mainly in the lower estuary where it meets the Gulf of Cadiz and decreases significantly further upstream the estuary (Guimarães et al., 2012). The distribution of the population highlights the importance of the lower estuary's economic value and abundance of recreational activities.

### 2.2.5 Managing the Guadiana Estuary: the SPICOSA Project

A recent case study on the Guadiana Estuary led by Tomasz Boski for the Science and Policy Integration for Coastal System Assessment (SPICOSA) project took place from 2007 to 2011 to evaluate the present situation of the Guadiana Estuary. The SPICOSA project integrated countries around the European Union and was funded by the EU's Sixth Framework Program. The goal of the SPICOSA project was to develop an operation research approach framework for policy options to manage coastal systems. Boski (2011) concluded that the closure of the Alqueva Dam will cause eutrophication and sediment starvation along the coast of Guadiana as it has significantly reduced freshwater flow into the estuary. Main anthropogenic inputs on the Portuguese side of the Guadiana River come from forestry and agriculture (Boski, 2011). On the Spanish side of the river, the Esuri real estate development

located 14 kilometers from the mouth of the river on salt marsh terrains has a high potential to be influenced by sea level rise and salt intrusion in the Guadiana Estuary.

Factors further influencing the ecology of the Guadiana Estuary include concentrations of toxic elements in the sediments caused by anthropogenic activities (Delgado et al., 2011). Salinity intrusion coupled with a trace of toxic elements in the Guadiana pose a high environmental risk for the estuary, which will further impact ecological services.

## 2.3 Salinity Intrusion

Several numerical model-based studies have found an increase in salinity in response to sea level rise (Ross et al., 2015). A study by Hilton et al. (2008) found an increase in salinity from 0.5 to 2.0 over the main Chesapeake Bay area due to sea level rise based on the results of a multiple linear regression model. An increase in salinity will have a profound effect on the physical properties of estuaries as the dynamic mixing of seawater and freshwater is the driving factor regulating stratification (Ross et al., 2015). The increase in salinity will cause the water to become denser and thus, increase the stratification of the water column. Salt intrusion is an inevitable consequence of sea level rise and will change horizontal and vertical salinity gradients, alter the estuarine circulation and further cause oxygen depletion (Hong & Shen, 2012). A study by Wiseman et al. (1990) found both positive and negative trends on the impact of salinity increase in Louisiana estuaries in the United States. These trends were attributed to the variability of freshwater flow rates due to the local effects of climate change (Wiseman et al., 1990). These authors found that an increase in salinity results in the death or decline in the productivity of marshes, which eventually leads to land loss (Wiseman et al., 1990). Further impacts of salinity intrusion include the contamination of water supplies of both human consumption and industrial purposes (Hilton et al., 2008).

As estuaries are sensitive environments and host complex and diverse ecosystems, an increase in salinity will change the distribution of species, as species have specific salt tolerances (Statham, 2012). This will impact the entire estuarine ecosystem as certain species move upstream from the salt intrusion caused by sea level rise.

## 2.4 Modeling the Impacts of Sea Level Change

### 2.4.1 Definition of Numerical Model

In order to evaluate the impact of future sea level rise scenarios in the Guadiana Estuary, a numerical model was implemented. In simple terms, a model is a conceptual representation

of reality. Analytical and quantitative models are based on physical, chemical and biological processes (Paola, 2000). Numerical models are quantitative based models and represent these scientific processes by solving mathematical equations (Paola, 2000). Several models have been used to study the projections and impacts of sea level rise including numerical, empirical and semi-empirical models (Church et al., 2013). Semi-empirical models project sea level based on statistical relationships between observed global mean sea level and global mean temperature, but do not simulate the underlying processes of changes to mean sea level (Church et al., 2013).

### 2.4.2 Previous Models of the Guadiana Estuary

The hydrodynamics of the Guadiana Estuary have been simulated with numerical models since the early 2000s (Quesada et al., 2019). A lack of bathymetric data for the first few simulations of the Guadiana Estuary limited the early models to evaluate the hydrodynamics for only the first 50 kilometers of the estuary. As the tidal limit of the estuary is located 80 kilometers upstream, improved bathymetries have been developed in order to completely evaluate the dynamics of the estuary. One example was created on a high resolution curvilinear grid that used bathymetric data collected from 2005 to 2010 (Basos, 2013).

A model produced by Quesada et al. (2019) recently used the MOHID water modeling system in 2D barotropic mode in a study simulating the effects of freshwater discharge and tidal forcing on tidal propagation in the Guadiana Estuary. The model simulations were run over the same high resolution curvilinear grid produced by Basos (2013). The model was accurately able to produce phase values of tidal elevations and currents compared with results obtained from a harmonic analysis (Quesada et al., 2019). The results of the model demonstrated how tidal forcing has the largest influence on tidal wave amplitude downstream the estuary, whereas freshwater discharge controls tidal wave amplitude upstream (Quesada et al., 2019).

Of relevance are the results of a study by Mills et al. (2019) as the present study is a continuation of the work and methodologies used to simulate hydrodynamics and evolution of salt transport with respect to mean sea level rise. These authors used MOHID in 2D to simulate the hydrodynamics of the Guadiana Estuary considering different sea level rise scenarios up to the year 2100 along with varying freshwater flow rates of the Guadiana River (Mills et al., 2019). Results of the model demonstrated an overall increase in salinity in the estuary as well as flooding areas around the estuary with respect to mean sea level rise. Mean sea level rise led

to a reduction in velocity in the main channel, most likely due to an increase in depth and water volume (Mills et al., 2019). The model considered only the present bathymetry as well as a tidal amplitude equivalent to the average tidal amplitudes. The horizontal distribution of salinity in estuaries is dependent on several factors. One major variable is the equilibrium between spring and neap tidal cycles and freshwater flow (Varga et al., 2017). It is thus the purpose of this work to expand upon the methodologies of Mills et al. (2019) to determine how the horizontal distribution of salinity varies between spring and neap tide as well as across a bathymetry that will allow flooding of the marshes and low-lying areas.

# 3 Methods

## 3.1 MOHID

The MOHID water modeling system (MARETEC, 2017) was used to simulate the hydrodynamics and water properties of the Guadiana Estuary in response to different scenarios of sea level rise. MOHID simulates physical and biogeochemical processes in the water column and sediments using an object-oriented programming approach (MARETEC, 2017). MOHID is programmed in ANSI FORTRAN 95 in order to produce object-oriented models integrating hydrodynamic processes for different marine systems and at different scales (MARETEC, 2017). The model can be used in one, two or three dimensions as well as incorporate nested models. The present study used MOHID in 2D, as the Guadiana Estuary is classified as a well-mixed estuary (Garel & D'Alimonte, 2017) and thus the hydrodynamics and water properties are the same throughout the water column. The Guadiana Estuary can become stratified, but only under freshwater flows of 1000 $m^3/s$ (Fortunato et al., 2002). The present study ran simulations for freshwater flows of 10 $m^3/s$ and 100 $m^3/s$ as these are typical conditions of the system, thus it was not necessary to use a three-dimensional model.

MOHID water has been widely used throughout Europe to simulate the hydrodynamics of coastal and estuarine systems such as the major estuaries of Portugal, the Netherlands, France and Ireland (Quesada et al., 2019). The program consists of models for hydrodynamics, Eulerian transport, Lagrangian transport, water quality and sediment (Morais et al., 2012). For this study, MOHID Studio graphical interface was used. This is a Bentley Systems software integrating all models available in the MOHID system into a user-friendly graphical interface. MOHID studio allows the performance of all tasks related to model implementation, validation, execution and result visualization. It also contains several features and tools to help users

prepare all necessary data and set up model simulations, grids, initial conditions and boundary conditions.

## 3.2 Model Simulations

In order to simulate the hydrodynamics of a marine system using the hydrodynamic model MOHID, it is necessary to set up each simulation with several data components (Basos, 2013). Bathymetric gridded data, water level and forcing such as water discharge and tides all must be included in the model setup. The following section explains the setup of each simulation used in the present study. The main variables for the present study include the bathymetry, water level, river discharge and tides. Atmospheric conditions such as wind are considered negligible due to the limited fetch along the estuary (Morais et al., 2012).

### 3.2.1 Model Setup

The main objective of this dissertation is to determine how the hydrodynamics and salt transport will change along the Guadiana Estuary with respect to sea level rise. The previous numerical model of the estuary by Mills et al. (2019) used the finite volume method with an Alternating Direction Implicit (ADI) method to solve Navier-stokes and transport equations. The finite volume method allows for the transport equations to be applied to the entire cell volume at specific points in discrete time (Neves et al., 2000). The present study implements the same general setup of the model by Mills et al. (2019) and uses the same Cartesian computational grid of 1400 x 350 cells with a constant space step of 30 meters. This computational mesh was chosen as it provides the most appropriate spatial resolution for the study without incurring excessive calculation time. The calculation time for each simulation is quite high, especially when the river discharge is low. For example, it takes more than two weeks to calculate two months of simulated time when the river flow is 10 $m^3/s$. The two months of simulation time is required as that is how long it takes for the salinity field to stabilize. This is due to the high residence time of particles in the estuary when the freshwater flow rate is low (Oliveira et al., 2006).

The hydrodynamic MOHID model of the Guadiana Estuary has been previously validated, calibrated and used in several studies. An ecohydrology study by Morais et al. (2012) on the abundance of anchovy eggs in the Guadiana Estuary used the MOHID model to simulate the transport and distribution of anchovy larvae in the estuary in response to different river discharge scenarios. The model was calibrated with field measurements of several

hydrodynamic parameters such as water level, velocity and direction as well as water properties such as salinity and sediments (Lopes et al., 2003).

### 3.2.2 Model Bathymetries

The present model considers of two separate bathymetries: (1) a bathymetry in which maximum human intervention is taken to keep the coastline maintained and (2) a bathymetry that allows flooding of the saltmarshes and low-lying areas. The first bathymetry represented in Figure 3.1 is the current bathymetry of the Guadiana Estuary. It was computed by triangular interpolation of measured bathymetric data on the Cartesian grid of 1400 x 350 cells with a space of 30 meters (Mills et al., 2019). The results of the simulations computed on this bathymetry correspond to a future scenario in which the coastline does not change even as the mean sea level is rising.

The second bathymetry as shown in Figure 3.2 was computed by Sampath et al. (2011) in a behavior-oriented model. This bathymetry was used because MOHID is a process-based model and cannot compute long-term geomorphological dynamics. This bathymetry allows the surrounding saltmarshes and low-lying areas of the estuary to be flooded. It was solved based on the rate of sea level change, accommodation space for the deposition of sediments and vertical accretion of sediments dependent on inundation (Sampath et al., 2011).

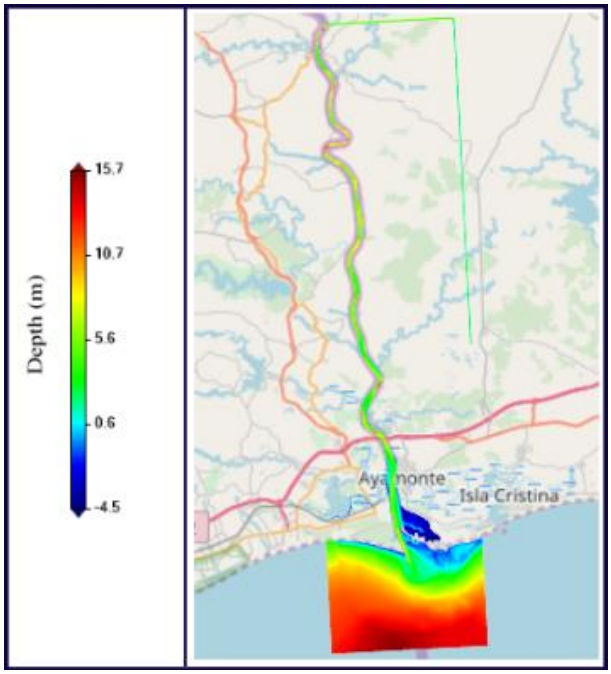


*Figure 3.1* Computational bathymetry of the Guadiana Estuary if the coastline is maintained on a mesh of 1400 x 350 cells with a space step of 30 m (Mills et al., 2019)

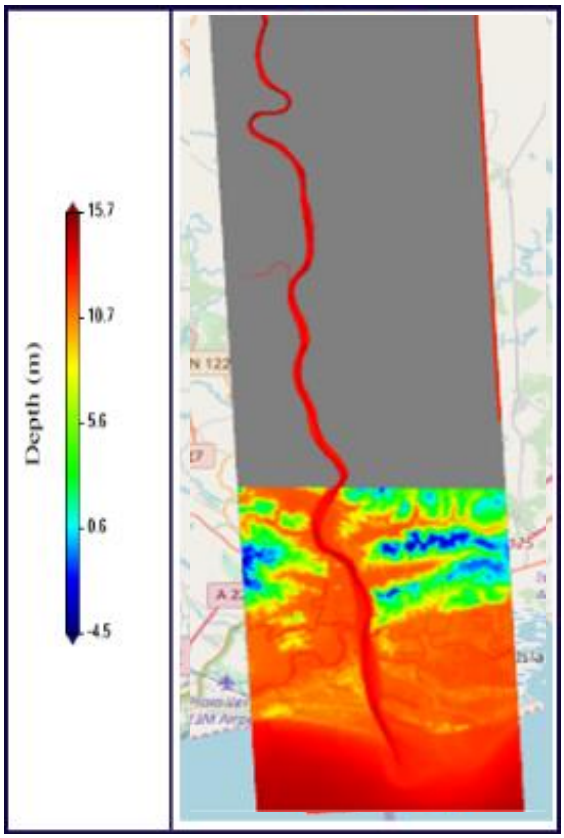


*Figure 3.2* Computational bathymetry of the Guadiana Estuary, allowing flooding (1400 x 350 cells with a space step of 30 m). The grey area represents land. (Sampath et al., 2011)

### 3.2.3 Sea Level Rise Scenarios

Following the work of Mills et al. (2019) various sea level scenarios were chosen based on future sea level rise projections from the 5$^{th}$ assessment report produced by the IPCC. The 5$^{th}$ assessment report includes sea level rise forecasts up to the year 2100 for different Representative Concentration Pathways (RCP), more commonly known as greenhouse gas emissions (Church et al., 2013). The study by Mills et al. (2019) considered the values forecasted by the IPCC for a case of low greenhouse gas emissions (RCP 4.5) and a case of very high greenhouse gas emissions (RCP 8.5). Table 3.1 outlines the IPCC sea level rise predictions for the years 2045-2065, 2081-2100 and 2100 for both RCP values along with the values used by Mills et al. (2019). The predictions made by the IPCC were based on sea level rise throughout the years 1986 to 2005 (Church et al., 2013).

*Table 3.1* Predictions for the rise in global mean sea level in meter based on sea level rise from the years 1986-2005 for RCP 4.5 and RCP 8.5 (Adapted from the 5th IPCC Report, Church et al. (2013) along with scenarios used by Mills et al. (2019)

| | | RCP 4.5 | Mills et al. (2019) | RCP 8.5 | Mills et al. (2019) |
|---|---|---|---|---|---|
| **2046-2065** | P95 | 0.30 | | 0.38 | 0.24 |
| | Median. | 0.26 | 0.24 | 0.30 | |
| | P05 | 0.19 | | 0.22 | 0.79 |
| **2081-2100** | P95 | 0.63 | | 0.82 | |
| | Median. | 0.47 | 0.48 | 0.63 | 0.48 |
| | P05 | 0.32 | | 0.45 | |
| **2100** | P95 | 0.71 | | 0.98 | |
| | Median. | 0.53 | 0.48 | 0.74 | 0.79 |
| | P05 | 0.36 | | 0.52 | |

The sea level rise scenarios chosen by Mills et al. (2019) are indicative of a sea level rise of 0.24 meters for the year 2040, a sea live rise of 0.48 meters for the year 2070 and 0.79 meters for the year 2100. These values were chosen as they cover all possibilities of sea level rise for the years previously mentioned for both cases of greenhouse gas emissions projected by the IPCC. As opposed to running simulations for each possible scenario for each greenhouse gas emission predicted by the IPCC with a 5%, 50% and 95% likelihood as shown in Table 3.1, it was decided to use three scenarios of sea level rise to demonstrate the evolution of the estuary every thirty years up to the year 2100. Simulating each possibility of sea level rise predicted by the IPCC would require an unnecessary number of simulations for the model and would be redundant considering the overlap of several of the values of mean sea level rise predictions. Thus, the present model utilizes the same sea level rise scenarios from Mills et al. (2019) and includes a sea level rise of 0 for the present year, 0.24 m for the year 2040, 0.48 m for the year 2070 and 0.79 m for the year 2100.

### 3.2.4 Freshwater Flow Scenarios

Freshwater flow scenarios were chosen based on the high variability of the flow of the Guadiana River. The study by Mills et al. (2019) considered four different river discharges: (1) Q = 10 $m^3$/s, indicative of the flow of the river in summer when there is a lack of rain (Morais et al., 2012), (2) Q = 50 $m^3$/s for an intermediate discharge scenario, (3) Q = 100 $m^3$/s for a high discharge scenario and (4) Q = 500 $m^3$/s for a very high flow scenario. The scenarios of Q = 50 $m^3$/s and Q = 500 $m^3$/s were not imposed in the present model as the latter situation has

only been known to occur prior to the closure of the Alqueva Dam and should now only occur in extreme cases of river discharge. The intermediate flow of Q = 50 $m^3$/s was also not imposed in the model as the present study will already include 32 simulations. It was thus decided to consider only two cases of freshwater flow from the river: a low discharge of 10 $m^3$/s representing the summer months when there is little rain and a high discharge of 100 $m^3$/s for the remaining months of the year when there is more rainfall. These two values for river discharge are appropriate as the freshwater flow has been strongly regulated since the closure of the Alqueva Dam, yielding a reduction in the yearly and seasonal variability of the river discharge (Quesada et al., 2019).

### 3.2.5 Tidal Scenarios

The model used by Mills et al. (2019) was not associated with any specific tidal event as it represents typical system conditions. All 16 simulations were forced with the same tidal amplitude equivalent to the average amplitude of an external tide of type M2 and S2 in phase and M2 and S2 out of phase, yielding an amplitude of 1 meter (Mills et al., 2019). Therefore, the previous model did not consider how the dynamics of the estuary will evolve with respect to different tidal amplitudes. The present study examines the differences in spring and neap tidal ranges. The spring tide, with the highest differences between high and low tide occurs twice per month and has a tidal range of 2.56 meters (Garel, 2017). Likewise, the neap tide, with the smallest differences between high and low tides occurs twice per month with a tidal range of 1.28 meters. Thus, the value imposed in the model representing a spring tidal cycle is 1.28 meters and the value for neap tide is 0.64 meters

In summary, the model consists of two separate bathymetries, four different scenarios of sea level rise, two different cases of river discharge and two different tidal scenarios for a total of 32 simulations. Table 3.2, Table 3.3, Table 3.4 and Table 3.5 summarize the variables implemented in the model.

*Table 3.2* Bathymetry Scenarios

| **Scenario** | **Bathymetry** |
|---|---|
| **1** | Present Bathymetry |
| **2** | Bathymetry allowing flooding |

*Table 3.3* Sea Level Rise Scenarios

| Year | Sea Level Rise (m) |
|---|---|
| **Present** | 0 |
| **2040** | 0.24 |
| **2070** | 0.48 |
| **2100** | 0.79 |

*Table 3.4* Freshwater Flow Scenarios

| Scenario | Freshwater Flow Rate ($m^3/s$) |
|---|---|
| **1** | 10 |
| **2** | 100 |

*Table 3.5* Tidal Scenarios

| Tidal Scenario | Tidal Amplitude (m) |
|---|---|
| **Spring Tide** | 1.28 |
| **Neap Tide** | 0.64 |

### 3.2.6 Model Runs

Each of the 32 simulations was set up with the data components previously mentioned. Each simulation was composed with a set of runs that run the model for a specified length of time. The first eight runs for each model were run for 2 hours of simulated time, slowly increasing the Courant number with each run. The ninth run for each simulation was run for 20 days followed by a run with 30 days, as this is the time for the salinity field to stabilize, as previously mentioned. Another one-day run was executed after the two months of required time to stabilize the salinity field in order to show the evaluation of both hydrodynamics and salinity over two tidal cycles. The model setup is shown in Figure 3.3.

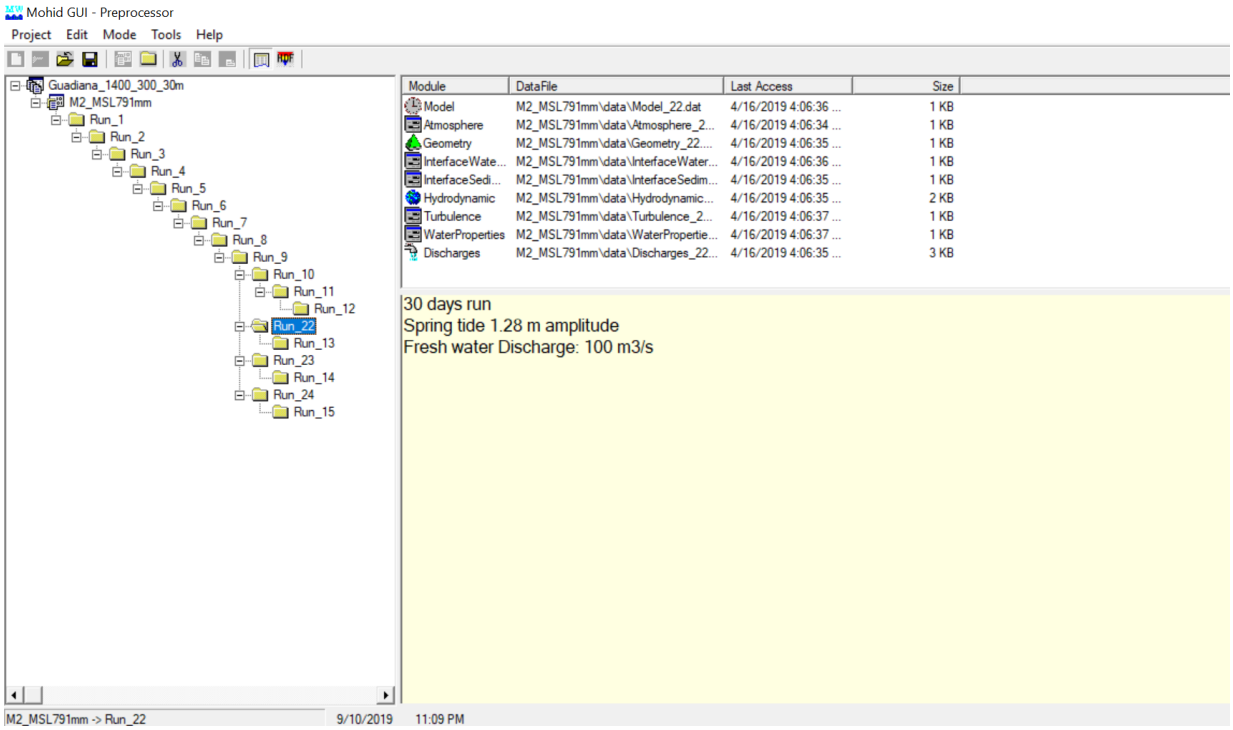


*Figure 3.3* Model setup for one simulation.

### 3.2.7 Areas of Inundation

To determine the areas of inundation for the various scenarios of sea level rise combined with the various river discharge scenarios classes of flooding were computed as a function of submersion time over one tidal cycle. 10 classes of flooding were chosen based on intervals of submersion time over 1 tidal cycle. For example, class 1 corresponds to a submersion time of 0 to 1.2 hours, class 2 corresponds to a submersion time of 1.2 hours to 2.4 hours, and so forth up to 12.2 hours of submersion time. The classes of flooding were computed up to 12.2 hours because the Guadiana Estuary is semidiurnal and thus has a tidal cycle of 12.25 hours (Garel, 2017). Each spring and neap tide scenario combined with the various freshwater discharge scenarios and various sea level rise scenarios were run over the bathymetry allowing flooding of the estuary. Each output file was then run in a script in Python to produce both a histogram data file and an HDF file showing the areas of inundation. The Python script was used to determine the time a cell in the grid was covered by water for one tidal cycle. Classes of flooding were then determined based on the percentage of time an area was covered in water. Table 3.6 shows the setup of the histogram computed in Python to calculate total land submersion area for each class of flooding.

*Table 3.6* Histogram chart computed in Python to calculate land inundation for each class of flooding.

| Class | Bin(wet%) | Submersion Time (hours) | |
|---|---|---|---|
| **1** | 0.0001-0.1 | 0.0 | 1.2 |
| **2** | 0.1-0.2 | 1.2 | 2.4 |
| **3** | 0.2-0.3 | 2.4 | 3.7 |
| **4** | 0.3-0.4 | 3.7 | 4.9 |
| **5** | 0.4-0.5 | 4.9 | 6.1 |
| **6** | 0.5-0.6 | 6.1 | 7.3 |
| **7** | 0.6-0.7 | 7.3 | 8.6 |
| **8** | 0.7-0.8 | 8.6 | 9.8 |
| **9** | 0.8-0.9 | 9.8 | 11.0 |
| **10** | 0.9-0.9999 | 11.0 | 12.2 |

# 4 Results

The results of the model allow for an evaluation of the hydrodynamics, salinity distribution and transport, and flooding areas of the Guadiana Estuary. Time series graphs were produced along several locations of the estuary allowing an examination of the evolution of velocity, water elevation and salinity. The following section portrays the time series results of velocity, water elevation and salinity, horizontal distribution maps of salinity and areas of inundation.

## 4.1 Time Series Locations

Time series graphs of velocity modulus and salinity were produced along several locations of the estuary. Six location points were constructed along the main channel allowing an evaluation of velocity and salinity over two tidal cycles (24 hours). Five location points were also constructed in the saltmarshes on the Portuguese side of the estuary, near Castro Marim. The locations and nomenclature for the points used in the time series are shown in Figure 4.1.

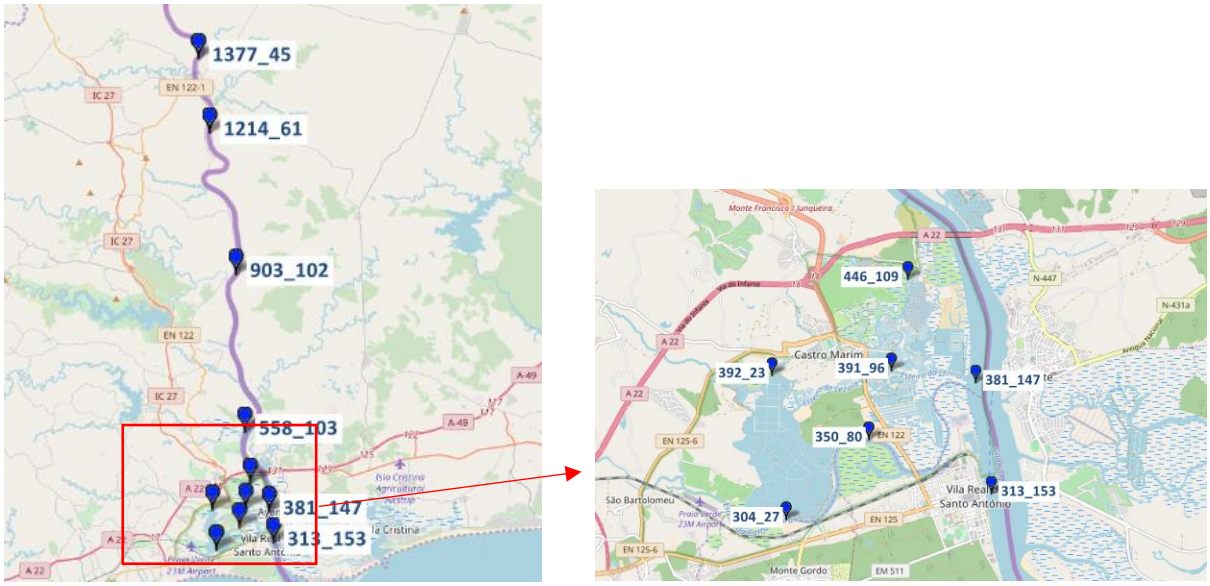


*Figure 4.1* Location and nomenclature for points used in the time series along the main channel (left) and saltmarshes (right).

## 4.2 Temporal Evolution of Velocity

As the hydrodynamics were modeled over two separate bathymetries, for four different scenarios of sea level rise combined with two varying freshwater discharge scenarios along two different types of tide, the total number of time series results for the 11 location points on the map is quite high. Therefore, the time series results at the following locations are displayed: one in the upper section of the estuary (1377_45), one in the middle section of the estuary (558_103), one at the inlet into the marsh area (381_147), one in the westernmost region of Castro Marim (392_23), one in the easternmost region of Castro Marim (391_96), one downstream Esteiro da Carrasqueira and one in the lower section of the estuary closest to the mouth (313_153). The remaining time series graphs are shown in the appendix.

### 4.2.1 Velocity Time Series at Neap Tide for a High Freshwater Flow

Figure 4.2, Figure 4.3, Figure 4.4, Figure 4.5, Figure 4.6, Figure 4.7 and Figure 4.8 show the time series results at the previously mentioned locations for the present bathymetry compared with the bathymetry that allows flooding of the marshes and low-lying areas at neap tide combined with a freshwater flow rate of 100 $m^3/s$ over two tidal cycles (24 hours).

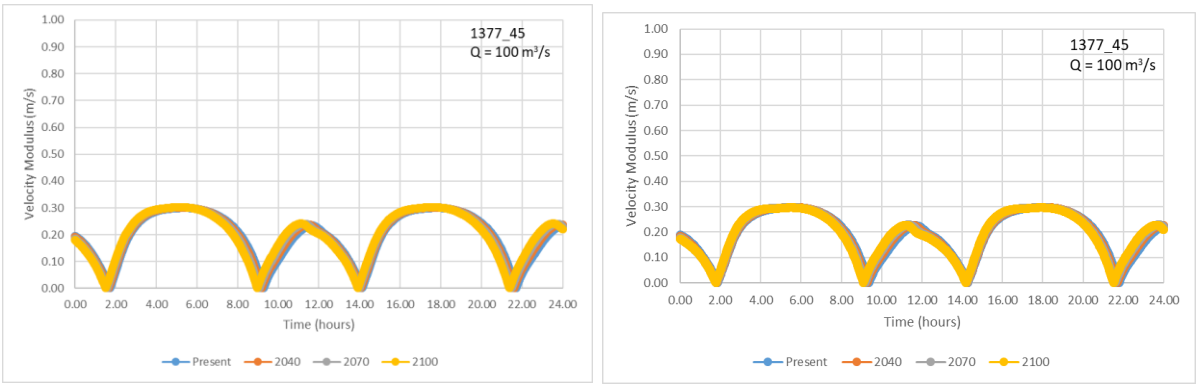


*Figure 4.2* Velocity time series over two tidal cycles for a river discharge of 100 $m^3/s$ at neap tide in the upper estuary for the present bathymetry (left) and bathymetry that allows flooding (right).

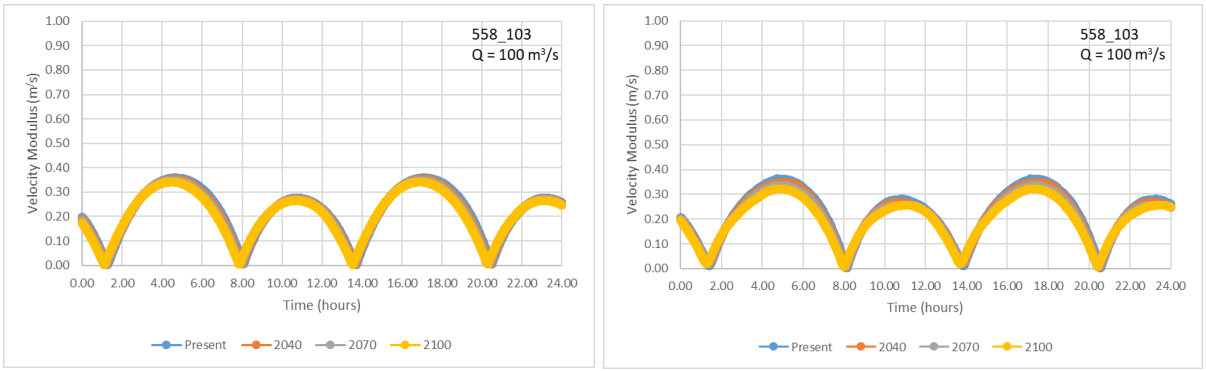


*Figure 4.3* Velocity time series over two tidal cycles for a river discharge of 100 $m^3/s$ at neap tide in the middle estuary for the present bathymetry (left) and bathymetry that allows flooding (right).

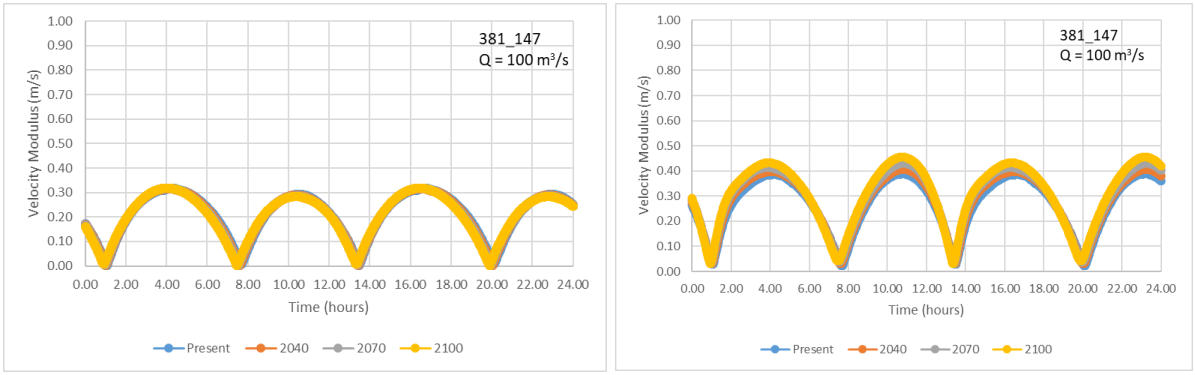


*Figure 4.4* Velocity time series over two tidal cycles for a river discharge of 100 $m^3/s$ at neap tide at the inlet into the marshes for the present bathymetry (left) and bathymetry that allows flooding (right).

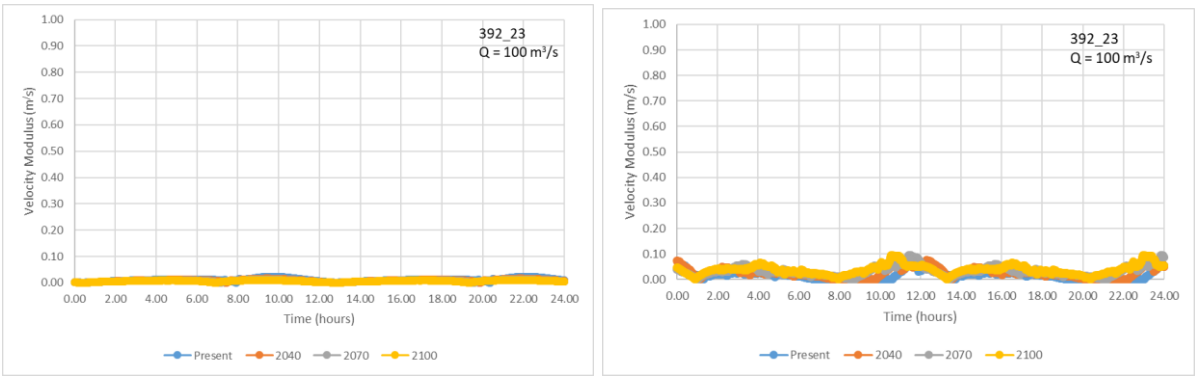


*Figure 4.5* Velocity time series over two tidal cycles for a river discharge of 100 $m^3/s$ at neap tide in the westernmost region of Castro Marim for the present bathymetry (left) and bathymetry that allows flooding (right).

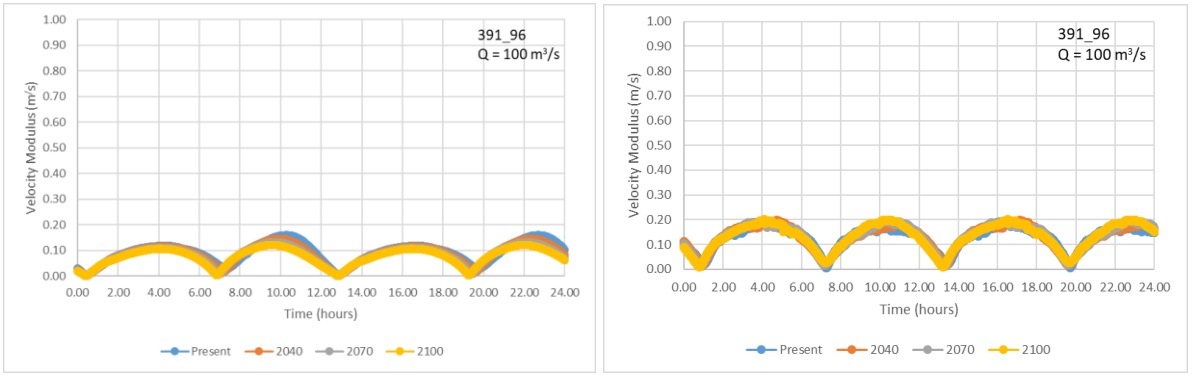


*Figure 4.6* Velocity time series over two tidal cycles for a river discharge of 100 $m^3/s$ at neap tide at the easternmost region of Castro Marim for the present bathymetry (left) and bathymetry that allows flooding (right).

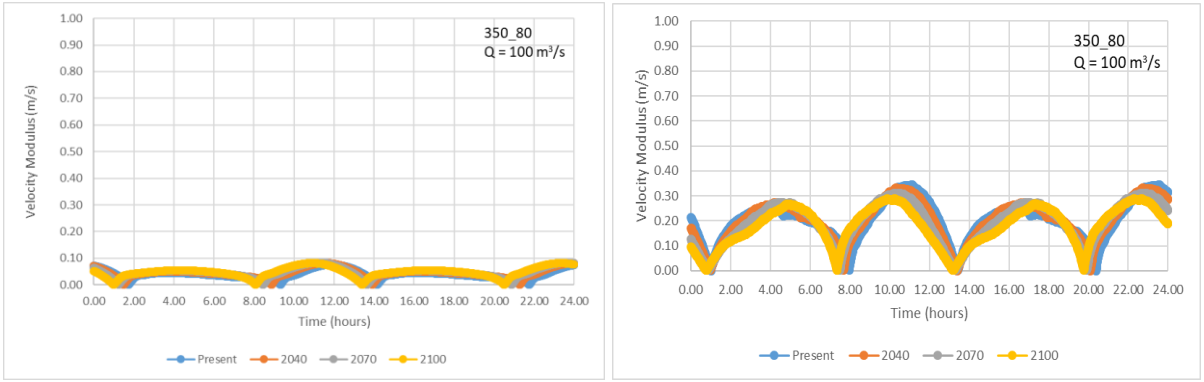


*Figure 4.7* Velocity time series over two tidal cycles for a river discharge of 100 $m^3/s$ at neap tide downstream Esteiro da Carrasqueira for the present bathymetry (left) and bathymetry that allows flooding (right).

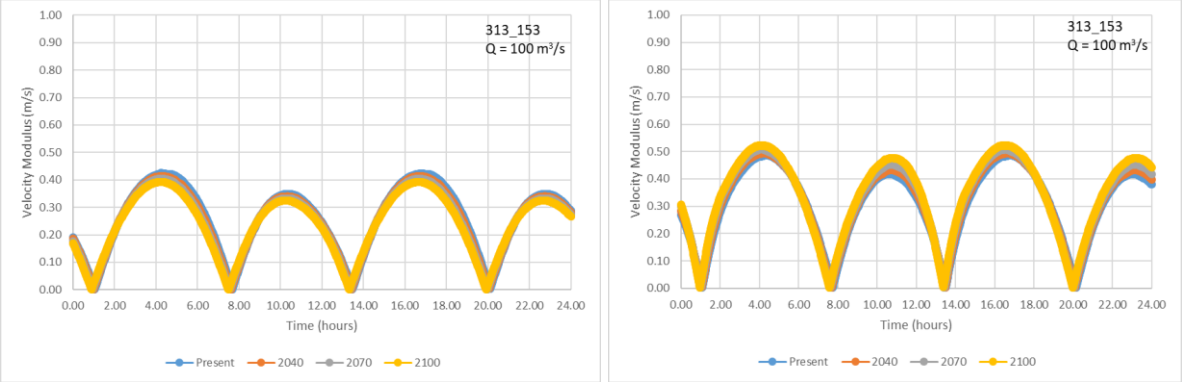


*Figure 4.8* Velocity time series over two tidal cycles for a river discharge of 100 $m^3/s$ at neap tide in the lower estuary for the present bathymetry (left) and bathymetry that allows flooding (right).

For the case of high freshwater discharge at neap tide over the present bathymetry, there is a general decrease in velocity modulus at all locations in the estuary. For the bathymetry that allows flooding, the results in the upper and middle sections of the estuary are consistent with the results obtained from the present bathymetry. However, in the lower section of the estuary and in the salt marshes, there is an increase in velocity modulus. It can also be noted that velocity values are generally higher for the bathymetry allowing flooding compared to the present bathymetry. This is especially true in the lower estuary close to the mouth and at the inlet of Esteiro da Leziria, as shown in Figure 4.4.

To determine the average change in velocity modulus every thirty years for each location along the estuary, the average velocity over the 24-hour period at each location used in the time series was computed and then subtracted to examine the differences between the present year and 2040, 2040 and 2070, and 2070 and 2100. The average change in velocity for each thirty-year period for the present bathymetry is shown in Table 4.1.

*Table 4.1* Changes in velocity modulus for a discharge of 100 $m^3/s$ at neap tide over the present bathymetry.

| | | Change in Velocity Modulus (m/s) | | |
|---|---|---|---|---|
| **Location** | | **Present - 2040** | **2040 - 2070** | **2070 - 2100** |
| **Upper Estuary** | 1377_45 | 1.51E-03 | 8.95E-04 | 2.35E-04 |
| | 1214_61 | 1.05E-03 | 6.35E-04 | 8.79E-05 |
| **Middle Estuary** | 903_102 | 1.52E-03 | 1.14E-03 | 6.00E-04 |
| | 558_103 | -3.73E-03 | -3.80E-03 | -4.12E-03 |
| **Lower Estuary** | 381_147 | -1.04E-03 | -1.24E-03 | -1.31E-03 |
| | 313_153 | -6.38E-03 | -6.41E-03 | -6.61E-03 |
| **Marshes** | 446_109 | -6.45E-04 | -5.19E-04 | -4.27E-04 |
| | 392_23 | -1.99E-03 | -1.51E-03 | -1.11E-03 |
| | 391_96 | -4.73E-03 | -5.29E-03 | -5.18E-03 |
| | 350_80 | 5.10E-03 | 2.65E-03 | 7.20E-04 |
| | 304_27 | 6.14E-04 | 1.33E-05 | -3.69E-04 |

*Table 4.2* Changes in velocity modulus for a discharge of 100 $m^3/s$ at neap tide over the bathymetry allowing flooding.

| | | Change in Velocity Modulus (m/s) | | |
|---|---|---|---|---|
| **Location** | | **Present - 2040** | **2040 - 2070** | **2070 - 2100** |
| **Upper Estuary** | 1377_45 | 9.72E-04 | 6.33E-04 | 3.01E-04 |
| | 1214_61 | 6.75E-04 | 4.03E-04 | 5.29E-05 |
| **Middle Estuary** | 903_102 | 1.26E-03 | 8.05E-04 | 2.63E-04 |
| | 558_103 | -6.82E-03 | -7.33E-03 | -7.62E-03 |
| **Lower Estuary** | 381_147 | 1.30E-02 | 1.25E-02 | 1.17E-02 |
| | 313_153 | 8.16E-03 | 9.56E-03 | 1.11E-02 |
| **Marshes** | 446_109 | 4.01E-04 | -6.31E-04 | -6.17E-04 |
| | 392_23 | 9.75E-03 | 6.67E-03 | 5.10E-03 |
| | 391_96 | 1.39E-03 | 2.60E-03 | 1.92E-04 |
| | 350_80 | -3.52E-04 | -8.74E-03 | -1.38E-02 |
| | 304_27 | 3.17E-03 | 1.97E-03 | -3.04E-04 |

Both types of bathymetry do not experience any change in velocity modulus until the middle to lower portion of the estuary. The bathymetry allowing flooding experiences an increase in velocity toward the mouth of the estuary (location 313_153) and at the inlet at Esteiro da Leziria. The present bathymetry has a decrease in velocity at the mouth of the estuary, most likely attributed to the deepening of the channel. The bathymetry allowing flooding results in an increase in velocity close to the saltmarshes of Castro Marim (392_23), whereas the present bathymetry experiences no change in velocity at this location. It can also be noted in the time series that the present bathymetry has velocity values close to 0 at this location compared to values close to 0.1 $m^3/s$ for the bathymetry allowing flooding, which shows the impacts the bathymetry has on horizontal velocity. In general, the present bathymetry shows how the channel deepens with respect to sea level rise and thus results in a decrease in horizontal velocity, whereas the bathymetry allowing flooding allows the water to spread horizontally to the marshes and low-lying areas.

### 4.2.2 Velocity Time Series at Neap Tide for a Low Freshwater Flow

The results for a low freshwater discharge at neap tide over the present bathymetry in comparison to bathymetry allowing flooding are presented in Figure 4.9, Figure 4.10, Figure 4.11, Figure 4.12, Figure 4.13, Figure 4.14 and Figure 4.15.

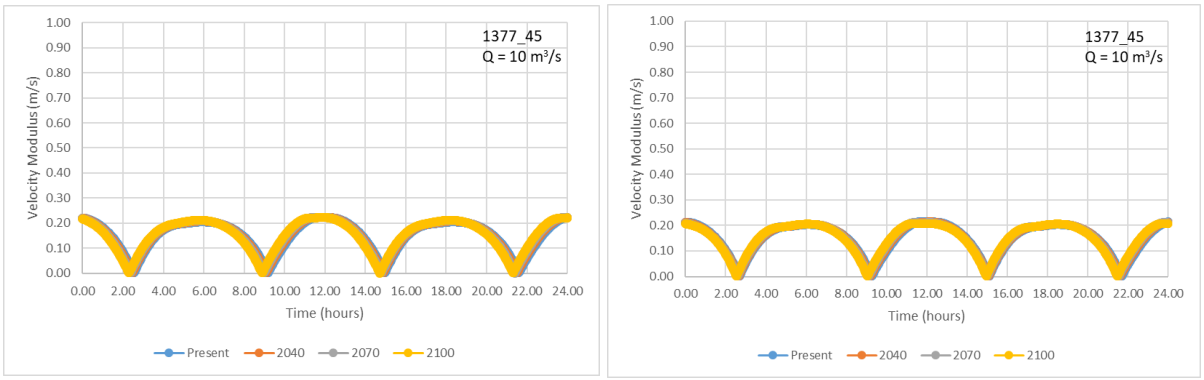


*Figure 4.9* Velocity time series over two tidal cycles for a river discharge of 10 $m^3/s$ at neap tide in the upper estuary for the present bathymetry (left) and bathymetry that allows flooding (right).

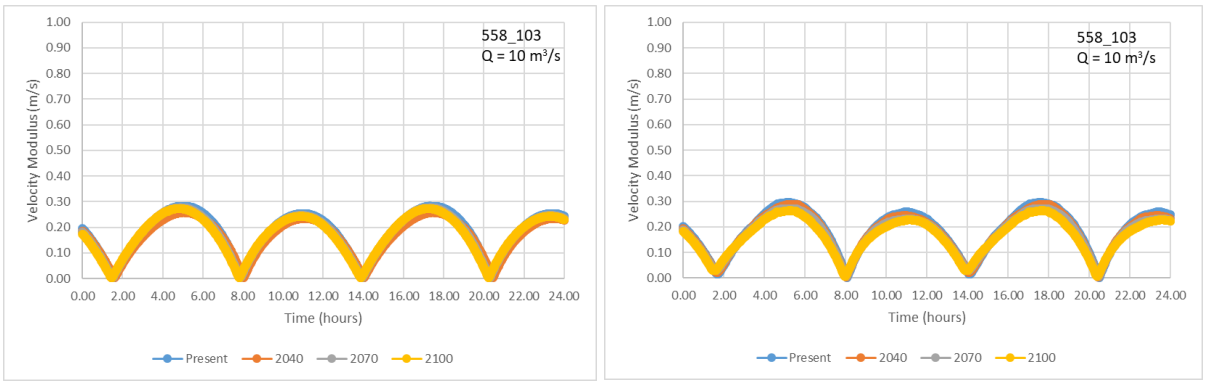


*Figure 4.10* Velocity time series over two tidal cycles for a river discharge of 10 $m^3/s$ at neap tide in the middle estuary for the present bathymetry (left) and bathymetry that allows flooding (right).

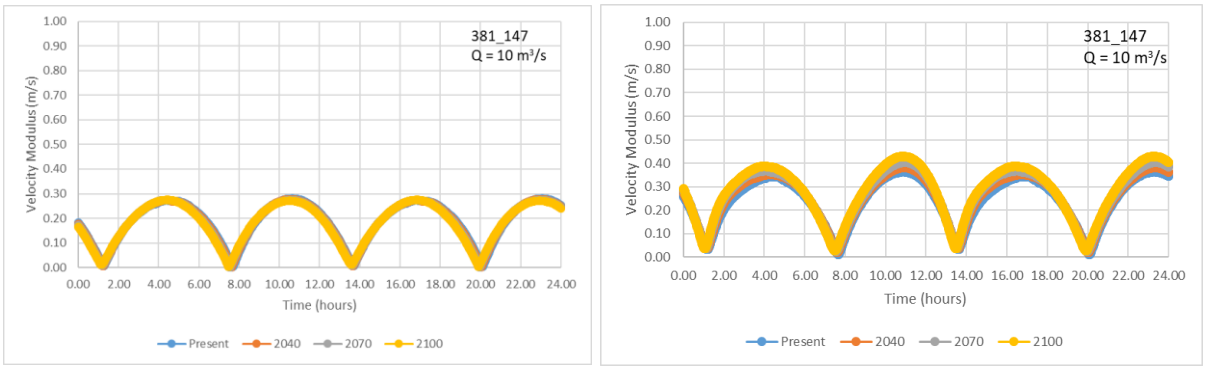


*Figure 4.11* Velocity time series over two tidal cycles for a river discharge of 10 $m^3/s$ at neap tide at the inlet into the marshes for the present bathymetry (left) and bathymetry that allows flooding (right).

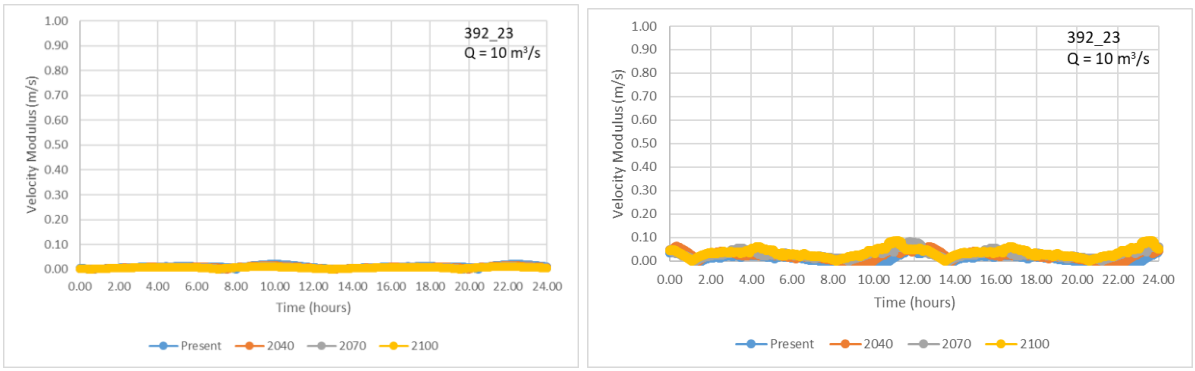


*Figure 4.12* Velocity time series over two tidal cycles for a river discharge of 10 $m^3/s$ at neap tide in the westernmost region of Castro Marim for the present bathymetry (left) and bathymetry that allows flooding (right).

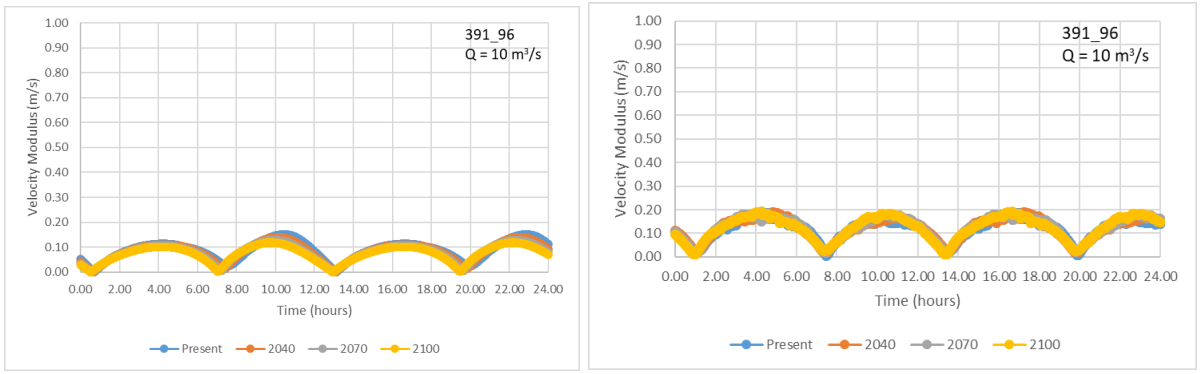


*Figure 4.13* Velocity time series over two tidal cycles for a river discharge of 10 $m^3/s$ at neap tide in the marsh area for the present bathymetry (left) and bathymetry that allows flooding (right).

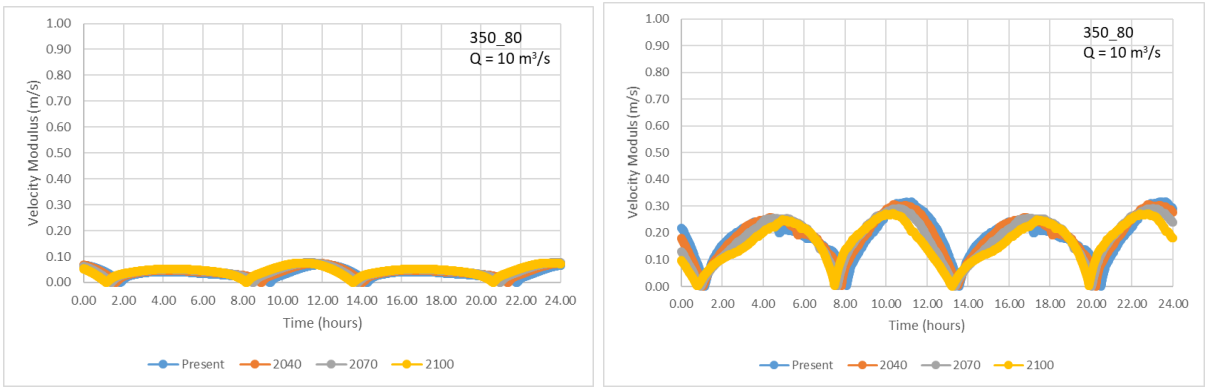


*Figure 4.14* Velocity time series over two tidal cycles for a river discharge of 10 $m^3/s$ at neap tide downstream Esteiro da Carrasqueira for the present bathymetry (left) and bathymetry that allows flooding (right).

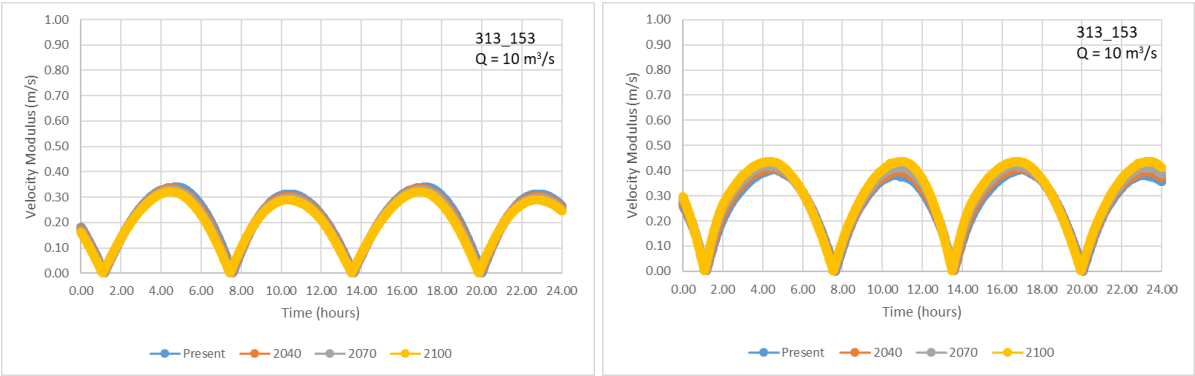


*Figure 4.15* Velocity time series over two tidal cycles for a river discharge of 10 $m^3/s$ at neap tide in the lower estuary for the present bathymetry (left) and bathymetry that allows flooding (right).

The results of a low discharge at neap tide over the present bathymetry also yield a decrease in velocity modulus with respect to mean sea level rise. However, the decrease in velocity is much less pronounced compared to the results observed for a high discharge. Again, closer to the marshes and the mouth of the estuary, there is an increase in velocity modulus for the bathymetry allowing flooding. A table summarizing the changes in velocity for the various locations in the estuary for the present bathymetry is shown in Table 4.3 and for the bathymetry allowing flooding in Table 4.4.

*Table 4.3* Changes in velocity modulus for a discharge of 10 $m^3/s$ at neap tide over the present bathymetry.

| | | Change in Velocity Modulus (m/s) | | |
|---|---|---|---|---|
| **Location** | | **Present - 2040** | **2040 - 2070** | **2070 - 2100** |
| **Upper Estuary** | 1377_45 | 9.87E-04 | 6.41E-04 | 1.17E-04 |
| | 1214_61 | 8.63E-04 | 5.80E-04 | 1.20E-04 |
| **Middle Estuary** | 903_102 | 1.45E-03 | 1.23E-03 | 7.26E-04 |
| | 558_103 | -1.37E-02 | 8.15E-03 | -3.05E-03 |
| **Lower Estuary** | 381_147 | -1.19E-03 | -1.46E-03 | -1.75E-03 |
| | 313_153 | -5.23E-03 | -4.69E-03 | -5.49E-03 |
| **Marshes** | 446_109 | -5.45E-04 | -4.66E-04 | -3.90E-04 |
| | 392_23 | -1.81E-03 | -1.37E-03 | -1.01E-03 |
| | 391_96 | -3.86E-03 | -4.70E-03 | -4.66E-03 |
| | 350_80 | 4.68E-03 | 2.49E-03 | 7.86E-04 |
| | 304_27 | 5.30E-04 | 1.54E-05 | -3.15E-04 |

*Table 4.4* Changes in velocity modulus for a discharge of 10 $m^3/s$ at neap tide over the bathymetry allowing flooding.

| | | Change in Velocity Modulus (m/s) | | |
|---|---|---|---|---|
| **Location** | | **Present - 2040** | **2040 - 2070** | **2070 - 2100** |
| **Upper Estuary** | 1377_45 | 8.80E-04 | 4.58E-04 | -5.98E-05 |
| | 1214_61 | 7.64E-04 | 3.68E-04 | -8.98E-05 |
| **Middle Estuary** | 903_102 | 1.38E-03 | 8.95E-04 | 3.71E-04 |
| | 558_103 | -6.02E-03 | -5.88E-03 | -6.46E-03 |
| **Lower Estuary** | 381_147 | 1.24E-02 | 1.17E-02 | 1.16E-02 |
| | 313_153 | 7.76E-03 | 9.61E-03 | 1.13E-02 |
| **Marshes** | 446_109 | 4.00E-04 | -4.90E-04 | -7.18E-04 |
| | 392_23 | 9.47E-03 | 6.12E-03 | 4.69E-03 |
| | 391_96 | 2.35E-03 | 2.33E-03 | -6.41E-04 |
| | 350_80 | -2.85E-04 | -8.05E-03 | -1.40E-02 |
| | 304_27 | 3.09E-03 | 1.88E-03 | -4.64E-04 |

### 4.2.3 Velocity Time Series at Spring Tide for a High Freshwater flow

The velocity modulus time series results at spring tide with a freshwater flow of 100 $m^3/s$ over the present bathymetry and bathymetry allowing flooding are shown in Figure 4.16, Figure 4.17, Figure 4.18, Figure 4.19, Figure 4.20, Figure 4.21 and Figure 4.22.

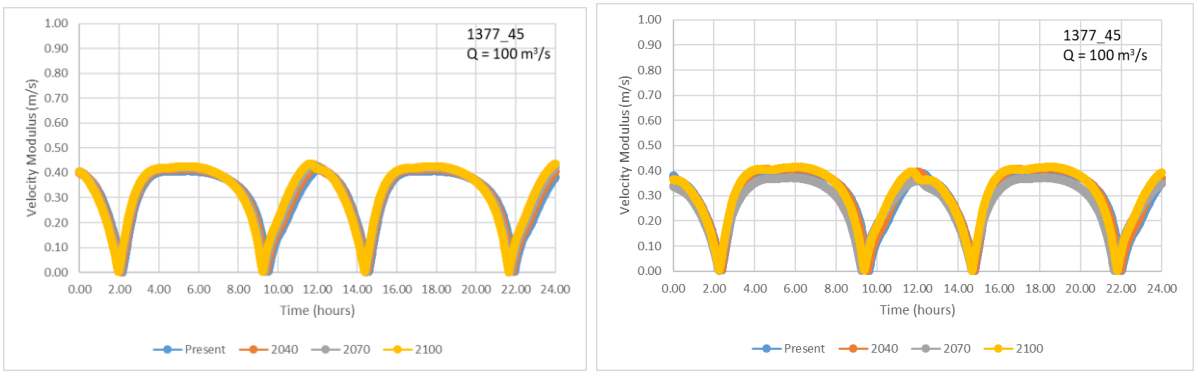


*Figure 4.16* Velocity time series over two tidal cycles for a river discharge of 100 $m^3/s$ at spring tide in the upper estuary for the present bathymetry (left) and bathymetry that allows flooding (right).

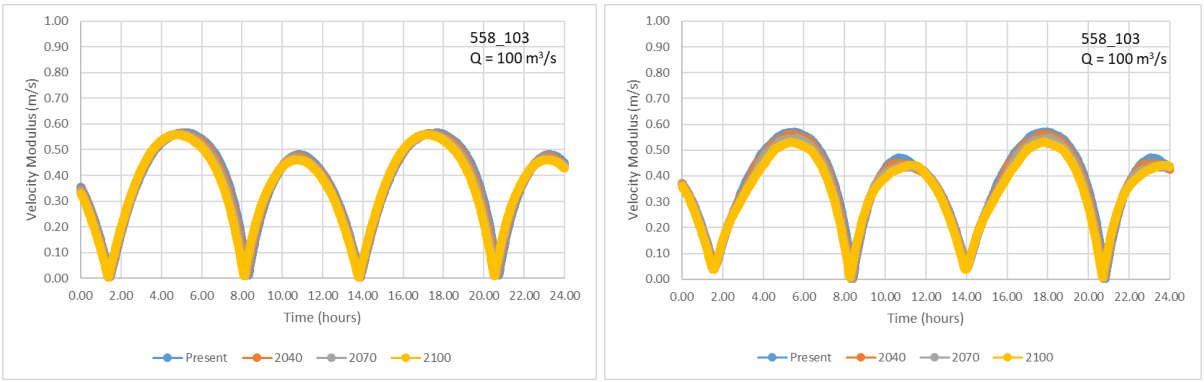


*Figure 4.17* Velocity time series over two tidal cycles for a river discharge of 100 $m^3/s$ at spring tide in the middle estuary for the present bathymetry (left) and bathymetry that allows flooding (right).

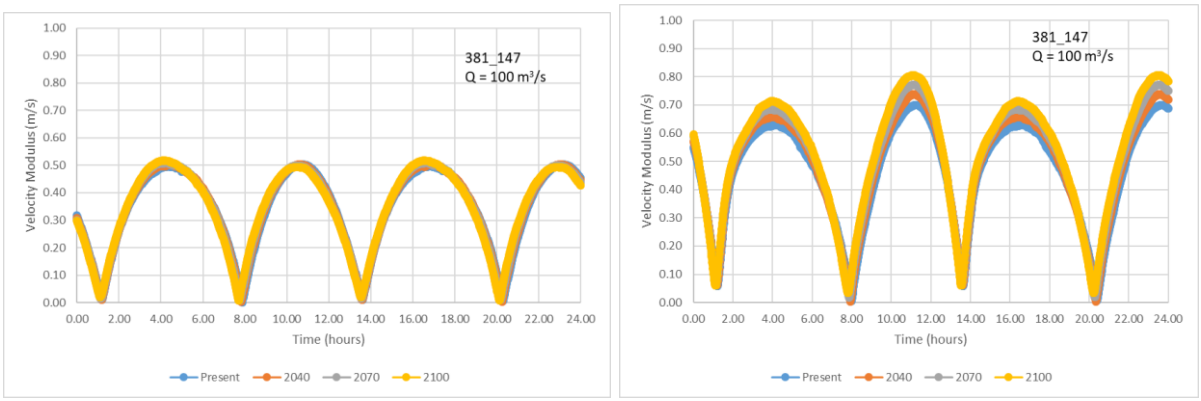


*Figure 4.18* Velocity time series over two tidal cycles for a river discharge of 100 $m^3/s$ at spring tide at the inlet into the marshes for the present bathymetry (left) and bathymetry that allows flooding (right).

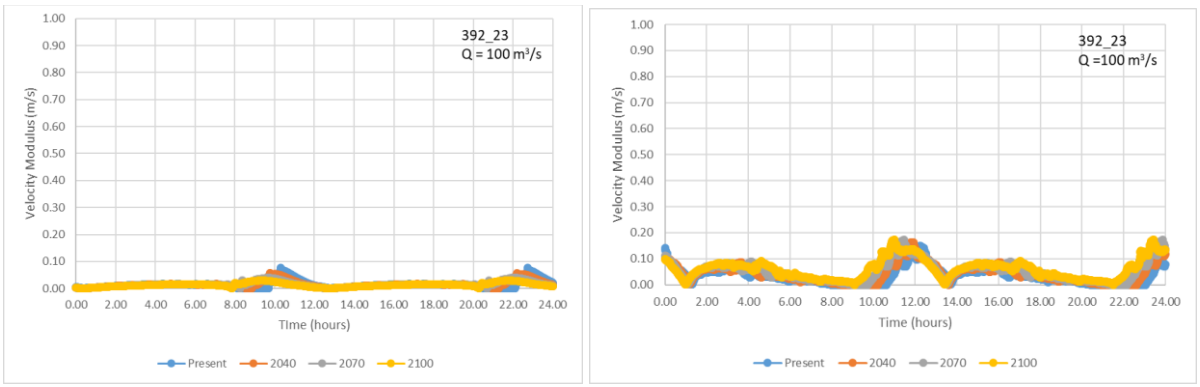


*Figure 4.19* Velocity time series over two tidal cycles for a river discharge of 100 $m^3/s$ at neap tide in the marsh area at the westernmost region of Castro Marim for the present bathymetry (left) and bathymetry that allows flooding (right).

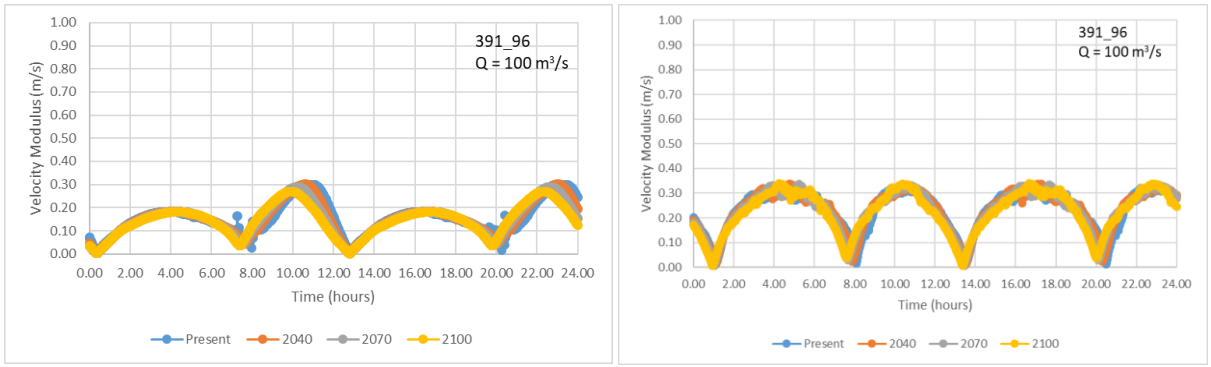


*Figure 4.20* Velocity time series over two tidal cycles for a river discharge of 100 $m^3/s$ at spring tide in the easternmost area of Castro Marim for the present bathymetry (left) and bathymetry that allows flooding (right).

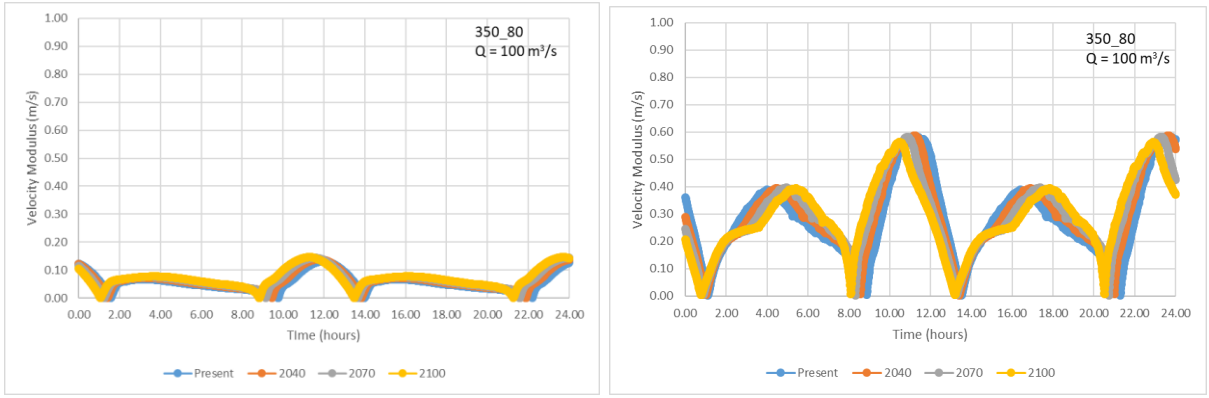


*Figure 4.21* Velocity time series over two tidal cycles for a river discharge of 100 $m^3/s$ at spring tide downstream Esteiro da Carrasqueira for the present bathymetry (left) and bathymetry that allows flooding (right).

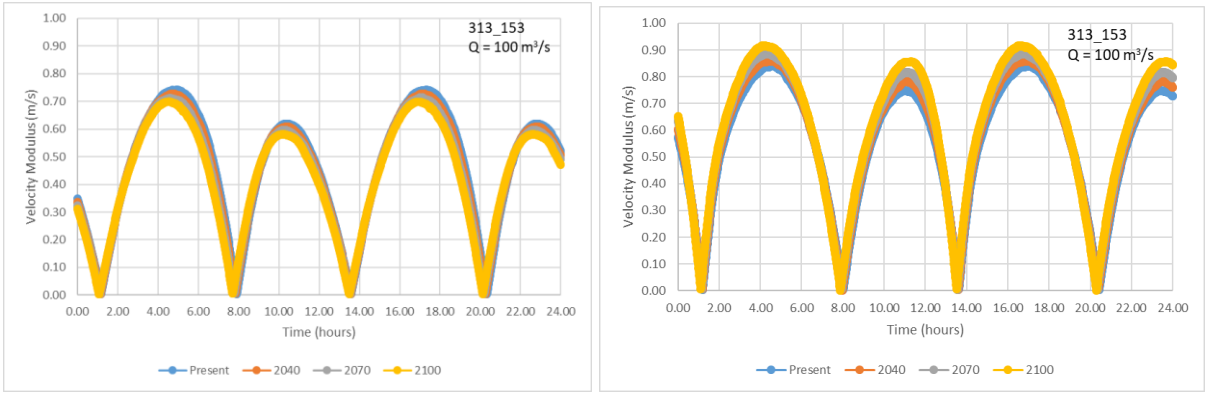


*Figure 4.22* Velocity time series over two tidal cycles for a river discharge of 100 $m^3/s$ at spring tide in the lower estuary for the present bathymetry (left) and bathymetry that allows flooding (right).

The results at spring tide combined with a high discharge from the Guadiana River are comparable to the results of neap tide combined with a high discharge from the Guadiana River. There is a general decrease in velocity with respect to an increase in mean sea level rise over the present bathymetry. There is an increase in velocity with respect to sea level rise close to the mouth of the estuary and in the marshes for the bathymetry allowing flooding. The velocity

values are much higher for spring tide compared to the velocity values for neap tide for both bathymetries. It can also be noted that downstream the estuary and in the marsh area velocity values are much higher for the bathymetry allowing flooding compared to the velocity values for the present bathymetry. These results are synonymous with the results produced at neap tide and again shows the impacts the bathymetry has on horizontal velocity. A summary of the evolution of velocity at spring tide for a high discharge of freshwater over the present bathymetry is shown in Table 4.5 and a summary for the results over the bathymetry allowing flooding is shown in Table 4.6.

*Table 4.5* Changes in velocity modulus for a discharge of 100 $m^3/s$ at spring tide over the present bathymetry.

| | | Change in Velocity Modulus (m/s) | | |
|---|---|---|---|---|
| **Location** | | **Present - 2040** | **2040 - 2070** | **2070 - 2100** |
| **Upper Estuary** | 1377_45 | 5.02E-03 | 4.21E-03 | 3.32E-03 |
| | 1214_61 | 4.03E-03 | 3.33E-03 | 2.69E-03 |
| **Middle Estuary** | 903_102 | 5.23E-03 | 4.31E-03 | 3.78E-03 |
| | 558_103 | -3.49E-03 | -3.84E-03 | -4.15E-03 |
| **Lower Estuary** | 381_147 | 2.71E-03 | 1.38E-03 | 2.97E-04 |
| | 313_153 | -9.06E-03 | -1.02E-02 | -1.03E-02 |
| **Marshes** | 446_109 | 4.78E-04 | -6.45E-04 | -7.96E-04 |
| | 392_23 | 4.56E-04 | -9.88E-04 | -1.71E-03 |
| | 391_96 | 3.20E-04 | -3.00E-03 | -4.80E-03 |
| | 350_80 | 5.72E-03 | 4.56E-03 | 3.45E-03 |
| | 304_27 | 8.31E-04 | 5.49E-04 | 2.94E-04 |

*Table 4.6* Changes in velocity modulus for a discharge of 100 $m^3/s$ at spring tide over the bathymetry allowing flooding.

| | | Change in Velocity Modulus (m/s) | | |
|---|---|---|---|---|
| **Location** | | **Present - 2040** | **2040 - 2070** | **2070 - 2100** |
| **Upper Estuary** | 1377_45 | 3.75E-03 | -2.94E-02 | 3.60E-02 |
| | 1214_61 | 2.87E-03 | 2.52E-03 | 2.01E-03 |
| **Middle Estuary** | 903_102 | 3.91E-03 | 3.16E-03 | 2.10E-03 |
| | 558_103 | -8.15E-03 | -9.03E-03 | -9.71E-03 |
| **Lower Estuary** | 381_147 | 2.10E-02 | 2.04E-02 | 1.76E-02 |
| | 313_153 | 1.79E-02 | 1.81E-02 | 1.77E-02 |
| **Marshes** | 446_109 | 4.64E-04 | 1.34E-03 | 2.38E-03 |
| | 392_23 | 8.53E-03 | 8.85E-03 | 7.92E-03 |
| | 391_96 | 1.16E-03 | -2.59E-03 | -5.38E-03 |
| | 350_80 | 1.06E-02 | 2.89E-03 | -3.35E-03 |
| | 304_27 | 6.52E-03 | 4.38E-03 | 2.68E-03 |

At spring tide with a high freshwater discharge there is no change in velocity modulus in the upper estuary for the present bathymetry. The uppermost region of the bathymetry allowing flooding, however results in a decrease in velocity modulus at first, followed by an increase in velocity after the year 2070. This could be attributed to the water being transported more outward toward the marshes and less upstream the main channel.

### 4.2.4 Velocity Time Series at Spring Tide for a Low Freshwater Discharge

The velocity time series results of a low discharge at spring tide are shown in Figure 4.23, Figure 4.24, Figure 4.25, Figure 4.26, Figure 4.27, Figure 4.28 and Figure 4.29.

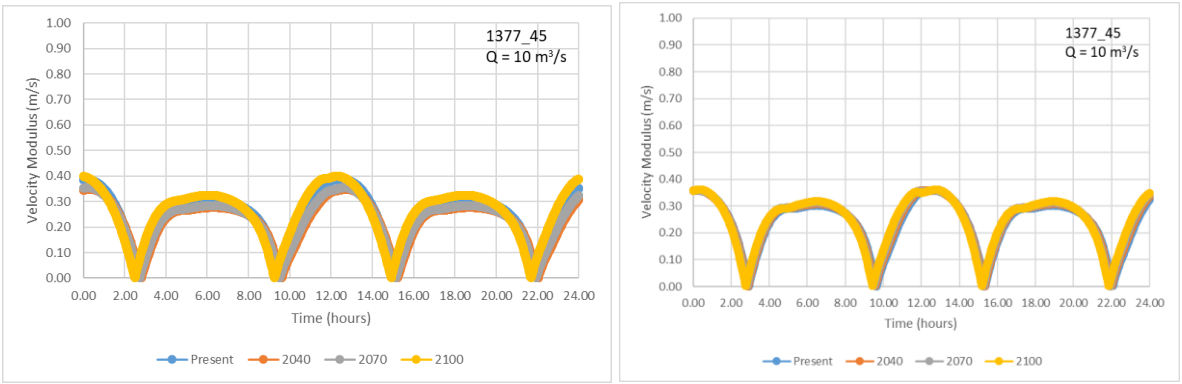


*Figure 4.23* Velocity time series over two tidal cycles for a river discharge of 10 $m^3/s$ at spring tide in the upper estuary for the present bathymetry (left) and bathymetry allowing flooding (right).

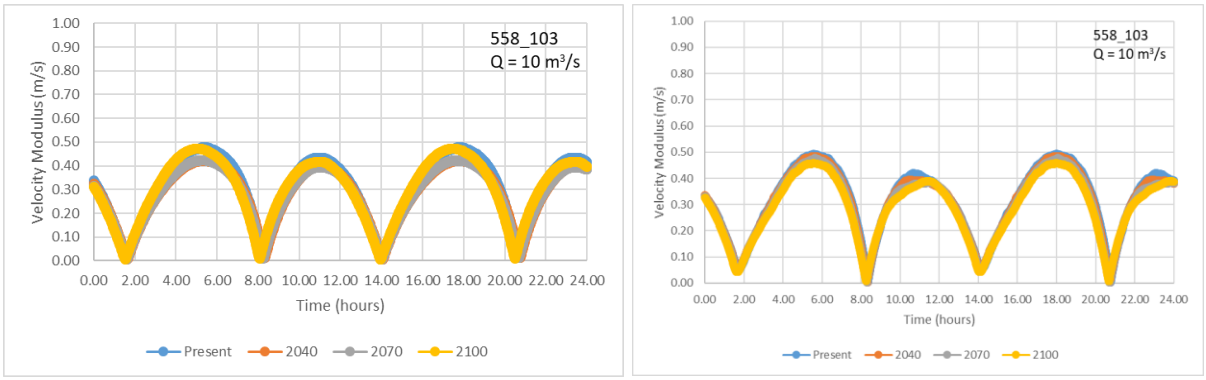


*Figure 4.24* Velocity time series over two tidal cycles for a river discharge of 10 $m^3/s$ at spring tide in the middle estuary for the present bathymetry (left) and bathymetry allowing flooding (right).

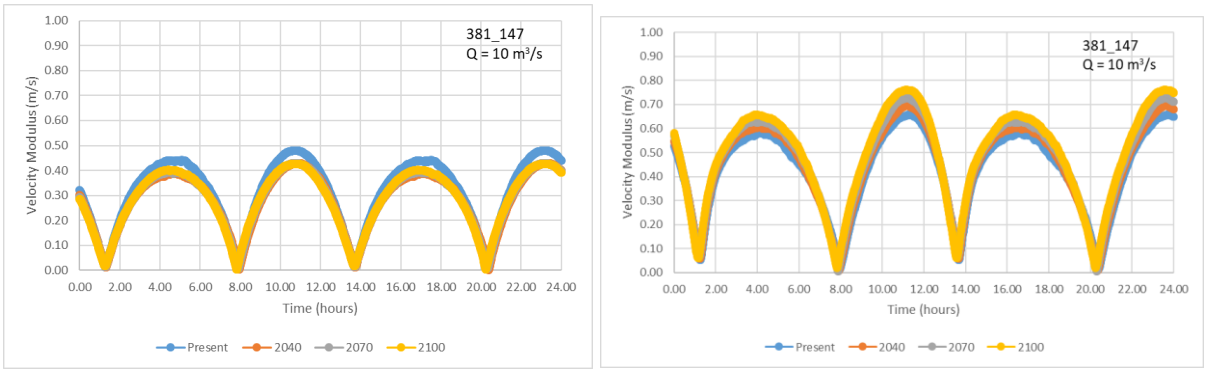


*Figure 4.25* Velocity time series over two tidal cycles for a river discharge of 10 $m^3/s$ at spring tide in the inlet into the marshes for the present bathymetry (left) and bathymetry allowing flooding (right).

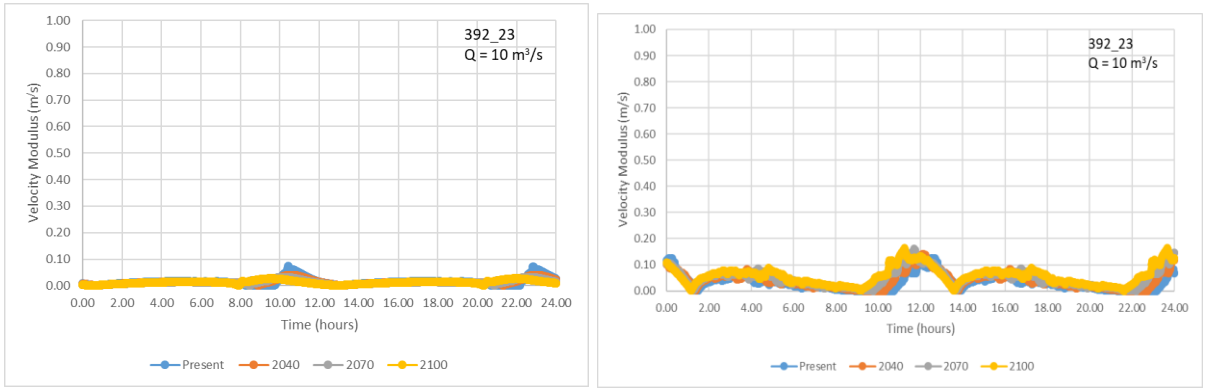


*Figure 4.26* Velocity time series over two tidal cycles for a river discharge of 10 $m^3/s$ at spring tide in the westernmost region of Castro Marim for the present bathymetry (left) and bathymetry allowing flooding (right).

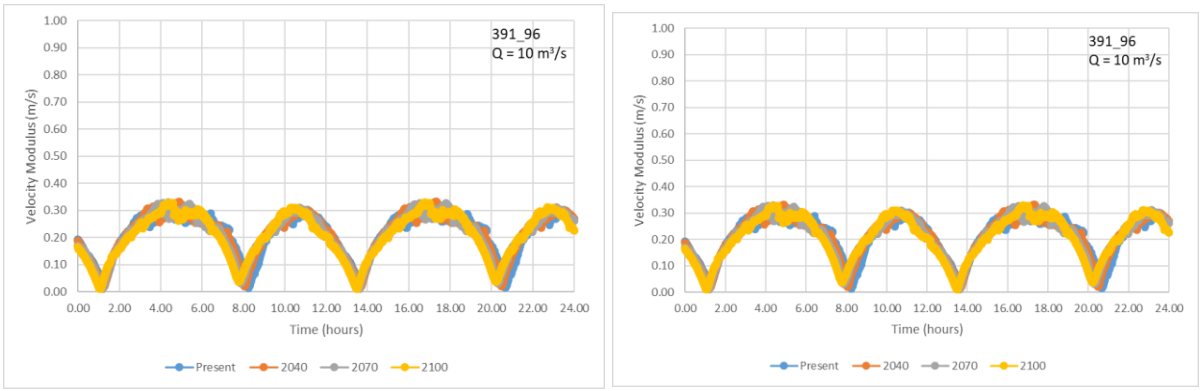


*Figure 4.27* Velocity time series over two tidal cycles for a river discharge of 10 $m^3/s$ at spring tide in the marsh area for the present bathymetry (left) and bathymetry allowing flooding (right).

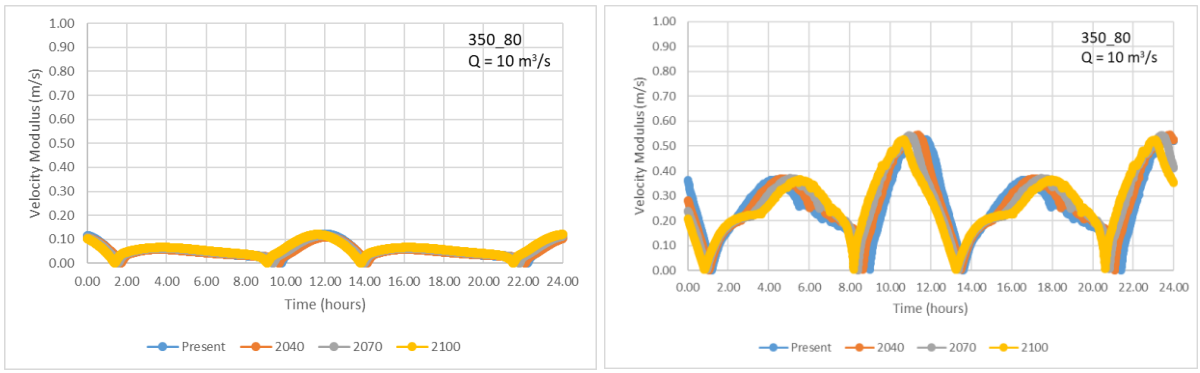


*Figure 4.28* Velocity time series over two tidal cycles for a river discharge of 10 $m^3/s$ at spring tide downstream Esteiro da Carrasqueira for the present bathymetry (left) and bathymetry that allows flooding (right).

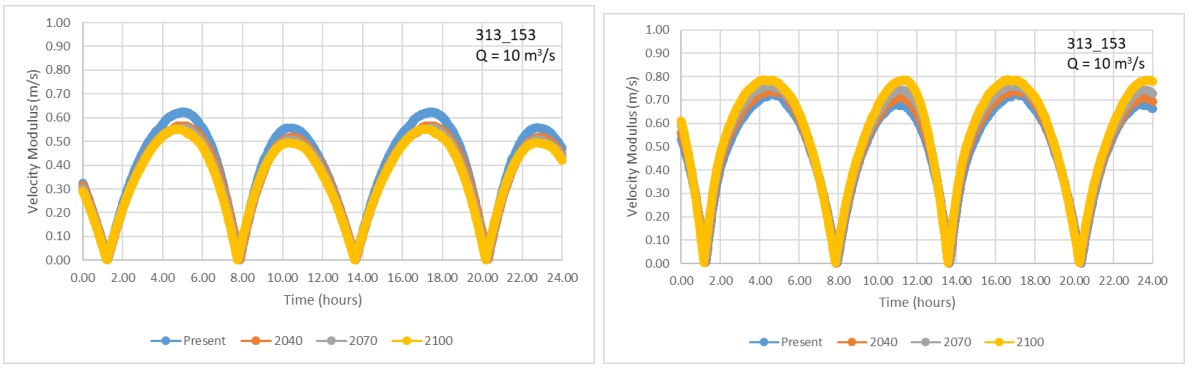


*Figure 4.29* Velocity time series over two tidal cycles for a river discharge of 10 $m^3/s$ at spring tide in the lower estuary for the present bathymetry (left) and bathymetry allowing flooding (right).

Again, velocity decreases with respect to mean sea level rise in the present bathymetry and increases for the bathymetry allowing flooding of the estuary. In the middle section of the main channel there is a consistent decrease in velocity as sea level increases for the bathymetry that allows flooding. However, for the present bathymetry at this location velocity decreases with the first change in mean sea level, but then begins to increase.

At the lower section of the estuary, the most dramatic decrease in velocity is for the present bathymetry between the present year and 2040. This could be due to the deepening of the channel as sea level increases. After 2040, there is a much smaller decrease in velocity in

response to the increase in sea level. For the bathymetry allowing flooding, there is a consistent increase in velocity for this section of the estuary.

The differences are much more pronounced near the mouth of the estuary and in the wetlands. The results are most likely attributed to the deepening of the channel due to the increase in mean sea level for the present bathymetry. The alternate bathymetry allows the surrounding land area to be flooded, thus water is transported by advection and results in an increase in velocity. The average change in velocity for each thirty-year period at each location in the estuary is shown in Table 4.7 for the present bathymetry and in Table 4.8

*Table 4.7* Changes in velocity modulus for a discharge of 10 $m^3/s$ at spring tide over the present bathymetry.

| | | Change in Velocity Modulus (m/s) | | |
|---|---|---|---|---|
| **Location** | | **Present - 2040** | **2040 - 2070** | **2070 - 2100** |
| **Upper Estuary** | 1377_45 | -2.23E-02 | 4.89E-03 | 2.86E-02 |
| | 1214_61 | -1.99E-02 | 4.04E-03 | 2.52E-02 |
| **Middle Estuary** | 903_102 | -2.02E-02 | 4.66E-03 | 2.76E-02 |
| | 558_103 | -2.84E-02 | -1.91E-03 | 2.08E-02 |
| **Lower Estuary** | 381_147 | -3.27E-02 | 1.90E-03 | 1.54E-03 |
| | 313_153 | -3.00E-02 | -6.86E-03 | -6.72E-03 |
| **Marshes** | 446_109 | -3.20E-04 | -6.18E-04 | -2.47E-04 |
| | 392_23 | -1.47E-03 | -8.97E-04 | -2.39E-04 |
| | 391_96 | -8.57E-03 | -1.01E-03 | -2.95E-03 |
| | 350_80 | -2.74E-03 | 4.52E-03 | 3.68E-03 |
| | 304_27 | -1.36E-03 | 6.10E-04 | 4.25E-04 |

*Table 4.8* Changes in velocity modulus for a discharge of 10 $m^3/s$ at spring tide over the bathymetry allowing flooding.

| | | Change in Velocity Modulus (m/s) | | |
|---|---|---|---|---|
| **Location** | | **Present - 2040** | **2040 - 2070** | **2070 - 2100** |
| **Upper Estuary** | 1377_45 | 3.62E-03 | 2.82E-03 | 1.84E-03 |
| | 1214_61 | 2.92E-03 | 2.18E-03 | 1.36E-03 |
| **Middle Estuary** | 903_102 | 3.57E-03 | 2.81E-03 | 1.74E-03 |
| | 558_103 | -7.19E-03 | -8.34E-03 | -8.89E-03 |
| **Lower Estuary** | 381_147 | 2.04E-02 | 2.03E-02 | 1.67E-02 |
| | 313_153 | 1.81E-02 | 1.79E-02 | 1.65E-02 |
| **Marshes** | 446_109 | 3.24E-04 | 8.38E-04 | 1.68E-03 |
| | 392_23 | 8.15E-03 | 8.58E-03 | 7.35E-03 |
| | 391_96 | 5.34E-04 | -1.89E-03 | -4.09E-03 |
| | 350_80 | 8.27E-03 | 2.14E-03 | -3.64E-03 |
| | 304_27 | 5.75E-03 | 3.50E-03 | 2.36E-03 |

The upper and middle sections of the estuary for the present bathymetry experience an initial decrease in velocity followed by an increase in velocity after the year 2070. These two sections of the estuary experience little to no change in velocity for a high freshwater discharge and at both freshwater discharge scenarios. The initial decrease in velocity could be attributed to the smaller discharge. The increase in velocity after the year 2070 could be attributed to the stronger influence of the tide with such a high sea level. The lower section of the estuary results in an overall decrease in velocity modulus for the present bathymetry, which could be attributed to the deepening of the channel. An increase in velocity is found at both the lower estuary and in the marsh area for the bathymetry allowing flooding.

## 4.3 Evolution of Water Elevation

The hydrodynamic results for water elevation are consistent with the water levels that were forced in the model. More explicitly, water level increased by 0.24 meters every thirty years at each location except for in the marsh area where the change in water level is more variable. As the number of time series graphs produced is high and shows nearly the same result at all locations, the time series results are displayed in the appendix. A summary of the changes in water elevation based on the average water elevation in a 24-hour period is shown in Table 4.9, Table 4.10, Table 4.11, Table 4.12, Table 4.13, Table 4.14, Table 4.15 and Table 4.16.

*Table 4.9* Change in water elevation for a freshwater discharge of 100 $m^3/s$ at neap tide over the present bathymetry.

| | | Change in Elevation (m) | | |
|---|---|---|---|---|
| **Location** | | **Present - 2040** | **2040 - 2070** | **2070 - 2100** |
| **Upper Estuary** | 1377_45 | 2.29E-01 | 2.30E-01 | 2.37E-01 |
| | 1214_61 | 2.30E-01 | 2.31E-01 | 2.38E-01 |
| **Middle Estuary** | 903_102 | 2.31E-01 | 2.33E-01 | 2.39E-01 |
| | 558_103 | 2.34E-01 | 2.35E-01 | 2.41E-01 |
| **Lower Estuary** | 381_147 | 2.35E-01 | 2.36E-01 | 2.42E-01 |
| | 313_153 | 2.36E-01 | 2.37E-01 | 2.43E-01 |
| **Marshes** | 446_109 | 2.33E-01 | 2.36E-01 | 2.42E-01 |
| | 392_23 | 2.34E-01 | 2.37E-01 | 2.43E-01 |
| | 391_96 | 2.32E-01 | 2.35E-01 | 2.42E-01 |
| | 350_80 | 1.85E-01 | 2.00E-01 | 2.16E-01 |
| | 304_27 | 1.85E-01 | 2.00E-01 | 2.16E-01 |

*Table 4.10* Change in water elevation for a freshwater discharge of 100 $m^3/s$ at neap tide over the bathymetry allowing flooding.

| | | Change in Elevation (m) | | |
|---|---|---|---|---|
| **Location** | | **Present - 2040** | **2040 - 2070** | **2070 - 2100** |
| **Upper Estuary** | 1377_45 | 2.31E-01 | 2.32E-01 | 2.38E-01 |
| | 1214_61 | 2.32E-01 | 2.33E-01 | 2.39E-01 |
| **Middle Estuary** | 903_102 | 2.33E-01 | 2.35E-01 | 2.40E-01 |
| | 558_103 | 2.35E-01 | 2.37E-01 | 2.42E-01 |
| **Lower Estuary** | 381_147 | 2.36E-01 | 2.37E-01 | 2.43E-01 |
| | 313_153 | 2.36E-01 | 2.37E-01 | 2.43E-01 |
| **Marshes** | 446_109 | 2.35E-01 | 2.36E-01 | 2.41E-01 |
| | 392_23 | 1.30E-01 | 1.63E-01 | 2.14E-01 |
| | 391_96 | 2.35E-01 | 2.36E-01 | 2.41E-01 |
| | 350_80 | 2.24E-01 | 2.30E-01 | 2.38E-01 |
| | 304_27 | 2.25E-01 | 2.30E-01 | 2.37E-01 |

*Table 4.11* Change in water elevation for a freshwater discharge of 10 $m^3/s$ at neap tide over the present bathymetry.

| | | Change in Elevation (m) | | |
|---|---|---|---|---|
| **Location** | | **Present - 2040** | **2040 - 2070** | **2070 - 2100** |
| **Upper Estuary** | 1377_45 | 2.34E-01 | 2.35E-01 | 2.41E-01 |
| | 1214_61 | 2.34E-01 | 2.35E-01 | 2.42E-01 |
| **Middle Estuary** | 903_102 | 2.34E-01 | 2.35E-01 | 2.42E-01 |
| | 558_103 | 2.40E-01 | 2.32E-01 | 2.43E-01 |
| **Lower Estuary** | 381_147 | 2.36E-01 | 2.37E-01 | 2.43E-01 |
| | 313_153 | 2.36E-01 | 2.37E-01 | 2.43E-01 |
| **Marshes** | 446_109 | 2.32E-01 | 2.35E-01 | 2.42E-01 |
| | 392_23 | 2.33E-01 | 2.36E-01 | 2.42E-01 |
| | 391_96 | 2.31E-01 | 2.35E-01 | 2.42E-01 |
| | 350_80 | 1.90E-01 | 2.04E-01 | 2.19E-01 |
| | 304_27 | 1.90E-01 | 2.04E-01 | 2.19E-01 |

*Table 4.12* Change in water elevation for a freshwater discharge of 10 $m^3/s$ at neap tide over the bathymetry allowing flooding.

| | | Change in Elevation (m) | | |
|---|---|---|---|---|
| **Location** | | **Present - 2040** | **2040 - 2070** | **2070 - 2100** |
| **Upper Estuary** | 1377_45 | 2.35E-01 | 2.37E-01 | 2.42E-01 |
| | 1214_61 | 2.36E-01 | 2.37E-01 | 2.42E-01 |
| **Middle Estuary** | 903_102 | 2.36E-01 | 2.38E-01 | 2.43E-01 |
| | 558_103 | 2.37E-01 | 2.38E-01 | 2.44E-01 |
| **Lower Estuary** | 381_147 | 2.36E-01 | 2.38E-01 | 2.43E-01 |
| | 313_153 | 2.36E-01 | 2.38E-01 | 2.43E-01 |
| **Marshes** | 446_109 | 2.34E-01 | 2.36E-01 | 2.40E-01 |
| | 392_23 | 1.34E-01 | 1.70E-01 | 2.18E-01 |
| | 391_96 | 2.35E-01 | 2.37E-01 | 2.41E-01 |
| | 350_80 | 2.23E-01 | 2.29E-01 | 2.37E-01 |
| | 304_27 | 2.23E-01 | 2.29E-01 | 2.36E-01 |

*Table 4.13* Change in water elevation for a freshwater discharge of 100 $m^3/s$ at spring tide over the present bathymetry.

| | | Change in Elevation (m) | | |
|---|---|---|---|---|
| **Location** | | **Present - 2040** | **2040 - 2070** | **2070 - 2100** |
| **Upper Estuary** | 1377_45 | 2.23E-01 | 2.24E-01 | 2.30E-01 |
| | 1214_61 | 2.24E-01 | 2.25E-01 | 2.31E-01 |
| **Middle Estuary** | 903_102 | 2.25E-01 | 2.27E-01 | 2.33E-01 |
| | 558_103 | 2.28E-01 | 2.30E-01 | 2.36E-01 |
| **Lower Estuary** | 381_147 | 2.31E-01 | 2.33E-01 | 2.39E-01 |
| | 313_153 | 2.32E-01 | 2.34E-01 | 2.40E-01 |
| **Marshes** | 446_109 | 1.92E-01 | 2.21E-01 | 2.34E-01 |
| | 392_23 | 1.83E-01 | 2.13E-01 | 2.32E-01 |
| | 391_96 | 2.13E-01 | 2.21E-01 | 2.32E-01 |
| | 350_80 | 1.57E-01 | 1.64E-01 | 1.76E-01 |
| | 304_27 | 1.57E-01 | 1.64E-01 | 1.76E-01 |

*Table 4.14* Change in water elevation for a freshwater discharge of 100 $m^3/s$ at spring tide over the bathymetry allowing flooding.

| | | Change in Elevation (m) | | |
|---|---|---|---|---|
| **Location** | | **Present - 2040** | **2040 - 2070** | **2070 - 2100** |
| **Upper Estuary** | 1377_45 | 2.27E-01 | 2.28E-01 | 2.33E-01 |
| | 1214_61 | 2.28E-01 | 2.29E-01 | 2.34E-01 |
| **Middle Estuary** | 903_102 | 2.29E-01 | 2.30E-01 | 2.36E-01 |
| | 558_103 | 2.32E-01 | 2.33E-01 | 2.39E-01 |
| **Lower Estuary** | 381_147 | 2.33E-01 | 2.35E-01 | 2.41E-01 |
| | 313_153 | 2.33E-01 | 2.35E-01 | 2.41E-01 |
| **Marshes** | 446_109 | 2.12E-01 | 2.22E-01 | 2.33E-01 |
| | 392_23 | 1.29E-01 | 1.44E-01 | 1.68E-01 |
| | 391_96 | 2.19E-01 | 2.24E-01 | 2.33E-01 |
| | 350_80 | 1.85E-01 | 1.96E-01 | 2.10E-01 |
| | 304_27 | 1.86E-01 | 1.97E-01 | 2.11E-01 |

*Table 4.15* Change in water elevation for a freshwater discharge of 10 $m^3/s$ at spring tide over the present bathymetry.

| | | Change in Elevation (m) | | |
|---|---|---|---|---|
| **Location** | | **Present - 2040** | **2040 - 2070** | **2070 - 2100** |
| **Upper Estuary** | 1377_45 | 2.44E-01 | 2.30E-01 | 2.22E-01 |
| | 1214_61 | 2.44E-01 | 2.30E-01 | 2.22E-01 |
| **Middle Estuary** | 903_102 | 2.46E-01 | 2.30E-01 | 2.21E-01 |
| | 558_103 | 2.47E-01 | 2.31E-01 | 2.23E-01 |
| **Lower Estuary** | 381_147 | 2.45E-01 | 2.33E-01 | 2.39E-01 |
| | 313_153 | 2.43E-01 | 2.34E-01 | 2.40E-01 |
| **Marshes** | 446_109 | 2.14E-01 | 2.18E-01 | 2.18E-01 |
| | 392_23 | 2.05E-01 | 2.10E-01 | 2.18E-01 |
| | 391_96 | 2.28E-01 | 2.16E-01 | 2.28E-01 |
| | 350_80 | 1.92E-01 | 1.71E-01 | 1.81E-01 |
| | 304_27 | 1.92E-01 | 1.71E-01 | 1.81E-01 |

*Table 4.16* Change in water elevation for a freshwater discharge of 10 $m^3/s$ at spring tide over the bathymetry allowing flooding.

| | | Change in Elevation (m) | | |
|---|---|---|---|---|
| **Location** | | **Present - 2040** | **2040 - 2070** | **2070 - 2100** |
| **Upper Estuary** | 1377_45 | 2.33E-01 | 2.34E-01 | 2.39E-01 |
| | 1214_61 | 2.33E-01 | 2.35E-01 | 2.40E-01 |
| **Middle Estuary** | 903_102 | 2.33E-01 | 2.35E-01 | 2.40E-01 |
| | 558_103 | 2.35E-01 | 2.37E-01 | 2.42E-01 |
| **Lower Estuary** | 381_147 | 2.34E-01 | 2.37E-01 | 2.42E-01 |
| | 313_153 | 2.34E-01 | 2.36E-01 | 2.42E-01 |
| **Marshes** | 446_109 | 2.09E-01 | 2.17E-01 | 2.29E-01 |
| | 392_23 | 1.34E-01 | 1.48E-01 | 1.73E-01 |
| | 391_96 | 2.18E-01 | 2.22E-01 | 2.30E-01 |
| | 350_80 | 1.84E-01 | 1.95E-01 | 2.08E-01 |
| | 304_27 | 1.85E-01 | 1.95E-01 | 2.08E-01 |

## 4.4 Temporal Evolution of Salinity

The time series results of salinity are shown for the same locations mentioned in section 4.1 allowing an assessment of how salinity changes at each location for a period of two tidal cycles with respect to sea level rise. The model simulations for salt transport assume a salinity value of 0 for freshwater from the Guadiana River and a value of 36 for seawater from the Gulf of Cadiz. Thus, the salinity values for the Guadiana Estuary will lie between 0 and 36. The salinity values are represented as simply numbers without units, which is recommended by UNESCO (1981).

### 4.4.1 Salinity Time Series at Neap Tide with a High Freshwater Discharge

Figure 4.30, Figure 4.31, Figure 4.32, Figure 4.33, Figure 4.34, Figure 4.35 and Figure 4.36 show the temporal evolution of salinity in the Guadiana Estuary with a high discharge from the Guadiana River during neap tide.

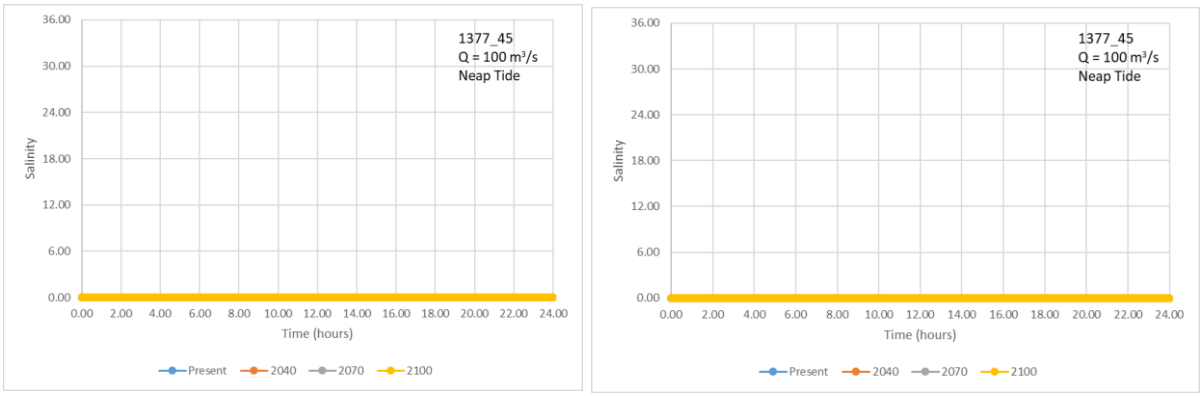


*Figure 4.30* Salinity time series over two tidal cycles for a river discharge of 100 $m^3/s$ at neap tide in the upper estuary for the present bathymetry (left) and bathymetry allowing flooding (right).

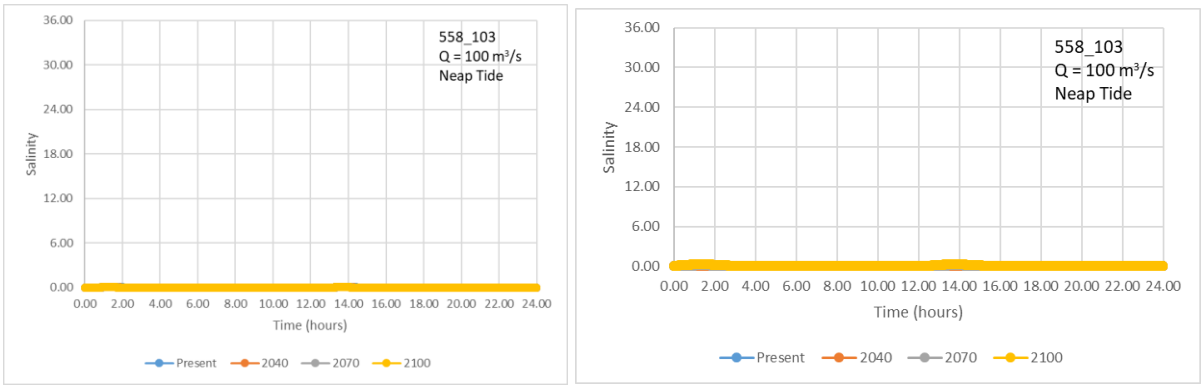


*Figure 4.31* Salinity time series over two tidal cycles for a river discharge of 100 $m^3/s$ at neap tide in the middle estuary for the present bathymetry (left) and bathymetry allowing flooding (right).

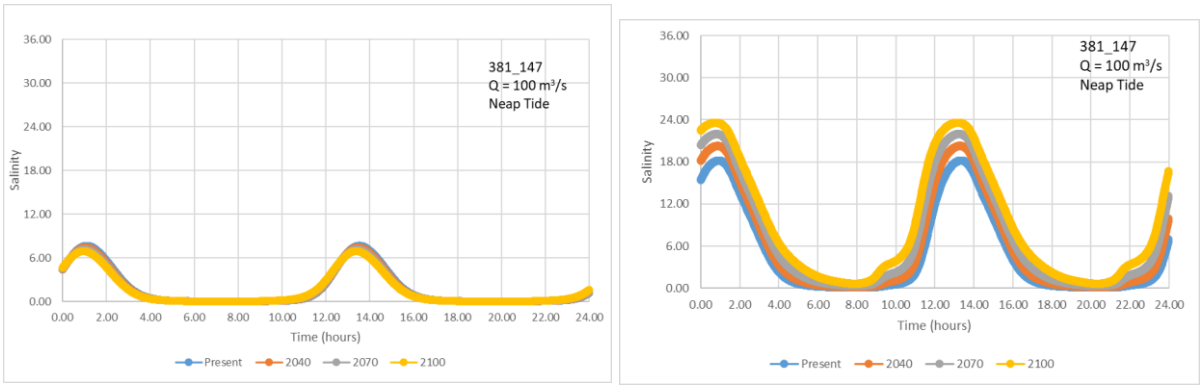


*Figure 4.32* Salinity time series over two tidal cycles for a river discharge of 100 $m^3/s$ at neap tide at the inlet into the marshes for the present bathymetry (left) and bathymetry allowing flooding (right).

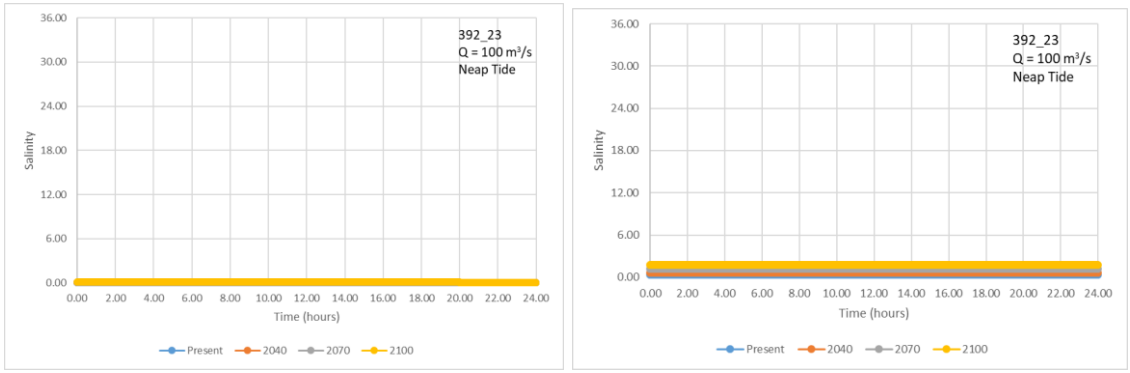


*Figure 4.33* Salinity time series over two tidal cycles for a river discharge of 100 $m^3/s$ at neap tide at the westernmost region of Castro Marim for the present bathymetry (left) and bathymetry allowing flooding (right).

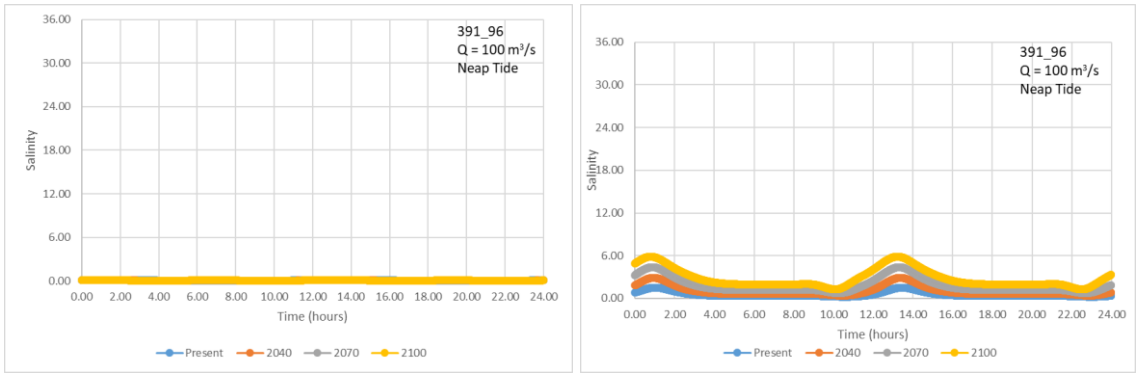


*Figure 4.34* Salinity time series over two tidal cycles for a river discharge of 100 $m^3/s$ at neap tide in the easternmost region of Castro Marim for the present bathymetry (left) and bathymetry allowing flooding (right).

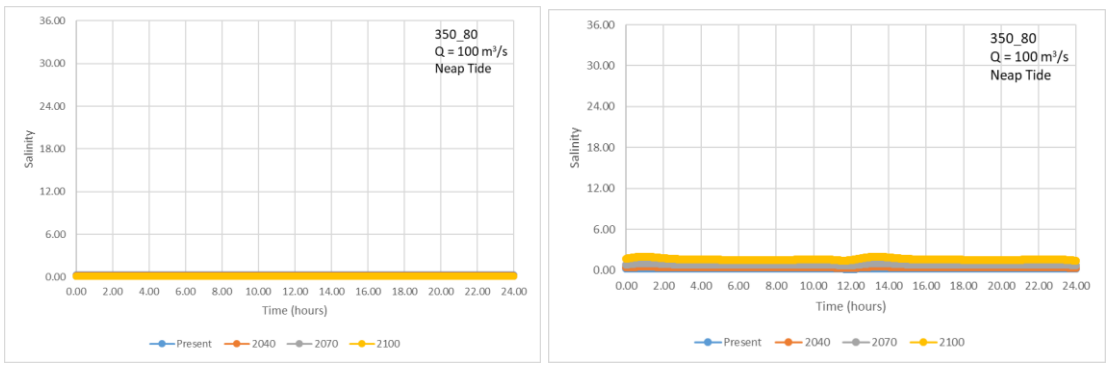


*Figure 4.35* Salinity time series over two tidal cycles for a river discharge of 100 $m^3/s$ at neap tide downstream Esteiro da Carrasqueira for the present bathymetry (left) and bathymetry that allows flooding (right).

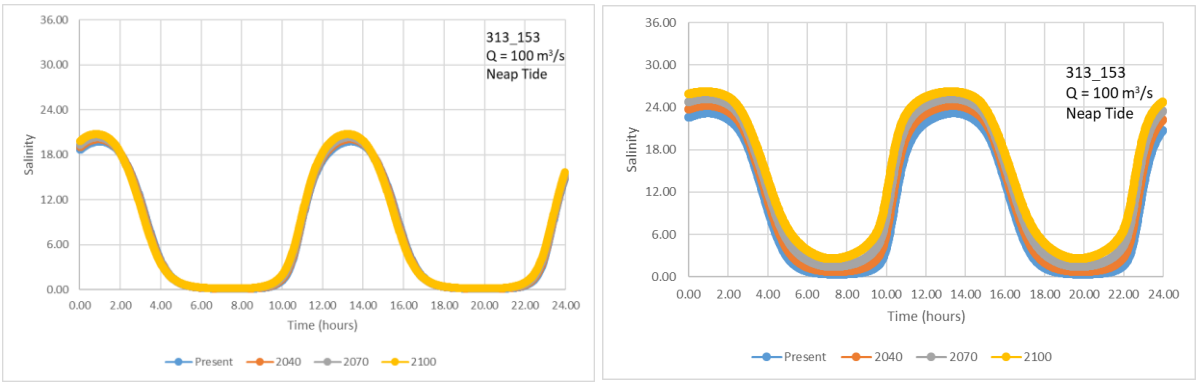


*Figure 4.36* Salinity time series over two tidal cycles for a river discharge of 100 $m^3/s$ at neap tide in the lower estuary for the present bathymetry (left) and bathymetry allowing flooding (right).

There is a slight increase in salinity due to mean sea level rise over the present bathymetry at neap tide for a high freshwater discharge. The increase in salinity is much more pronounced for the bathymetry allowing flooding. It can be noted that the increase in salinity corresponds with a decrease in velocity modulus based on the hydrodynamic results in section 4.2. The average change in salinity for each thirty-year interval at each point used in the time series was computed in excel and displayed in Table 4.17. The average change in salinity for the bathymetry allowing flooding is shown in Table 4.18.

*Table 4.17 Change in salinity for a discharge of 100 $m^3/s$ at neap tide over the present bathymetry.*

| | | Change in Salinity | | |
|---|---|---|---|---|
| **Location** | | **Present – 2040** | **2040 – 2070** | **2070 – 2100** |
| **Upper Estuary** | 1377_45 | -2.46E-11 | 1.14E-10 | -9.19E-11 |
| | 1214_61 | 1.77E-11 | 1.50E-10 | -1.20E-10 |
| **Middle Estuary** | 903_102 | 9.45E-11 | -3.92E-12 | -2.47E-10 |
| | 558_103 | -6.53E-05 | -1.78E-05 | 6.43E-06 |
| **Lower Estuary** | 381_147 | -5.05E-02 | -5.26E-02 | -2.83E-02 |
| | 313_153 | 6.33E-02 | 4.63E-02 | 1.27E-01 |
| **Marshes** | 446_109 | -9.91E-03 | 2.73E-03 | 2.54E-02 |
| | 392_23 | -8.09E-03 | 7.70E-03 | 4.19E-02 |
| | 391_96 | -1.29E-02 | -4.66E-03 | 6.06E-03 |
| | 350_80 | -1.24E-01 | -4.85E-02 | -1.28E-02 |
| | 304_27 | -1.48E-01 | -4.93E-02 | -2.23E-03 |

*Table 4.18* Changes in salinity for a discharge of 100 $m^3/s$ at neap tide over bathymetry allowing flooding.

| | | Change in Salinity | | |
|---|---|---|---|---|
| **Location** | | **Present - 2040** | **2040 - 2070** | **2070 - 2100** |
| **Upper Estuary** | 1377_45 | 1.76E-10 | 1.10E-10 | 3.43E-11 |
| | 1214_61 | 3.15E-10 | 4.79E-11 | 1.23E-10 |
| **Middle Estuary** | 903_102 | 5.74E-08 | 2.15E-08 | 5.57E-02 |
| | 558_103 | 5.27E-03 | 1.39E-02 | 3.20E-02 |
| **Lower Estuary** | 381_147 | 1.03E+00 | 1.19E+00 | 1.49E+00 |
| | 313_153 | 1.10E+00 | 1.19E+00 | 1.44E+00 |
| **Marshes** | 446_109 | 3.69E-01 | 7.18E-01 | 9.01E-01 |
| | 392_23 | 2.55E-01 | 5.50E-01 | 5.65E-01 |
| | 391_96 | 4.92E-01 | 7.68E-01 | 9.89E-01 |
| | 350_80 | 1.90E-01 | 4.37E-01 | 7.66E-01 |
| | 304_27 | 1.76E-01 | 4.10E-01 | 7.10E-01 |

Table 4.17 and Table 4.18 portray the differences in the evolution of salinity between the two bathymetries. Both bathymetries have zero change in salinity in the upper estuary because the salinity does not reach these two locations given the high freshwater discharge and smaller tidal amplitude. The middle section of the estuary, close to the lower estuary, experiences a small increase in salinity only for the bathymetry allowing flooding. For the present bathymetry, the lower estuary experiences a decrease in salinity at the location closest to the inlet at Esteiro da Leziria. However, for the bathymetry allowing flooding at this location shows an increase in salinity. The salinity values here are also much higher for the bathymetry allowing flooding, which demonstrates the ability of the flooding bathymetry to transport salt horizontally to the wetlands. Nearly all marshes and wetlands for the present bathymetry experience a small decrease in salinity, however the salinity increases drastically at these locations when the bathymetry allows flooding. This is most likely attributed to the salt being transported horizontally in these directions, as this bathymetry allows the water to spread horizontally in these areas, as opposed to being confined in the basin.

### 4.4.2 Salinity Time Series at Neap Tide with a Low Freshwater Discharge

The results for a low discharge at neap tide at each location of the estuary are shown in Figure 4.37, Figure 4.38, Figure 4.39, Figure 4.40, Figure 4.41, Figure 4.42 and Figure 4.43.

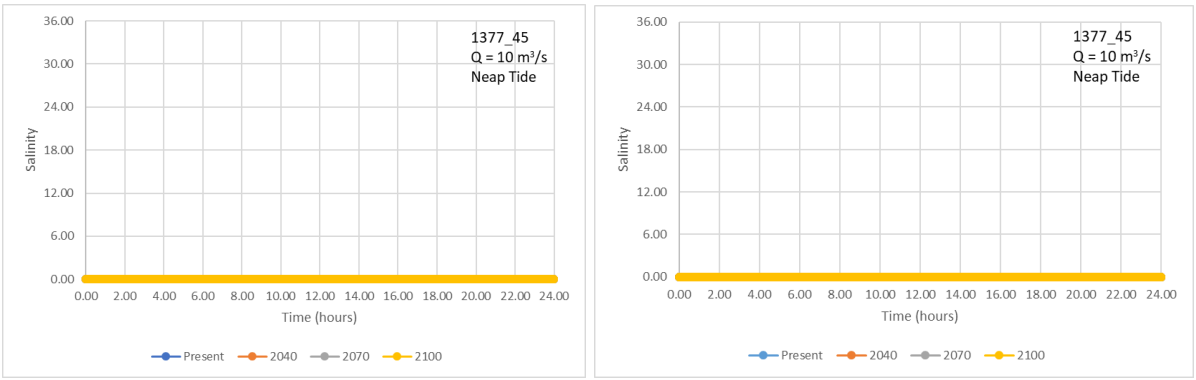


*Figure 4.37* Salinity time series over two tidal cycles for a river discharge of 10 $m^3/s$ at neap tide in the upper estuary for the present bathymetry (left) and bathymetry allowing flooding (right).

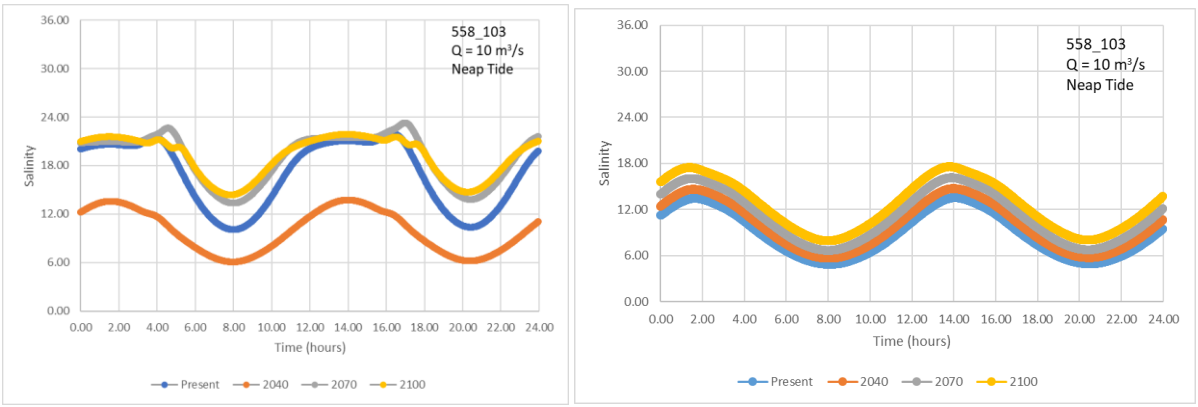


*Figure 4.38* Salinity time series over two tidal cycles for a river discharge of 10 $m^3/s$ at neap tide in the middle estuary for the present bathymetry (left) and bathymetry allowing flooding (right).

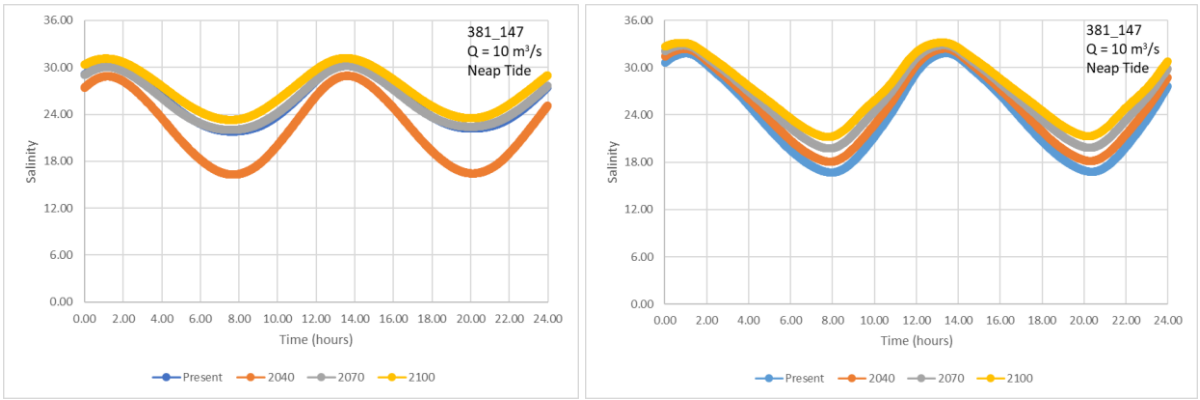


*Figure 4.39* Salinity time series over two tidal cycles for a river discharge of 10 $m^3/s$ at neap tide at the inlet into the marshes for the present bathymetry (left) and bathymetry allowing flooding (right).

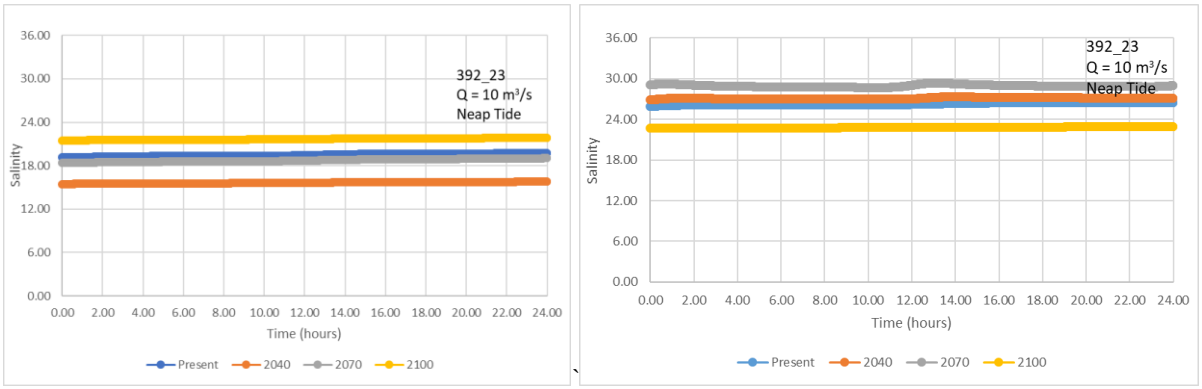


*Figure 4.40* Salinity time series over two tidal cycles for a river discharge of 10 $m^3/s$ at neap tide at the westernmost region of Castro Marim for the present bathymetry (left) and bathymetry allowing flooding (right).

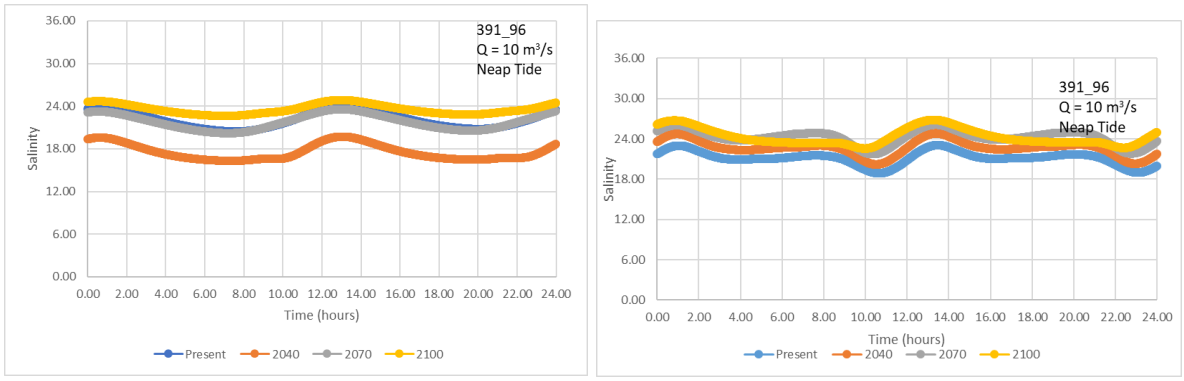


*Figure 4.41* Salinity time series over two tidal cycles for a river discharge of 10 $m^3/s$ at neap tide in the easternmost region of Castro Marim for the present bathymetry (left) and bathymetry allowing flooding (right).

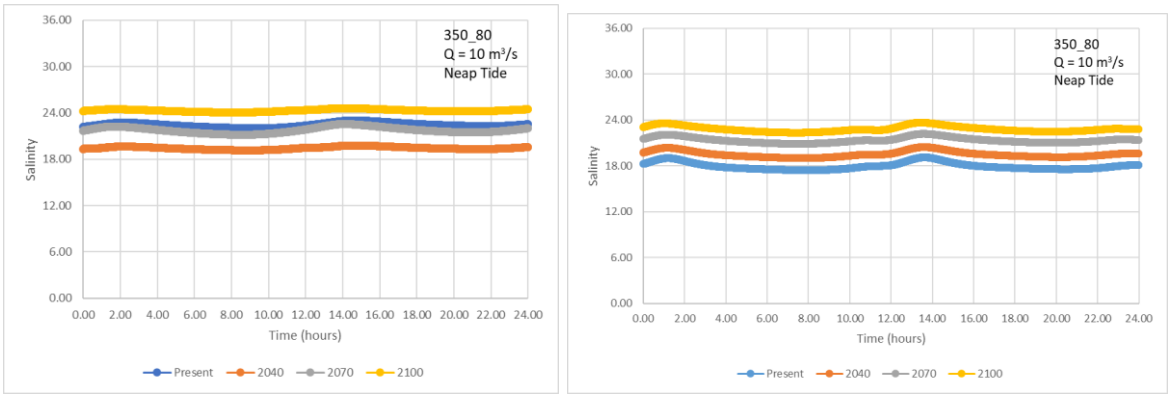


*Figure 4.42* Salinity time series over two tidal cycles for a river discharge of 10 $m^3/s$ at neap tide downstream Esteiro da Carrasqueira for the present bathymetry (left) and bathymetry that allows flooding (right).

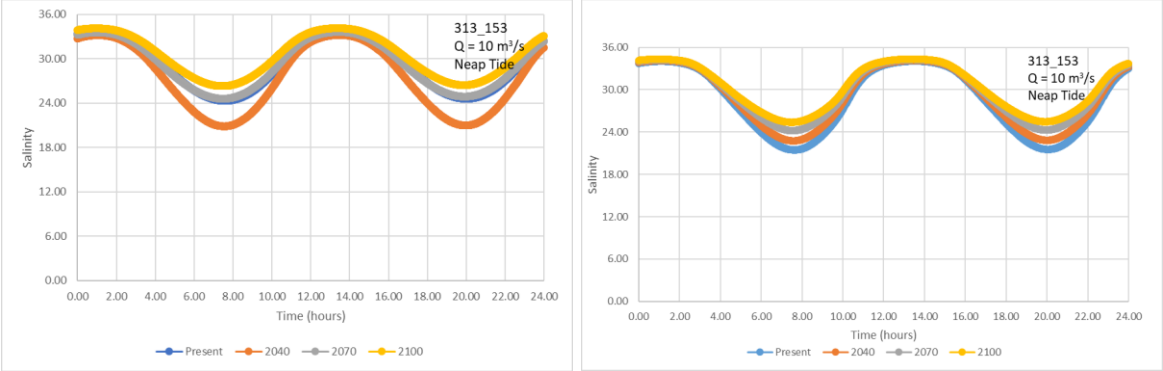


*Figure 4.43* Salinity time series over two tidal cycles for a river discharge of 10 $m^3/s$ at neap tide in the lower estuary for the present bathymetry (left) and bathymetry allowing flooding (right).

The increase in salinity is much more pronounced for a low discharge of freshwater compared to the increase in salinity for a high discharge of freshwater at neap tide. The year 2040, corresponding to a sea level rise of 0.24 meters also has a much lower value of salinity compared to the other values of salinity resulting from the other cases of sea level rise. It can be noted in the velocity time series that there is a reduction in velocity in the year 2040 followed by an increase in velocity in the year 2070 and then a very small decrease in velocity between the years 2070 and 2100. This result is further explained in the discussion. A table summarizing the changes in salinity for each thirty-year period is shown in Table 4.19.

*Table 4.19* Changes in salinity for a discharge of 10 $m^3/s$ at neap tide over the present bathymetry

| | | Change in Salinity | | |
|---|---|---|---|---|
| **Location** | | **Present - 2040** | **2040 - 2070** | **2070 - 2100** |
| **Upper Estuary** | 1377_45 | -3.68E-05 | 1.77E-04 | 9.17E-04 |
| | 1214_61 | -7.69E-04 | 2.51E-03 | 8.78E-03 |
| **Middle Estuary** | 903_102 | -1.70E-01 | 3.44E-01 | 3.75E-01 |
| | 558_103 | -6.99E+00 | 9.09E+00 | 1.36E-01 |
| **Lower Estuary** | 381_147 | -3.42E+00 | 3.43E+00 | 1.32E+00 |
| | 313_153 | -1.87E+00 | 1.88E+00 | 1.14E+00 |
| **Marshes** | 446_109 | -3.82E+00 | 3.46E+00 | 2.77E+00 |
| | 392_23 | -3.83E+00 | 3.07E+00 | 2.96E+00 |
| | 391_96 | -4.56E+00 | 4.26E+00 | 1.77E+00 |
| | 350_80 | -3.00E+00 | 2.33E+00 | 2.53E+00 |
| | 304_27 | -2.53E+00 | 1.68E+00 | 3.37E+00 |

*Table 4.20* Changes in salinity for a discharge of 10 $m^3/s$ at neap tide over the bathymetry allowing flooding.

| | | Change in Salinity | | |
|---|---|---|---|---|
| **Location** | | **Present - 2040** | **2040 - 2070** | **2070 - 2100** |
| **Upper Estuary** | 1377_45 | 1.09E-04 | 1.57E-04 | 2.34E-04 |
| | 1214_61 | 1.20E-03 | 1.68E-03 | 2.38E-03 |
| **Middle Estuary** | 903_102 | 8.06E-02 | 1.06E-01 | 1.38E-01 |
| | 558_103 | 1.03E+00 | 1.29E+00 | 1.41E+00 |
| **Lower Estuary** | 381_147 | 1.07E+00 | 1.17E+00 | 9.66E-01 |
| | 313_153 | 6.49E-01 | 6.53E-01 | 5.07E-01 |
| **Marshes** | 446_109 | 1.68E+00 | 1.57E+00 | 5.24E-01 |
| | 392_23 | 8.39E-01 | 1.82E+00 | -6.11E+00 |
| | 391_96 | 1.50E+00 | 1.58E+00 | 5.72E-02 |
| | 350_80 | 1.55E+00 | 1.85E+00 | 1.46E+00 |
| | 304_27 | 1.60E+00 | 1.88E+00 | 1.49E+00 |

### 4.4.3 Salinity Time Series at Spring Tide with a High Freshwater Discharge

Figure 4.44, Figure 4.45, Figure 4.46, Figure 4.47, Figure 4.48, Figure 4.49 and Figure 4.50 show the temporal evolution of salinity at spring tide for a high discharge of freshwater.

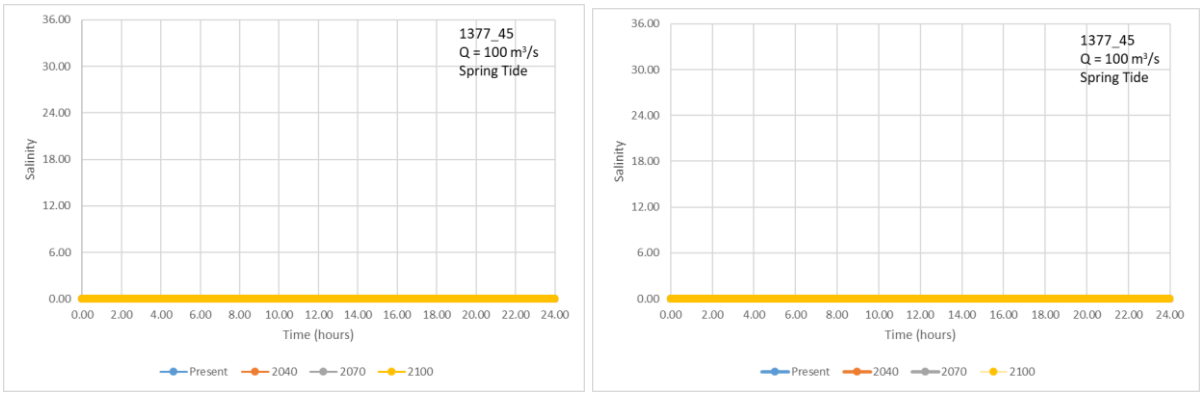


*Figure 4.44* Salinity time series over two tidal cycles for a river discharge of 100 $m^3/s$ at spring tide in the upper estuary for the present bathymetry (left) and bathymetry allowing flooding (right).

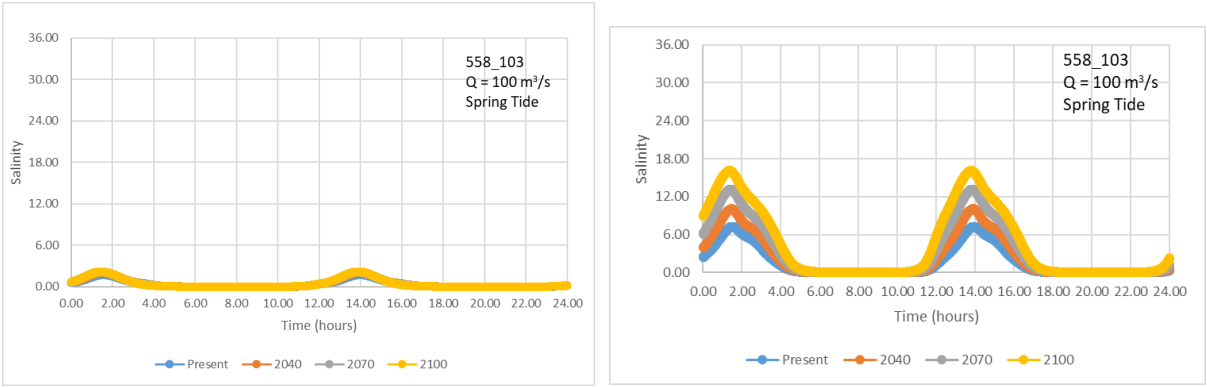

*Figure 4.45* Salinity time series over two tidal cycles for a river discharge of 100 $m^3/s$ at spring tide in the middle estuary for the present bathymetry (left) and bathymetry allowing flooding (right).

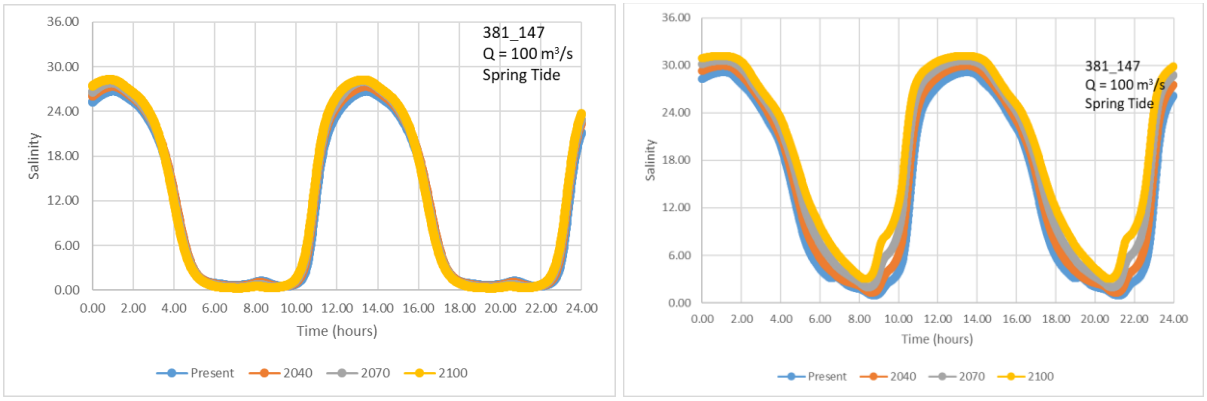


*Figure 4.46* Salinity time series over two tidal cycles for a river discharge of 100 $m^3/s$ at spring tide at the inlet into the marshes for the present bathymetry (left) and bathymetry allowing flooding (right).

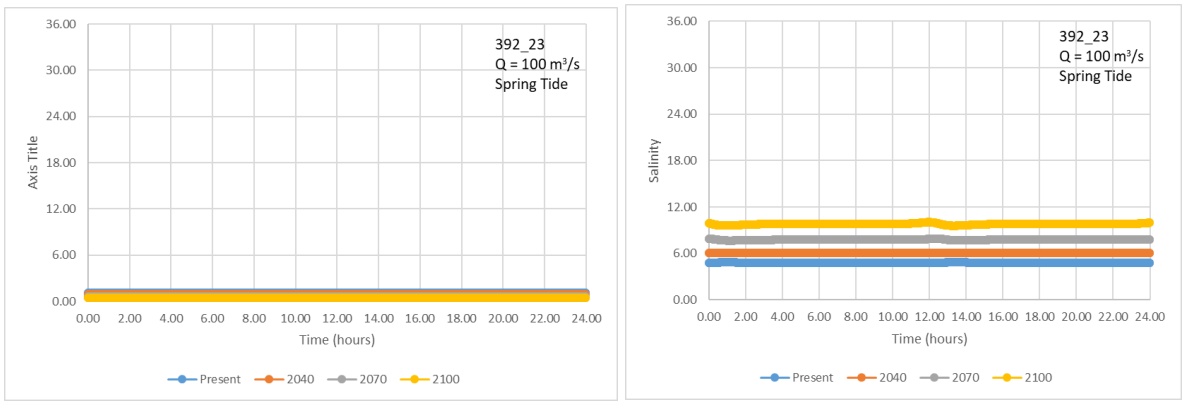


*Figure 4.47* Salinity time series over two tidal cycles for a river discharge of 100 $m^3/s$ at spring tide at the westernmost region of Castro Marim for the present bathymetry (left) and bathymetry allowing flooding (right).

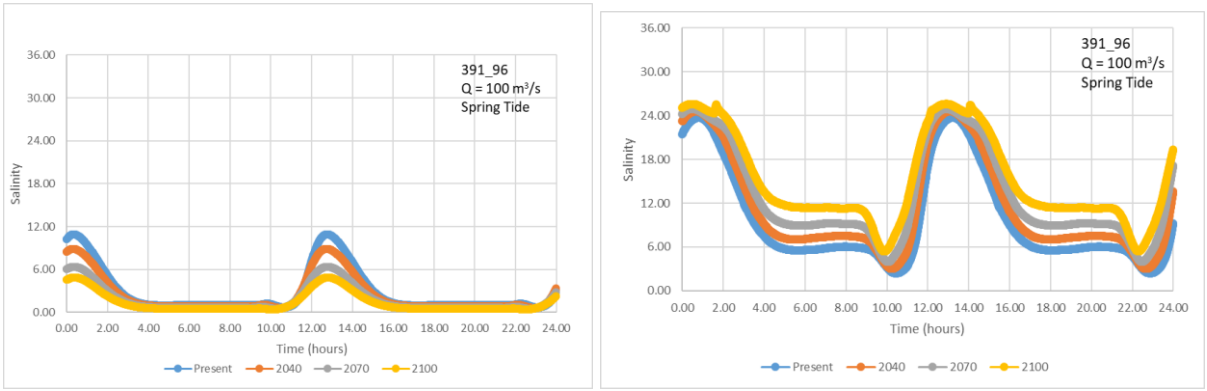


*Figure 4.48* Salinity time series over two tidal cycles for a river discharge of 100 $m^3/s$ at spring tide in the marsh area for the present bathymetry (left) and bathymetry allowing flooding (right).

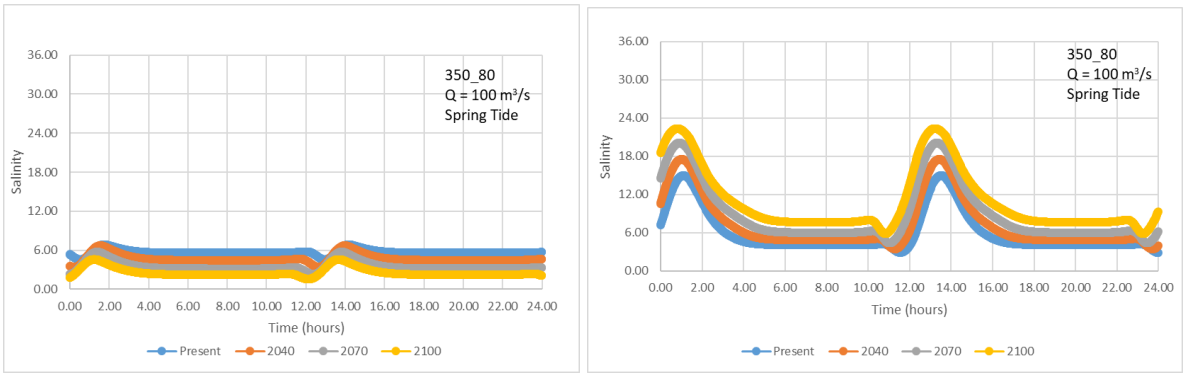


*Figure 4.49* Salinity time series over two tidal cycles for a river discharge of 100 $m^3/s$ at spring tide downstream Esteiro da Carrasqueira for the present bathymetry (left) and bathymetry that allows flooding (right).

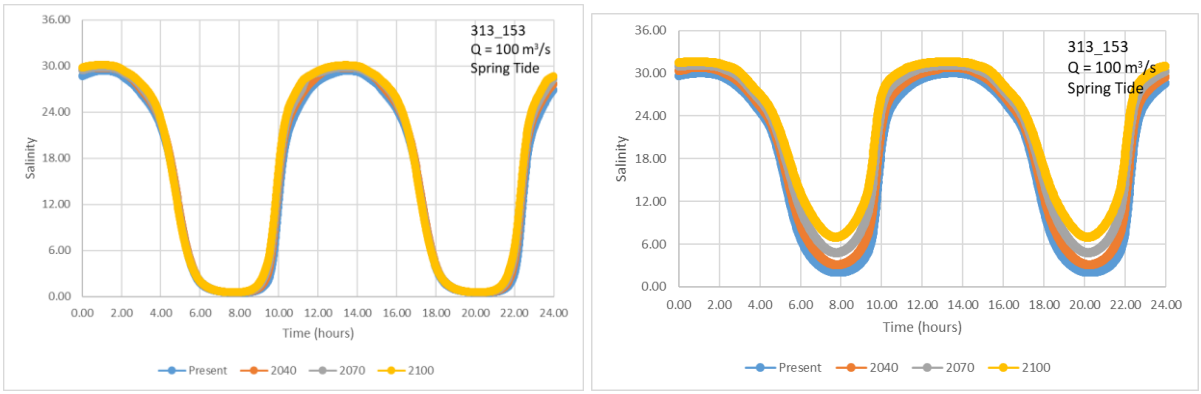


*Figure 4.50* Salinity time series over two tidal cycles for a river discharge of 100 $m^3/s$ at spring tide in the lower estuary for the present bathymetry (left) and bathymetry allowing flooding (right).

The differences in salinity between the two bathymetries are quite pronounced at spring tide with a river discharge of 100 $m^3/s$. There is a decrease in salinity with respect to mean sea level rise in the present bathymetry, while on the other hand there is an increase in salinity for the bathymetry allowing flooding. The differences in salinity trends between the two bathymetries are especially pronounced at the marshes and in the middle of the estuary. A summary of the differences in salinity between the thirty-year periods is shown in Table 4.21 for the present bathymetry and in Table 4.22 for the bathymetry allowing flooding.

*Table 4.21* Changes in salinity for a discharge of 100 $m^3/s$ at spring tide over the present bathymetry.

| | | Change in Salinity | | |
|---|---|---|---|---|
| **Location** | | **Present - 2040** | **2040 - 2070** | **2070 - 2100** |
| **Upper Estuary** | 1377_45 | 3.68E-11 | 2.44E-11 | -8.99E-11 |
| | 1214_61 | 8.61E-11 | 1.05E-11 | -8.08E-11 |
| **Middle Estuary** | 903_102 | 1.60E-09 | 4.41E-09 | 5.68E-09 |
| | 558_103 | 5.01E-02 | 1.18E-02 | 1.92E-03 |
| **Lower Estuary** | 381_147 | 3.80E-01 | 8.32E-02 | 1.21E-01 |
| | 313_153 | 5.84E-01 | 1.74E-01 | 2.71E-01 |
| **Marshes** | 446_109 | -1.51E-01 | -2.35E-01 | -1.84E-01 |
| | 392_23 | -1.52E-01 | -2.39E-01 | -1.86E-01 |
| | 391_96 | -4.32E-01 | -6.09E-01 | -4.16E-01 |
| | 350_80 | -9.70E-01 | -1.19E+00 | -9.28E-01 |
| | 304_27 | -1.12E+00 | -1.27E+00 | -9.15E-01 |

*Table 4.22* Changes in salinity for a discharge of 100 $m^3/s$ at spring tide over the bathymetry allowing flooding.

| | | Change in Salinity | | |
|---|---|---|---|---|
| Location | | **Present - 2040** | **2040 - 2070** | **2070 - 2100** |
| Upper Estuary | 1377_45 | -1.42E-10 | 3.10E-12 | 4.29E-11 |
| | 1214_61 | -1.30E-10 | 4.08E-11 | 8.80E-11 |
| Middle Estuary | 903_102 | 1.76E-08 | 3.80E-08 | 7.51E-08 |
| | 558_103 | 7.10E-01 | 9.21E-01 | 1.06E+00 |
| Lower Estuary | 381_147 | 1.24E+00 | 1.41E+00 | 1.54E+00 |
| | 313_153 | 1.29E+00 | 1.34E+00 | 1.43E+00 |
| Marshes | 446_109 | 2.04E+00 | 1.80E+00 | 2.12E+00 |
| | 392_23 | 1.23E+00 | 1.72E+00 | 2.04E+00 |
| | 391_96 | 1.59E+00 | 1.71E+00 | 1.99E+00 |
| | 350_80 | 1.32E+00 | 1.66E+00 | 1.97E+00 |
| | 304_27 | 7.66E-01 | 1.15E+00 | 1.63E+00 |

A high discharge during spring tide does not yield any change in salinity values in the upper estuary as mean sea level increases for both bathymetries. The salinity does not reach the estuary until the middle to lower section (558_103). Both bathymetries experience an increase in salinity at this location, but the salinity change for the bathymetry allowing flooding is much more pronounced. There is also an increase in salinity in the lower estuary, but again the bathymetry allowing flooding results in a much higher increase in salinity. The time series graphs also depict much higher salinity values for the bathymetry allowing flooding compared to the present bathymetry. The salinity values in the marshes all result in a decrease in salinity for the present bathymetry, but for the bathymetry allowing flooding the salinity increases

dramatically. The salinity values at spring tide are also much higher than they are at neap tide for both bathymetries, which demonstrates the influence of the tide on salt intrusion.

### 4.4.4 Salinity Time Series at Spring Tide with a Low Freshwater Discharge

The time series of salinity for a low freshwater discharge at spring tide are shown in Figure 4.51, Figure 4.52, Figure 4.53, Figure 4.54, Figure 4.55, Figure 4.56 and Figure 4.57.

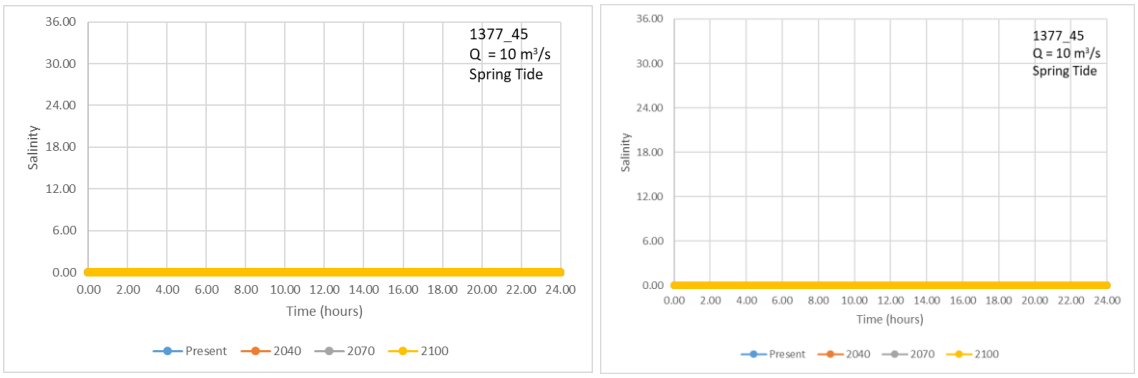


*Figure 4.51* Salinity time series over two tidal cycles for a river discharge of 10 $m^3/s$ at spring tide in the upper estuary for the present bathymetry (left) and bathymetry allowing flooding (right).

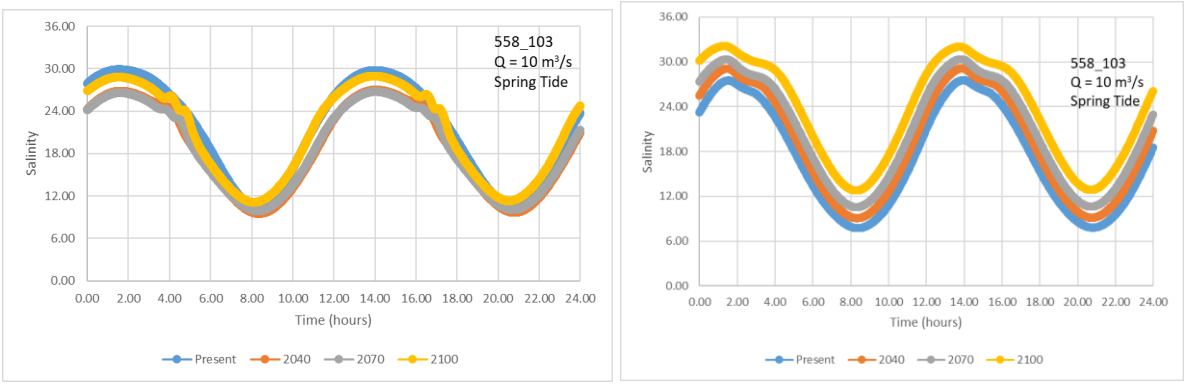


*Figure 4.52* Salinity time series over two tidal cycles for a river discharge of 10 $m^3/s$ at spring tide in the middle estuary for the present bathymetry (left) and bathymetry allowing flooding (right).

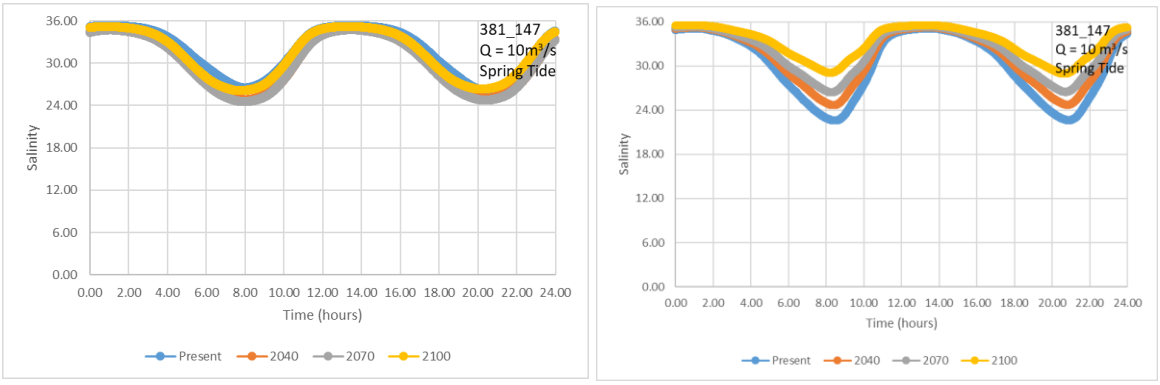


*Figure 4.53* Salinity time series over two tidal cycles for a river discharge of 10 $m^3/s$ at spring tide at the inlet into the marshes for the present bathymetry (left) and bathymetry allowing flooding (right).

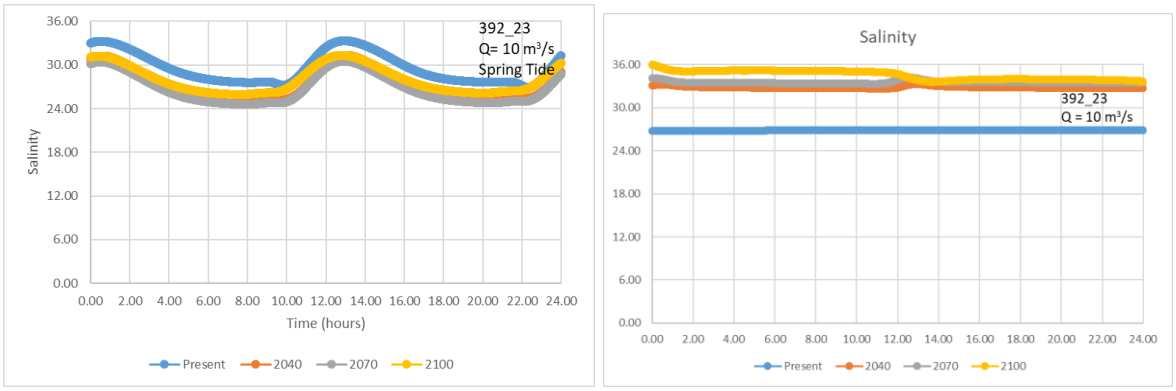


*Figure 4.54* Salinity time series over two tidal cycles for a river discharge of 10 $m^3/s$ at spring tide at the westernmost region of Castro Marim for the present bathymetry (left) and bathymetry allowing flooding (right).

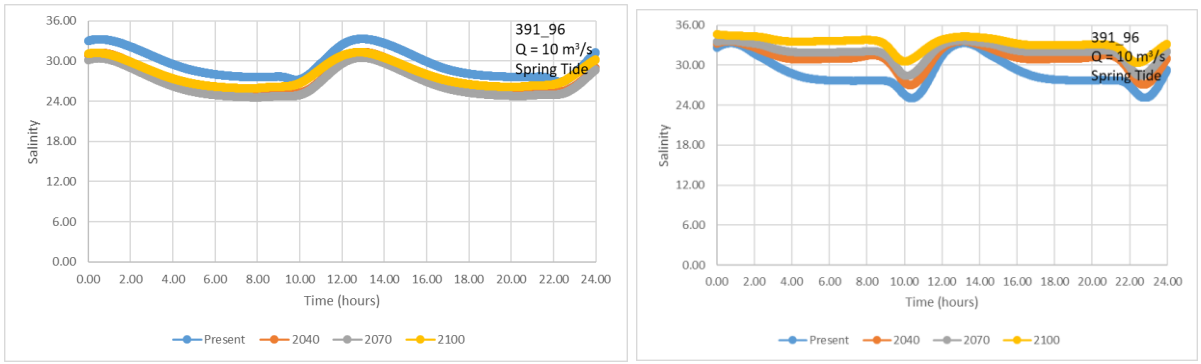


*Figure 4.55* Salinity time series over two tidal cycles for a river discharge of 10 $m^3/s$ at spring tide in the marsh area for the present bathymetry (left) and bathymetry allowing flooding (right).

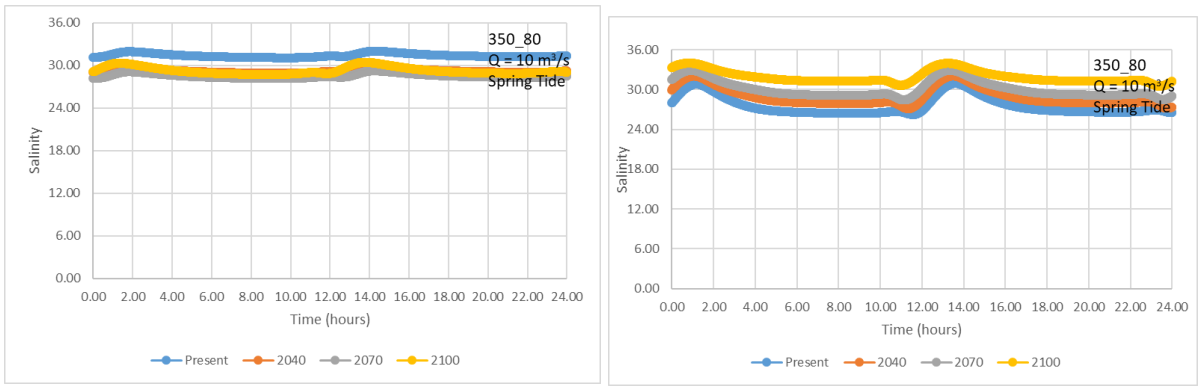


*Figure 4.56* Salinity time series over two tidal cycles for a river discharge of 10 $m^3/s$ at spring tide downstream Esteiro da Carrasqueira for the present bathymetry (left) and bathymetry that allows flooding (right).

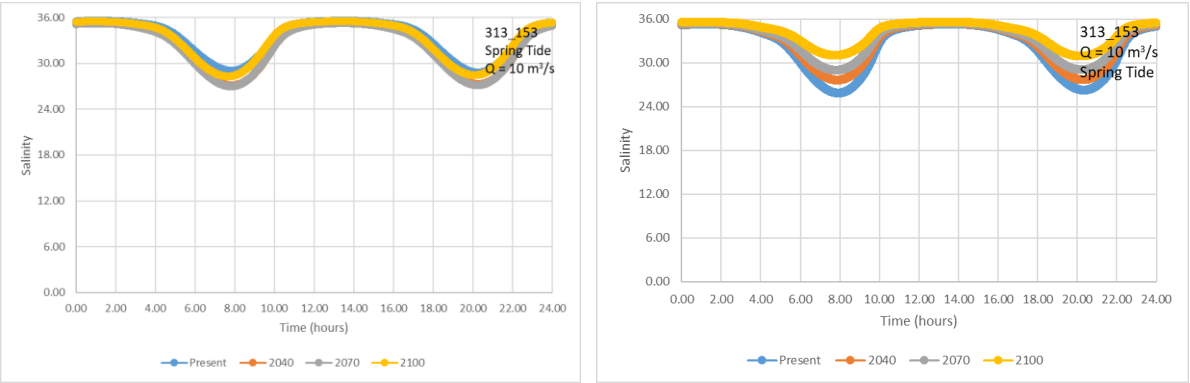


*Figure 4.57* Salinity time series over two tidal cycles for a river discharge of 10 $m^3/s$ at spring tide in the lower estuary for the present bathymetry (left) and bathymetry allowing flooding (right).

Again, there is a very consistent increase in salinity every thirty years for the bathymetry allowing flooding. In the middle channel of the estuary and in the marsh area there is a decrease in salinity for the present bathymetry, but then rises after the year 2070. Changes in salinity for a low freshwater discharge at spring tide is summarized in Table 4.23 for the present bathymetry and in Table 4.24 for the bathymetry allowing flooding.

*Table 4.23* Changes in salinity for a discharge of 10 $m^3/s$ at spring tide over the present bathymetry.

| | | Change in Salinity | | |
|---|---|---|---|---|
| **Location** | | **Present - 2040** | **2040 - 2070** | **2070 - 2100** |
| **Upper Estuary** | 1377_45 | -8.27E-04 | 3.89E-04 | 1.98E-03 |
| | 1214_61 | -7.85E-03 | 3.35E-03 | 1.67E-02 |
| **Middle Estuary** | 903_102 | -3.42E-01 | 1.14E-01 | 5.47E-01 |
| | 558_103 | -2.38E+00 | 3.68E-02 | 2.02E+00 |
| **Lower Estuary** | 381_147 | -1.31E+00 | -2.12E-01 | 1.11E+00 |
| | 313_153 | -9.44E-01 | -9.57E-02 | 7.74E-01 |
| **Marshes** | 446_109 | -2.46E+00 | -4.60E-01 | 1.37E+00 |
| | 392_23 | -2.29E+00 | -5.51E-01 | 1.24E+00 |
| | 391_96 | -2.29E+00 | -5.51E-01 | 1.24E+00 |
| | 350_80 | -2.20E+00 | -6.82E-01 | 7.54E-01 |
| | 304_27 | -2.23E+00 | -7.25E-01 | 6.18E-01 |

*Table 4.24* Changes in salinity for a discharge of 10 m3/s at spring tide over the bathymetry allowing flooding.

| | | Change in Salinity | | |
|---|---|---|---|---|
| **Location** | | **Present - 2040** | **2040 - 2070** | **2070 - 2100** |
| **Upper Estuary** | 1377_45 | 1.19E-03 | 1.61E-03 | 2.38E-03 |
| | 1214_61 | 9.74E-03 | 1.25E-02 | 1.82E-02 |
| **Middle Estuary** | 903_102 | 3.11E-01 | 3.60E-01 | 5.27E-01 |
| | 558_103 | 1.74E+00 | 1.64E+00 | 2.49E+00 |
| **Lower Estuary** | 381_147 | 1.06E+00 | 7.84E-01 | 1.17E+00 |
| | 313_153 | 6.06E-01 | 4.82E-01 | 7.77E-01 |
| **Marshes** | 446_109 | 2.20E+00 | 8.34E-01 | 1.41E+00 |
| | 392_23 | 5.99E+00 | 6.84E-01 | 1.86E-01 |
| | 391_96 | 2.16E+00 | 8.30E-01 | 1.27E+00 |
| | 350_80 | 1.35E+00 | 1.16E+00 | 1.85E+00 |
| | 304_27 | 1.49E+00 | 1.23E+00 | 2.13E+00 |

A low discharge at spring tide results in an increase in salinity in the upper estuary for both bathymetries. There is an initial decrease in salinity for the present bathymetry from the present year to the year 2040 followed by a very small change in salinity and then a more significant increase in salinity from 2070 to 2100. On the other hand, the bathymetry allowing flooding shows a very consistent increase in salinity for every thirty-year interval and at every location. This is especially true in the marshes where flooding is allowed. The increase in water volume in these areas results in a very high salinity increase. The increase in salinity from the present year to 2040 is quite high. It then slows down after 2070 but increases drastically again by the year 2100. The values in salinity are much higher at spring tide compared to neap tide, which is to be expected considering the higher volume of water entering the estuary from the higher tidal amplitude.

## 4.5 Horizontal Distribution Maps of Salinity

The model produced horizontal distribution maps showing the evolution of salinity in the 1400 x 350 Cartesian grid at all locations in and around the estuary. Again, the number of maps produced is quite high considering the number of simulations. The following section presents the changes in the horizontal distribution of salinity up to the year 2100 for each case: neap tide with a high freshwater discharge for both types of bathymetry at both high and low tide (Figure 4.58, Figure 4.59, Figure 4.60 and Figure 4.61), neap tide with a low freshwater discharge for both types of bathymetry in high and low water conditions (Figure 4.62, Figure 4.63, Figure 4.64 and Figure 4.65), spring tide with a high freshwater discharge for both types

of bathymetry in high and low water conditions (Figure 4.66, Figure 4.67, Figure 4.68 and Figure 4.69), spring tide with a low freshwater discharge for both types of bathymetry in high and low water conditions (Figure 4.70, Figure 4.71, Figure 4.72 and Figure 4.73) for a total of 16 maps.

### 4.5.1 Salinity Distribution Maps at Neap Tide with a High Freshwater Flow

The horizontal distribution maps for simulations over the present bathymetry at neap tide combined with a high freshwater discharge are shown in Figure 4.58 and Figure 4.59 and the horizontal distribution maps for the bathymetry allowing flooding at neap tide for a high freshwater discharge are shown in Figure 4.60 and Figure 4.61.

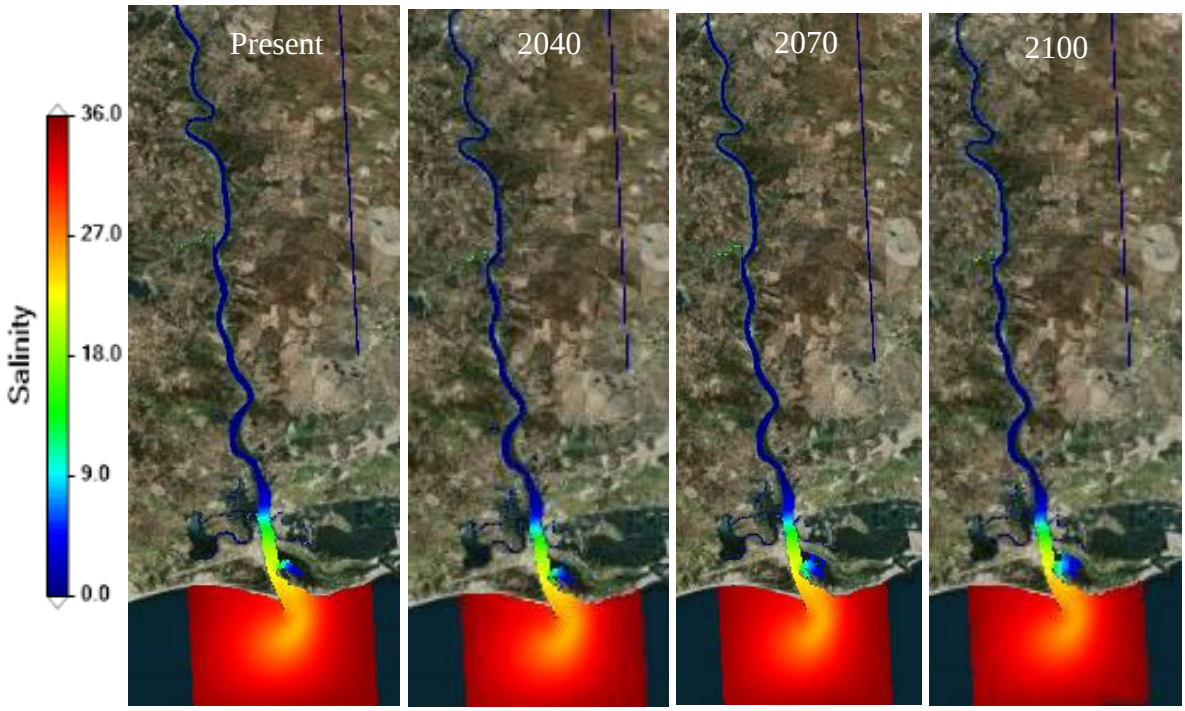


*Figure 4.58* Salinity distribution maps in high water conditions for a river discharge of 100 $m^3/s$ for the present year, 2040, 2070 and 2100 at neap tide over the present bathymetry.

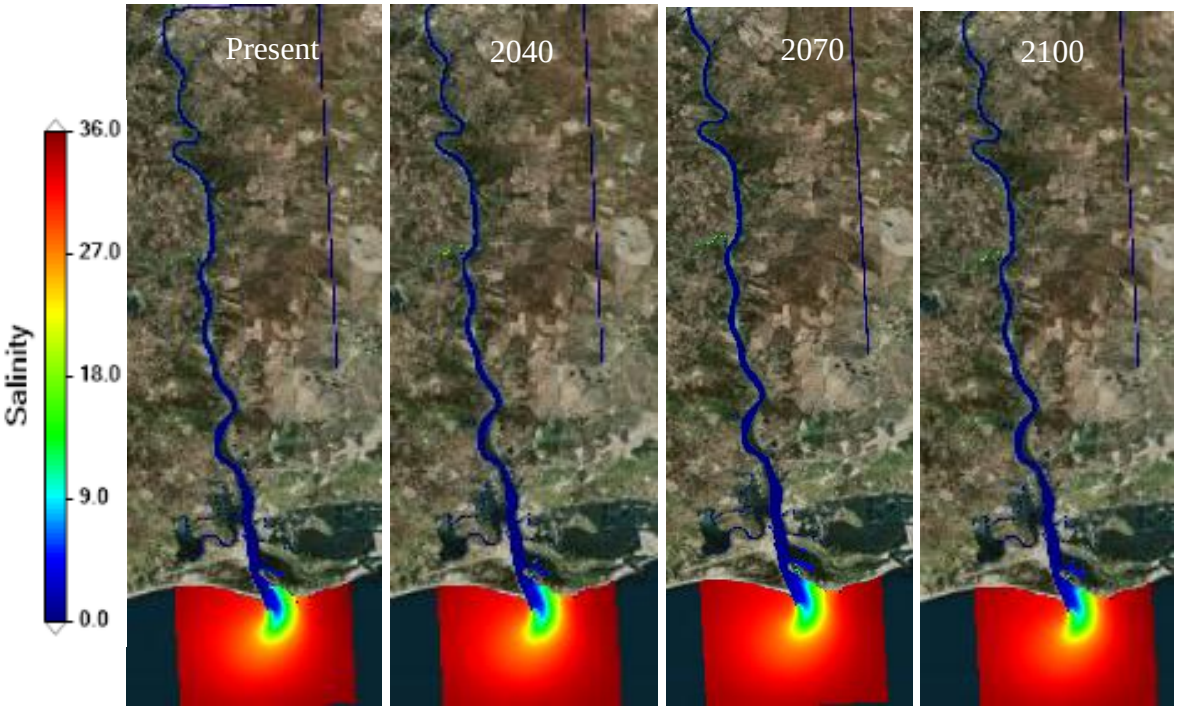


*Figure 4.59* Salinity distribution maps in low water conditions for a river discharge of 100 $m^3/s$ for the present year, 2040, 2070 and 2100 at neap tide over the present bathymetry.

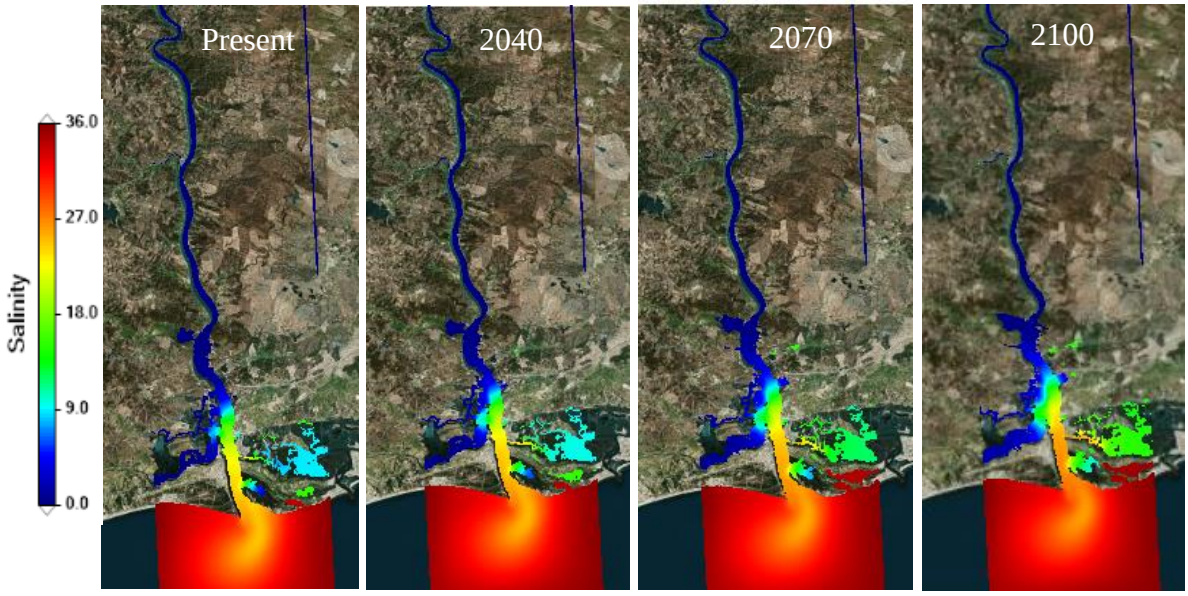


*Figure 4.60* Salinity distribution maps in high water conditions for a river discharge of 100 $m^3/s$ for the present year, 2040, 2070 and 2100 at neap tide over the bathymetry allowing flooding.

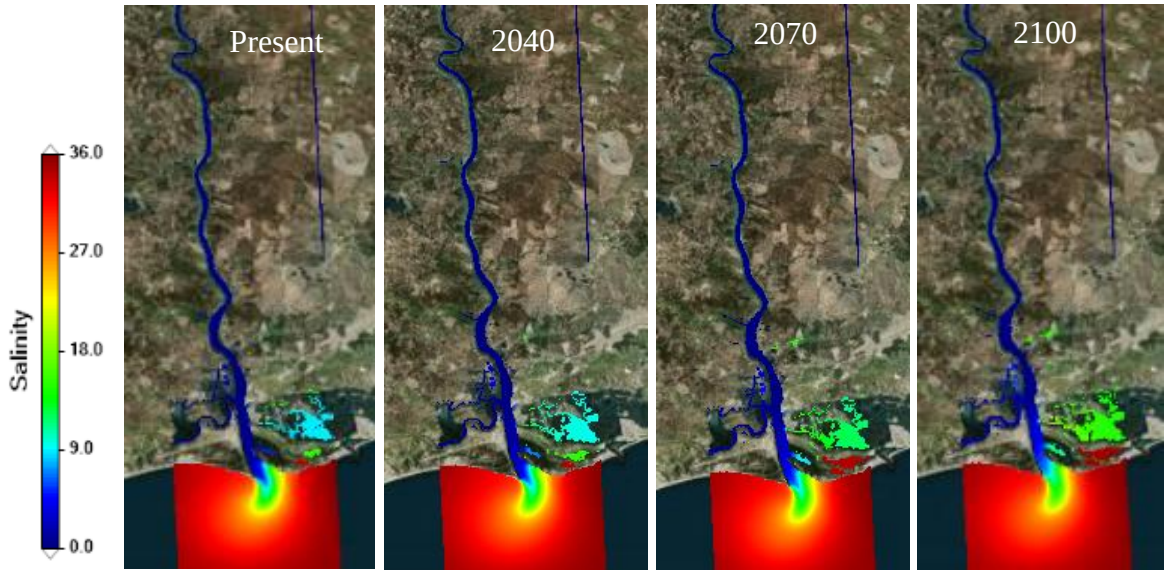


*Figure 4.61* Salinity distribution maps in low water conditions for a river discharge of 100 $m^3/s$ for the present year, 2040, 2070 and 2100 at neap tide over the bathymetry allowing flooding.

There is a marked increase in salinity along all point of the estuary from the present year to the year 2100 for all maps showing a high freshwater discharge at neap tide. The changes in salinity are much more pronounced at high tide, as to be expected considering the higher volume of seawater entering the estuary. The salinity distribution maps (Figure 4.60 and Figure 4.61) portray the extension of salt intrusion into the marshes near Ayamonte with salinity values of approximately 18 by the year 2100 compared to salinity values of 9 at present.

### 4.5.2 Salinity Distribution Maps at Neap Tide with a Low Freshwater Flow

Horizontal distribution maps of salinity at neap tide combined with a river discharge of 10 $m^3/s$ over the present bathymetry are shown in Figure 4.62 and Figure 4.63. The evolution of salinity transport for the bathymetry allowing flooding are showing in Figure 4.64 and Figure 4.65.

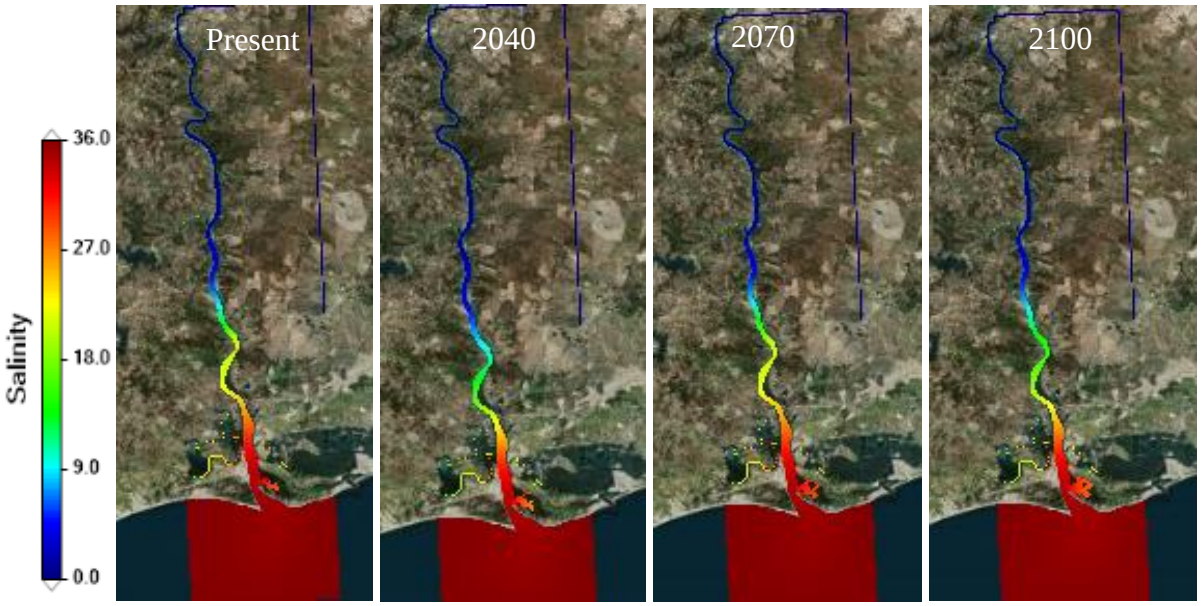


*Figure 4.62* Salinity distribution maps in high water conditions for a river discharge of 10 $m^3/s$ for the present year, 2040, 2070 and 2100 at neap tide over the present bathymetry.

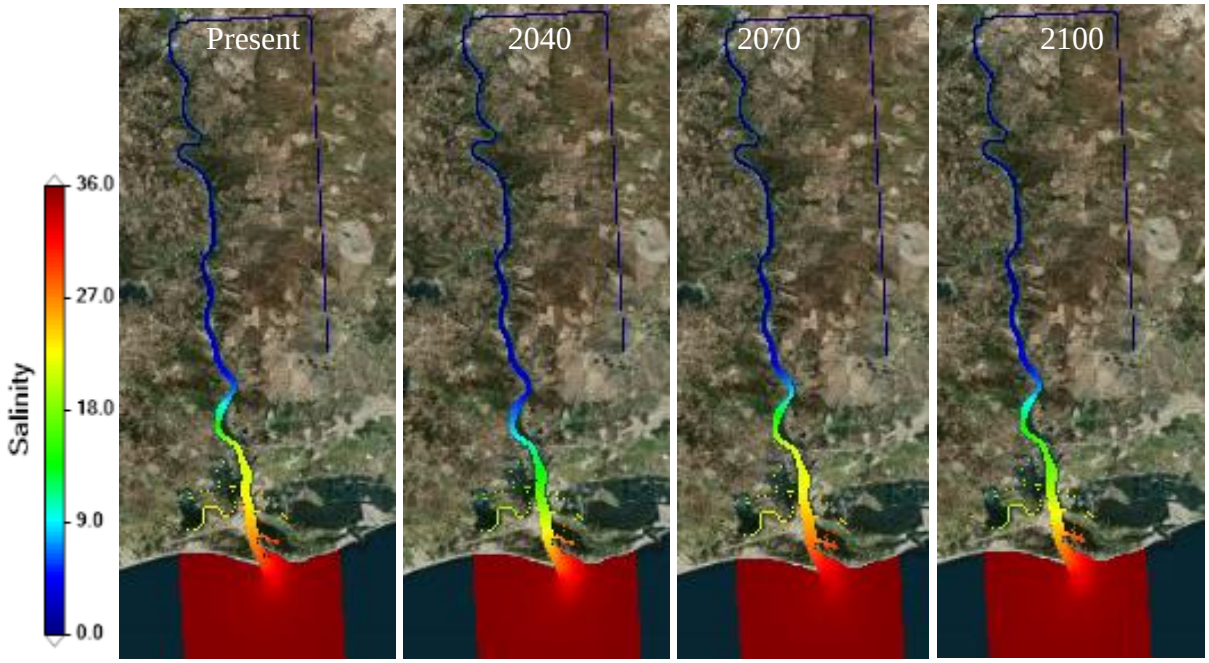


*Figure 4.63* Salinity distribution maps in low water conditions for a river discharge of 10 $m^3/s$ for the present year, 2040, 2070 and 2100 at neap tide over the present bathymetry.

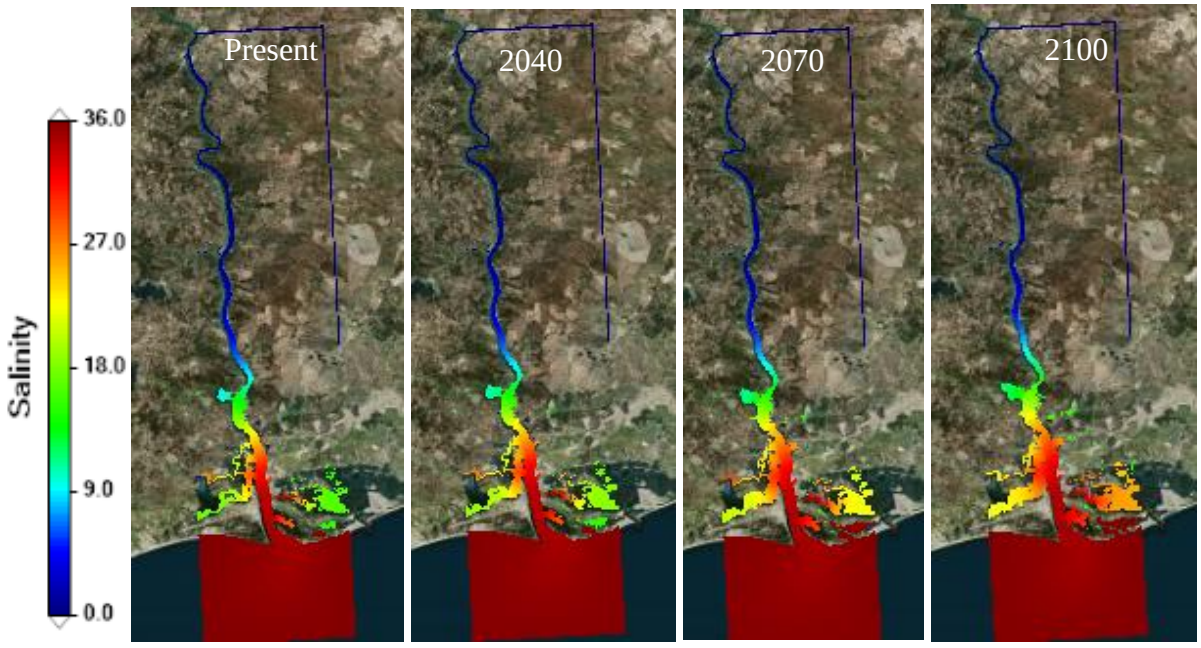


*Figure 4.64* Salinity distribution maps in high water conditions for a river discharge of 10 $m^3/s$ for the present year, 2040, 2070 and 2100 at neap tide over the bathymetry allowing flooding.

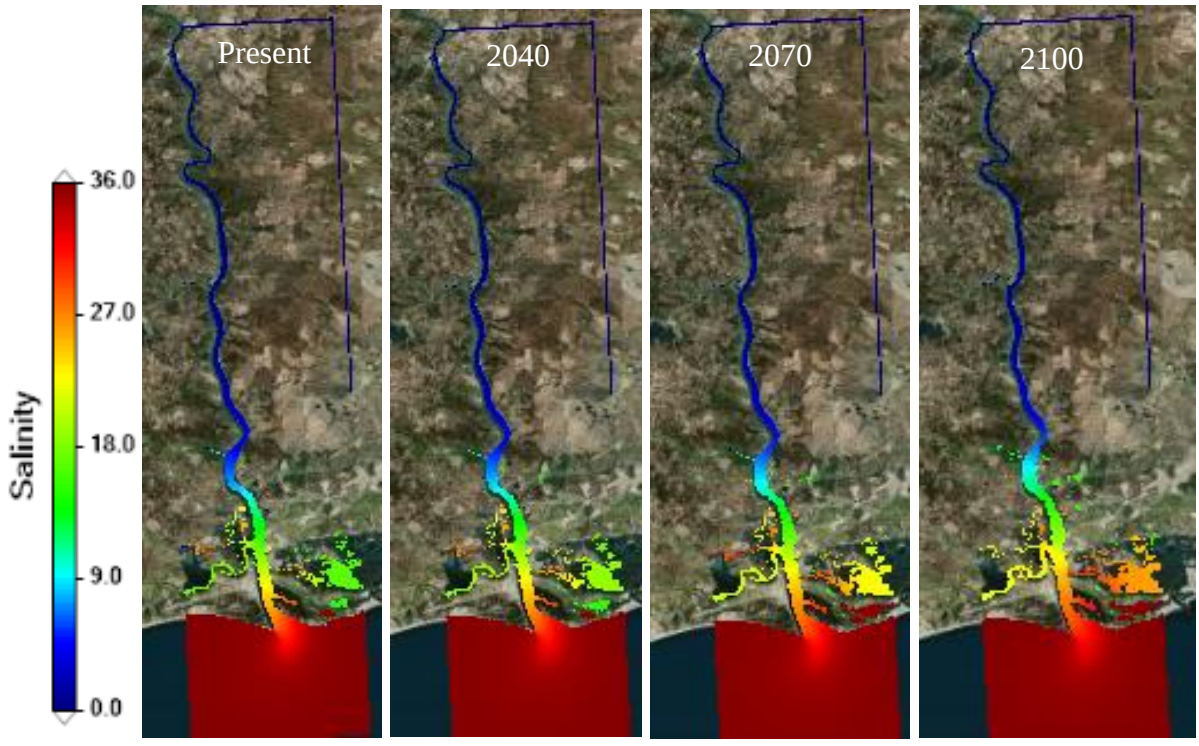


*Figure 4.65* Salinity distribution maps in low water conditions for a river discharge of 10 $m^3/s$ for the present year, 2040, 2070 and 2100 at neap tide over the bathymetry allowing flooding.

The overall results for a low freshwater discharge at neap tide portray an increase in salinity for both types of bathymetry in response to sea level rise. The only exception is the scenario in the year 2040 for the present bathymetry. It can be noted that salinity decreases from the present to the year 2040. It then increases from 2040 to 2070 and decreases again in

2100. Figure 4.62 and Figure 4.63 also reveal how the salt is transported further up the main channel compared to the present year and 2040. This result is also evident in the time series analysis in section 4.4.2. The salinity results for the bathymetry allowing flooding into the marshes portray a much more consistent increase in salinity over the various scenarios of sea level rise compared to the results obtained from the present bathymetry.

### 4.5.3 Salinity Distribution Maps at Spring Tide with a High Freshwater Flow

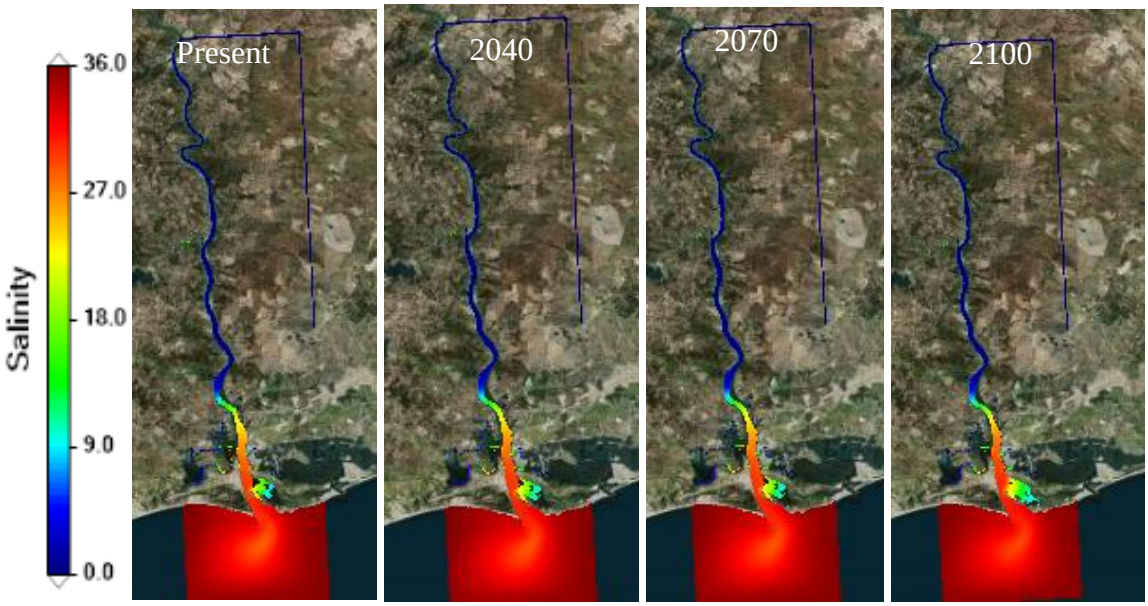


*Figure 4.66* Salinity distribution maps in high water conditions for a river discharge of 100 $m^3/s$ for the present year, 2040, 2070 and 2100 at spring tide over the present bathymetry.

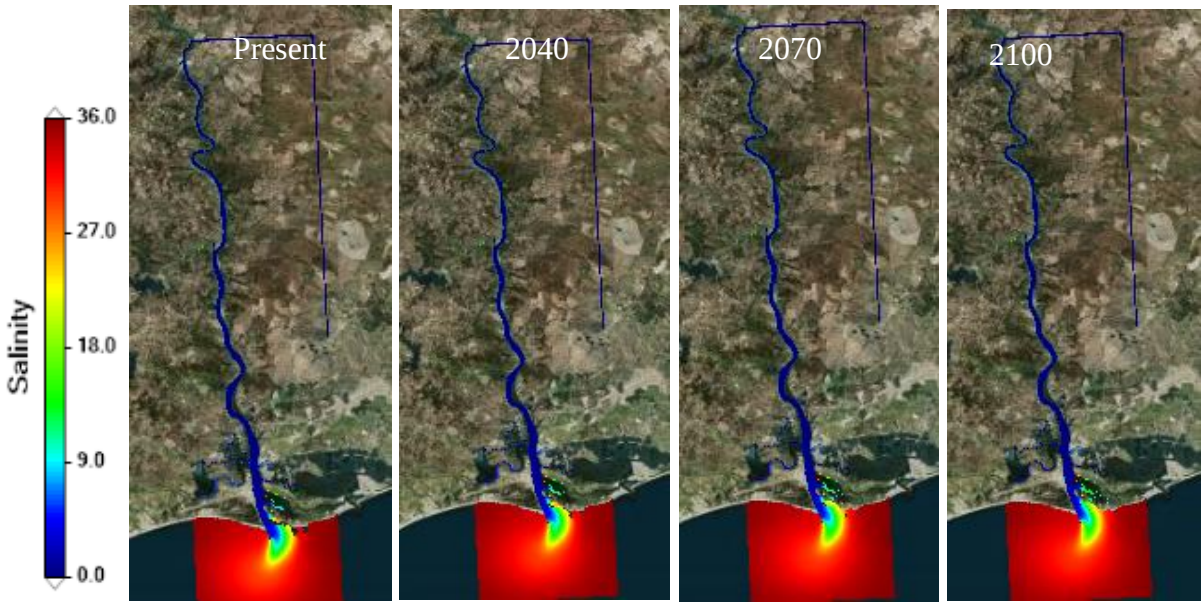


*Figure 4.67* Salinity distribution maps in low water conditions for a river discharge of 100 $m^3/s$ for the present year, 2040, 2070 and 2100 at spring tide over the present bathymetry.

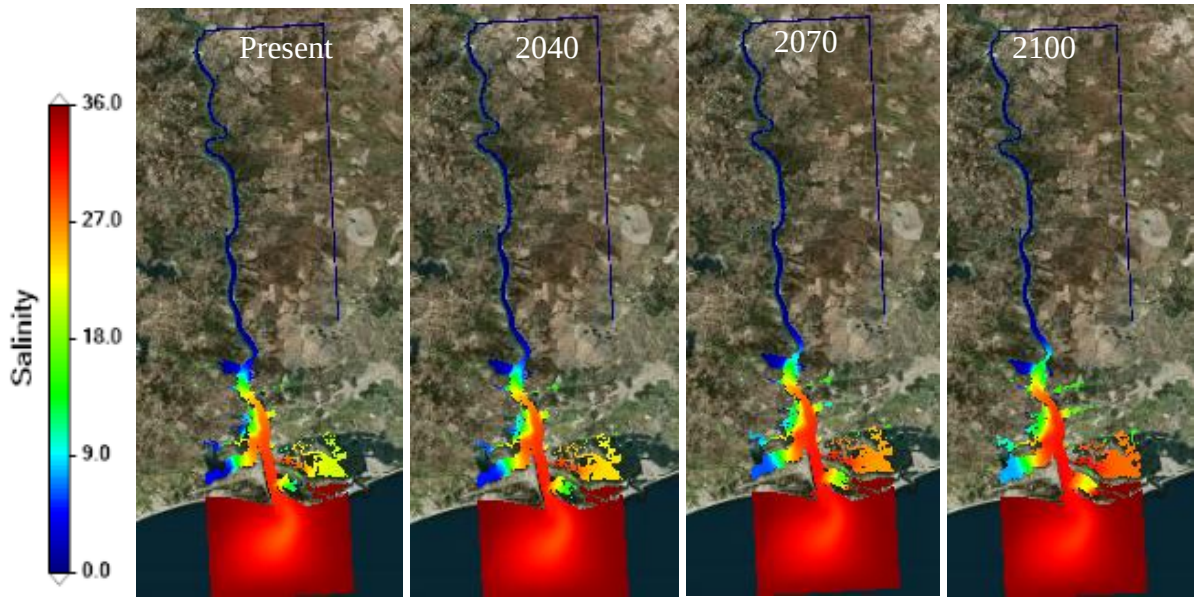


*Figure 4.68* Salinity distribution maps in high water conditions for a river discharge of 100 $m^3/s$ for the present year, 2040, 2070 and 2100 at spring tide over the bathymetry allowing flooding.

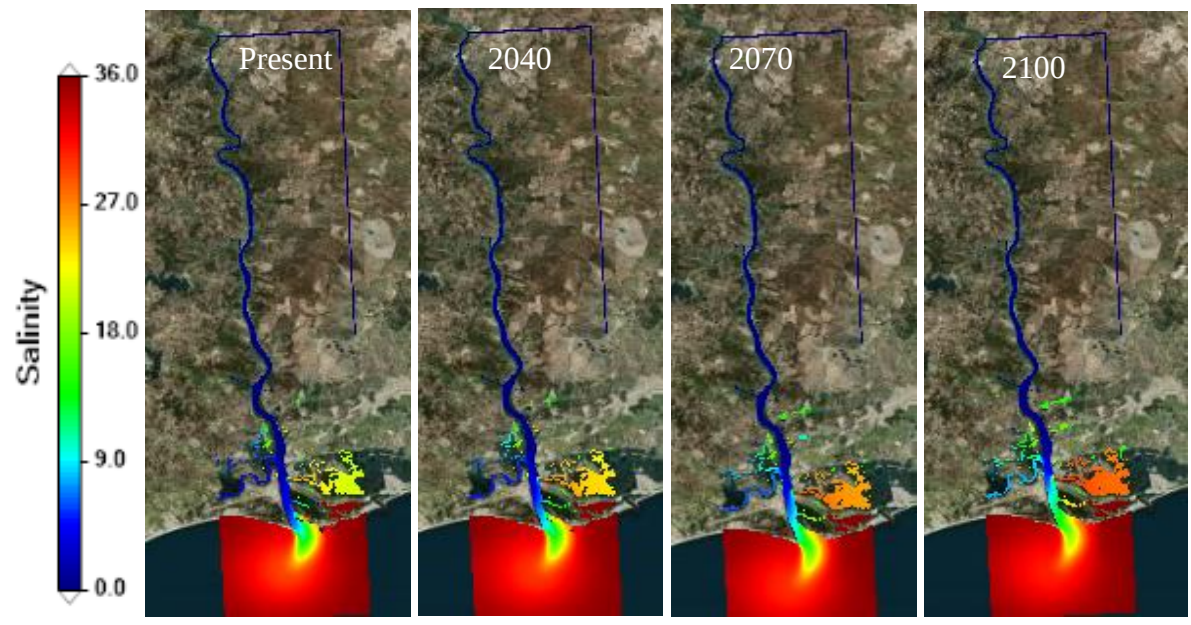


*Figure 4.69* Salinity distribution maps in low water conditions for a river discharge of 100 $m^3/s$ for the present year, 2040, 2070 and 2100 at spring tide over the bathymetry allowing flooding.

An increase in salinity can be seen for all scenarios of a high freshwater discharge at spring tide. The increase in salinity is most pronounced at high tide. Salinity increases further up the channel and in the marshes for the bathymetry allowing flooding compared to the present bathymetry where the salt intrusion is confined in the main channel. The values in salinity for spring tide are also much higher compared to the values of salinity at neap tide.

### 4.5.4 Salinity Distribution Maps at Spring Tide with a Low Freshwater Flow

The horizontal distribution maps of salinity at spring tide combined with a river discharge of 10 $m^3/s$ at high and low tide for the present bathymetry are shown in Figure 4.70 and Figure 4.71, respectively. The results for the bathymetry allowing flooding are shown in Figure 4.72 and Figure 4.73.

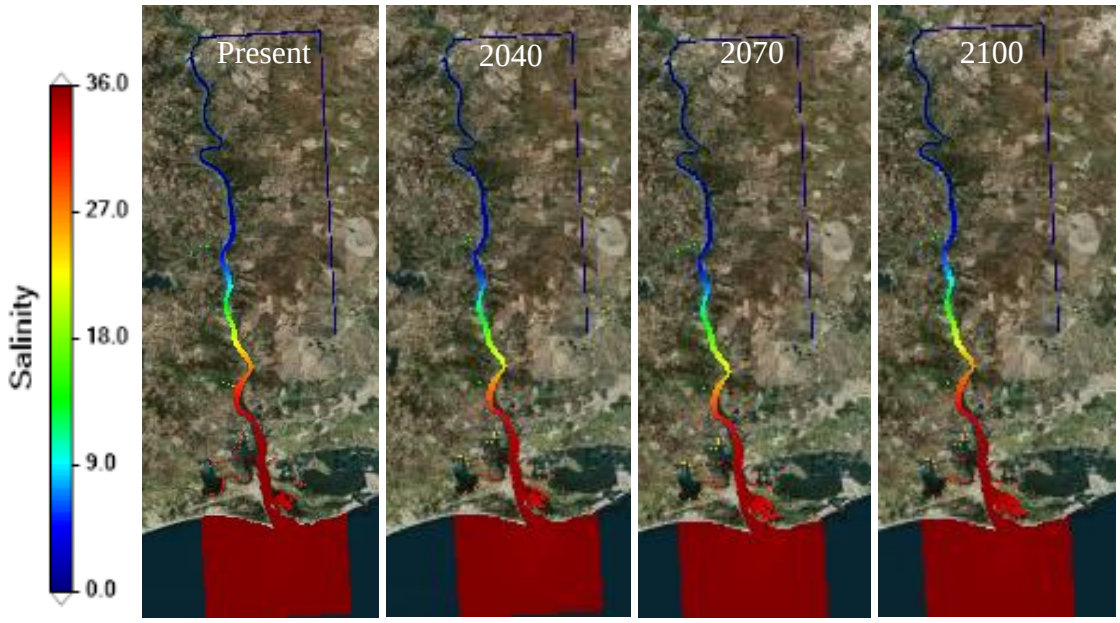


*Figure 4.70* Salinity distribution maps in high water conditions for a river discharge of 10 $m^3/s$ for the present year, 2040, 2070 and 2100 at spring tide over the present bathymetry.

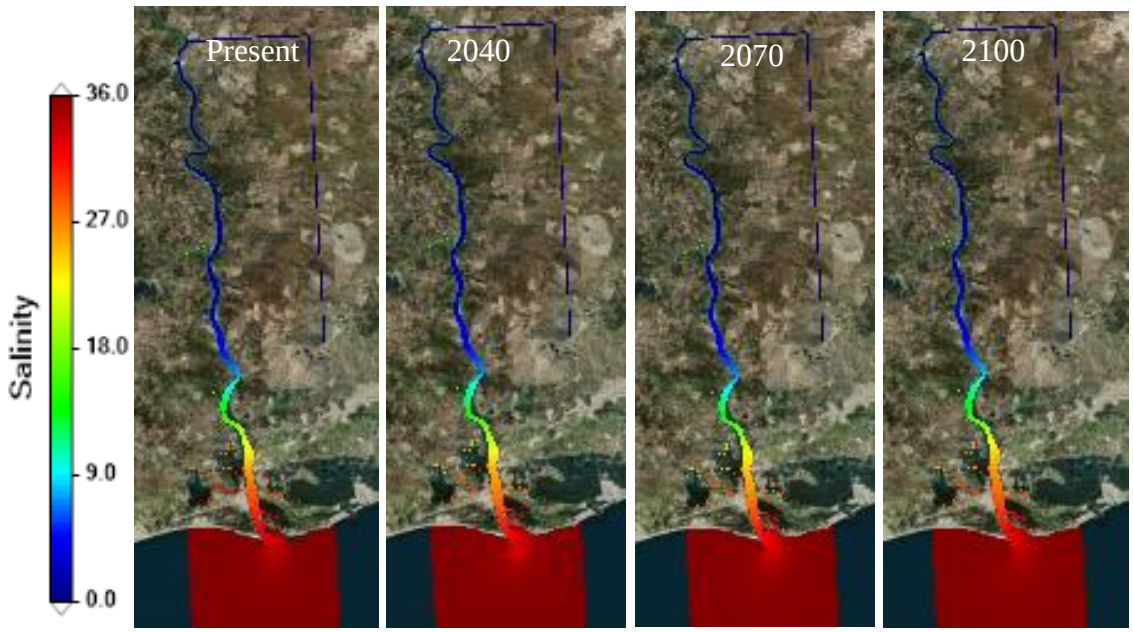


*Figure 4.71* Salinity distribution maps in low water conditions for a river discharge of 10 $m^3/s$ for the present year, 2040, 2070 and 2100 at spring tide over the present bathymetry.

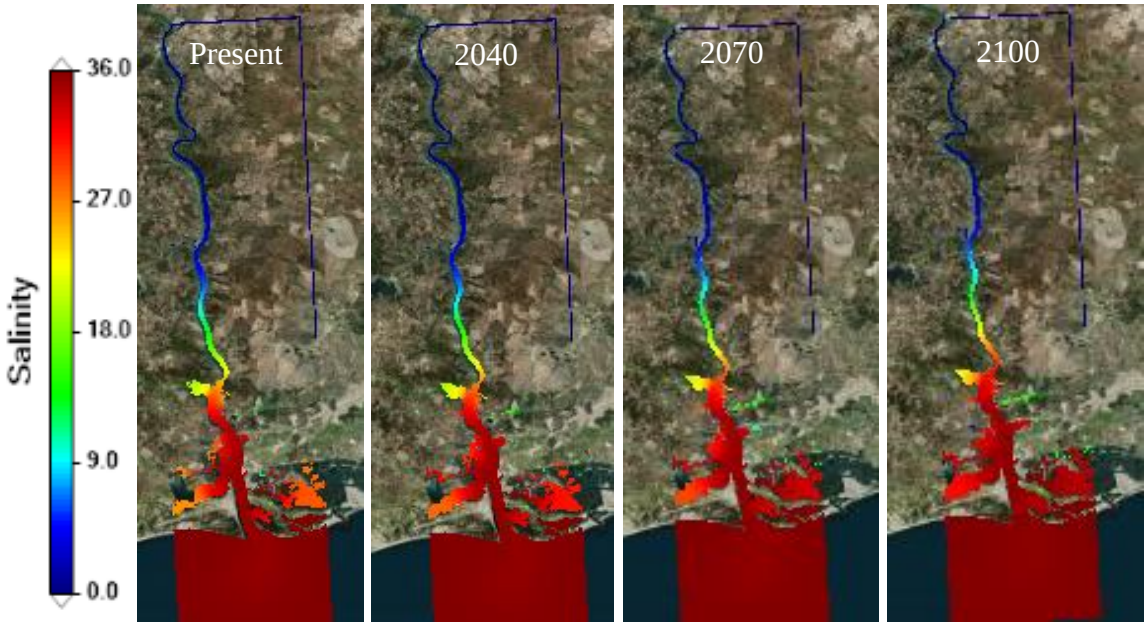


*Figure 4.72* Salinity distribution maps in high water conditions for a river discharge of 10 $m^3/s$ for the present year, 2040, 2070 and 2100 at spring tide over the bathymetry allowing flooding.

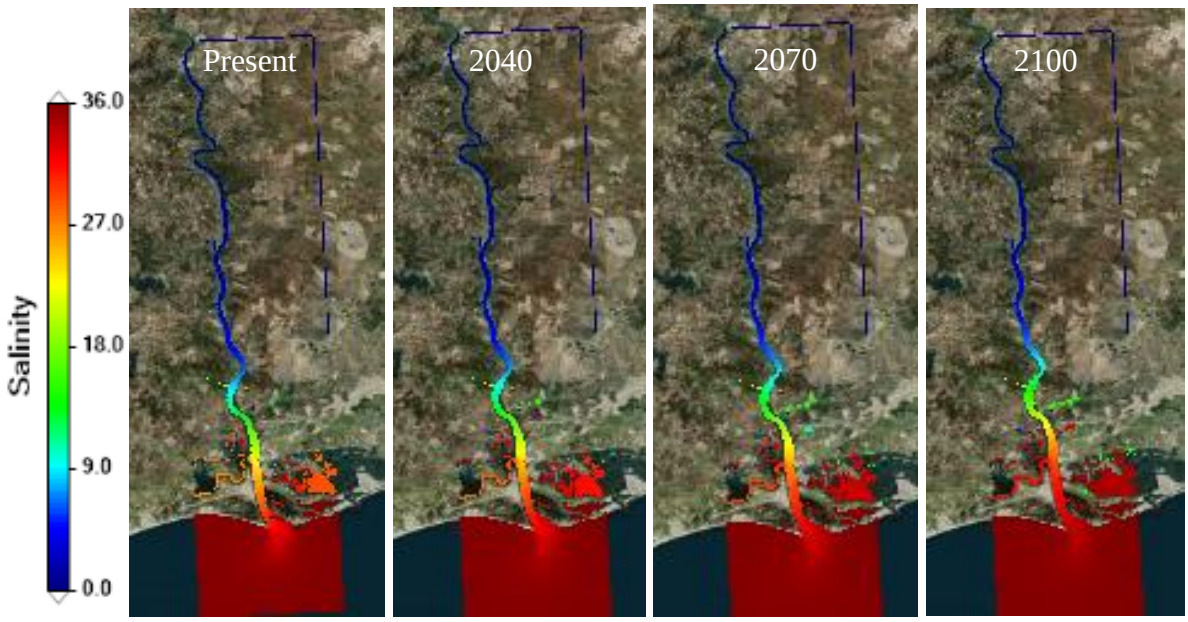


*Figure 4.73* Salinity distribution maps in low water conditions for a river discharge of 10 $m^3/s$ for the present year, 2040, 2070 and 2100 at spring tide over the bathymetry allowing flooding.

For the case of a low freshwater discharge at spring tide for both types of bathymetries, salinity increases up the mainstream with respect to mean sea level rise. The salinity progresses both upstream the main channel and extends far into the marshes for the bathymetry allowing flooding. The salinity values reach almost 36 by the year 2100 at both high and low tide, as can be seen in Figure 4.72 and Figure 4.73.

### 4.5.5 Areas of Inundation: Flooding Classes

Areas of inundation were computed for one tidal cycle for the various scenarios of sea level rise. The methodologies follow those of Mills et al. (2019) who computed flooding area as a function of the number of hours of land submersion over one tidal cycle for each scenario of sea level rise, but only for a very high freshwater discharge of 500 $m^3/s$. The results for the areas of inundation for the present study allow an analysis of land inundation for the various river discharge scenarios (10 $m^3/s$ and 100 $m^3/s$) combined with the various scenarios of sea level rise along with different tidal amplitudes over the bathymetry allowing flooding. The results are presented in the form of a histogram, showing land area for each class of submersion time over one tidal cycle. As previously mentioned in the methods in section 3.2.7, classes of submersion time were derived based on the number of hours of flooding within the duration of one tidal cycle. Class 1 refers to a submersion time of 0 – 1.2 hours, whereas class 10 refers to land that is submerged for an entire tidal cycle. The histogram for neap tide combined with a high freshwater discharge is shown in Figure 4.74. A table summarizing the inundation results throughout the years of sea level rise for the case of a high freshwater flow at neap tide is also shown in Table 4.25. Figure 4.75 and Table 4.26 show the areas of flooding for a low freshwater discharge at neap tide. Figure 4.76 and Table 4.27 show the areas of flooding for a high freshwater discharge at spring tide. Figure 4.77 and Table 4.28 show the areas of flooding for a low freshwater discharge at spring tide.Figure 4.76 Histogram showing classes of flooding as a function of submersion time for one tidal cycle for the various scenarios of sea level rise at spring tide with a high freshwater flow.

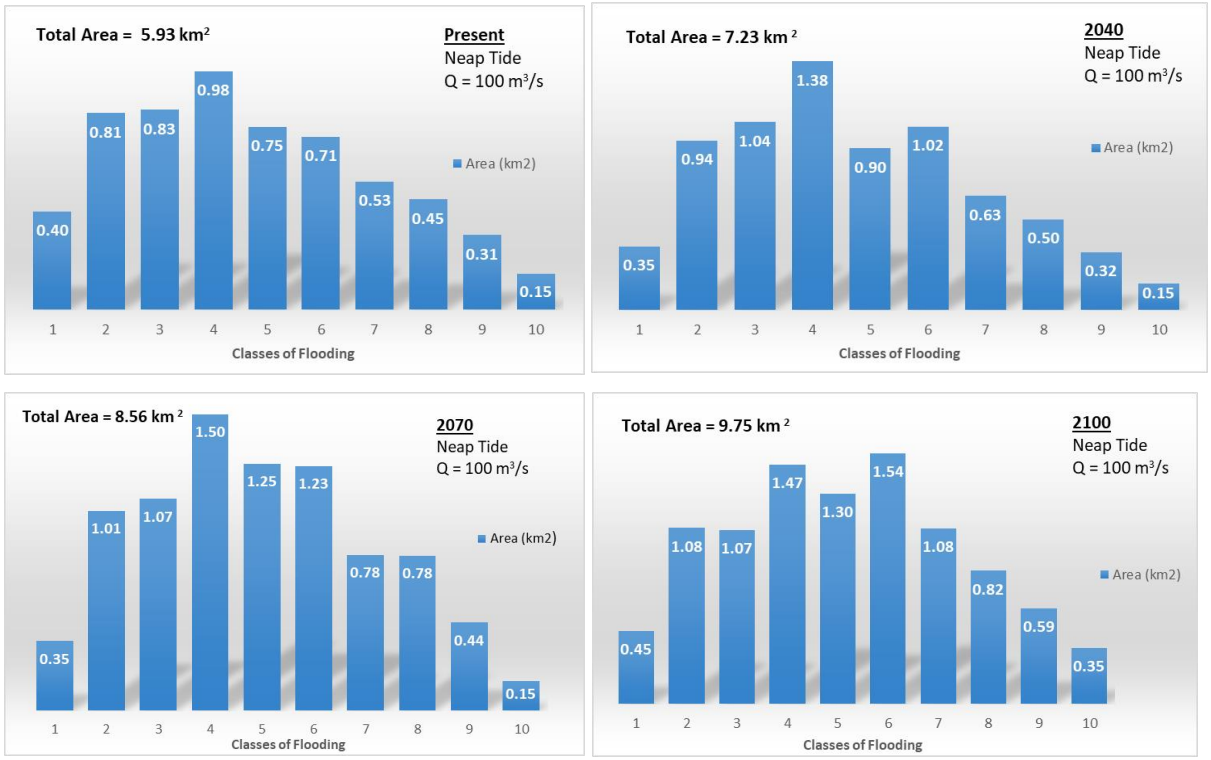


*Figure 4.74* Histogram showing classes of flooding as a function of submersion time for one tidal cycle for the various scenarios of sea level rise at neap tide with a high freshwater flow.

*Table 4.25* Areas of inundation over one tidal cycle at neap tide with a high freshwater flow.

| | | Area (km²) | | | |
|---|---|---|---|---|---|
| **Class** | **Submersion Time (hours)** | **Present** | **2040** | **2070** | **2100** |
| 1 | 0 - 1.2 | 0.40 | 0.35 | 0.35 | 0.45 |
| 2 | 1.2 - 2.4 | 0.81 | 0.94 | 1.01 | 1.08 |
| 3 | 2.4 - 3.7 | 0.83 | 1.04 | 1.07 | 1.07 |
| 4 | 3.7 - 4.9 | 0.98 | 1.38 | 1.50 | 1.47 |
| 5 | 4.9 - 6.1 | 0.75 | 0.90 | 1.25 | 1.30 |
| 6 | 6.1 - 7.3 | 0.71 | 1.02 | 1.23 | 1.54 |
| 7 | 7.3 -8.6 | 0.53 | 0.63 | 0.78 | 1.08 |
| 8 | 8.6 - 9.8 | 0.45 | 0.50 | 0.78 | 0.82 |
| 9 | 9.8 - 11.0 | 0.31 | 0.32 | 0.44 | 0.59 |
| 10 | 11.0 - 12.24 | 0.15 | 0.15 | 0.15 | 0.35 |
| | **Total** | **5.93** | **7.23** | **8.56** | **9.75** |

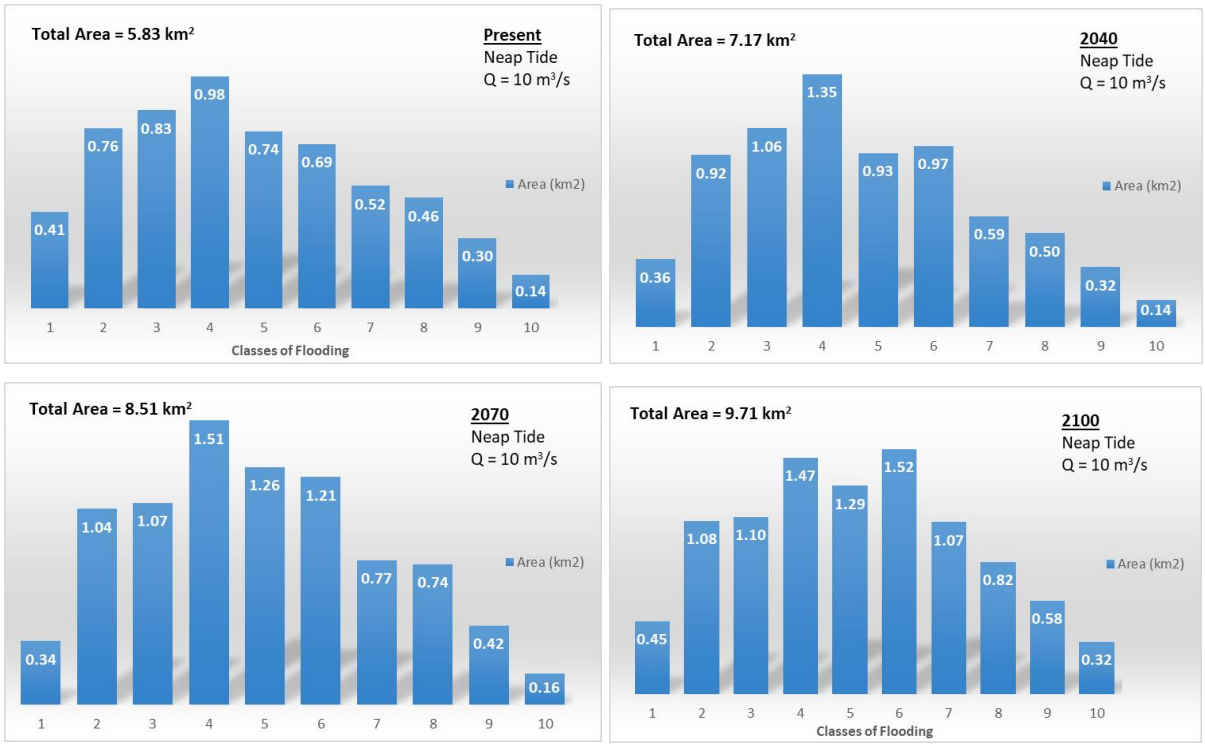


*Figure 4.75* Histogram showing classes of flooding as a function of submersion time for one tidal cycle for the various scenarios of sea level rise at neap tide with a low freshwater flow.

*Table 4.26* Areas of inundation over one tidal cycle at neap tide with a low freshwater flow.

| | | Area ($km^2$) | | | |
|---|---|---|---|---|---|
| **Class** | **Submersion Time (hours)** | **Present** | **2040** | **2070** | **2100** |
| 1 | 0 - 1.2 | 0.41 | 0.36 | 0.34 | 0.45 |
| 2 | 1.2 - 2.4 | 0.76 | 0.92 | 1.04 | 1.08 |
| 3 | 2.4 - 3.7 | 0.83 | 1.06 | 1.07 | 1.10 |
| 4 | 3.7 - 4.9 | 0.98 | 1.35 | 1.51 | 1.47 |
| 5 | 4.9 - 6.1 | 0.74 | 0.93 | 1.26 | 1.29 |
| 6 | 6.1 - 7.3 | 0.69 | 0.97 | 1.21 | 1.52 |
| 7 | 7.3 -8.6 | 0.52 | 0.59 | 0.77 | 1.07 |
| 8 | 8.6 - 9.8 | 0.46 | 0.50 | 0.74 | 0.82 |
| 9 | 9.8 - 11.0 | 0.30 | 0.32 | 0.42 | 0.58 |
| 10 | 11.0 - 12.24 | 0.14 | 0.14 | 0.16 | 0.32 |
| | **Total** | **5.83** | **7.17** | **8.51** | **9.71** |

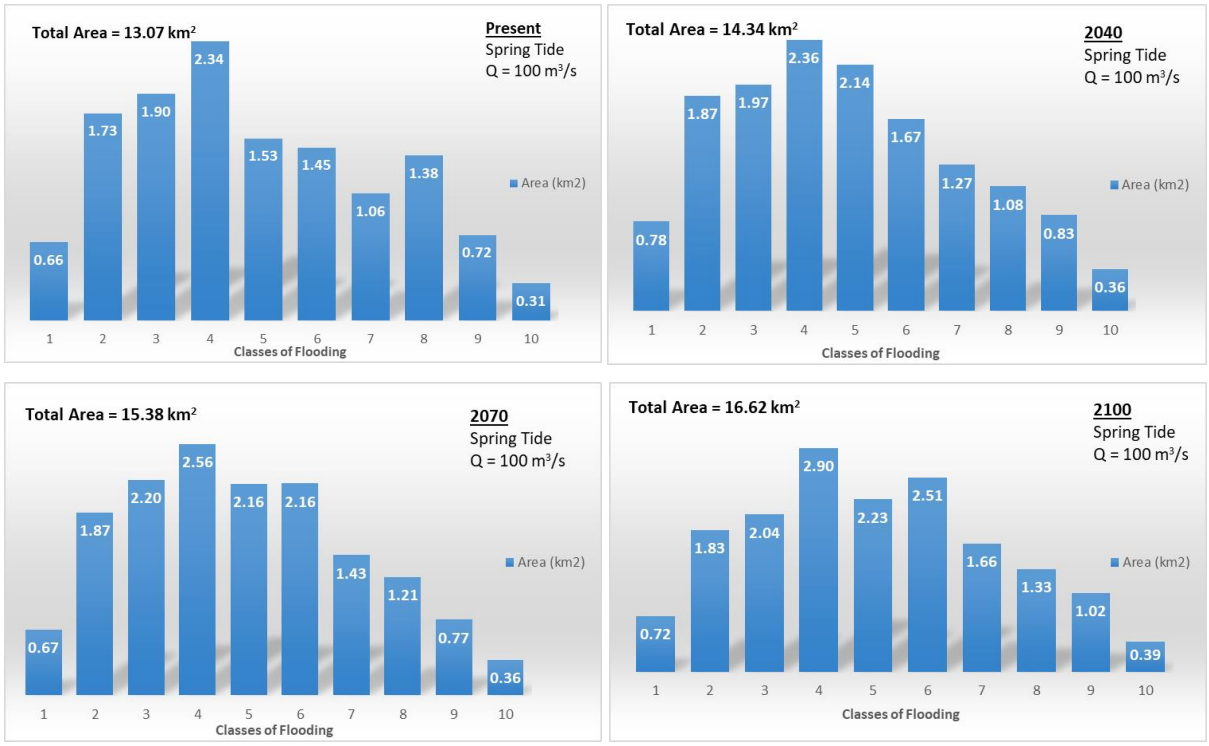


*Figure 4.76* Histogram showing classes of flooding as a function of submersion time for one tidal cycle for the various scenarios of sea level rise at spring tide with a high freshwater flow.

*Table 4.27* Areas of inundation over one tidal cycle at spring tide with a high freshwater flow.

| | | Area ($km^2$) | | | |
|---|---|---|---|---|---|
| **Class** | **Submersion Time (hours)** | **Present** | **2040** | **2070** | **2100** |
| 1 | 0 - 1.2 | 0.66 | 0.78 | 0.67 | 0.72 |
| 2 | 1.2 - 2.4 | 1.73 | 1.87 | 1.87 | 1.83 |
| 3 | 2.4 - 3.7 | 1.90 | 1.97 | 2.20 | 2.04 |
| 4 | 3.7 - 4.9 | 2.34 | 2.36 | 2.56 | 2.90 |
| 5 | 4.9 - 6.1 | 1.53 | 2.14 | 2.16 | 2.23 |
| 6 | 6.1 - 7.3 | 1.45 | 1.67 | 2.16 | 2.51 |
| 7 | 7.3 -8.6 | 1.06 | 1.27 | 1.43 | 1.66 |
| 8 | 8.6 - 9.8 | 1.38 | 1.08 | 1.21 | 1.33 |
| 9 | 9.8 - 11.0 | 0.72 | 0.83 | 0.77 | 1.02 |
| 10 | 11.0 - 12.24 | 0.31 | 0.36 | 0.36 | 0.39 |
| | **Total** | **13.07** | **14.34** | **15.38** | **16.62** |

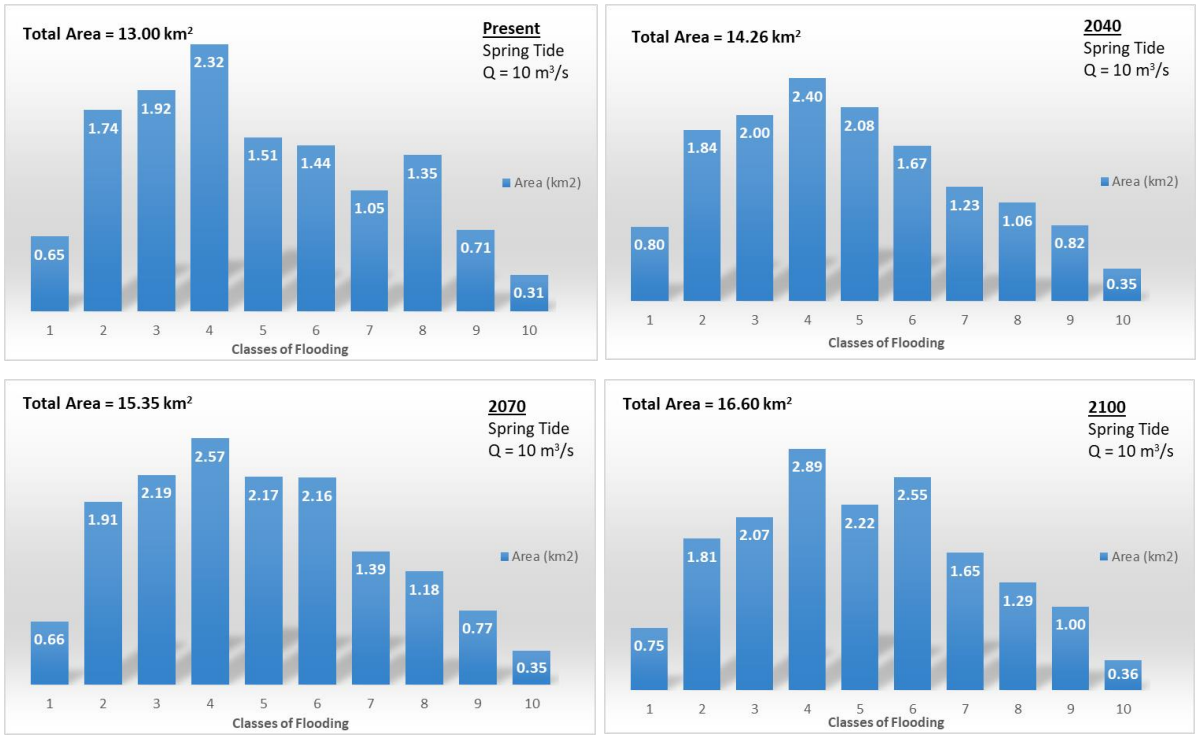


*Figure 4.77* Histogram showing classes of flooding as a function of submersion time for one tidal cycle for the various scenarios of sea level rise at spring tide with a low freshwater flow.

*Table 4.28* Areas of inundation over one tidal cycle at spring tide with a low freshwater flow.

| | | Area ($km^2$) | | | |
|---|---|---|---|---|---|
| **Class** | **Submersion Time (hours)** | **Present** | **2040** | **2070** | **2100** |
| 1 | 0 - 1.2 | 0.65 | 0.80 | 0.66 | 0.75 |
| 2 | 1.2 - 2.4 | 1.74 | 1.84 | 1.91 | 1.81 |
| 3 | 2.4 - 3.7 | 1.92 | 2.00 | 2.19 | 2.07 |
| 4 | 3.7 - 4.9 | 2.32 | 2.40 | 2.57 | 2.89 |
| 5 | 4.9 - 6.1 | 1.51 | 2.08 | 2.17 | 2.22 |
| 6 | 6.1 - 7.3 | 1.44 | 1.67 | 2.16 | 2.55 |
| 7 | 7.3 -8.6 | 1.05 | 1.23 | 1.39 | 1.65 |
| 8 | 8.6 - 9.8 | 1.35 | 1.06 | 1.18 | 1.29 |
| 9 | 9.8 - 11.0 | 0.71 | 0.82 | 0.77 | 1.00 |
| 10 | 11.0 - 12.24 | 0.31 | 0.35 | 0.35 | 0.36 |
| | **Total** | **13.00** | **14.26** | **15.35** | **16.60** |

All varying hydrodynamic factors result in an increase in inundation due to mean sea level rise. The area of inundation is much smaller at neap tide compared to the area of inundation at spring tide, which reflects how much the sea level and tide contribute to the amount of land submerged. It can also be noted that the amount of land area in the higher flooding classes increases with respect to sea level rise. For example, for the present situation with a low freshwater flow during spring tide, 1.44 $km^2$ of land belongs in flooding class 6 (6.1 – 7.3 hours of submersion time during a tidal cycle), but by 2100, 2.55 $km^2$ of land belongs in flooding class 6.

### 4.5.6 Areas of Inundation: Flood Distribution Maps

As previously mentioned, the Python script used to compute flooding areas during one tidal cycle also resulted in flood distribution maps to view the areas of inundation. The maps show the land submerged for any portion of time in a tidal cycle. Each flooding class is represented by color. The flood distribution map for a high freshwater discharge at neap tide is shown in Figure 4.78, for a low freshwater at neap tide in Figure 4.79, for a high freshwater discharge at spring tide in Figure 4.80 and for a low freshwater discharge at spring tide in Figure 4.81.

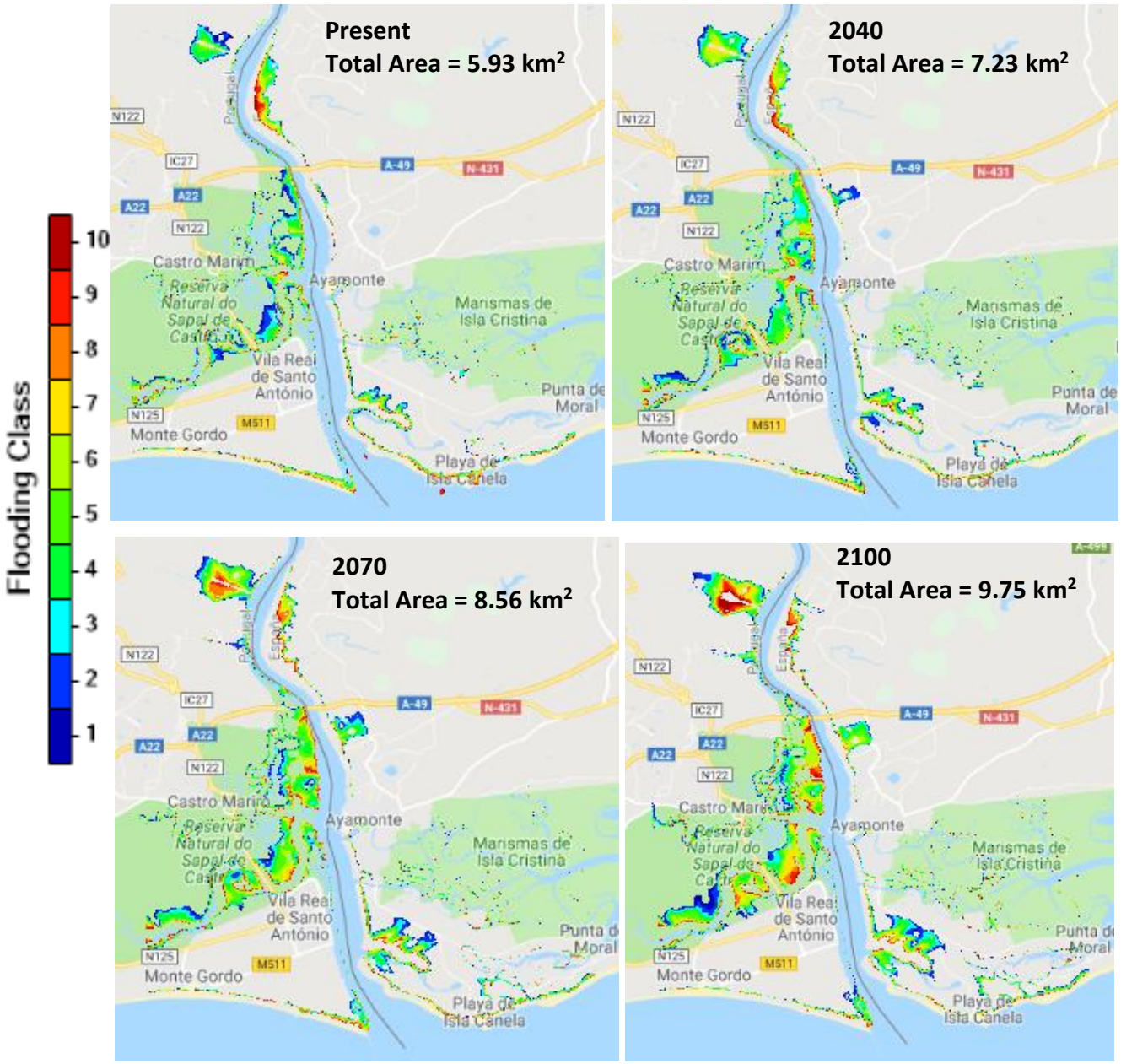


*Figure 4.78* Flood distribution maps for a high freshwater discharge during neap tide for the various scenarios of sea level rise.

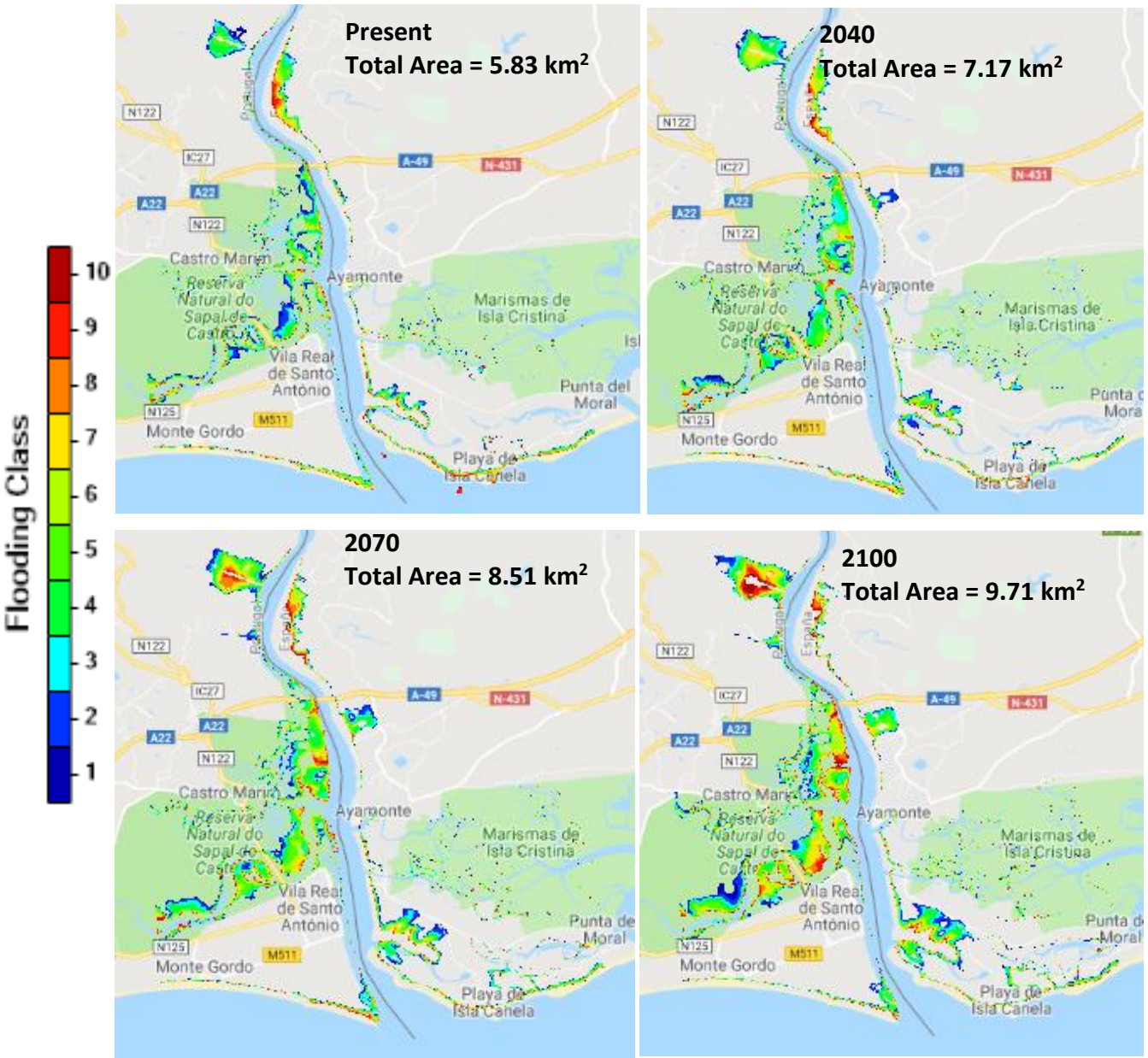


*Figure 4.79* Flood distribution maps for a low freshwater discharge during neap tide for the various scenarios of sea level rise.

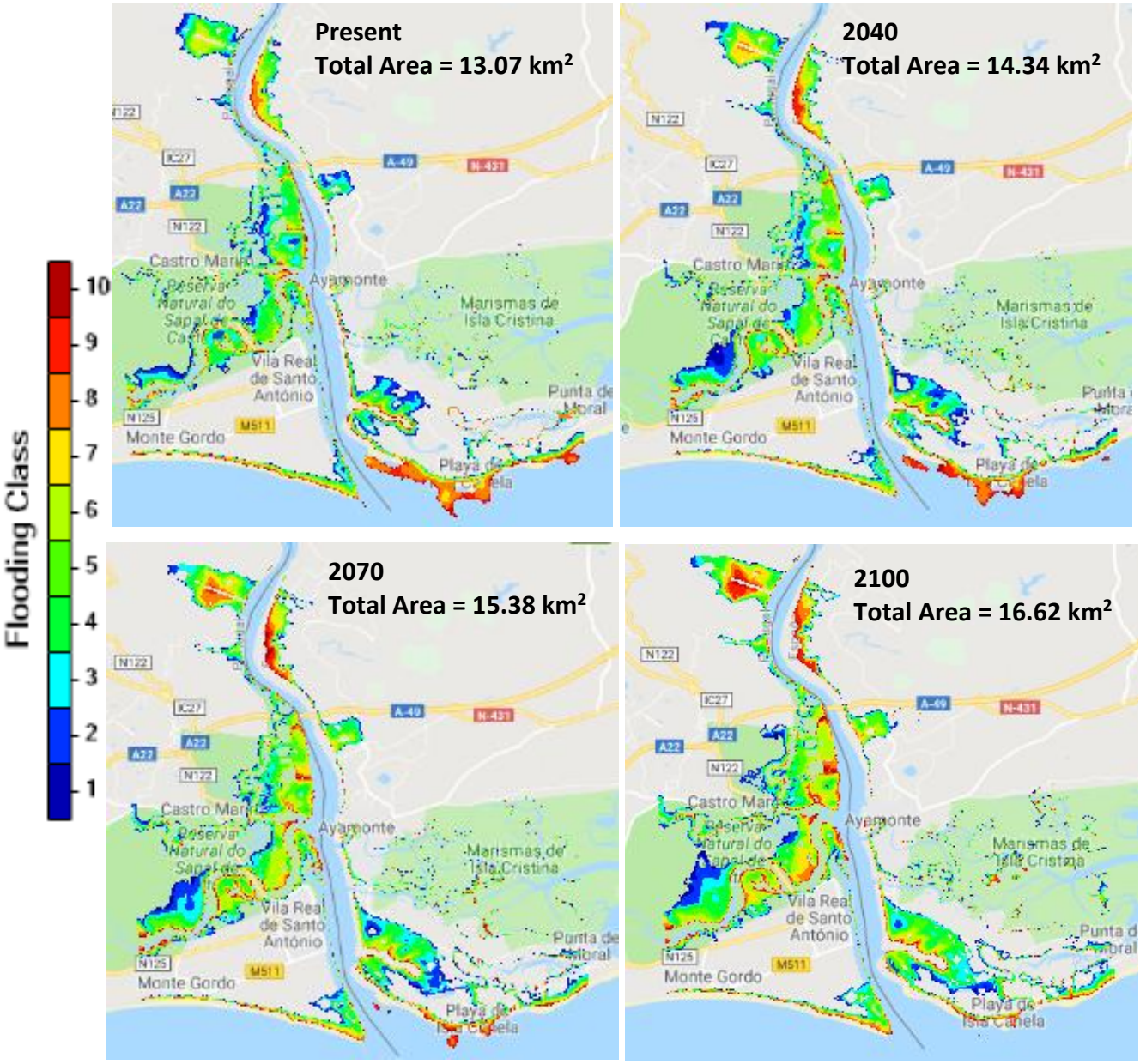


*Figure 4.80* Flood distribution maps for a high freshwater discharge during spring tide for the various scenarios of sea level rise.

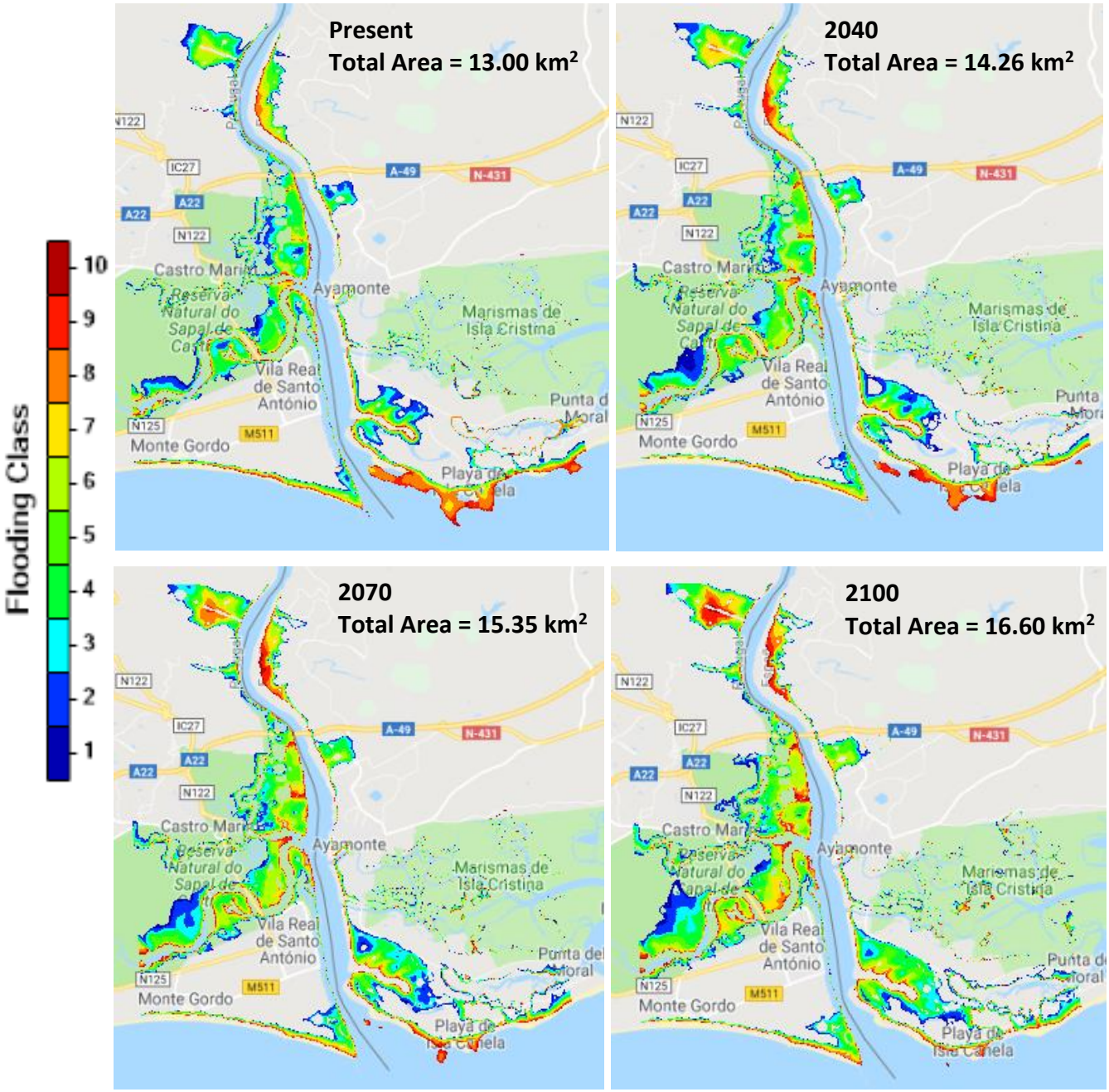


*Figure 4.81* Flood distribution maps for a low freshwater discharge during spring tide for the various scenarios of sea level rise.

# 5 Discussion

The two main objectives of this work were to evaluate how climate change will impact (1) salinity distribution and (2) flooding areas in and around the Guadiana Estuary. Thus, the following section discusses and analyzes the results of salinity and land inundation. It begins with an analysis of all model results and how they compare to previous findings of the hydrodynamics of the Guadiana Estuary. This section further explores how changes in the dynamics of the Guadiana Estuary will impact socioeconomic activities.

## 5.1 Hydrodynamic and Salinity Results

The hydrodynamics of the Guadiana Estuary are complex and several different output results were observed based on the varying inputs of the model. The following section discusses the results of salinity for a high freshwater discharge at neap tide (5.1.1), a low freshwater discharge at neap tide (5.1.2), a high freshwater discharge at spring tide (5.1.3) and a low freshwater discharge at spring tide (5.1.4) for both types of bathymetry.

### 5.1.1 Evolution of Salinity for a High Freshwater Discharge at Neap Tide

For the present bathymetry, salinity does not reach the upper and middle regions of the estuary for the situation of a high freshwater discharge at neap tide. The furthest extension of the salt intrusion is at the inlet into Esteiro da Leziria (381_147), which has salinity values of approximately 6 in high water conditions. There is a small decrease in salinity at this location with respect to sea level rise. The velocity results at this location also portray a consistent decrease in velocity of approximately 0.1 m/s every thirty years. The decrease in velocity could be attributed to the deepening of the channel from the increase in water volume. This result has been known to occur in shallow ebb-dominated estuaries and further enhances tidal asymmetries (Friedrichs et al., 1990). In order to gain further insight into the effects the decrease in velocity has on salinity at specific points in the estuary, velocity direction was viewed over the salinity distribution maps. MOHID studio allows the visualization of different module layers, so each horizontal distribution map of salinity was viewed along with the associated velocity vectors from the hydrodynamics file. Figure 5.1 shows velocity direction and salinity values at a time instant of one hour before high tide at the inlets of Esteiro da Leziria and Esteiro da Carrasqueira for the various scenarios of sea level rise.

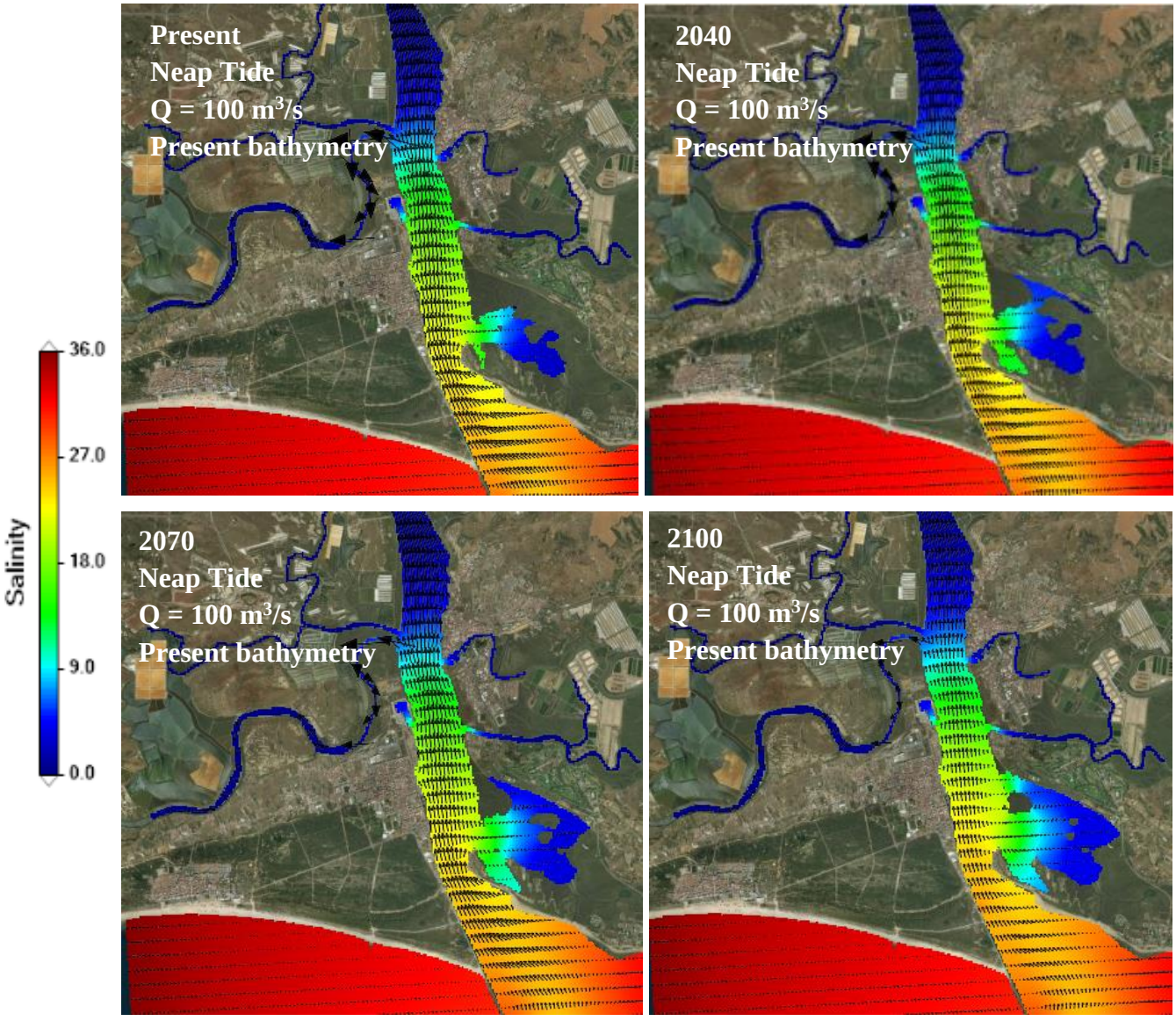


*Figure 5.1* Velocity direction and salinity distribution near the inlet into the marshes for a high freshwater flow at neap tide over the present bathymetry for the various scenarios of sea level rise at a time instant of one hour before high tide.

Figure 5.1 reveals how salt is transported into the stream of Esteiro da Carresqueira before reaching the inlet at Esteiro da Leziria. The magnitude of velocity at this area also increases with respect to sea level rise. This is further justified in the velocity time series result at the location downstream Esteiro da Carresqueira (350_80), as an increase in velocity modulus is portrayed with respect to sea level rise (Figure 4.7). Thus, the decrease in salinity at Esteiro da Leziria can be attributed to the transportation of seawater westward into Esteiro da Carresqueira. It can also be noted in Figure 5.1 that water is transported eastward toward Estero de Bruno on the Spanish side. The horizontal displacement of seawater entering the estuary prevents salinity from reaching the channel further upstream, which is why there is a decrease in salinity at several of the locations included in the time series results.

The mouth of the estuary (313_153) results in a small increase in salinity from the present year to 2040 and from 2040 to 2070, but by 2100 the increase in salinity accelerates by 0.13. The marshes all experience an initial decrease in salinity from the present to 2040, but this decrease in salinity decelerates by 2070 and then starts to increase in 2100.

The salinity results from the alternate bathymetry differ drastically from the results from the present bathymetry. The salinity does not reach the upper estuary, but the salt intrusion extends much further upstream by the year 2100 compared to the extension of salinity for the present bathymetry. The salt intrusion extends approximately 20 kilometers upstream at Foz de Odeleite (903_102) with an increase in salinity from 0 to 0.06 by the year 2100. The middle of the estuary (558_103) experiences a consistent increase of 0.01 in salinity but accelerates by 0.03 in the year 2100. The salinity increase in the lower estuary is much more pronounced with salinity increasing by more than 1 every thirty years. The rate of salinity increase is also accelerating at all points in the estuary. Salinity values in the marshes are generally below 6 apart from the easternmost region of Castro Marim (391_96) where salinity increases from 0 to slightly above 6 at high tide by the year 2100. Figure 5.2 demonstrates the transport and distribution of salinity in the marshes on both the Portuguese and Spanish side of the estuary. The bathymetry allowing flooding, allows saltwater to be transported far through Estero de Canela, as it completely floods the national park of Marismas de Isla Cristina by the year 2100.

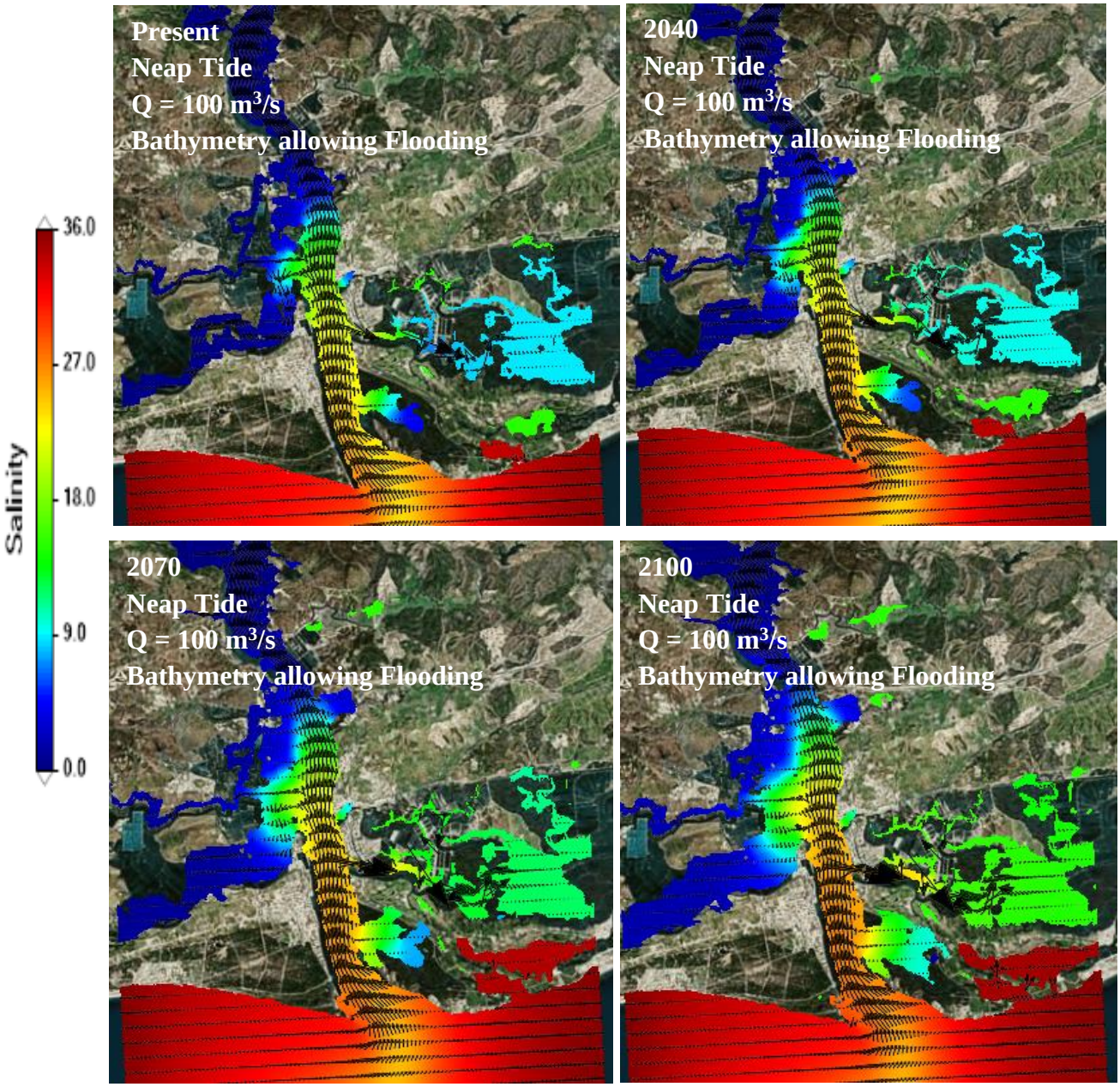


*Figure 5.2* Velocity direction and salinity distribution near the inlet into the marshes for a high freshwater flow at neap tide over the bathymetry allowing flooding for the various scenarios of sea level rise at a time instant of one hour before high tide.

### 5.1.2 Evolution of Salinity for a Low Freshwater Discharge at Neap Tide

The results for the present bathymetry at neap tide with a low freshwater discharge reveal that salinity decreases from the present year until 2040. This result is inconsistent with results obtained from the other scenarios. The simulation for the year 2040 was run several more times by altering the Courant number and thus decreasing the time-step, but the same result was still obtained. Another run was also inserted into this simulation to allow more time for the salinity field to stabilize, but again the same results were obtained. It was not in the time frame of this work to allow for another run considering the high computational time mentioned in the methods section. It can be noted from the summary of changes in velocity in Table 4.3 that velocity decreases in the middle and lower regions of the estuary as well as the regions in the marshes that are closest to the main channel. Figure 5.3 demonstrates the transport of salinity eastward on the Spanish side. Salinity then seems to remain in the main channel close to the mouth. The horizontal distribution maps portray the advection of salinity eastward toward Isla Cristina throughout the scenarios of sea level rise. The eastward movement of salinity can justify the decrease in salinity at several of the location points in the time series, as locations east of the estuary were not evaluated in the time series.

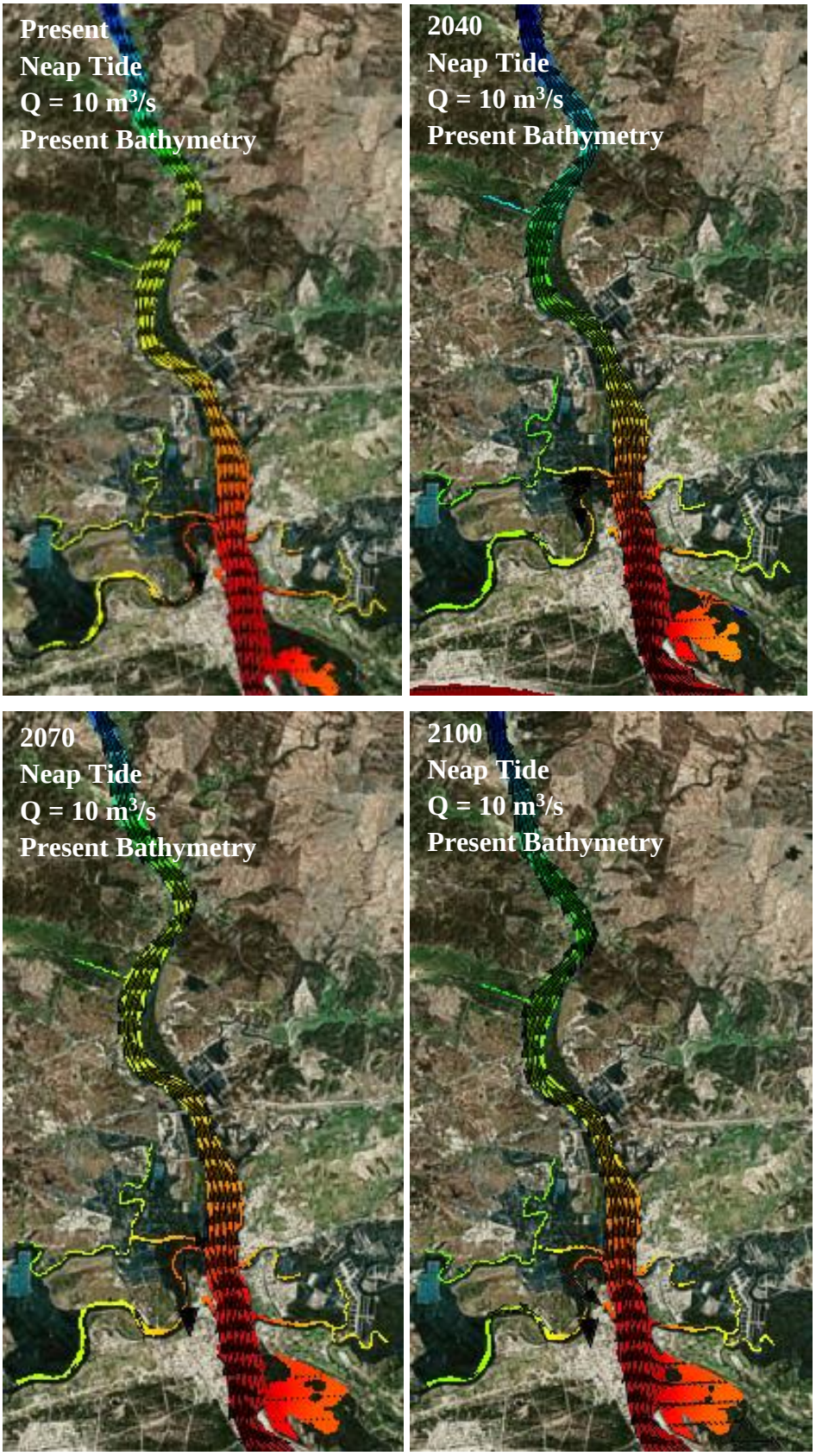


*Figure 5.3* Velocity direction and salinity distribution for a low freshwater flow at neap tide over the present bathymetry for the various scenarios of sea level rise at a time instant of one hour before high tide.

On the other hand, the bathymetry allowing flooding experiences an overall increase in salinity at all points in and around the estuary. The upper estuary experiences a very small change in salinity. The main channel and majority of the marsh area all experience an increase in salinity by about 1 for each thirty-year interval. The only exception is at the westernmost region of Castro Marim (392_23) where there is a large decrease in salinity from 2070 to 2100. It can be noted in the analysis of the velocity modulus that velocity decelerates from the year 2070 to 2100 in this same location. The decrease in salinity could be attributed to the saltwater being transported elsewhere, such as upstream the estuary.

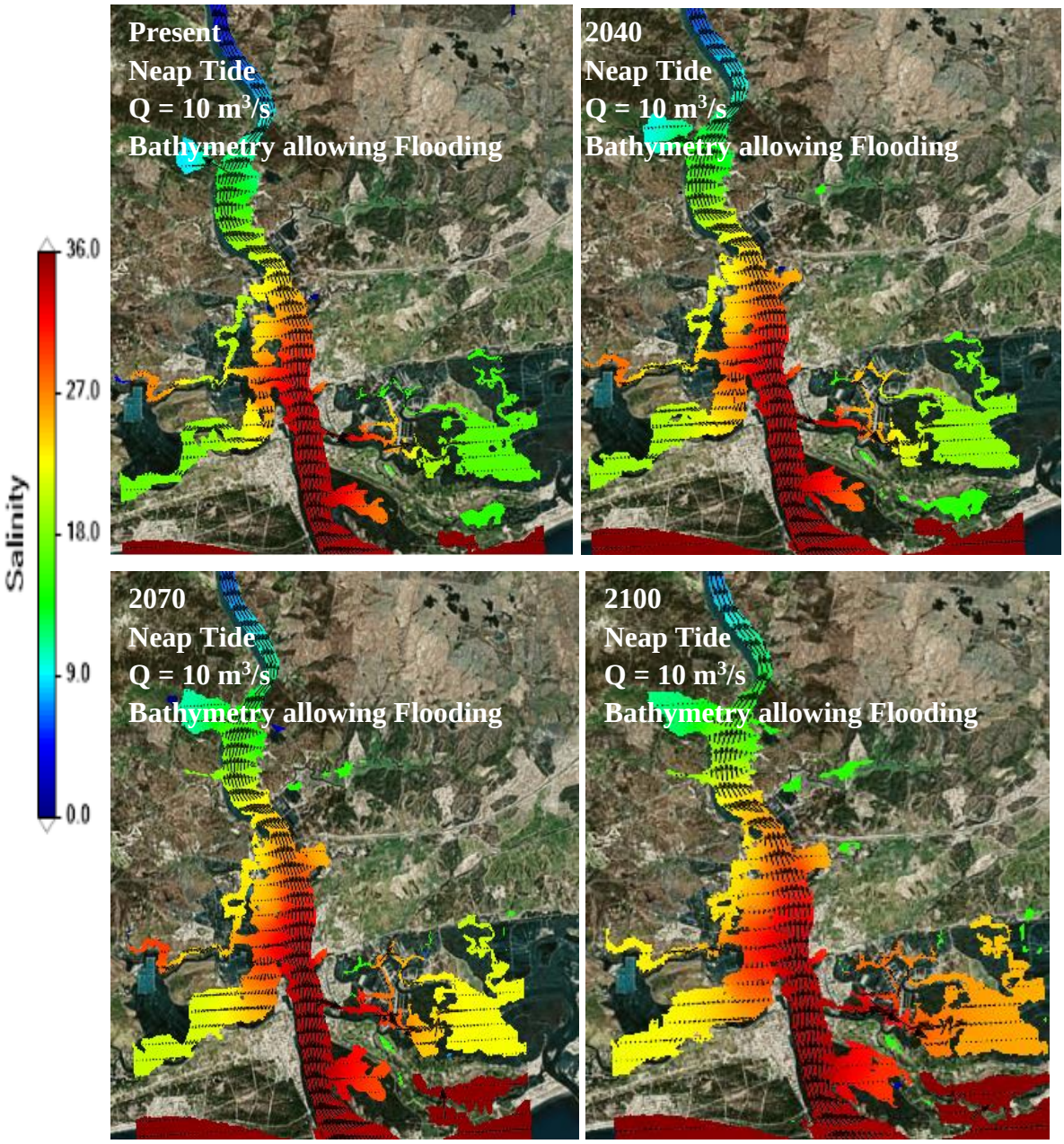


*Figure 5.4* Velocity direction and salinity distribution at all areas affected by the salinity front for a low freshwater flow at neap tide over the bathymetry allowing flooding one hour before high tide.

### 5.1.3 Evolution of Salinity for a High Freshwater Discharge at Spring Tide

The present bathymetry experiences an overall increase in salinity in response to sea level rise for a high freshwater discharge at spring tide. The change in salinity is very small in the upper estuary and is much more pronounced in the middle and lower estuary. It can also be noted in the time series analysis of velocity that velocity increases in the mid-upper estuary (903_102) by 2040, but then stays the same until 2100. There is also a consistent decrease in velocity of 0.01 m/s at the point closest to the mouth in front of Vila Real de Santo Antonio (313_153). This is consistent with the results obtained at neap tide for this location, and thus again can be attributed to the deepening of the channel. However, despite the increase in velocity, there is an increase in salinity at this point with respect to sea level rise. Figure 5.5 demonstrates the stronger penetration of seawater at this point, especially as sea level increases.

The marsh area experiences a small decrease in salinity. The largest decrease in salinity is found at the furthest point from the main channel at Esteiro da Carrasqueira (304_27). This could be attributed to the salinity being transported further up the main channel as the velocity time series show an increase in velocity at locations upstream the main channel (Figure 4.16 and Figure 4.18). The lower estuary in front of Vila Real de Santo Antonio (313_153) and at the inlet into the marshes at Esteiro da Leziria (381_147) both portray an increase in salinity with respect to sea level rise. It can also be noted in Figure 4.46 and Figure 4.50 that salinity values vary greatly with respect to the tide. At high tide, salinity values reach nearly 30 by 2100, but drop close to 0 during low tide. The velocity direction over the horizontal distribution maps is shown in Figure 5.5.

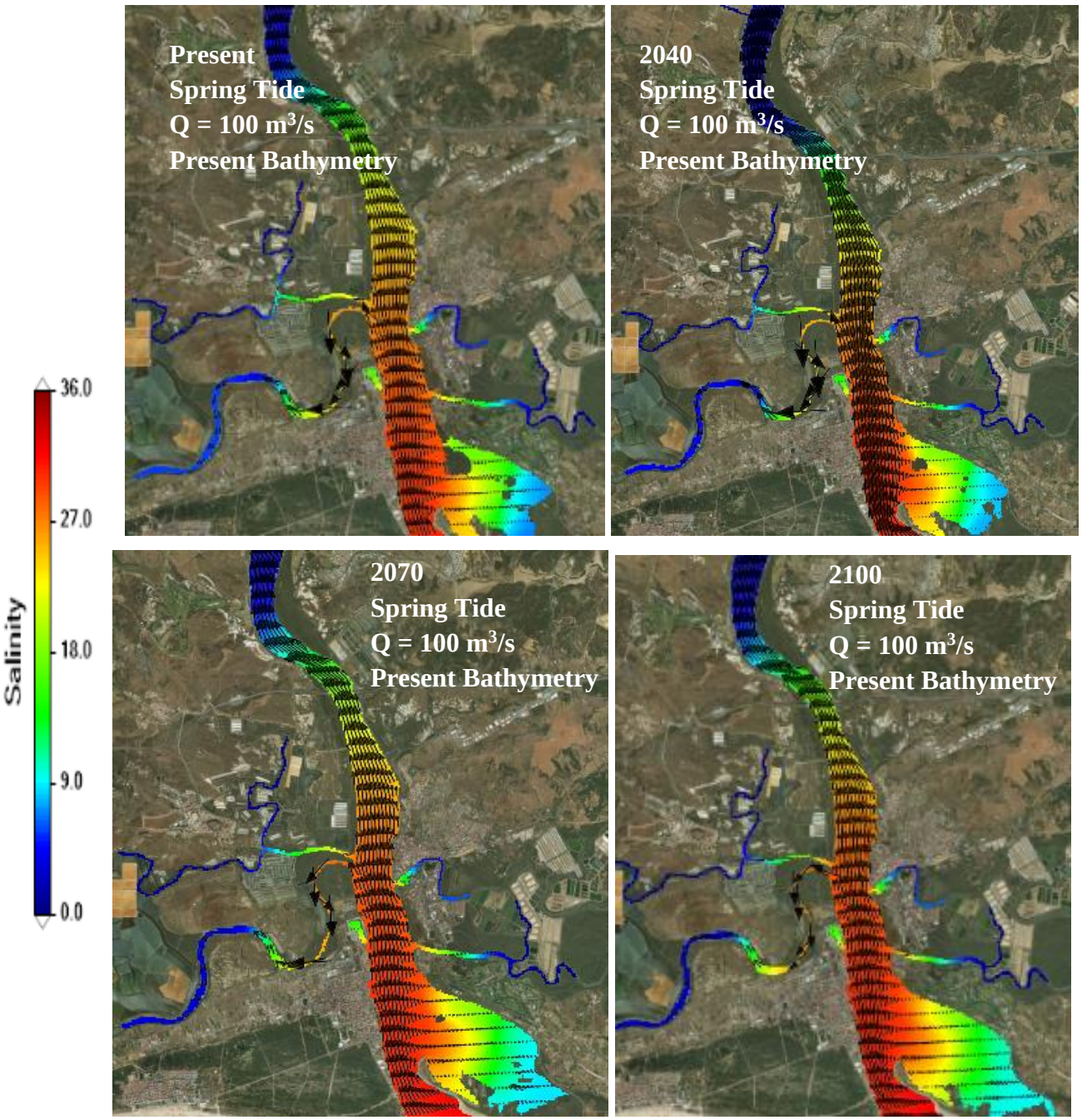


*Figure 5.5* Velocity direction and salinity distribution at all areas affected by the salinity front for a high freshwater flow at spring tide over the present bathymetry one hour before high tide.

For the bathymetry allowing flooding there is an increase in salinity at all points in the estuary with respect to sea level rise. The upper estuary experiences a minute decrease in salinity from the present year to 2040, which then increases by 2070 and 2100. Unlike velocity results from the present bathymetry, the bathymetry that allows flooding does not experience an increase in velocity in the upper estuary. There is a decrease in velocity of 0.03 m/s at the uppermost region of the estuary (1377_45) between the years 2040 and 2070, which then returns to the original value by the year 2100. This can explain the small decrease in salinity in the upper estuary.

The middle to lower regions of the main channel as well as the marshes result in an increase in salinity by roughly 1.5 every thirty years. Similar to the results obtained for the present bathymetry, the area in front of Vila Real de Santo Antonio (313_153) and the inlet into the marshes at Esteiro da Leziria (381_147) yield the highest salinity values, with salinity values above 30 by the year 2100 in both locations. These two areas also have the highest values of velocity as shown in Figure 4.18 and Figure 4.22.

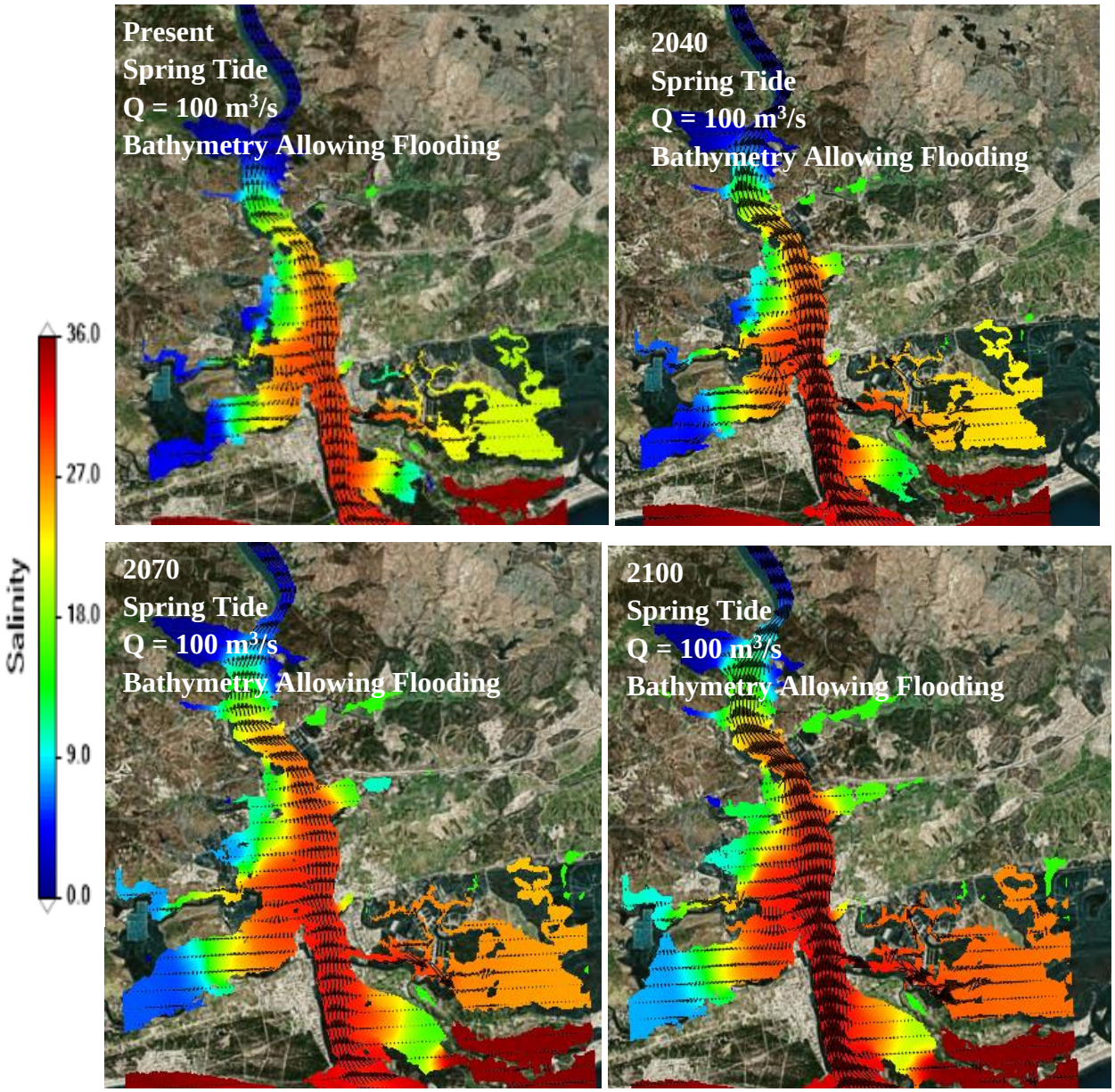


*Figure 5.6* Velocity direction and salinity distribution at all areas affected by the salinity front for a high freshwater flow at spring tide over the bathymetry allowing flooding.

### 5.1.4 Temporal Evolution of Salinity for a Low Freshwater Discharge at Spring Tide

The present bathymetry results in a small decrease in salinity for a low freshwater discharge at spring tide for all points in the estuary. This result coincides with the velocity results in the sense that there is an overall decrease in velocity. The decrease in salinity is smallest in the upper estuary. The initial decrease from the present year to 2040 is the largest, with salinity values decreasing by approximately 2 in the marsh area and middle estuary. The decrease in salinity decelerates by the year 2070 and then starts to increase again from 2070 to 2100. The decrease in salinity could be attributed to the reduction in velocity modulus as shown in the time series results (Figures Figure 4.23 - Figure 4.29). Figure 5.7 reveals an overall decrease in velocity, especially in the marsh area. Salinity continues to propagate further upstream by the year 2100 but does not extend into the marshes on either side of the estuary.

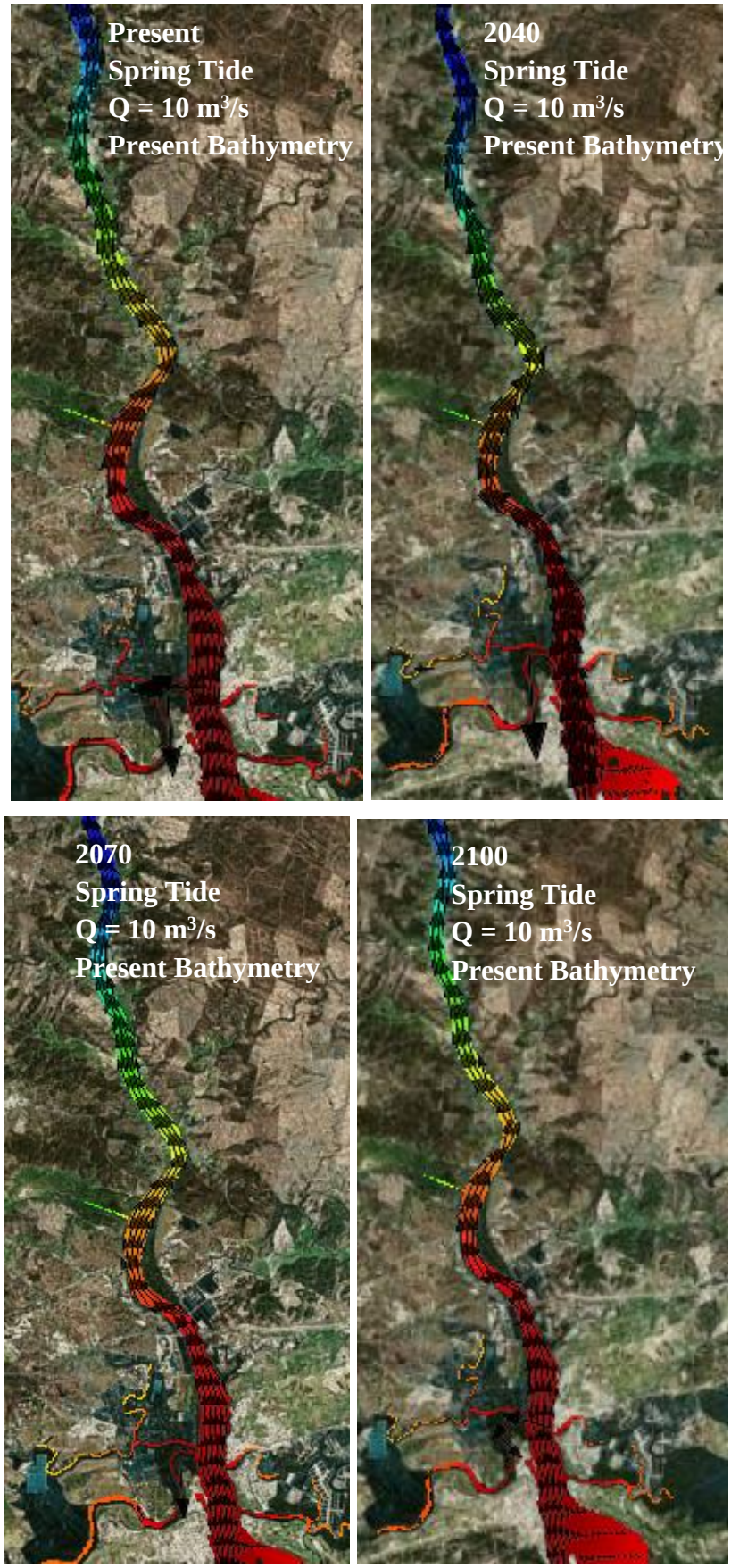


*Figure 5.7* Velocity direction and salinity distribution at all areas affected by the salinity front for a high freshwater flow at spring tide over the bathymetry allowing flooding.

The results obtained from the alternate bathymetry differ drastically compared to the results from the present bathymetry. Salinity values are positively correlated with respect to mean sea level rise at all points in the estuary. Salinity extends to the furthest point upstream the estuary at Alcoutim (1377_45) by the year 2100. The middle and lower regions of the estuary experience an increase in salinity by approximately 1 every thirty years. The marsh area is greatly impacted by the sea level rise as the salinity increases by approximately 2 from the present year until 2040. The westernmost region of Castro Marim (392_23) has the most drastic increase in salinity by the year 2040, with salinity increasing by about 6 from the present year until 2040. The salinity continues to increase, but at a much slower rate by 2070 and by 2100. By the year 2100, salinity values reach almost 36. The variability in salinity values throughout the 24-hour period is much less compared to variability in salinity for the higher discharge. This result highlights the impacts the flow has on the residence time of salinity at certain locations in the estuary.

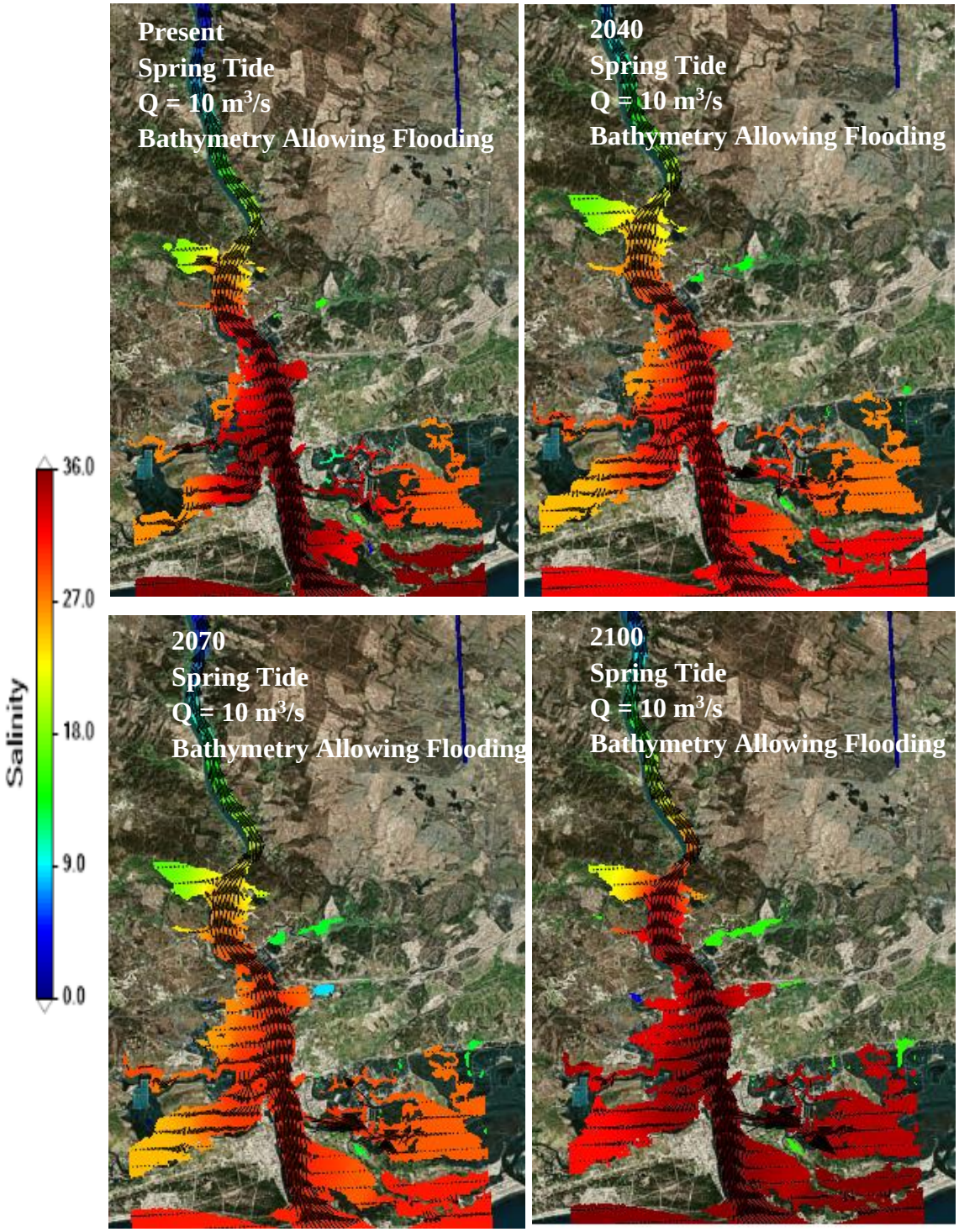


*Figure 5.8* Velocity direction and salinity distribution at all areas affected by the salinity front for a high freshwater flow at spring tide over the bathymetry allowing flooding.

### 5.1.5 Overall Impact of Salinity Change on the Guadiana Estuary

The results obtained from the MOHID model have shown the dynamics of the Guadiana Estuary to be quite complex, especially with respect to the tides. Furthermore, the results from the bathymetry that allow flooding of the saltmarshes and low-lying areas differ drastically from the results for the present bathymetry. For the bathymetry allowing flooding, salinity increases almost linearly with respect to mean sea level rise for all cases of freshwater flow and each tidal scenario. On the other hand, the present bathymetry that does not allow the coastline to be changed and thus keeps water in the present-day basin, results in a highly complex dynamic where salinity values vary at different locations with respect to mean sea level rise.

All salinity results for each type of bathymetry, freshwater discharge scenario and tidal scenario demonstrate that the western margin in front of Vila Real de Santo Antonio (313_153) have the highest values in salinity. This is most likely due to the penetration of salt water from the Gulf of Cadiz at this location where tidal currents are strongest (Fortunato et al., 2002). The spatial distribution of salinity intrusion depends on the freshwater flow and tidal scenario. Salinity extends horizontally into the marshes when the freshwater flow from the Guadiana River is high. Salinity extends further upstream when the river discharge is low. These results are consistent with those from Mills et al. (2019) who also found larger changes in velocity and salinity in the marshes near Esteiro da Leziria for higher freshwater discharges compared to changes in velocity and salinity in the main channel. Likewise, results from Mills et al. (2019) found larger changes in velocity and salinity upstream the main channel for low freshwater discharges. The bathymetry allowing flooding allows salinity to extend much further into the marshes, with some areas reaching salinity values close to 36 by 2100.

Salinity increases with respect to mean sea level rise. Although the results from the present bathymetry may not portray an increase in salinity at the points chosen for the time series, salinity does increase on the Spanish side of the estuary as shown in Figure 5.1 and Figure 5.3. The bathymetry allowing flooding reveals a more linear relationship at each of the time series locations between sea level rise and salinity. Results obtained from this model are consistent with results from other numerical models who have modeled changes in salinity in estuaries caused by sea level rise and have found an increase in salinity (Chua & Xu, 2014; Hong & Shen, 2012; Vargas et al., 2017). The results of this model indicate that bathymetry, freshwater flow and spring-neap tide variability impact the horizontal distribution of salinity intrusions caused by sea level rise.

### 5.1.6 Impact of Land Inundation

The flood distribution maps all reveal an overall increase in inundated land area caused by sea level rise. The area of inundation is much larger during spring tide compared to neap tide. For example, by the year 2100, 16.62 $km^2$ of land is inundated for a high freshwater discharge at spring tide compared to 9.75 $km^2$ of land inundated at neap tide in the same year. Results do not differ significantly for different freshwater flows, which demonstrates that the increase in land inundation is based on solely on the increase in sea level. Flooded areas also move up in flooding class with respect to sea level rise, meaning the number of hours submerged during one tidal cycle increases. Flooded areas will severely impact both society and the economy of the region. For example, the Esuri housing development mentioned in section 2.2.5 will contain a large amount of flooded area by 2100 at spring tide with some areas fully submerged during a tidal cycle as shown in Figure 5.9.

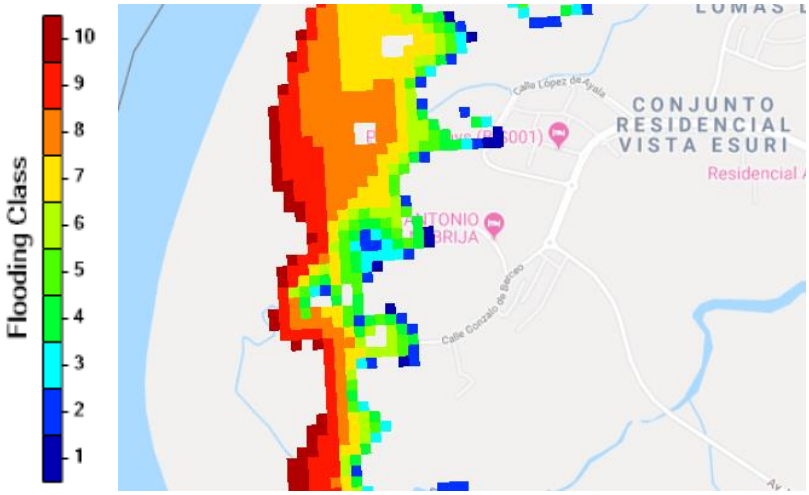


*Figure 5.9* Area of inundation in 2100 near the Esuri housing development at spring tide for a high freshwater flow.

Another important area affected by flooding caused by sea level rise is Castro Marim on the Portuguese side of the estuary. Castro Marim is an extensive area of salt marsh hosting a wide range of biodiversity (Gonçalves, 2015). The creeks of Esteiro da Leziria and Esteiro da Carrasqueira are highly valuable for the reproduction of many commercial fish. The density of fish larvae in this area is dependent on the balance of freshwater flow from the Guadiana River and flooding events. At present, Castro Marim is known to be completely inundated only during spring tide. It is under these conditions of irregular flooding and freshwater flow that fish larvae can survive (Gonçalves, 2015). However, changes in the environment will impact the abundance and diversity of species in Castro Marim. The reduction in freshwater flow has

already led to a reduction in primary production in the area (Gonçalves, 2015). As the survival of fish larvae is dependent on the delicate balance between freshwater flow and incoming seawater, the increase in mean sea level will have a large impact on the biodiversity in Castro Marim. Figure 5.10 shows the flooding areas of Castro Marim in the year 2100. It can be noted that even during neap tide several areas fall under flooding class 10, meaning these areas will be fully submerged under one tidal cycle.

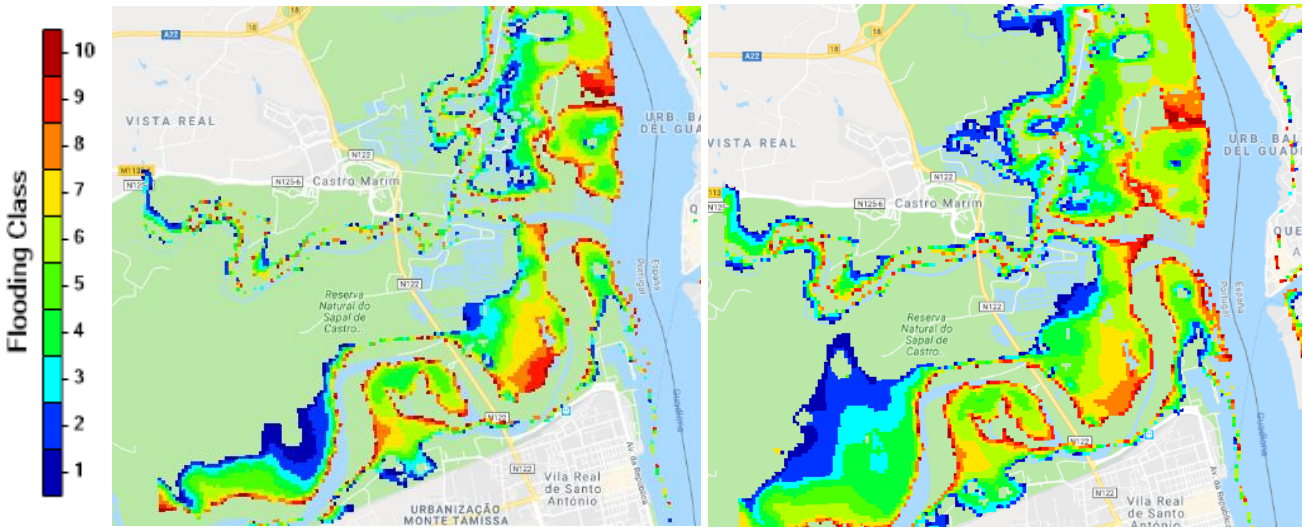


*Figure 5.10* Land submerged at Castro Marim during one tidal cycle at neap tide (left) and spring tide (right) in the year 2100.

# 6 Conclusion

The two-dimensional MOHID water model produced hydrodynamic, salt transport maps and flood distribution maps to gain further insight into the future state of the Guadiana Estuary as it responds to climate change. The results of the model demonstrate the dynamics of the estuary to be complex. The estuary responds differently to sea level rise based on freshwater flow, bathymetry and tidal amplitudes. The results of the model can be used to fully assess and predict the future state of the Guadiana Estuary for both a situation of an unchanged coastline and a likely situation in which the bathymetry evolves due to climate change.

All results portray an increase in salinity in response to sea level rise. The spatial distribution of salinity is highly dependent on the bathymetry as well as freshwater flow and tidal amplitude. When the freshwater flow is low in the spring and summer months, salinity extends upstream. When the freshwater flow is high due to rainfall in the winter, salinity extends westward and eastward into the marshes of Portugal and Spain.

Flooding areas were also computed and demonstrated that the amount of land submerged under one tidal cycle increases with respect to sea level rise. Results of the model can be used to further evaluate the impacts of flooding at specific points along the estuary and to predict length of submersion time during one tidal cycle.

The results obtained from the model can serve as a tool for coastal managers to evaluate the future state of the Guadiana Estuary and to manage areas that will be impacted by salinity intrusion and land inundation. The increase in saline waters and flooding areas in and around the Guadiana Estuary will not only impact the physical dynamics of the estuary, but also society who rely on the estuary for socioeconomic and commercial activities. It should be noted that the original plan of this dissertation was to also apply the results of the model from the work of Mills et al. (2019) on the current socioeconomic status of the Guadiana Estuary and how it will evolve due to climate change. However, due to the high computational time of the execution of more than 32 simulations to analyze how spring-neap tide variability, freshwater flow variability and changes in bathymetry will impact the estuary, it became time prohibitive to achieve the socioeconomic objective. The results of this model can be used by experts in the socioeconomic profession to assess more concretely how the physical evolution of the estuary in response to climate change will further impact society and the economy.

One limitation of this model is the use of a two-dimensional model as opposed to a three-dimensional model. This was justified because the estuary is well-mixed, but there may be some variability in the water column due to the complex dynamics of the system, especially at neap tide. Future studies could develop a three-dimensional model to provide a more complete evaluation of the estuary and how it responds to climate change.

# References


Basos, N. (2013). *GIS as a tool to aid pre- and post-processing of hydrodynamic models . Application to the Guadiana Estuary Faculdade de Ciências e Tecnologia e Instituto Superior de Engenharia GIS as a tool to aid pre- and post-processing of hydrodynamic models . Applica*. Faro, Portugal.

Bilskie, M. V., Hagen, S. C., Medeiros, S. C., & Passeri, D. L. (2014). Dynamics of sea level rise and coastal flooding on a changing landscape. Geophysical Research Letters. *Geophysical Research Letters*, *41*(3), 927–934. https://doi.org/10.1002/2013GL058759.Standard

Brown, S., Nicholls, R. J., Goodwin, P., Haigh, I. D., Lincke, D., Vafeidis, A. T., & Hinkel, J. (2018). Quantifying Land and People Exposed to Sea-Level Rise with No Mitigation and 1.5°C and 2.0°C Rise in Global Temperatures to Year 2300. *Earth's Future*, *6*(3), 583–600. https://doi.org/10.1002/2017EF000738

Carrasco, A. R., Ferreira, O., & Roelvink, D. (2016). Coastal lagoons and rising sea level: A review. *Earth-Science Reviews*, *154*, 356–368. https://doi.org/10.1016/j.earscirev.2015.11.007

Cazenave, A., & Cozannet, G. Le. (2013). *Earth ' s Future Sea level rise and its coastal impacts Earth ' s Future*. 15–34. https://doi.org/10.1002/2013EF000188.Received

Chua, V. P., & Xu, M. (2014). Impacts of sea-level rise on estuarine circulation: An idealized estuary and San Francisco Bay. *Journal of Marine Systems*, *139*, 58–67. https://doi.org/10.1016/j.jmarsys.2014.05.012

Church, J. A., Clark, P. U., Cazenave, A., Gregory, J. M., Jevrejeva, S., Levermann, A., … Unnikrishnan, A. S. (2013). 2013: Sea level change. *Climate Change 2013: The Physical Science Basis. Contribution of Working Group I to the Fifth Assessment Report of the Intergovernmental Panel on Climate Change*, 1137–1216. https://doi.org/10.1017/CB09781107415315.026

Church, J. A., & White, N. J. (2011). Sea-Level Rise from the Late 19th to the Early 21st Century. *Surveys in Geophysics*, *32*(4–5), 585–602. https://doi.org/10.1007/s10712-011-9119-1

Delgado, J., Boski, T., Nieto, J. M., Pereira, L., Moura, D., Gomes, A., … García-Tenorio, R. (2012). Sea-level rise and anthropogenic activities recorded in the late Pleistocene/Holocene sedimentary infill of the Guadiana Estuary (SW Iberia). *Quaternary Science Reviews*, *33*, 121–141. https://doi.org/10.1016/j.quascirev.2011.12.002

Delgado, Joaquín, Barba-Brioso, C., Nieto, J. M., & Boski, T. (2011). Speciation and ecological risk of toxic elements in estuarine sediments affected by multiple anthropogenic contributions (Guadiana saltmarshes, SW Iberian Peninsula): I. Surficial sediments. *Science of the Total Environment*, *409*(19), 3666–3679. https://doi.org/10.1016/j.scitotenv.2011.06.013

Fleming, K., Johnston, P., Zwartz, D., Yokoyama, Y., Lambeck, K., & Chappell, J. (1998). *Fleming_etal1998.pdf*. *163*, 327–342.

Fortunato, A. B., Oliveira, A., & Alves, E. T. (2002). Circulation and Salinity Intrusion in the Guadiana estuary (Portugal/Spain). *Thalassas*, *18(2)*(December 2015), 43–65.

Garel, E., & D'Alimonte, D. (2017). Continuous river discharge monitoring with bottom-mounted current profilers at narrow tidal estuaries. *Continental Shelf Research*, *133*(December 2016), 1–12. https://doi.org/10.1016/j.csr.2016.12.001

Garel, E., Pinto, L., Santos, A., & Ferreira, Ó. (2009). Tidal and river discharge forcing upon water and sediment circulation at a rock-bound estuary (Guadiana estuary, Portugal). *Estuarine, Coastal and Shelf Science*, *84*(2), 269–281. https://doi.org/10.1016/j.ecss.2009.07.002

Garel, Erwan. (2017). Present dynamics of the Guadiana estuary. In *Investigating the past , present and future*. https://doi.org/http://hdl.handle.net/10400.1/9887

Garel, Erwan, & Cai, H. (2018). Effects of Tidal-Forcing Variations on Tidal Properties Along a Narrow Convergent Estuary. *Estuaries and Coasts*, *41*(7), 1924–1942. https://doi.org/10.1007/s12237-018-0410-y

Gonzalez, R., Dias, J. M. A., Lobo, F., & Mendes, I. (2004). Sedimentological and paleoenvironmental characterisation of transgressive sediments on the Guadiana Shelf (Northern Gulf of Cadiz, SW Iberia). *Quaternary International*, *120*(1), 133–144. https://doi.org/10.1016/j.quaint.2004.01.012

Guimarães, M. H. E., Mascarenhas, A., Sousa, C., Boski, T., & Dentinho, T. P. (2012). The impact of water quality changes on the socio-economic system of the guadiana estuary: An assessment of management options. *Ecology and Society*, *17*(3). https://doi.org/10.5751/ES-05318-170338

Hilton, T. W., Najjar, R. G., Zhong, L., & Li, M. (2008). Is there a signal of sea-level rise in Chesapeake Bay salinity? *Journal of Geophysical Research: Oceans*, *113*(9), 1–12. https://doi.org/10.1029/2007JC004247

Hong, B., & Shen, J. (2012). Responses of estuarine salinity and transport processes to potential future sea-level rise in the Chesapeake Bay. *Estuarine, Coastal and Shelf Science*, *104*–

*105*, 33–45. https://doi.org/10.1016/j.ecss.2012.03.014

Lobo, F. ., Dias, J. M. A., Gonzalez, R., Hernandez-Molina, F.J. Morales, J. A., & Diaz del Rio, V. (2003). High-Resolution Seismic Stratigraphy of a Narrow, Bedrock-Controlled Estuary: The Guadiana Estuarine System, SW Iberia. *Journal of Sedimentary Research*, *73*(6), 973–986.

Lopes, J., Neves, R., Dias, J. M. A., & Martins, F. (2003). Calibração De Um Sistema De Modelação Para O Estuário Do. *4th Symposium on the Iberian Atlantic Margin*, 4–6.

MARETEC. (2017). MOHID Water. Retrieved April 4, 2019, from http://wiki.mohid.com/index.php?title=Mohid_Water

McLean, R. F., Tsyban, A., Burkett, V., Codignott, J. O., Forbes, D. L., Mimura, N., … Ittekkot, V. (2001). Coastal Zones and Marine Ecosystems. *Climate Change 2001: Impacts, Adaptation and Vulnerability*, pp. 343–379. Cambridge, UK.

Mills, L., Janeiro, J., & Martins, F. (2019). The impact of sea level rise in the Guadiana Estuary. *Rodrigues J. et Al. (Eds) Computational Science – ICCS 2019. ICCS 2019. Lecture Notes in Computer Science, Vol 11539*, 287–300. https://doi.org/https://doi.org/10.1007/978-3-030-22747-0_23

Morais, P., Martins, F., Chícharo, M. A., Lopes, J., & Chícharo, L. (2012). Merging anchovy eggs abundance into a hydrodynamic model as an assessment tool for estuarine ecohydrological management. *River Research and Applications*, *28*(2), 160–176. https://doi.org/10.1002/rra.1443

Neves, R., Silva, A., Delfino, J., Leitão, P., Leitão, J., Pina, P., … Coelho, H. (2000). Coastal management supported by modelling: Optimising the level of treatment of Urban discharges into coastal waters. *Environmental Studies*, *5*, 41–49.

Nicholls, R. J., Marinova, N., Lowe, J. A., Brown, S., Vellinga, P., De Gusmão, D., … Tol, R. S. J. (2011). Sea-level rise and its possible impacts given a “beyond 4°C world” in the twenty-first century. *Philosophical Transactions of the Royal Society A: Mathematical, Physical and Engineering Sciences*, *369*(1934), 161–181. https://doi.org/10.1098/rsta.2010.0291

Oliveira, A., Fortunato, A. B., & Pinto, L. (2006). Modelling the hydrodynamics and the fate of passive and active organisms in the Guadiana estuary. *Estuarine, Coastal and Shelf Science*, *70*(1–2), 76–84. https://doi.org/10.1016/j.ecss.2006.05.033

Paola, C. (2000). Quantitative models of sedimentary basin filling\rdoi:10.1046/j.1365-3091.2000.00006.x. *Sedimentology*, *47*(s1), 121–178. Retrieved from http://www.blackwell-synergy.com/doi/abs/10.1046/j.1365-3091.2000.00006.x

Quesada, M. C. C., García-Lafuente, J., Garel, E., Delgado Cabello, J., Martins, F., & Moreno-Navas, J. (2019). Effects of tidal and river discharge forcings on tidal propagation along the Guadiana Estuary. *Journal of Sea Research*, *146*(January), 1–13. https://doi.org/10.1016/j.seares.2019.01.006

Rahmstorf, S., Foster, G., & Cazenave, A. (2012). Comparing climate projections to observations up to 2011. *Environmental Research Letters*, *7*(4). https://doi.org/10.1088/1748-9326/7/4/044035

Ross, A. C., Najjar, R. G., Li, M., Mann, M. E., Ford, S. E., & Katz, B. (2015). Sea-level rise and other influences on decadal-scale salinity variability in a coastal plain estuary. *Estuarine, Coastal and Shelf Science*, *157*, 79–92. https://doi.org/10.1016/j.ecss.2015.01.022

Rovere, A., Stocchi, P., & Vacchi, M. (2016). Eustatic and Relative Sea Level Changes. *Current Climate Change Reports*, *2*(4), 221–231. https://doi.org/10.1007/s40641-016-0045-7

Sampath, D. M.R., & Boski, T. (2016). Morphological response of the saltmarsh habitats of the Guadiana estuary due to flow regulation and sea-level rise. *Estuarine, Coastal and Shelf Science*, *183*, 314–326. https://doi.org/10.1016/j.ecss.2016.07.009

Sampath, D. M.R., Boski, T., Loureiro, C., & Sousa, C. (2015). Modelling of estuarine response to sea-level rise during the Holocene: Application to the Guadiana Estuary-SW Iberia. *Geomorphology*, *232*, 47–64. https://doi.org/10.1016/j.geomorph.2014.12.037

Sampath, Dissanayake M.R., Boski, T., Silva, P. L., & Martins, F. A. (2011). Morphological evolution of the Guadiana estuary and intertidal zone in response to projected sea-level rise and sediment supply scenarios. *Journal of Quaternary Science*, *26*(2), 156–170. https://doi.org/10.1002/jqs.1434

Sella, G. F., Stein, S., Dixon, T. H., Craymer, M., James, T. S., Mazzotti, S., & Dokka, R. K. (2007). Observation of glacial isostatic adjustment in "stable" North America with GPS. *Geophysical Research Letters*, *34*(2), 1–6. https://doi.org/10.1029/2006GL027081

Statham, P. J. (2012). Nutrients in estuaries - An overview and the potential impacts of climate change. *Science of the Total Environment*, *434*, 213–227. https://doi.org/10.1016/j.scitotenv.2011.09.088

Vargas, C. I. C., Vaz, N., & Dias, J. M. (2017). An evaluation of climate change effects in estuarine salinity patterns: Application to Ria de Aveiro shallow water system. *Estuarine, Coastal and Shelf Science*, *189*, 33–45. https://doi.org/10.1016/j.ecss.2017.03.001

Wiseman, W. J., Swenson, E. M., & Power, J. (1990). Trends in Louisiana Estuaries Salinity.

*Estuaries*, *13*(3), 265–271.

Wolanski, E., Chicharo, L., Chicharo, M. A., & Morais, P. (2006). An ecohydrology model of the Guadiana Estuary (South Portugal). *Estuarine, Coastal and Shelf Science*, *70*(1–2), 132–143. https://doi.org/10.1016/j.ecss.2006.05.029

Wong, P. P., Losada, I. J., Gattuso, J.-P., Hinkel, J., Khattabi, A., McInnes, K. L., … Sallenger, A. (2014). Coastal Systems and Low-Lying Areas. In: Climate Change 2014: Impacts, Adaptation, and Vulnerability. *Climate Change 2014: Impacts, Adaptation, and Vulnerability. Part A: Global and Sectoral Aspects. Contribution of Working Group II to the Fifth Assessment Report of the Intergovernmental Panel on Climate Change*, 361–409. https://doi.org/10.1017/CBO9781107415379.010

# Appendix A Time Series Results of Water Elevation

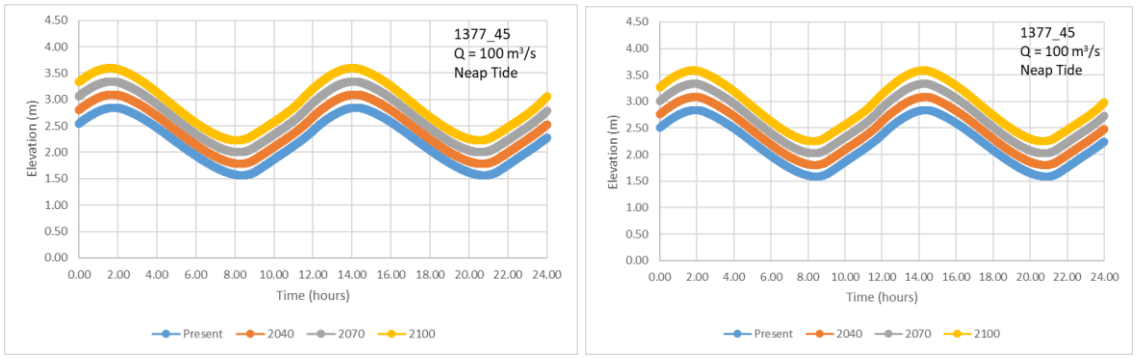


*Figure A.1* Time series of water elevation over two tidal cycles for a river discharge of 100 $m^3/s$ at neap tide in the upper estuary for the present bathymetry (left) and bathymetry that allows flooding (right).

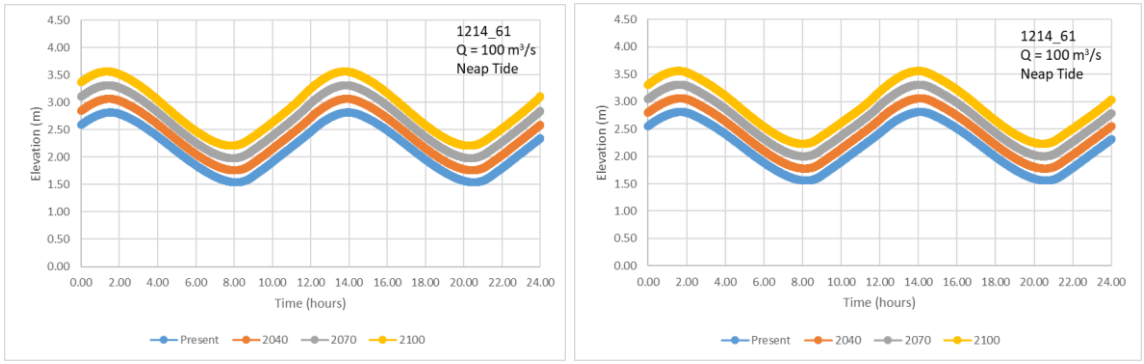


*Figure A.2* Time series of water elevation over two tidal cycles for a river discharge of 100 $m^3/s$ at neap tide in the upper estuary for the present bathymetry (left) and bathymetry that allows flooding (right).

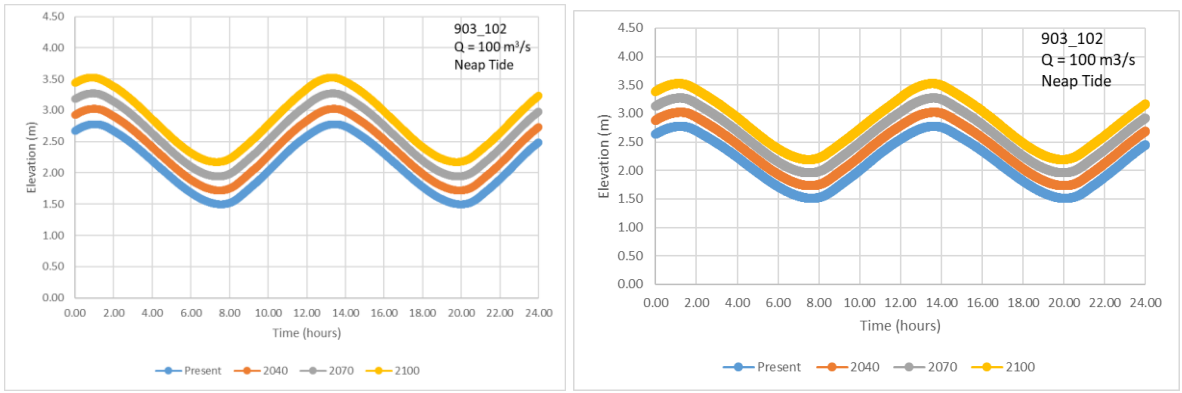


*Figure A.3* Time series of water elevation over two tidal cycles for a river discharge of 100 $m^3/s$ at neap tide in the middle estuary for the present bathymetry (left) and bathymetry that allows flooding (right).

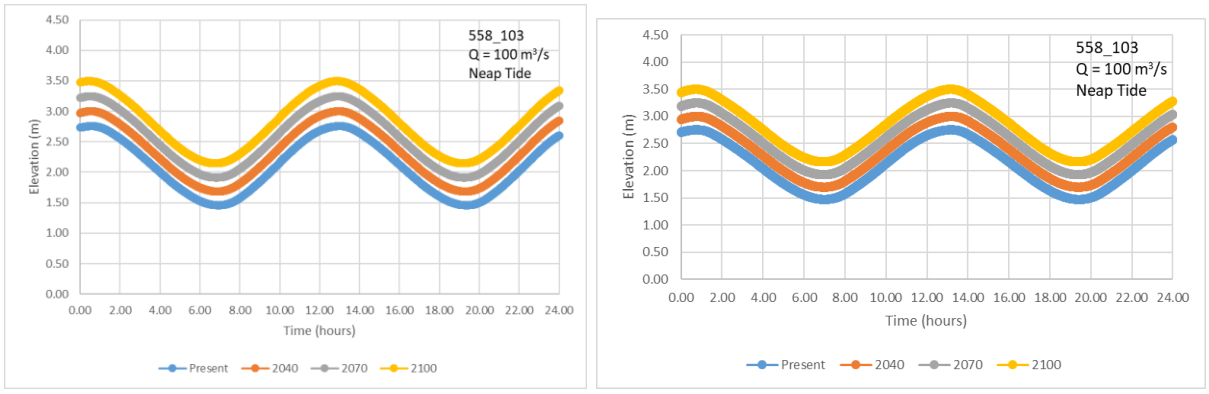


*Figure A.4* Time series of water elevation over two tidal cycles for a river discharge of 100 $m^3/s$ at neap tide in the middle estuary for the present bathymetry (left) and bathymetry that allows flooding (right).

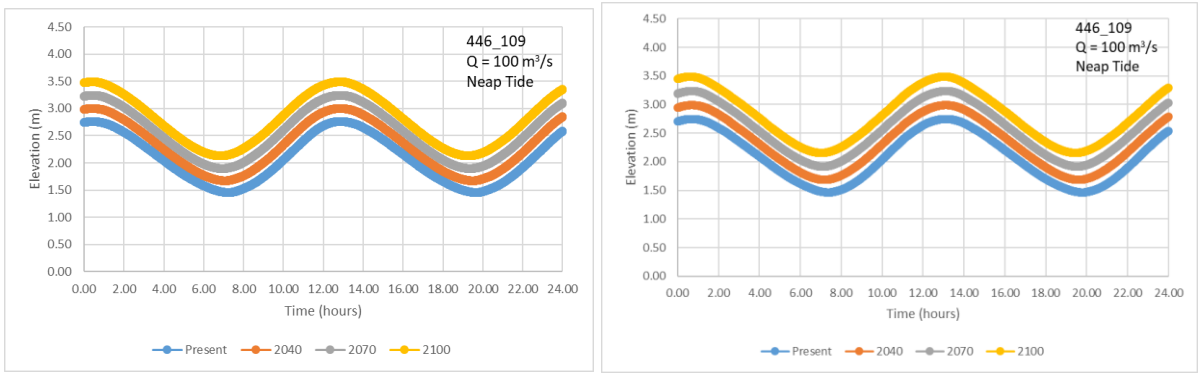


*Figure A.5* Time series of water elevation over two tidal cycles for a river discharge of 100 $m^3/s$ at neap tide in the northernmost region of Castro Marim for the present bathymetry (left) and bathymetry that allows flooding (right).

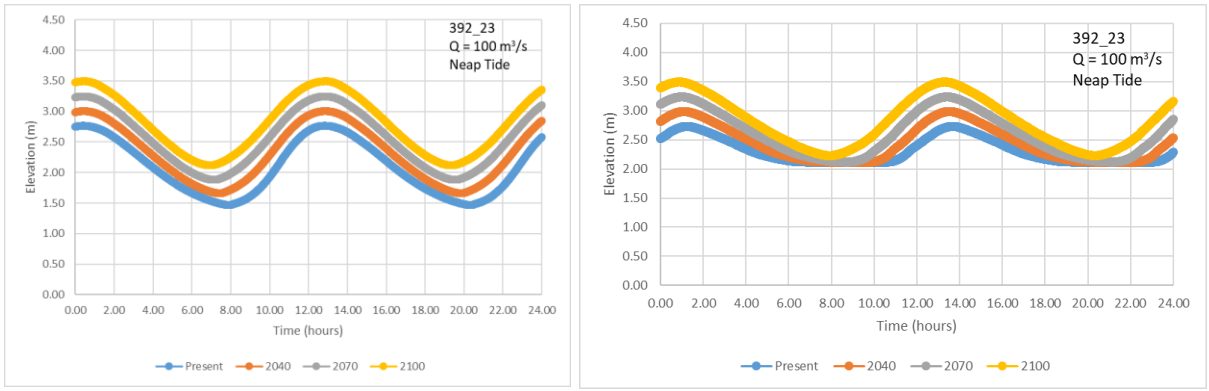


*Figure A.6* Time series of water elevation over two tidal cycles for a river discharge of 100 $m^3/s$ at neap tide in the westernmost region of Esteiro da Leziria for the present bathymetry (left) and bathymetry that allows flooding (right).

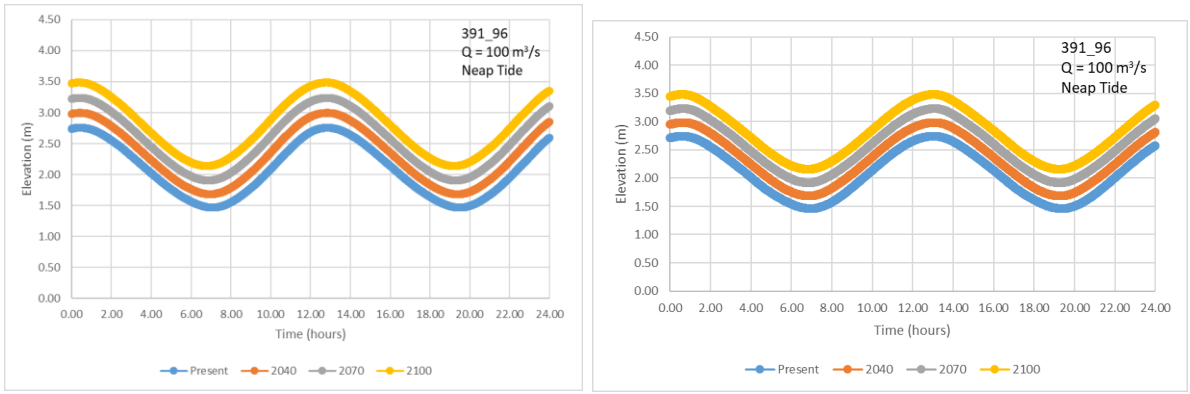


*Figure A.7* Time series of water elevation over two tidal cycles for a river discharge of 100 $m^3/s$ at neap tide in the easternmost region of Castro Marim for the present bathymetry (left) and bathymetry that allows flooding (right).

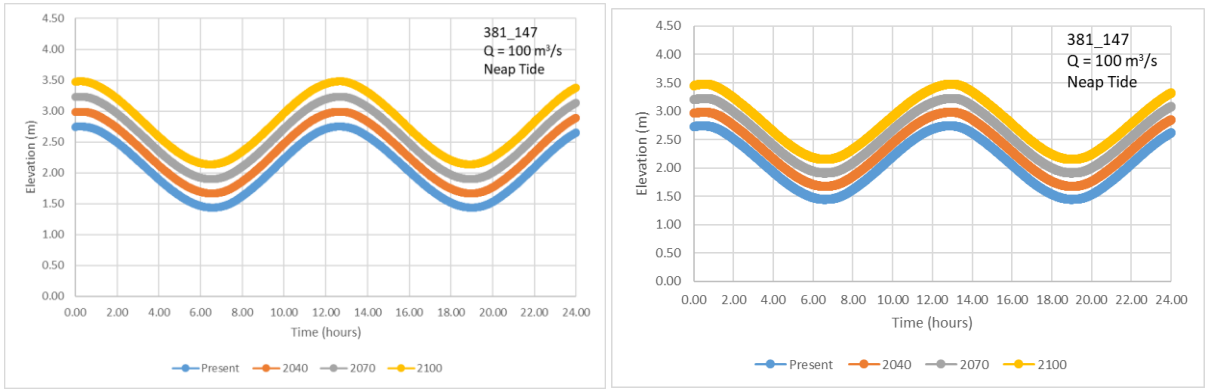


*Figure A.8* Time series of water elevation over two tidal cycles for a river discharge of 100 $m^3/s$ at neap tide in the inlet into Castro Marim for the present bathymetry (left) and bathymetry that allows flooding (right).

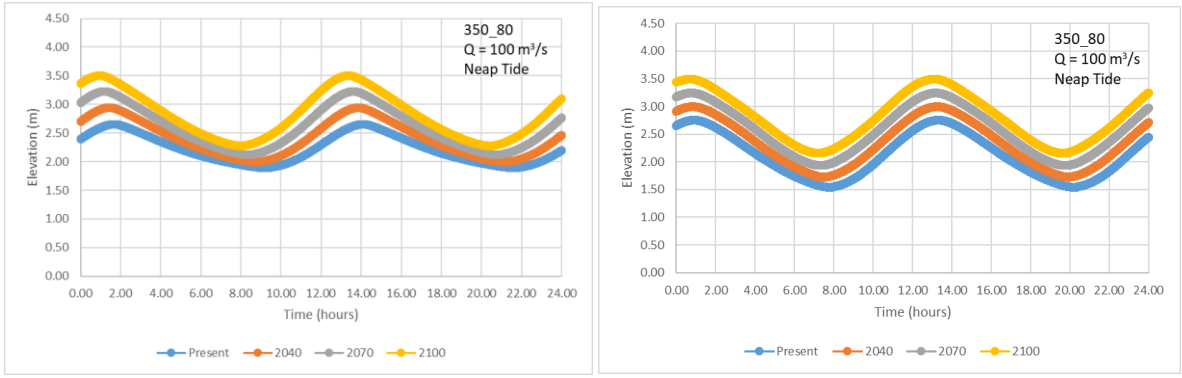


*Figure A.9* Time series of water elevation over two tidal cycles for a river discharge of 100 $m^3/s$ at neap tide downstream Esteiro da Carrasqueira for the present bathymetry (left) and bathymetry that allows flooding (right).

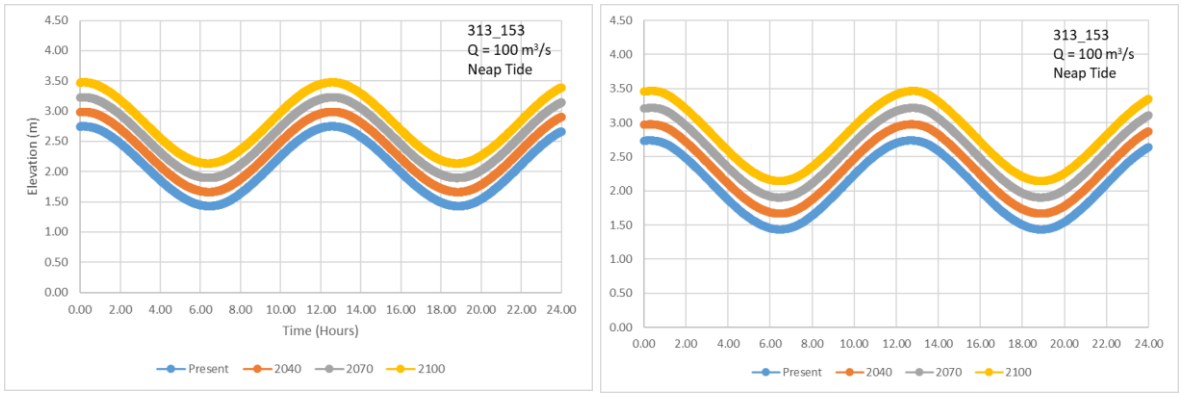


*Figure A.10* Time series of water elevation over two tidal cycles for a river discharge of 100 $m^3/s$ at neap tide in the lower estuary for the present bathymetry (left) and bathymetry that allows flooding (right).

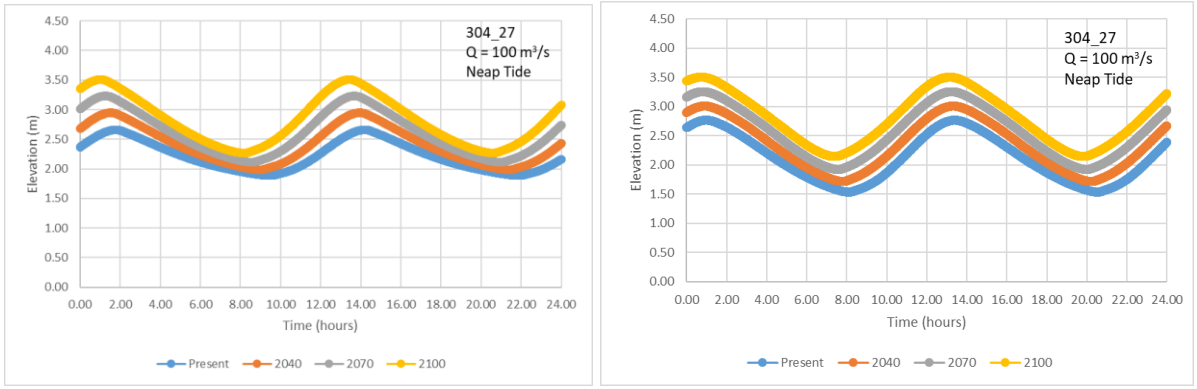


*Figure A.11* Time series of water elevation over two tidal cycles for a river discharge of 100 $m^3/s$ at neap tide in the westernmost region of Esteiro da Carrasqueira for the present bathymetry (left) and bathymetry that allows flooding (right).

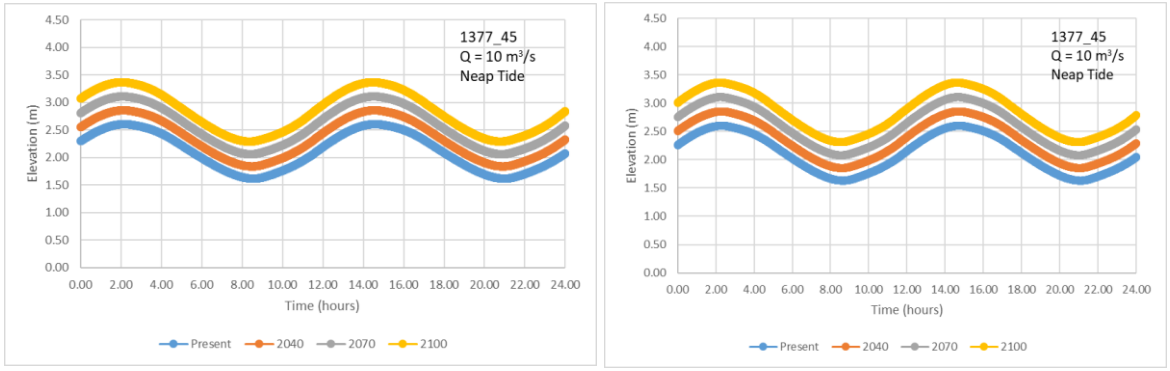


*Figure A.12* Time series of water elevation over two tidal cycles for a river discharge of 10 $m^3/s$ at neap tide in the upper estuary for the present bathymetry (left) and bathymetry that allows flooding (right).

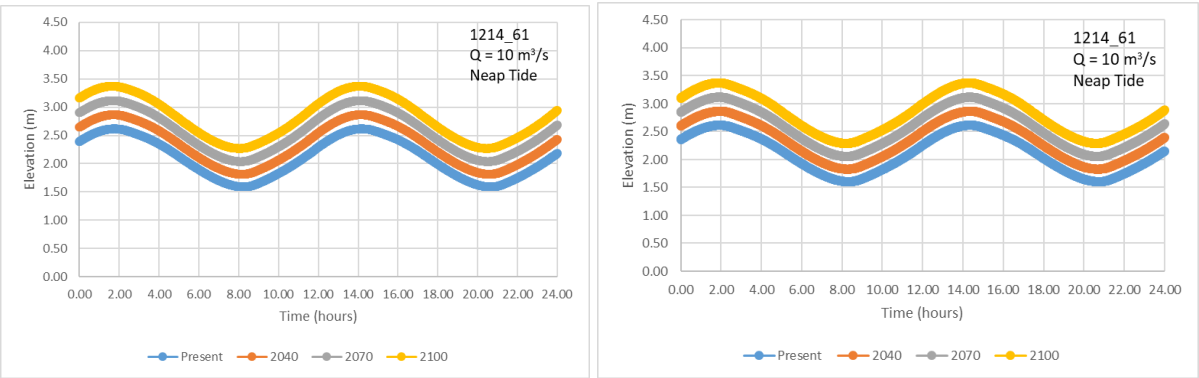


*Figure A.13* Time series of water elevation over two tidal cycles for a river discharge of 10 $m^3/s$ at neap tide in the upper estuary for the present bathymetry (left) and bathymetry that allows flooding (right).

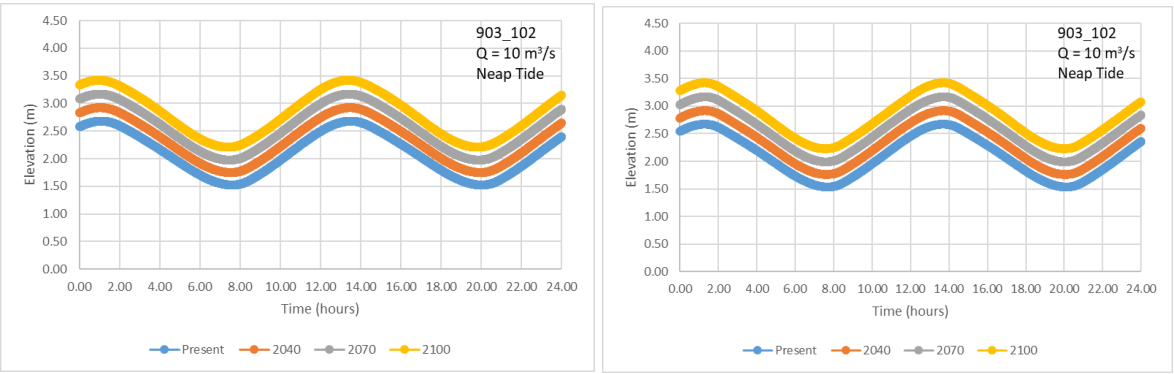


*Figure A.14* Time series of water elevation over two tidal cycles for a river discharge of 10 $m^3/s$ at neap tide in the middle estuary for the present bathymetry (left) and bathymetry that allows flooding (right).

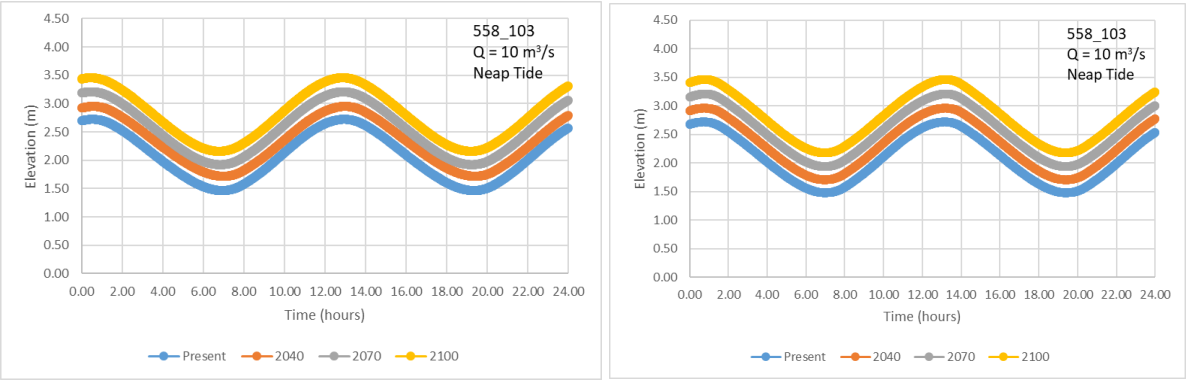


*Figure A.15* Time series of water elevation over two tidal cycles for a river discharge of 10 $m^3/s$ at neap tide in the middle estuary for the present bathymetry (left) and bathymetry that allows flooding (right).

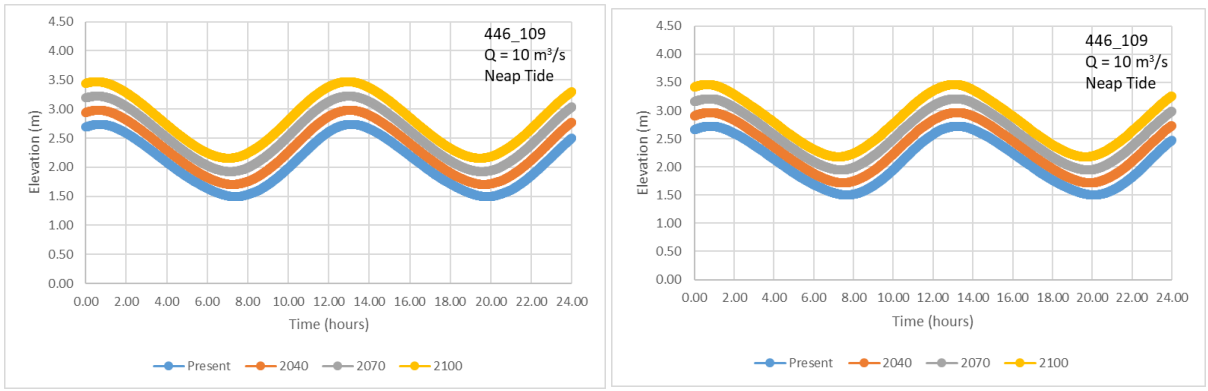


*Figure A.16* Time series of water elevation over two tidal cycles for a river discharge of 10 $m^3/s$ at neap tide in the northernmost region of Castro Marim for the present bathymetry (left) and bathymetry that allows flooding (right).

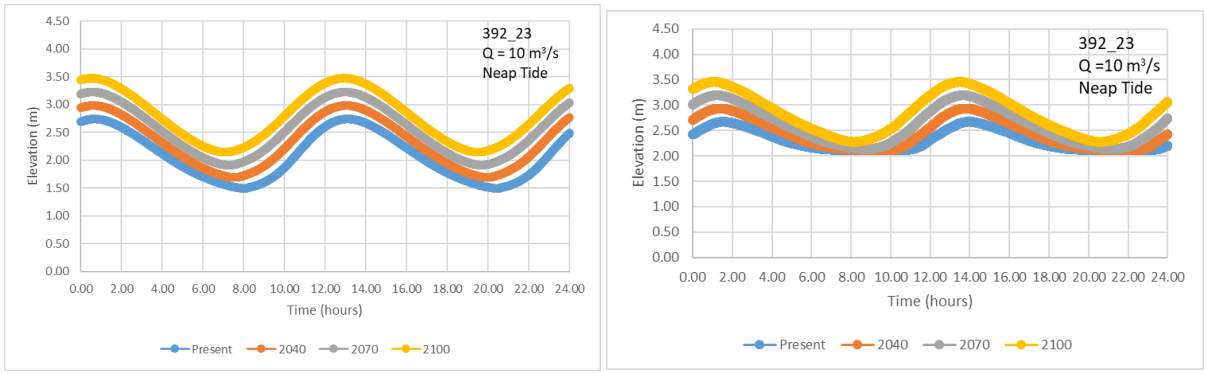


*Figure A.17* Time series of water elevation over two tidal cycles for a river discharge of 10 $m^3/s$ at neap tide in the westernmost region of Esteiro da Leziria for the present bathymetry (left) and bathymetry that allows flooding (right).

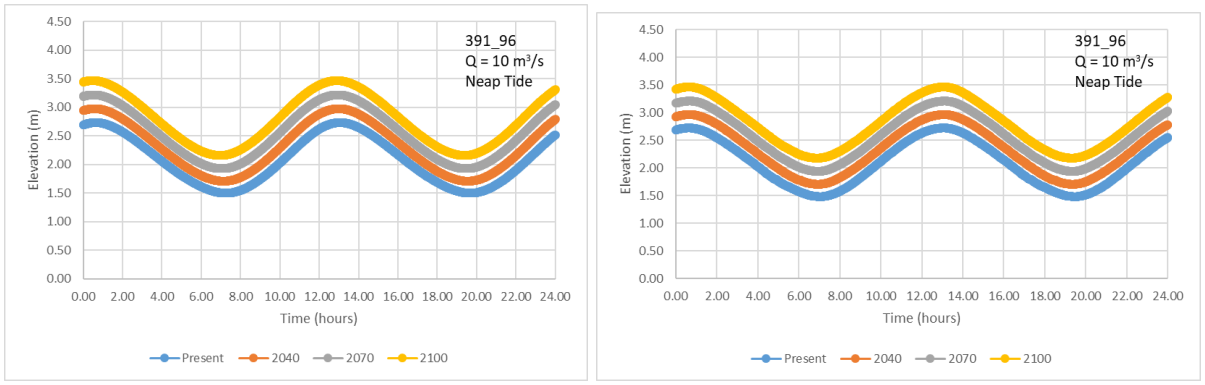


*Figure A.18* Time series of water elevation over two tidal cycles for a river discharge of 10 $m^3/s$ at neap tide in the easternmost region of Castro Marim for the present bathymetry (left) and bathymetry that allows flooding (right).

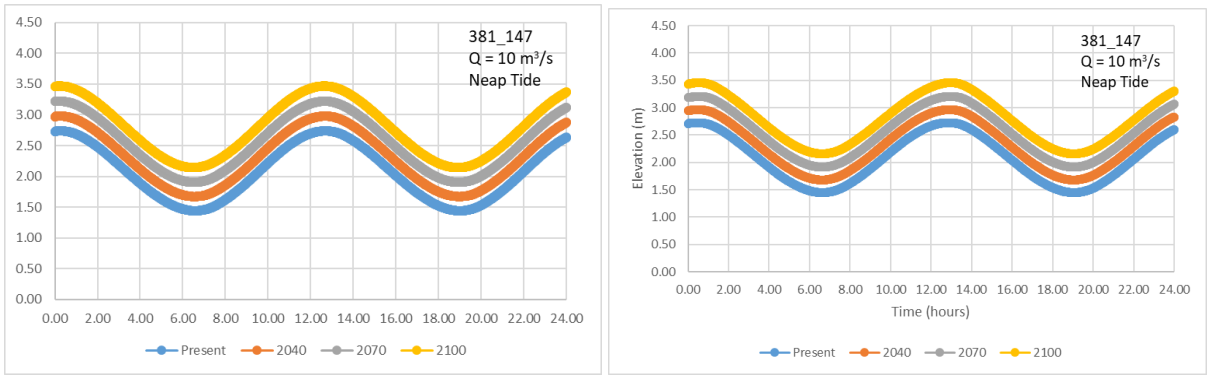


*Figure A.19* Time series of water elevation over two tidal cycles for a river discharge of 10 $m^3/s$ at neap tide in the inlet into Castro Marim for the present bathymetry (left) and bathymetry that allows flooding (right).

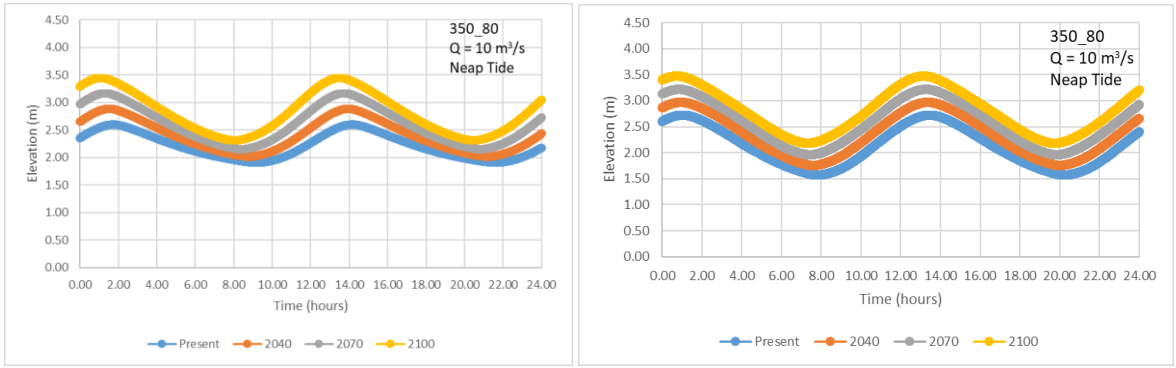


*Figure A.20* Time series of water elevation over two tidal cycles for a river discharge of 10 $m^3/s$ at neap tide downstream Esteiro da Carrasqueira for the present bathymetry (left) and bathymetry that allows flooding (right).

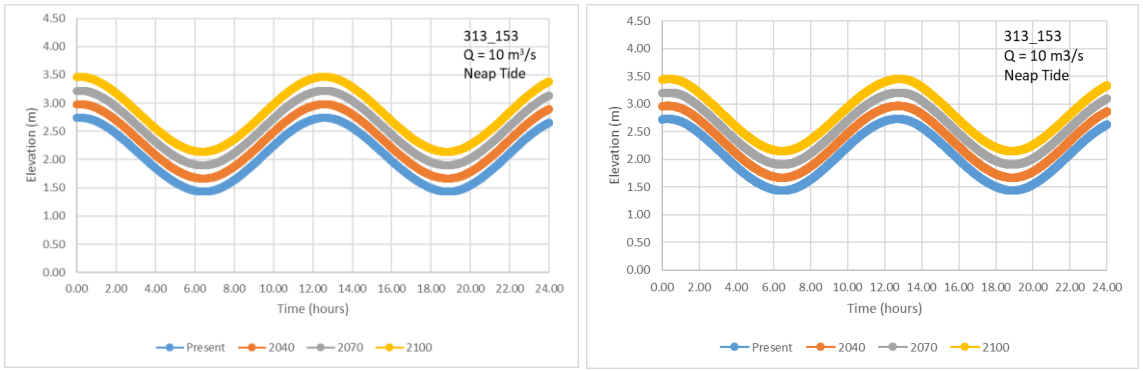


*Figure A.21* Time series of water elevation over two tidal cycles for a river discharge of 10 $m^3/s$ at neap tide in the lower estuary for the present bathymetry (left) and bathymetry that allows flooding (right).

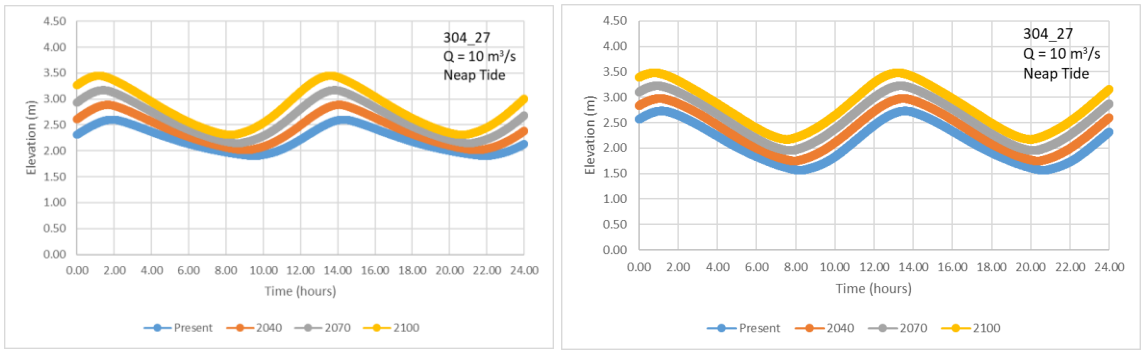


*Figure A.22* Time series of water elevation over two tidal cycles for a river discharge of 10 $m^3/s$ at neap tide in the westernmost region of Esteiro da Carrasqueira for the present bathymetry (left) and bathymetry that allows flooding (right).

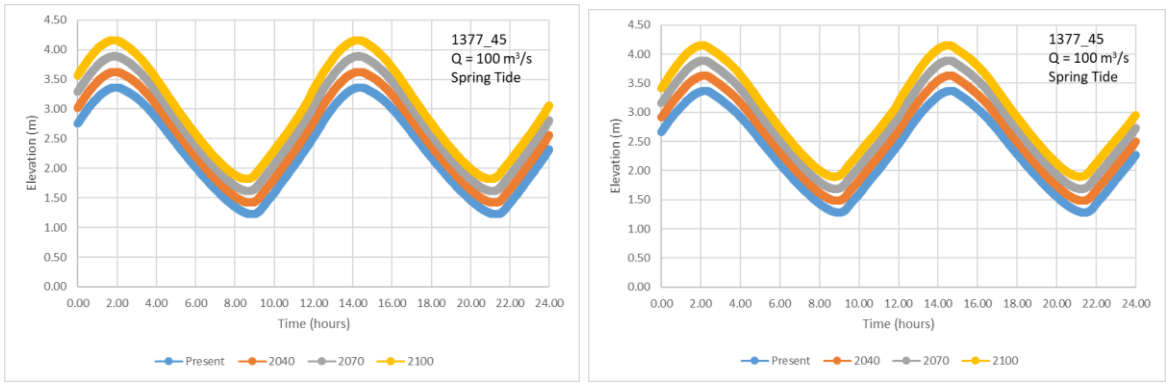


*Figure A.23* Time series of water elevation over two tidal cycles for a river discharge of 100 $m^3/s$ at spring tide in the upper estuary for the present bathymetry (left) and bathymetry that allows flooding (right).

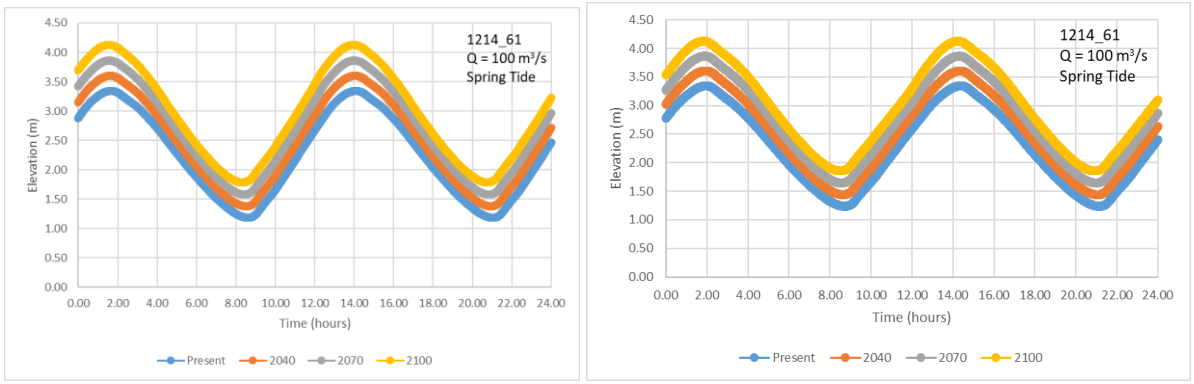


*Figure A.24* Time series of water elevation over two tidal cycles for a river discharge of 100 $m^3/s$ at spring tide in the upper estuary for the present bathymetry (left) and bathymetry that allows flooding (right).

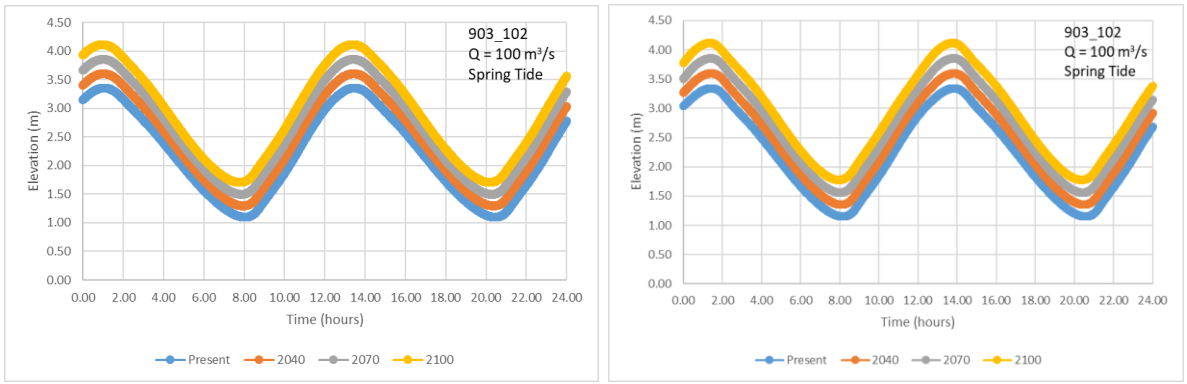


*Figure A.25* Time series of water elevation over two tidal cycles for a river discharge of 100 $m^3/s$ at spring tide in the middle estuary for the present bathymetry (left) and bathymetry that allows flooding (right).

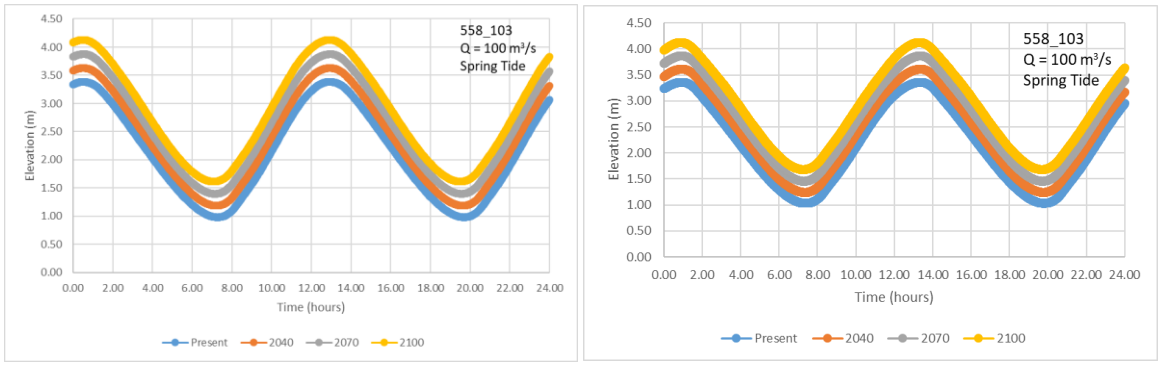


*Figure A.26* Time series of water elevation over two tidal cycles for a river discharge of 100 $m^3/s$ at spring tide in the middle estuary for the present bathymetry (left) and bathymetry that allows flooding (right).

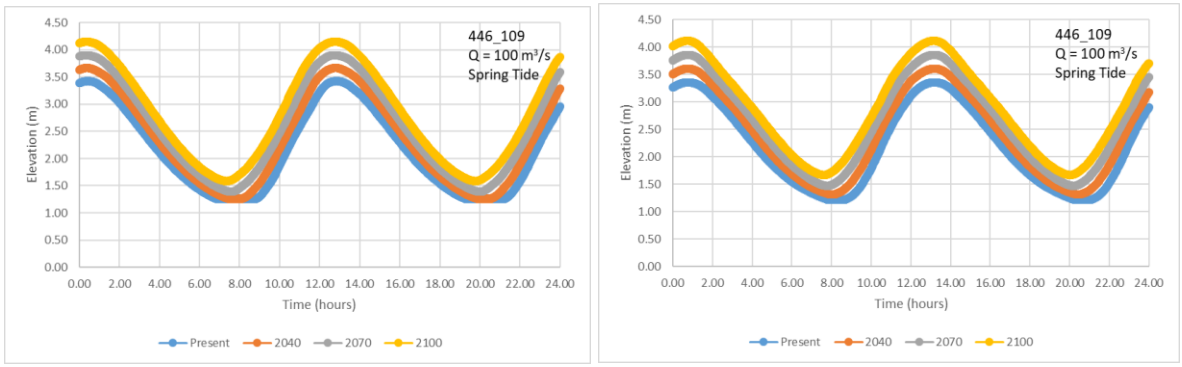


*Figure A.27* Time series of water elevation over two tidal cycles for a river discharge of 100 $m^3/s$ at spring tide in the northernmost region of Castro Marim for the present bathymetry (left) and bathymetry that allows flooding (right).

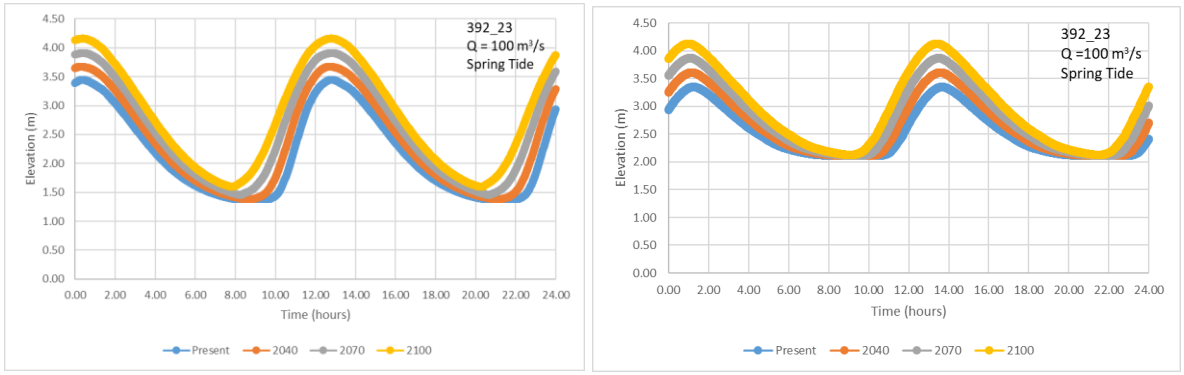


*Figure A.28* Time series of water elevation over two tidal cycles for a river discharge of 100 $m^3/s$ at spring tide in the westernmost region of Esteiro da Leziria for the present bathymetry (left) and bathymetry that allows flooding (right).

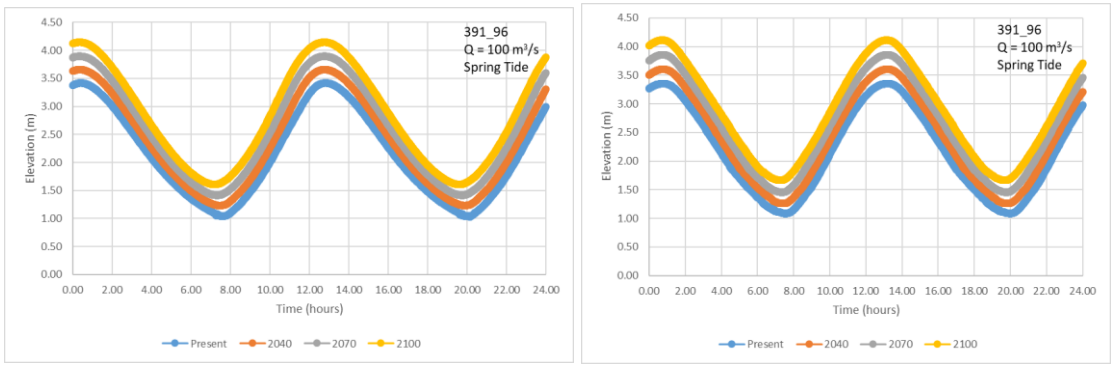


*Figure A.29* Time series of water elevation over two tidal cycles for a river discharge of 100 $m^3/s$ at spring tide in the easternmost region of Castro Marim for the present bathymetry (left) and bathymetry that allows flooding (right).

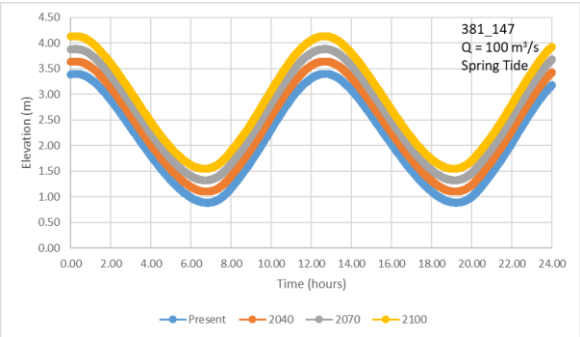


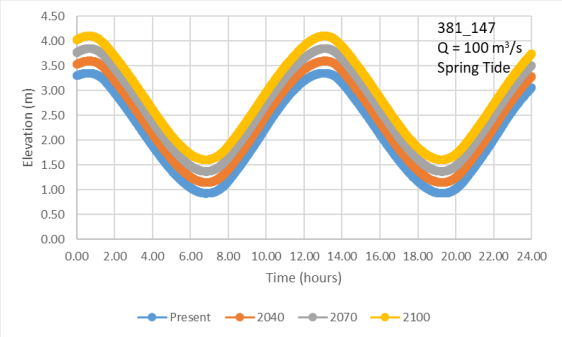


*Figure A.30* Time series of water elevation over two tidal cycles for a river discharge of 100 $m^3/s$ at spring tide at the inlet into Castro Marim for the present bathymetry (left) and bathymetry that allows flooding (right).

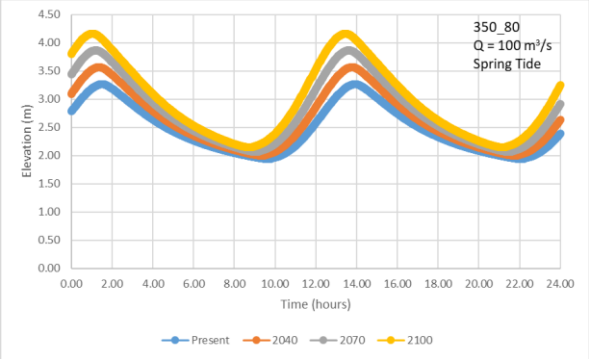


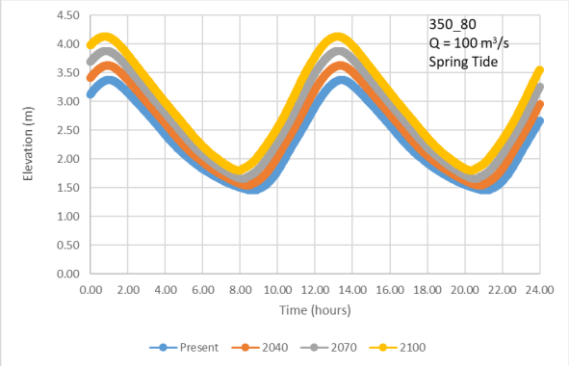


*Figure A.31* Time series of water elevation over two tidal cycles for a river discharge of 100 $m^3/s$ at spring tide downstream Esteiro da Carrasqueira for the present bathymetry (left) and bathymetry that allows flooding (right).

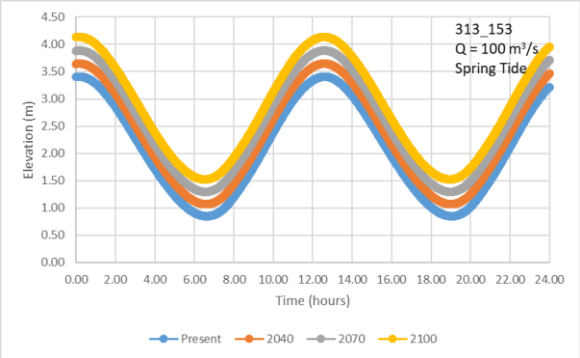


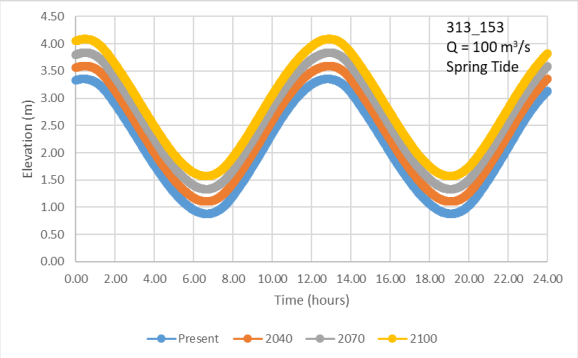


*Figure A.32* Time series of water elevation over two tidal cycles for a river discharge of 100 $m^3/s$ at spring tide in the lower estuary for the present bathymetry (left) and bathymetry that allows flooding (right).

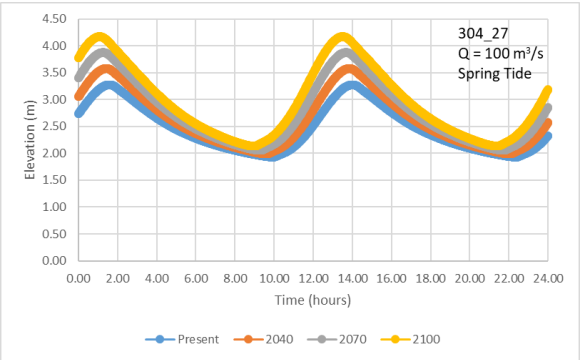


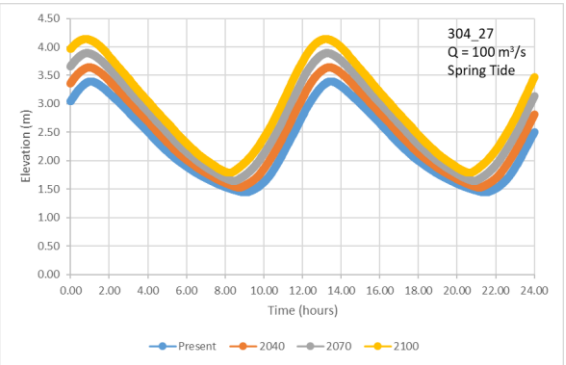


*Figure A.33* Time series of water elevation over two tidal cycles for a river discharge of 100 $m^3/s$ at spring tide in the westernmost region of Esteiro da Carresqueira for the present bathymetry (left) and bathymetry that allows flooding (right).

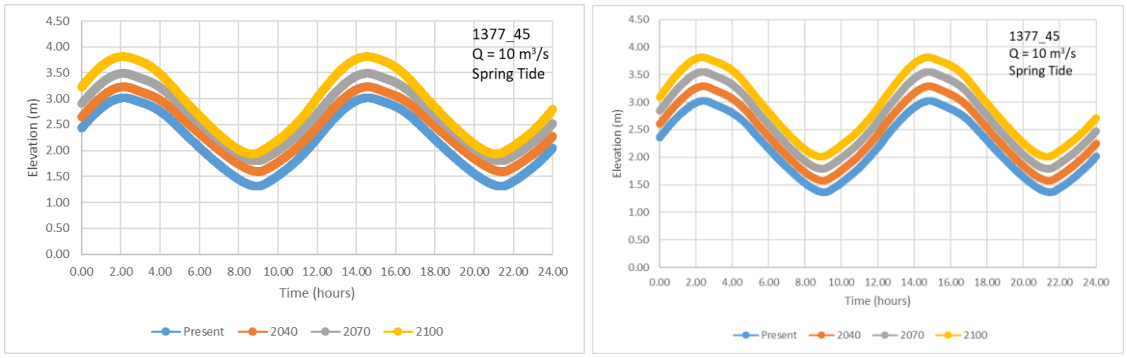


*Figure A.34* Time series of water elevation over two tidal cycles for a river discharge of 10 $m^3/s$ at spring tide in the upper estuary for the present bathymetry (left) and bathymetry that allows flooding (right).

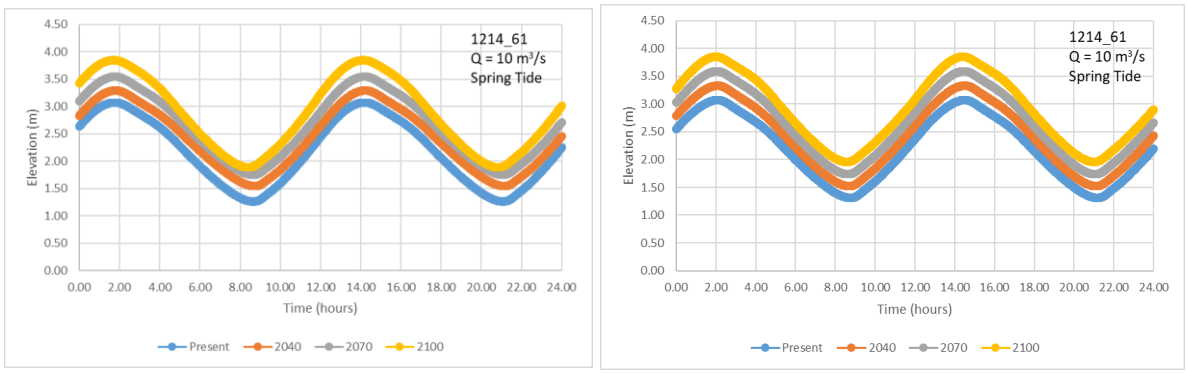


*Figure A.35* Time series of water elevation over two tidal cycles for a river discharge of 10 $m^3/s$ at spring tide in the upper estuary for the present bathymetry (left) and bathymetry that allows flooding (right).

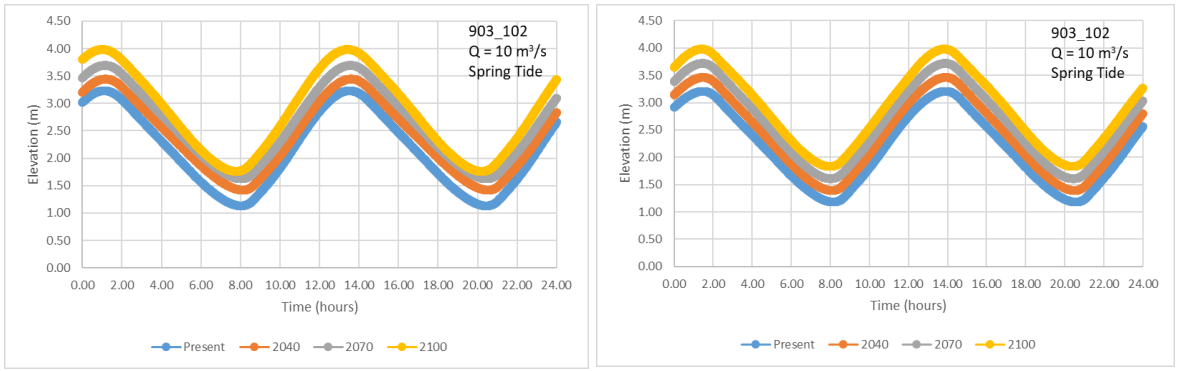


*Figure A.36* Time series of water elevation over two tidal cycles for a river discharge of 10 $m^3/s$ at spring tide in the middle estuary for the present bathymetry (left) and bathymetry that allows flooding (right).

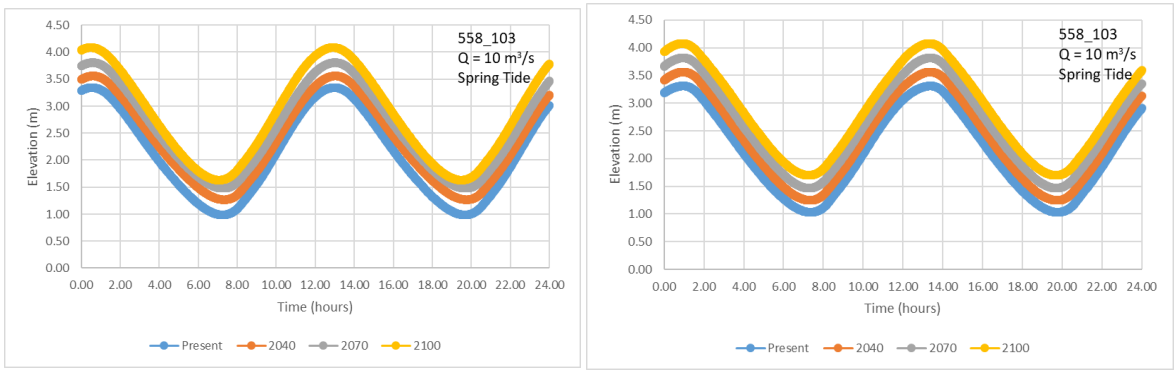


*Figure A.37* Time series of water elevation over two tidal cycles for a river discharge of 10 $m^3/s$ at spring tide in the middle estuary for the present bathymetry (left) and bathymetry that allows flooding (right).

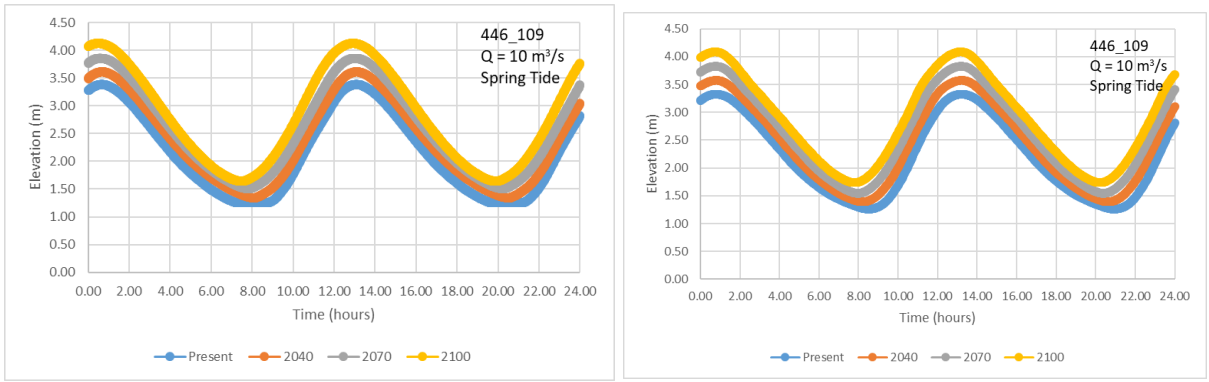


*Figure A.38* Time series of water elevation over two tidal cycles for a river discharge of 10 $m^3/s$ at spring tide in the northernmost region of Castro Marim for the present bathymetry (left) and bathymetry that allows flooding (right).

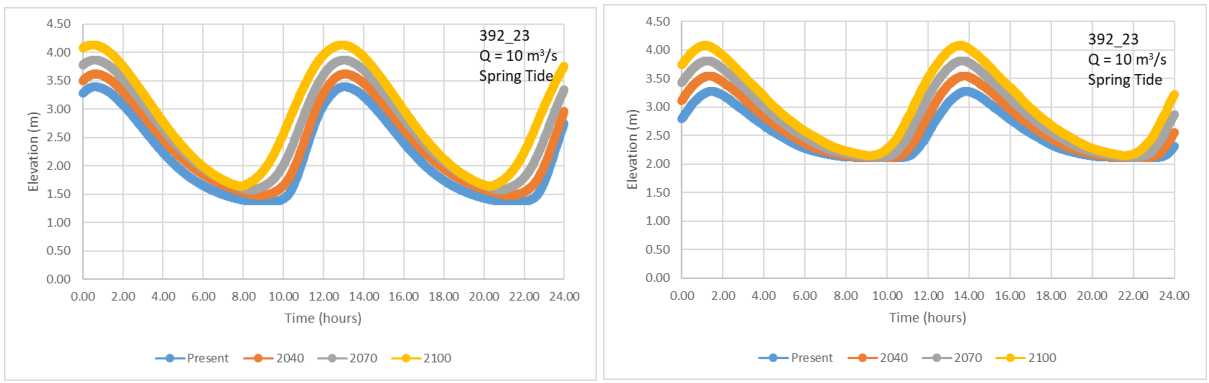


*Figure A.39* Time series of water elevation over two tidal cycles for a river discharge of 10 $m^3/s$ at spring tide in the westernmost region of Esteiro da Leziria for the present bathymetry (left) and bathymetry that allows flooding (right).

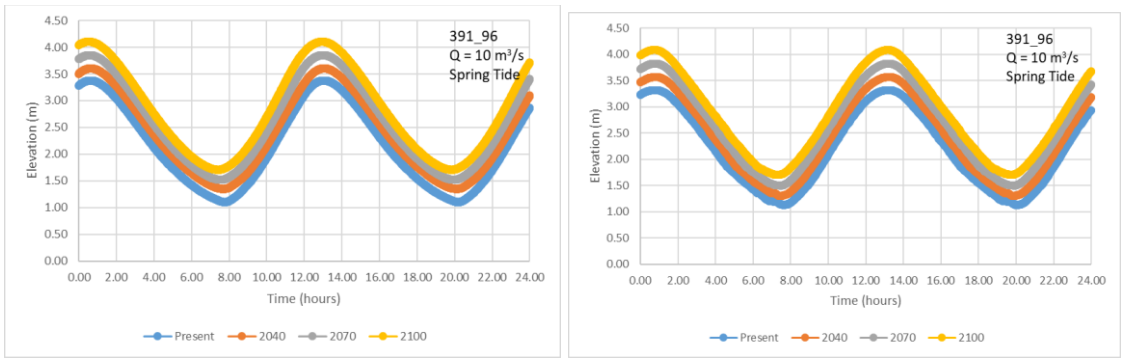


*Figure A.40* Time series of water elevation over two tidal cycles for a river discharge of 10 $m^3/s$ at spring tide in the easternmost region of Castro Marim for the present bathymetry (left) and bathymetry that allows flooding (right).

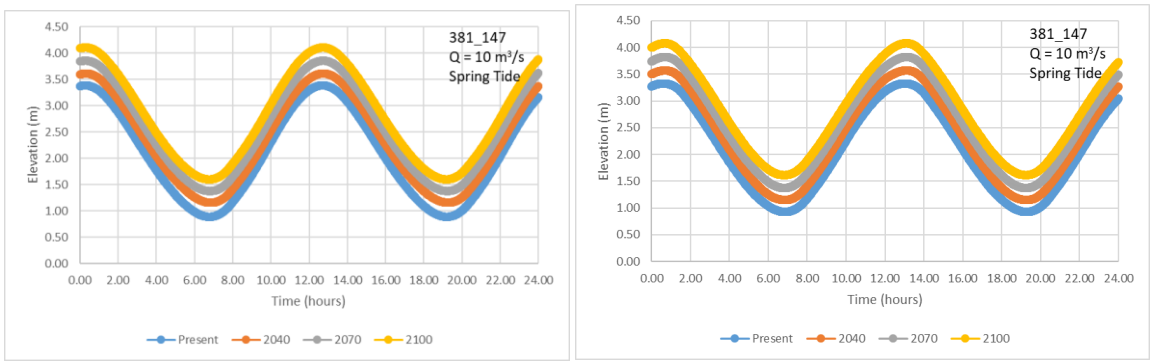


*Figure A.41* Time series of water elevation over two tidal cycles for a river discharge of 10 $m^3/s$ at spring tide at the inlet into Castro Marim for the present bathymetry (left) and bathymetry that allows flooding (right).

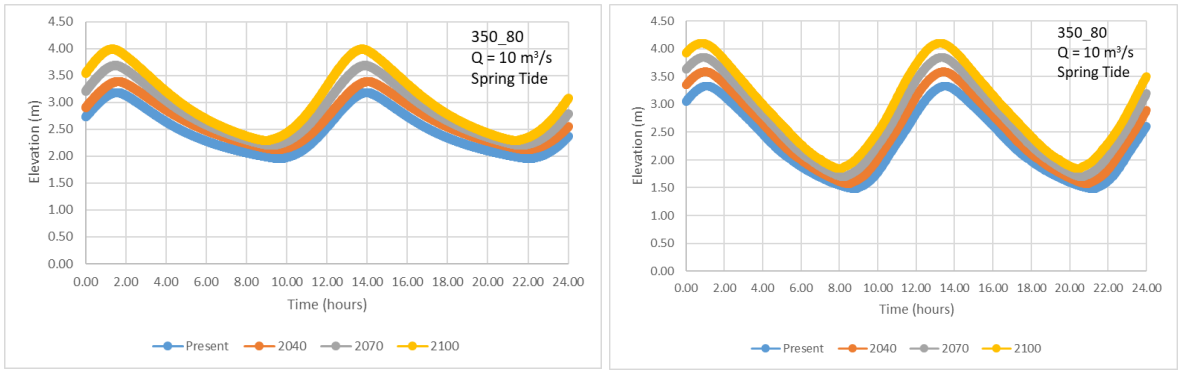


*Figure A.42* Time series of water elevation over two tidal cycles for a river discharge of 10 $m^3/s$ at spring tide downstream Esteiro da Carrasqueira for the present bathymetry (left) and bathymetry that allows flooding (right).

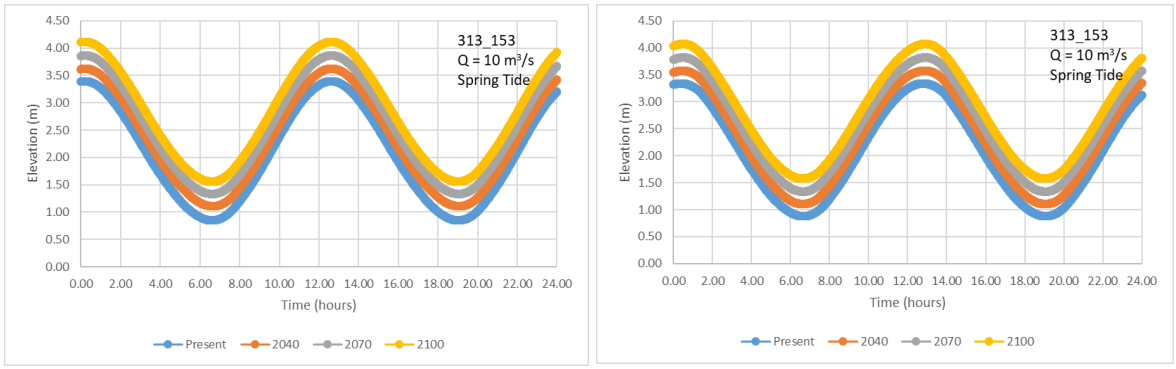


*Figure A.43* Time series of water elevation over two tidal cycles for a river discharge of 10 $m^3/s$ at spring tide in the lower estuary for the present bathymetry (left) and bathymetry that allows flooding (right).

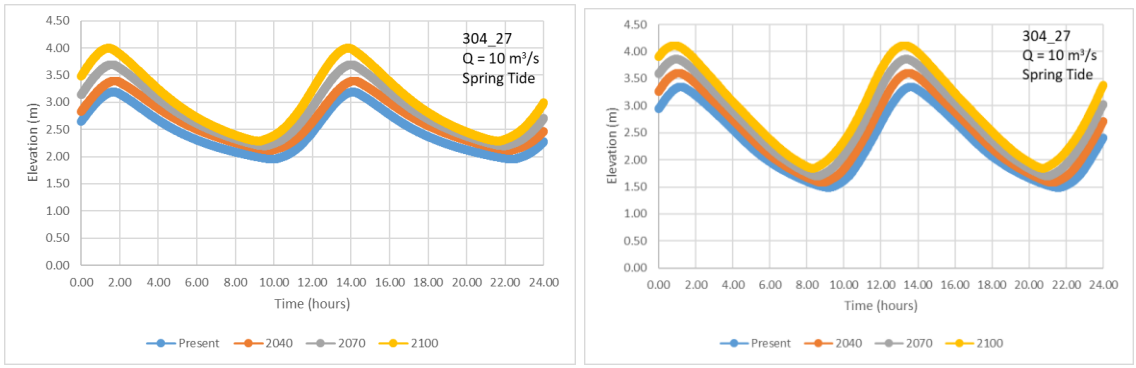


*Figure A.44* Time series of water elevation over two tidal cycles for a river discharge of 10 $m^3/s$ at spring tide in the westernmost region of Esteiro da Carrasqueira the present bathymetry (left) and bathymetry that allows flooding (right).

# Appendix B Time Series Results of Velocity

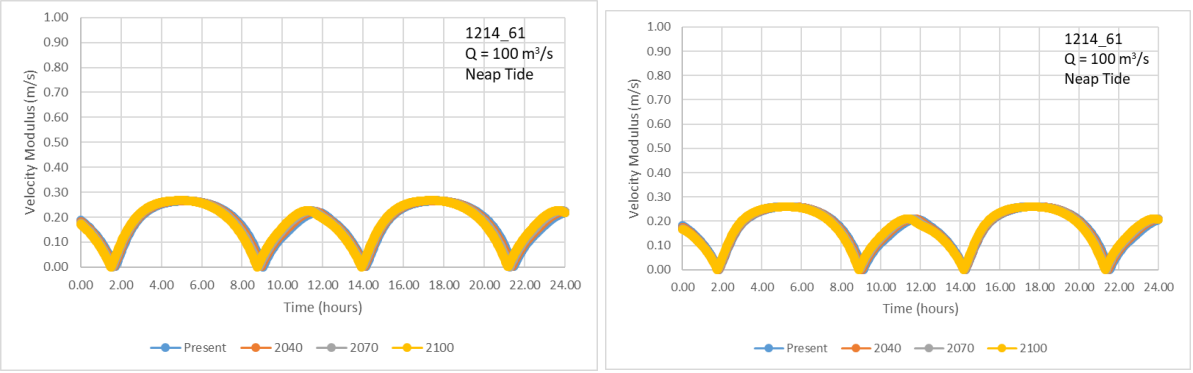


*Figure B.1* Velocity time series over two tidal cycles for a river discharge of 100 $m^3/s$ at neap tide in the upper estuary for the present bathymetry (left) and bathymetry that allows flooding (right).

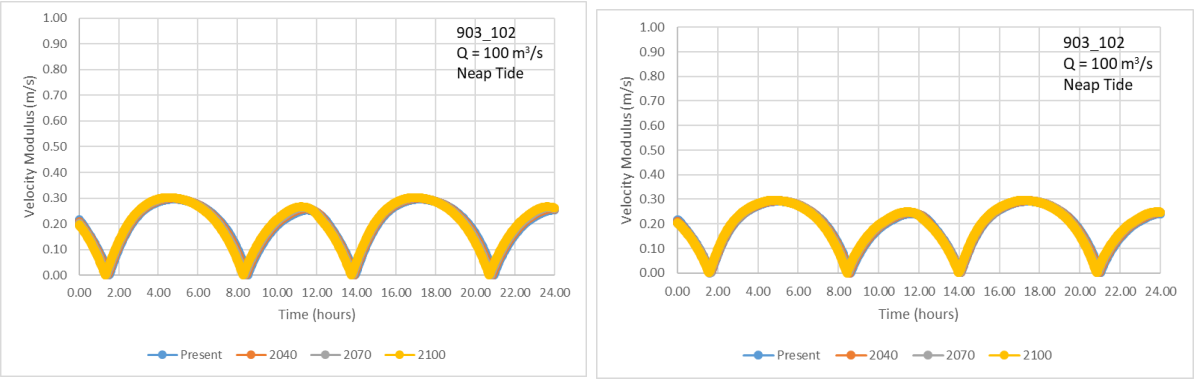


*Figure B.2* Velocity time series over two tidal cycles for a river discharge of 100 $m^3/s$ at neap tide in the middle estuary for the present bathymetry (left) and bathymetry that allows flooding (right).

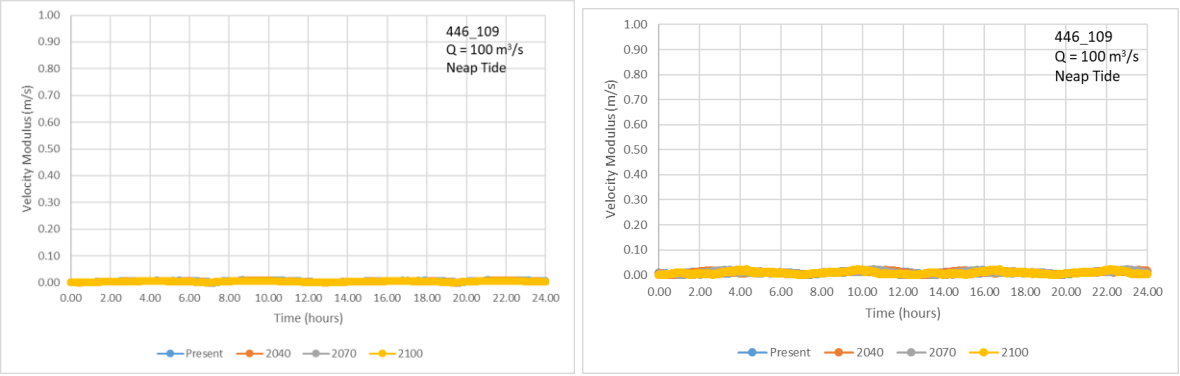


*Figure B.3* Velocity time series over two tidal cycles for a river discharge of 100 $m^3/s$ at neap tide in the northernmost region of Castro Marim for the present bathymetry (left) and bathymetry that allows flooding (right).

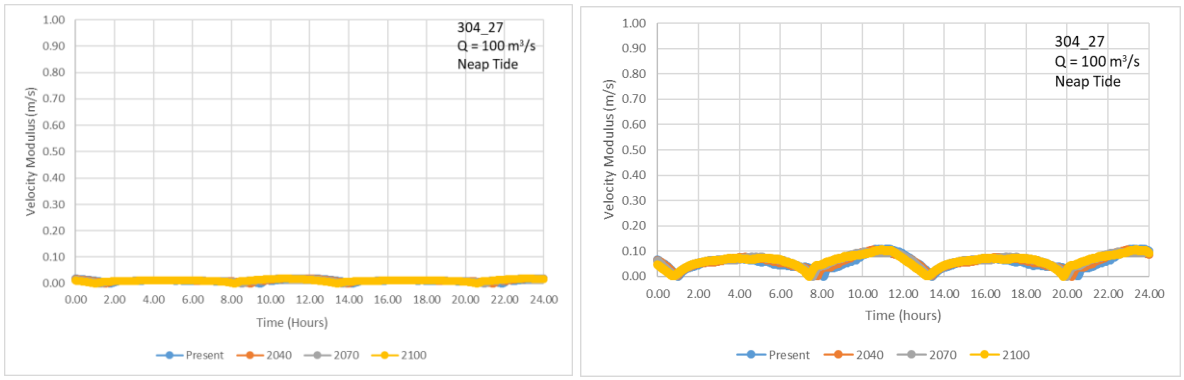


*Figure B.4* Velocity time series over two tidal cycles for a river discharge of 100 $m^3/s$ at neap tide in the westernmost region of Esteiro da Carrasqueira for the present bathymetry (left) and bathymetry that allows flooding (right).

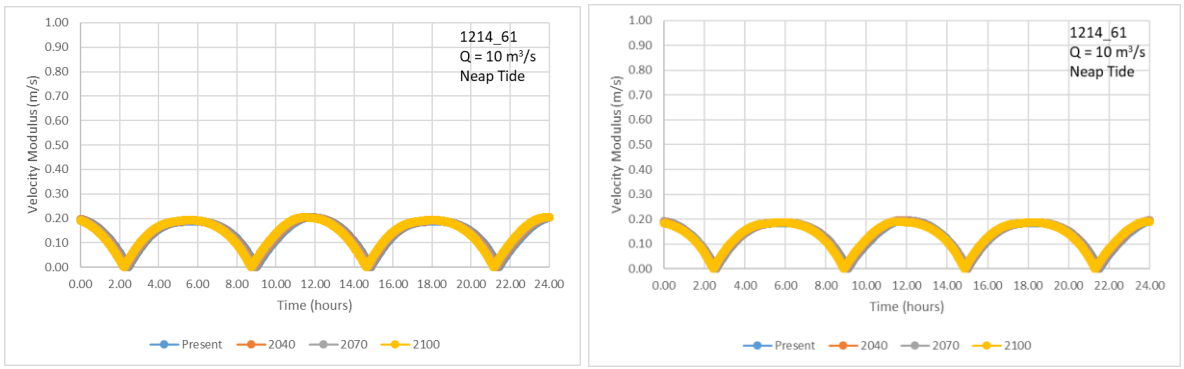


*Figure B.5* Velocity time series over two tidal cycles for a river discharge of 10 $m^3/s$ at neap tide in the upper estuary for the present bathymetry (left) and bathymetry that allows flooding (right).

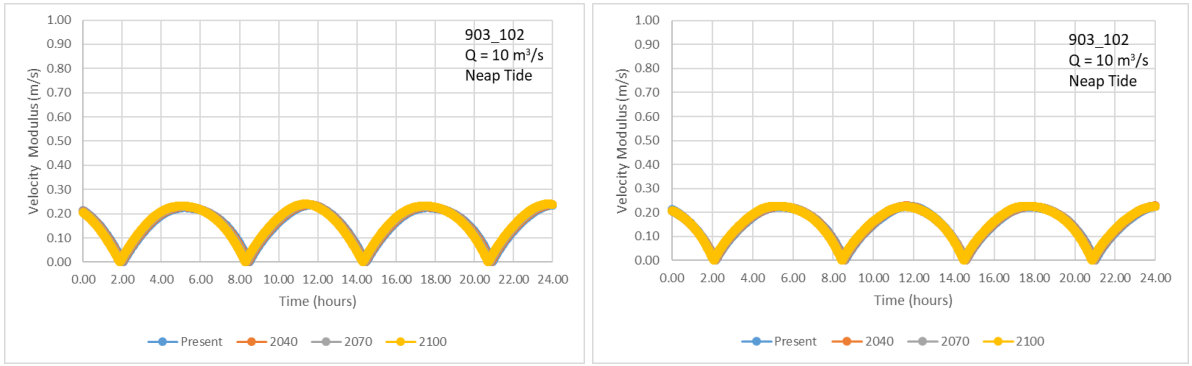


*Figure B.6* Velocity time series over two tidal cycles for a river discharge of 10 $m^3/s$ at neap tide in the middle estuary for the present bathymetry (left) and bathymetry that allows flooding (right).

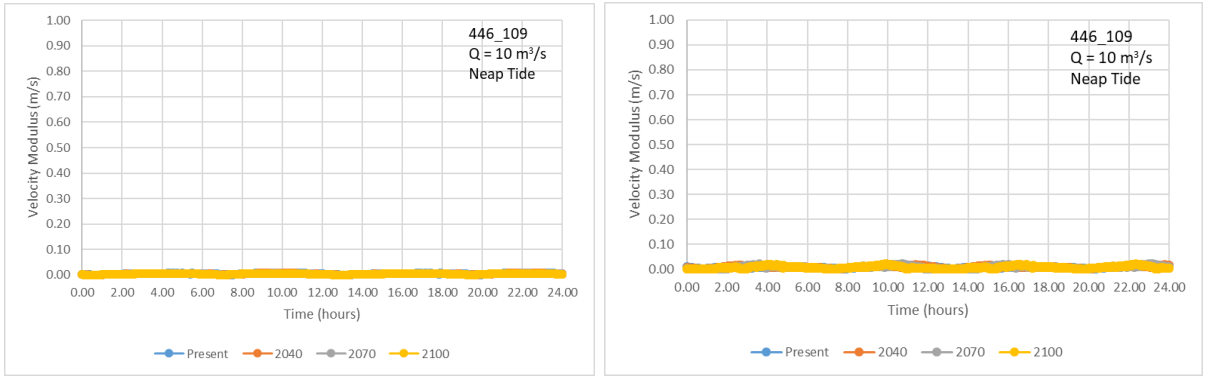


*Figure B.7* Velocity time series over two tidal cycles for a river discharge of 10 $m^3/s$ at neap tide in the northernmost region of Castro Marim for the present bathymetry (left) and bathymetry that allows flooding (right).

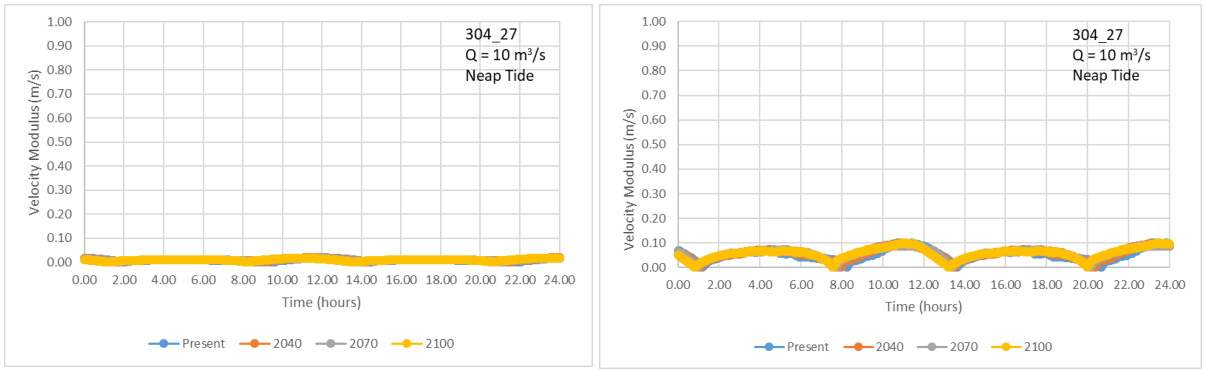


*Figure B.8* Velocity time series over two tidal cycles for a river discharge of 10 $m^3/s$ at neap tide in the westernmost region of Esteiro da Carrasqueira for the present bathymetry (left) and bathymetry that allows flooding (right).

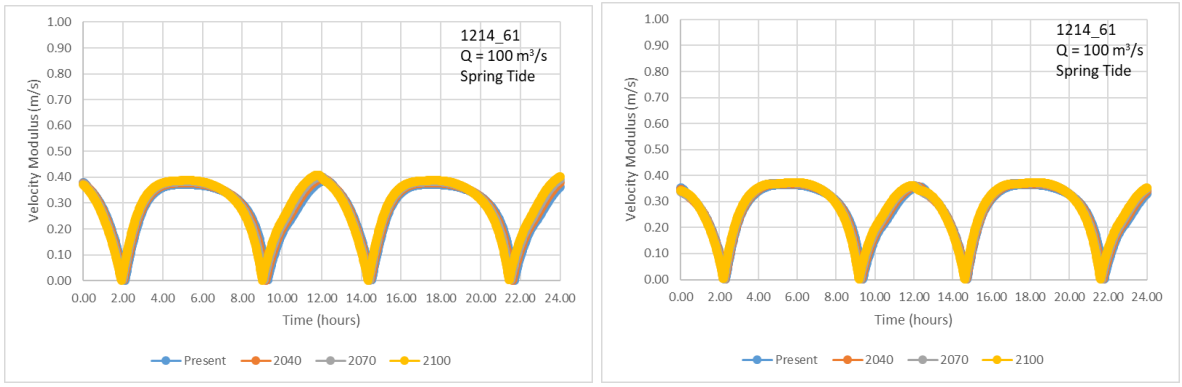


*Figure B.9* Velocity time series over two tidal cycles for a river discharge of 100 $m^3/s$ at spring tide in the upper estuary for the present bathymetry (left) and bathymetry that allows flooding (right).

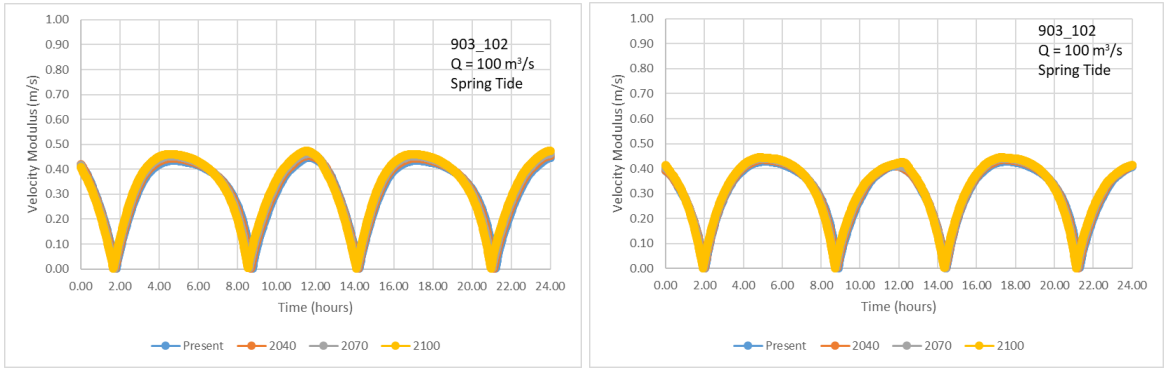


*Figure B.10* Velocity time series over two tidal cycles for a river discharge of 100 $m^3/s$ at spring tide in the middle estuary for the present bathymetry (left) and bathymetry that allows flooding (right).

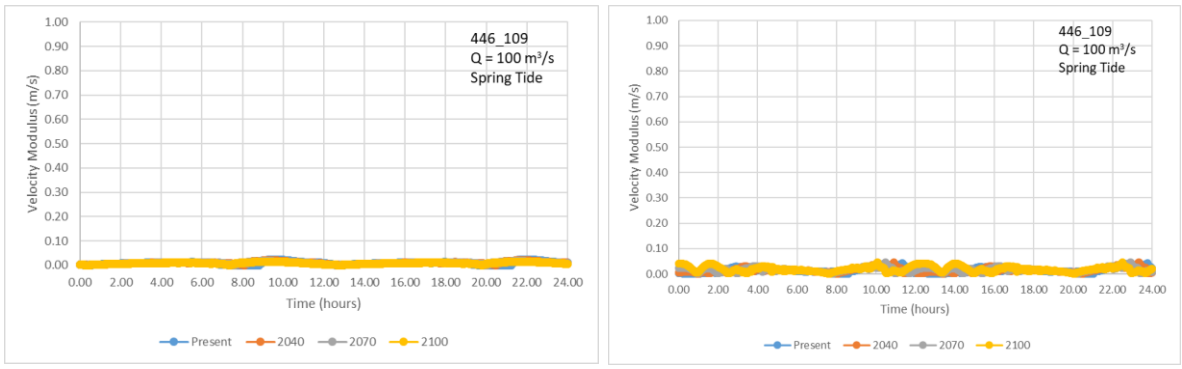


*Figure B.11* Velocity time series over two tidal cycles for a river discharge of 100 $m^3/s$ at spring tide in the northernmost region of Castro Marim for the present bathymetry (left) and bathymetry that allows flooding (right).

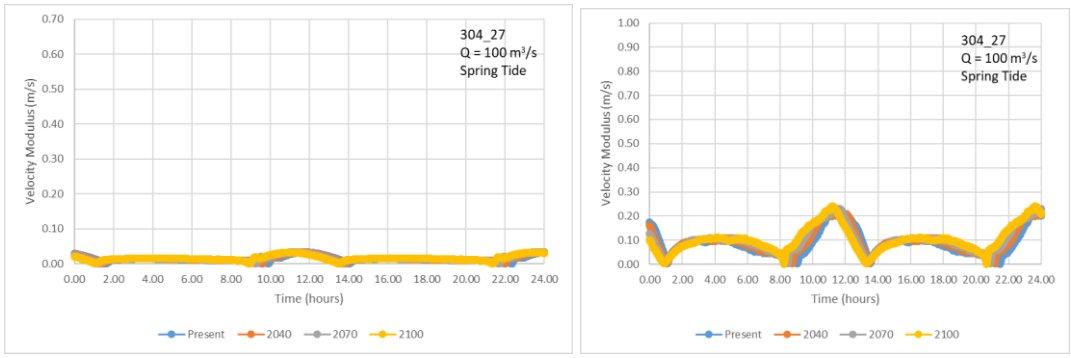


*Figure B.12* Velocity time series over two tidal cycles for a river discharge of 100 $m^3/s$ at spring tide in the westernmost region of Esteiro da Carrasqueira for the present bathymetry (left) and bathymetry that allows flooding (right).

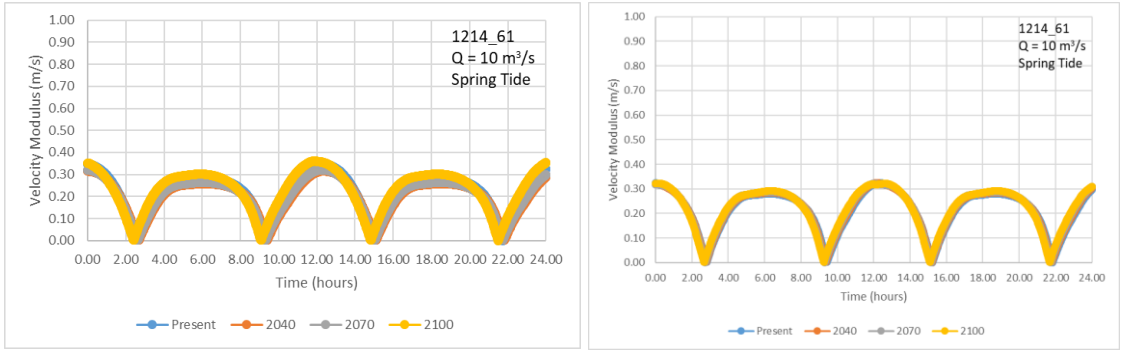


*Figure B.13* Velocity time series over two tidal cycles for a river discharge of 10 $m^3/s$ at spring tide in the upper estuary for the present bathymetry (left) and bathymetry that allows flooding (right).

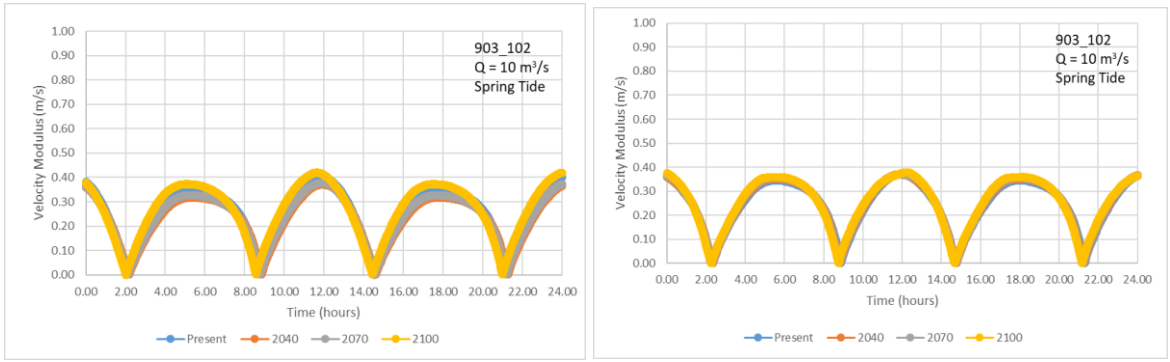


*Figure B.14* Velocity time series over two tidal cycles for a river discharge of 10 $m^3/s$ at spring tide in the middle estuary for the present bathymetry (left) and bathymetry that allows flooding (right).

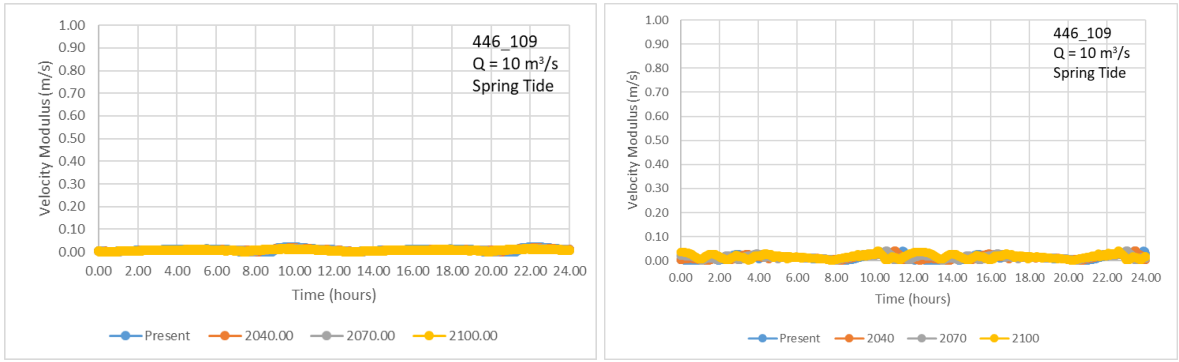


*Figure B.15* Velocity time series over two tidal cycles for a river discharge of 10 $m^3/s$ at spring tide in the northernmost region of Castro Marim for the present bathymetry (left) and bathymetry that allows flooding (right).

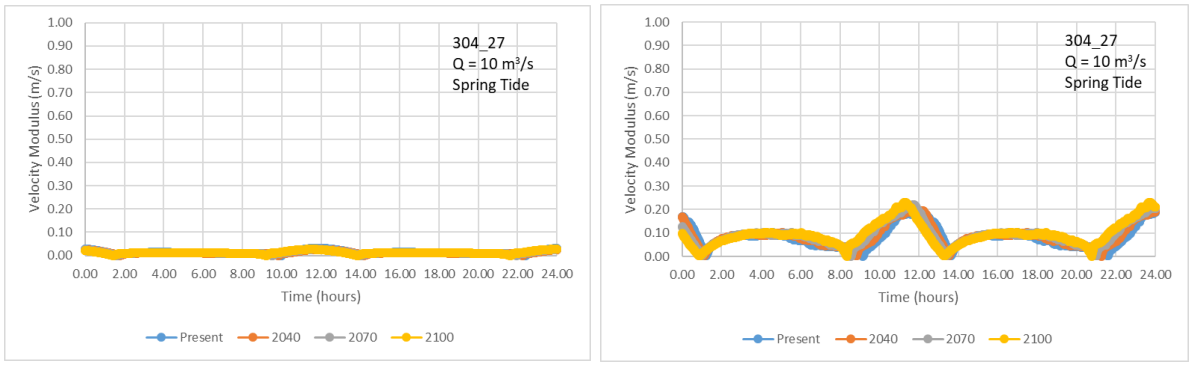


*Figure B.16* Velocity time series over two tidal cycles for a river discharge of 10 $m^3/s$ at spring tide in the westernmost region of Esteiro da Carrasqueira for the present bathymetry (left) and bathymetry that allows flooding (right).

# Appendix C Salinity Time Series

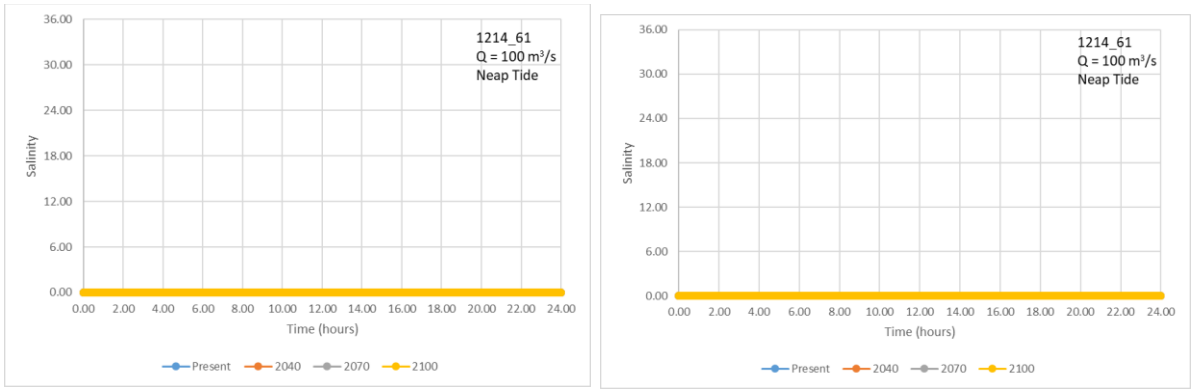


*Figure C.1* Salinity time series over two tidal cycles for a river discharge of 100 $m^3/s$ at neap tide in the upper estuary for the present bathymetry (left) and bathymetry that allows flooding (right).

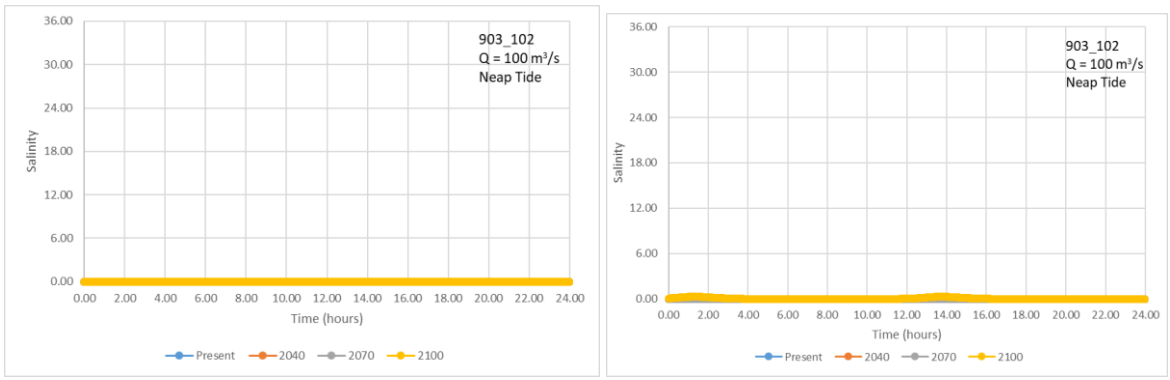


*Figure C.2* Salinity time series over two tidal cycles for a river discharge of 100 $m^3/s$ at neap tide in the middle estuary for the present bathymetry (left) and bathymetry that allows flooding (right).

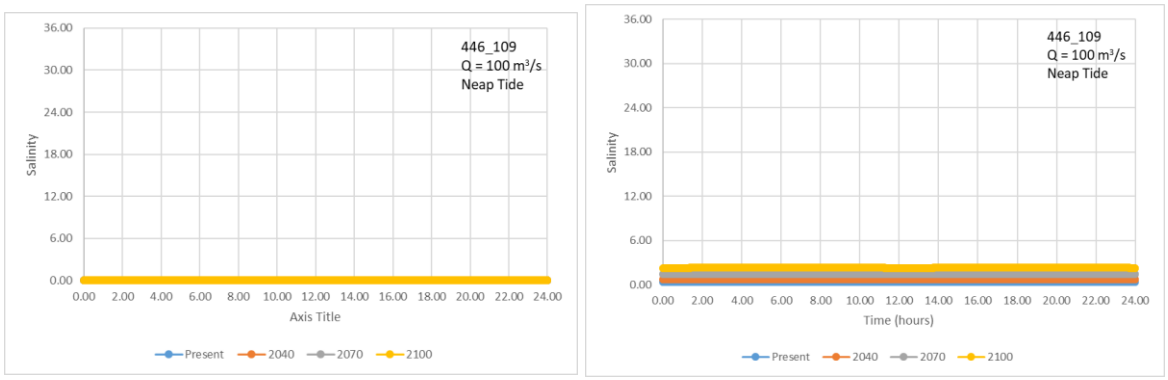


*Figure C.3* Salinity time series over two tidal cycles for a river discharge of 100 $m^3/s$ at neap tide in the northernmost region of Castro Marim for the present bathymetry (left) and bathymetry that allows flooding (right).

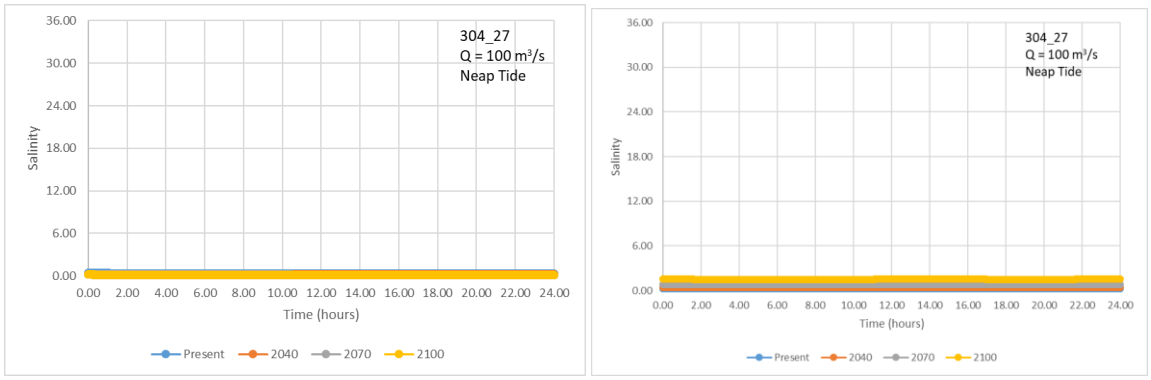


*Figure C.4* Salinity time series over two tidal cycles for a river discharge of 100 $m^3/s$ at neap tide in the westernmost region of Esteiro da Carrasqueira for the present bathymetry (left) and bathymetry that allows flooding (right).

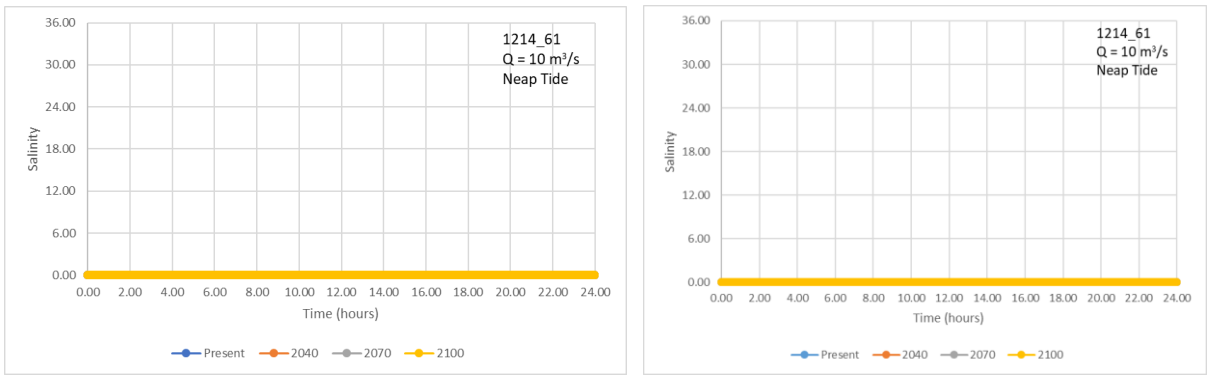


*Figure C.5* Salinity time series over two tidal cycles for a river discharge of 10 $m^3/s$ at neap tide in the upper estuary for the present bathymetry (left) and bathymetry that allows flooding (right).

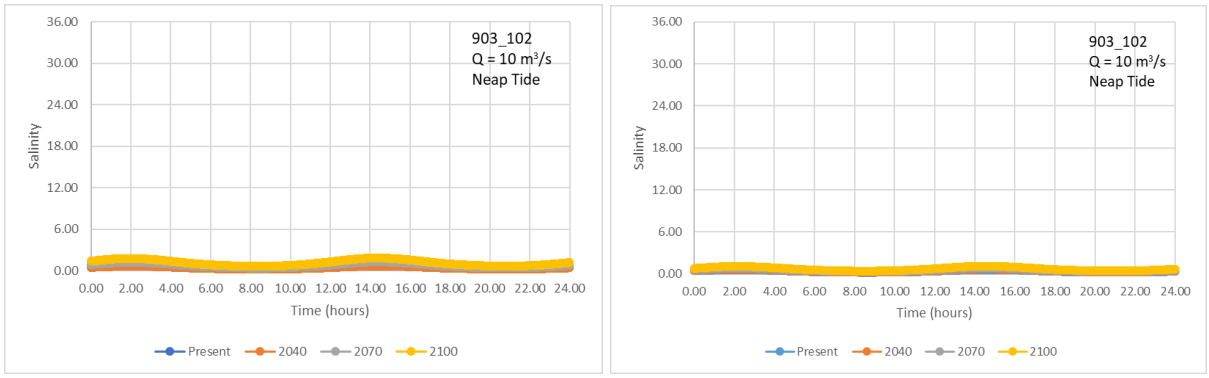


*Figure C.6* Salinity time series over two tidal cycles for a river discharge of 10 $m^3/s$ at neap tide in the middle estuary for the present bathymetry (left) and bathymetry that allows flooding (right).

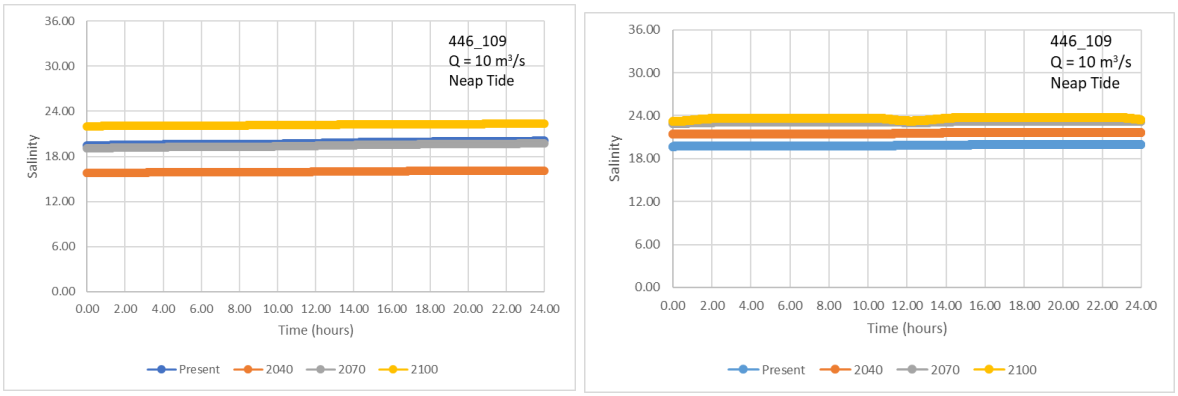


*Figure C.7* Velocity time series over two tidal cycles for a river discharge of 10 $m^3/s$ at neap tide in the northernmost region of Castro Marim for the present bathymetry (left) and bathymetry that allows flooding (right).

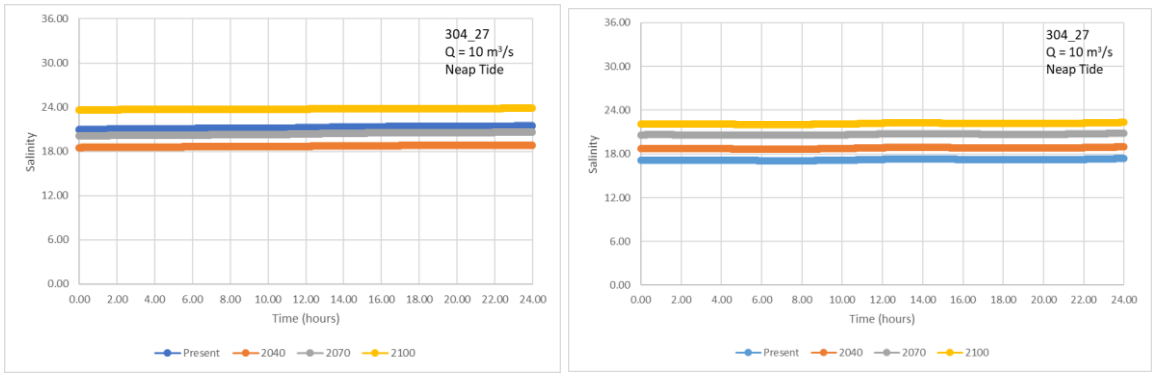


*Figure C.8* Salinity time series over two tidal cycles for a river discharge of 10 $m^3/s$ at neap tide in the westernmost region of Esteiro da Carrasqueira for the present bathymetry (left) and bathymetry that allows flooding (right).

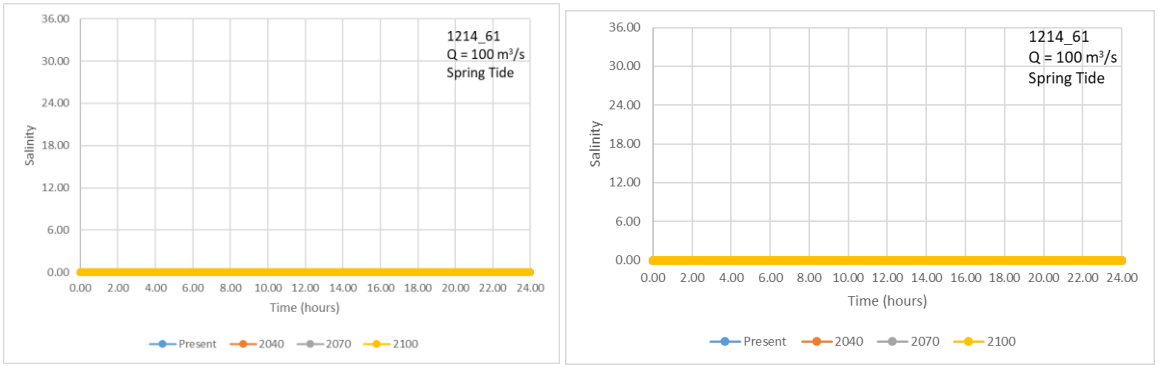


*Figure C.9* Salinity time series over two tidal cycles for a river discharge of 100 $m^3/s$ at spring tide in the upper estuary for the present bathymetry (left) and bathymetry that allows flooding (right).

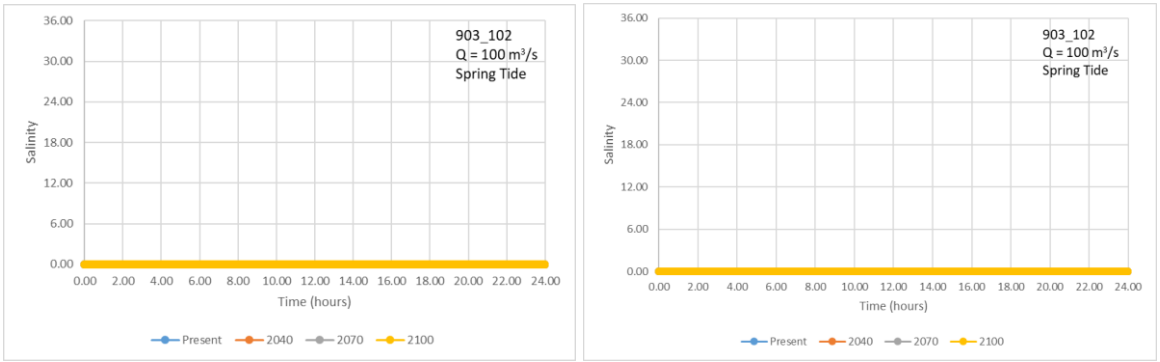


*Figure C.10* Salinity time series over two tidal cycles for a river discharge of 100 $m^3/s$ at spring tide in the middle estuary for the present bathymetry (left) and bathymetry that allows flooding (right).

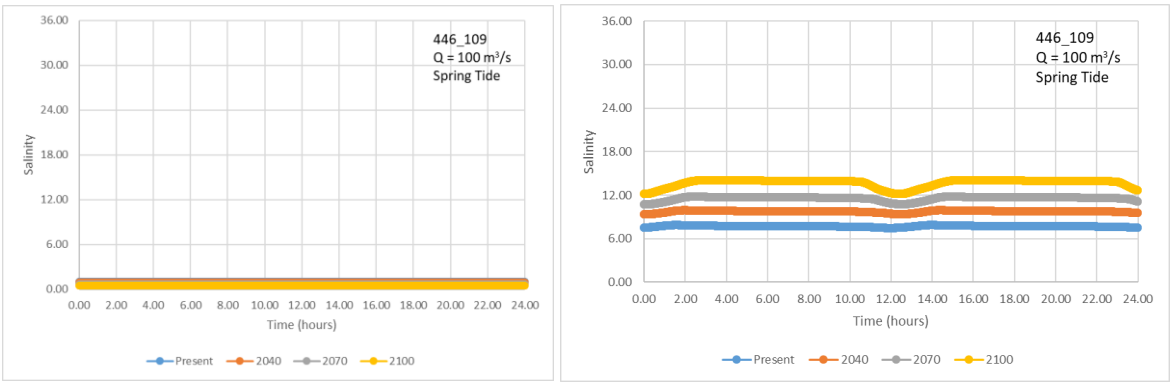


*Figure C.11* Salinity time series over two tidal cycles for a river discharge of 100 $m^3/s$ at spring tide in the northernmost region of Castro Marim for the present bathymetry (left) and bathymetry that allows flooding (right).

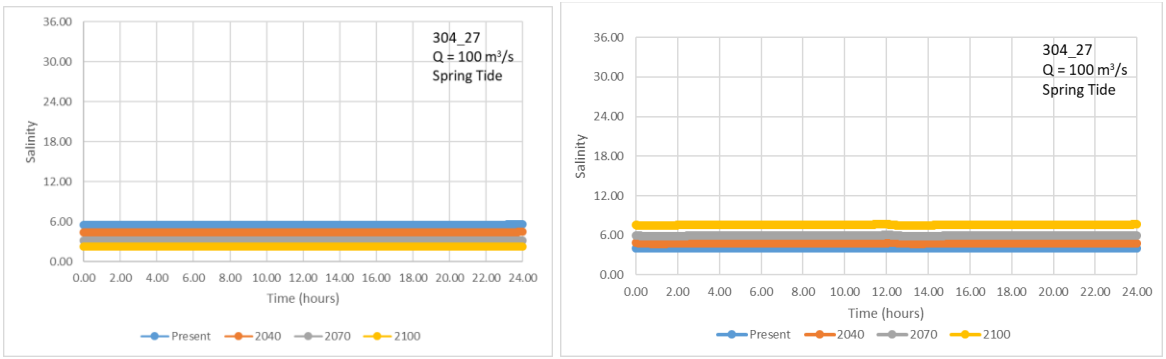


*Figure C.12* Salinity time series over two tidal cycles for a river discharge of 100 $m^3/s$ at spring tide in the westernmost region of Esteiro da Carrasqueira for the present bathymetry (left) and bathymetry that allows flooding (right).

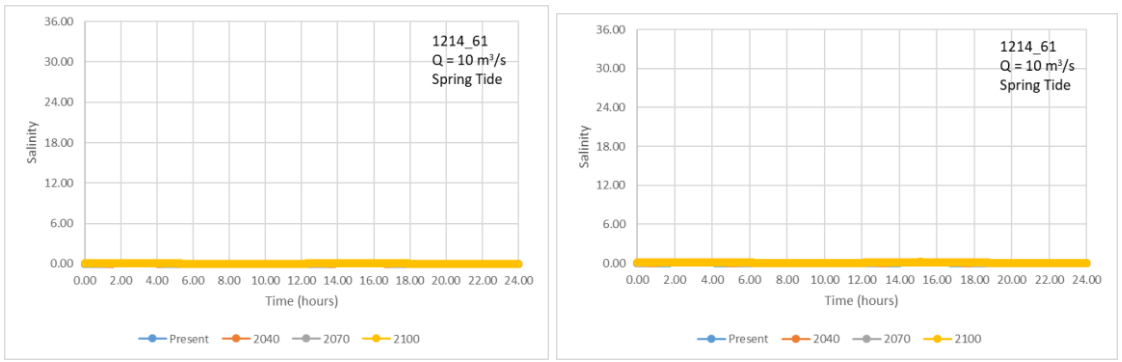


*Figure C.13* Salinity time series over two tidal cycles for a river discharge of 10 $m^3/s$ at spring tide in the upper estuary for the present bathymetry (left) and bathymetry that allows flooding (right).

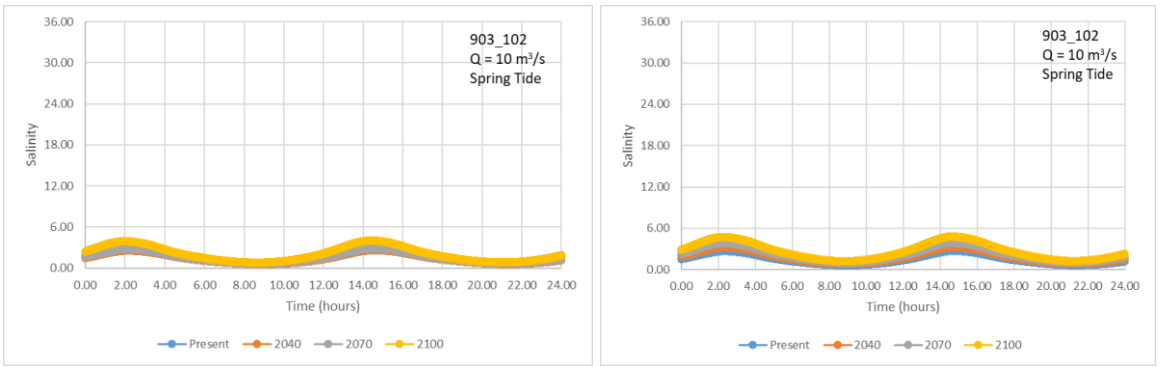


*Figure C.14* Salinity time series over two tidal cycles for a river discharge of 100 $m^3/s$ at spring tide in the middle estuary for the present bathymetry (left) and bathymetry that allows flooding (right).

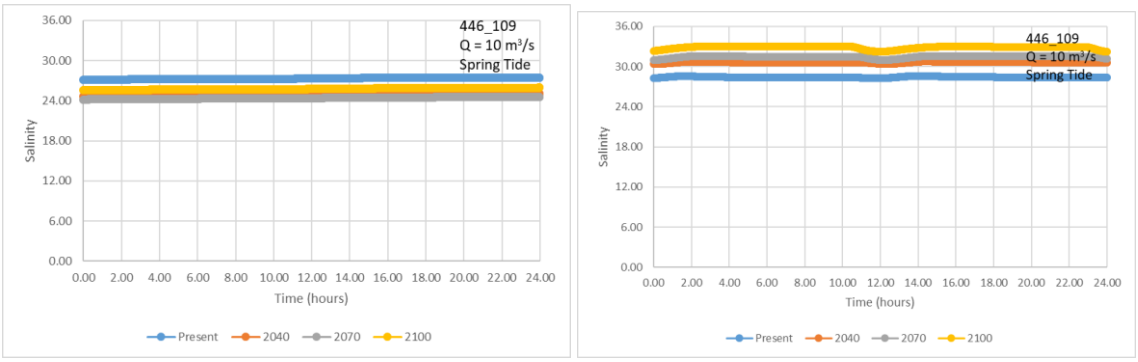


*Figure C.15* Salinity time series over two tidal cycles for a river discharge of 10 $m^3/s$ at spring tide in the northernmost region of Castro Marim for the present bathymetry (left) and bathymetry that allows flooding (right).

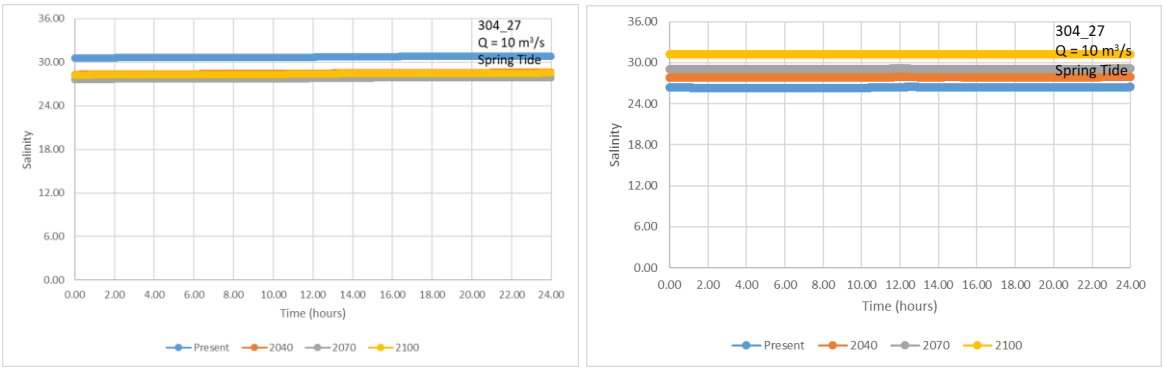


*Figure C.16* Salinity time series over two tidal cycles for a river discharge of 10 $m^3/s$ at spring tide in the westernmost region of Esteiro da Carrasqueira for the present bathymetry (left) and bathymetry that allows flooding (right).

# Appendix D ICCS Conference Paper – "The Impact of Sea Level Rise in the Guadiana Estuary"